Spectroscopic and Mechanistic Approach for Bio-Remediation of Heavy Metals

Thesis submitted to

The Maharaja Sayajirao University of Baroda

For the degree of

DOCTOR OF PHILOSOPHY

In

CHEMISTRY

सत्यं शिवं सुन्दरम्

Submitted by

Ms. Shilpi Kushwaha

Department of Chemistry
Faculty of Science
The Maharaja Sayajirao University of Baroda
Vadodara- 390 002
Gujarat (INDIA)

December-2011

Spectroscopic and Mechanistic Approach for Bio-Remediation of Heavy Metals

Thesis submitted to

The Maharaja Sayajirao University of Baroda

For the degree of

DOCTOR OF PHILOSOPHY

In

CHEMISTRY

Submitted by

Ms. Shilpi Kushwaha

Department of Chemistry
Faculty of Science
The Maharaja Sayajirao University of Baroda
Vadodara- 390 002
Gujarat (INDIA)

December-2011

Dedicated to my Grandparents, Parents, Sisters and Brothers

Tel: +91-265-2795552

सत्यं शिवं सुन्दरम्

Chemistry Department,
Faculty of Science,
The Maharaja Sayajirao University of Baroda,
Sayajiganj,
Vadodara-390 002
Gujarat (India)
Date: -13th December, 2011

CERTIFICATE

This is to certify that the thesis entitled "***Spectroscopic and Mechanistic Approach for Bio-Remediation of Heavy Metals***" submitted for Ph.D. Degree in Chemistry by ***Ms. Shilpi Kushwaha*** incorporates the original research work carried out by her under my supervision.

(Dr. Padmaja Sudhakar)
Research Guide

Head
Chemistry Department

HEAD,
CHEMISTRY DEPARTMENT
FACULTY OF SCIENCE
M. S. UNIVERSITY OF BARODA
VADODARA - 390 002

Dean,
Faculty of Science,
The M. S. University of Baroda,
Vadodara.

DEAN,
FACULTY OF SCIENCE
M. S. UNIVERSITY OF BARODA
VADODARA - 390 002

DECLARATION

I hereby declare that the matter embodied in the thesis entitled "**Spectroscopic and Mechanistic Approach for Bio-Remediation of Heavy Metals**" is a result of investigation carried out by me at Department of Chemistry, Faculty of Science, The Maharaja Sayajirao University of Baroda, Vadodara, Gujarat, India, under the supervision of Dr. Padmaja P. Sudhakar and that it has not been submitted elsewhere for the award of degree.

Date: 13.12.11

Place: Vadodara

(Shilpi Kushwaha)

Acknowledgements

This thesis is the result of the work whereby I have been accompanied and supported by many people. It is a pleasant opportunity for me to express my gratitude for all of them.

First and foremost, with a deep sense of gratitude, I wish to express my heartiest thanks to my guide, Dr. Padmaja P. Sudhakar for her never ending enthusiasm and continuous flow of suggestions and constant encouragement throughout the course of this investigation. She helped me to get a holistic view and a systematic approach of original research work.

I deeply thank Dr. B. Sreedhar, Division of Inorganic and Physical Chemistry, Indian Institute of Chemical Technology, Hyderabad for his constant support for various analusis.

I am thankful to BRNS (BARC, Mumbai) for the financial support.

I deeply thank the Department of Chemistry, The Maharaja Sayajirao University of Baroda for giving me the opportunity to work in this Department and making all the facilities available for my research work.

I would like to thank Prof. B.V. Kamath, Head and Prof. Surekha Devi, Earlier Head, Department of Chemistry, The Maharaja Sayajirao University of Baroda for their continuous support.

I would like to thank Dr. Unnikrishnan, IPCL, Baroda, for BET measurements.

I would like to thank Dr. P. K. Mehta, Department of Physics, The M. S. University of Baroda, for helping me in the XRD measurements.

I would like to thank Dr. Ganpati, Department of Geology, The M. S. University of Baroda, for helping me in the TGA measurements.

I would like to thank SPARC, Tandelja, Baroda, for NMR and CHN measurements.

I would like to thank Dr. Ansghuman Pal and Dr. Sunil Shah, for their constant support. I deeply thank Ketan, Jigar, Sarang, Srinivas, Bharat, Harnish, Ronak, Ageetha, Rahul, Neelesh, Kadu, Soyeb, Mayur, Hemant, Sanjay, Puran, Shardul, Komal, Akeel, Sharda, Ranjit, Parth, Parimal, Manisha, Nancy, Vriti, Apurva, Uloopi, Hiral, Piyush bhai, Abhilash, Aakash, Kunal, Deepak Pauravi for their encouragement, help and all time support. I have an endless list of friends who have enriched my life greatly and I thank them all for being with me.

I would like to thank Mrs. Revathi Ganesh, for documentation.

I am also thankful to all the teachers and non-teaching staff of the Department of Chemistry for supporting me throughout the research work.

As always it is impossible to mention everybody who had an impact to this work however there are those whose spiritual support is even more important. I feel a deep sense of gratitude for my mother, father and brother who *formed part of my vision and taught me good things that really matter in life. I am also very much grateful to all my family members for their endless love, constant inspiration and encouragement.*

Shilpi Kushwaha

Outline

Chapter 1

Introduction

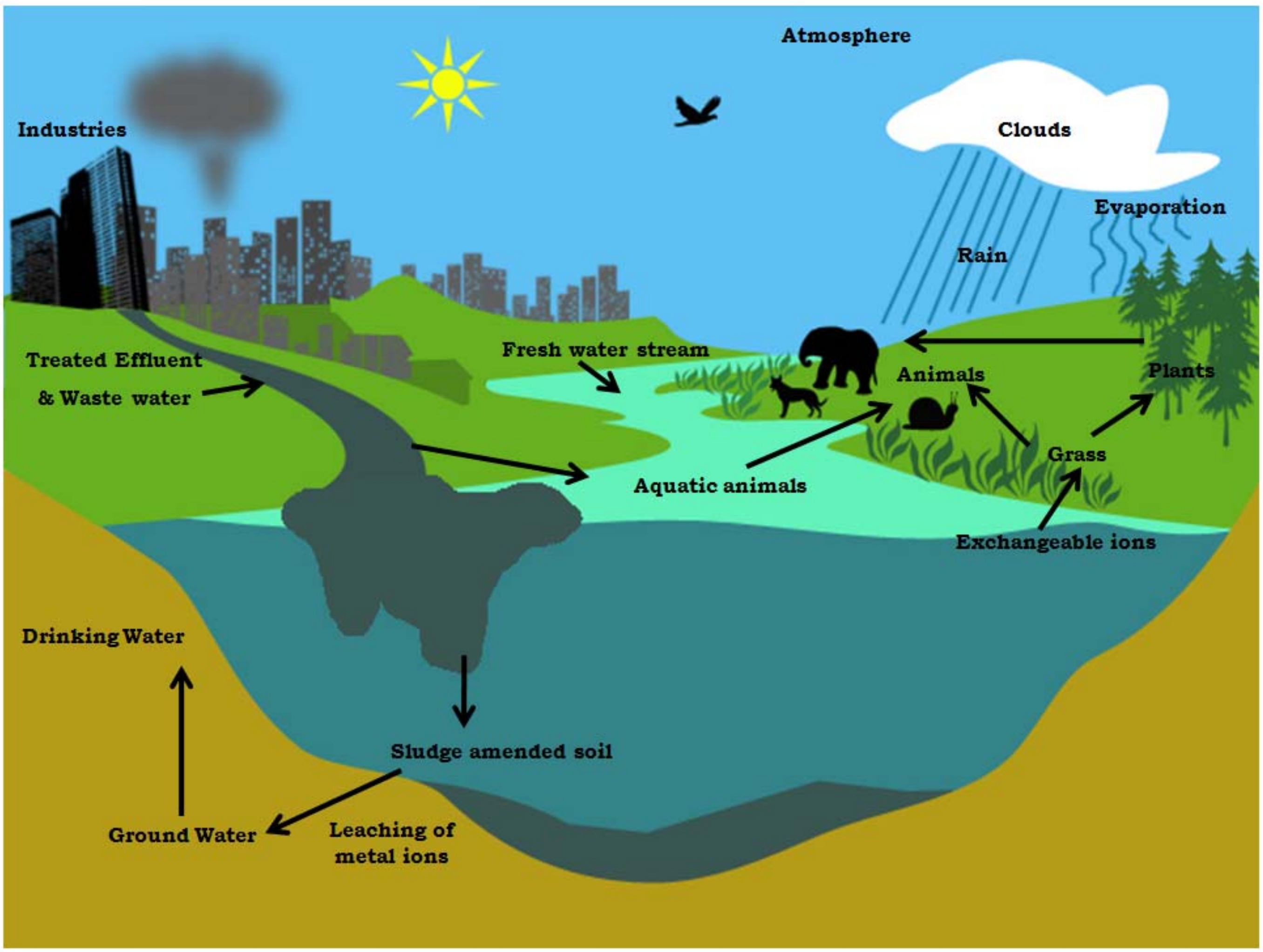

‘Heavy metals’ is a general collective term applied tothe group of metals and metalloids with an atomic densitygreater than 6 g/cm^3. Although it is only a loosely definedterm it is widely recognized and usually applied to the elementssuch as Cd (cadmium), Cr (chromium), Cu (copper),Hg (mercury), Ni (nickel), Pb (lead) and Zn (zinc) whichare commonly associated with pollution and toxicity problems.

Unlike most organic pollutants, heavy metals occurnaturally in rock-forming and ore minerals and so a rangeof normal background concentrations is associated witheach of these elements in soils, sediments, waters and livingorganisms. On an annual basis, significant quantities ofvarious heavy metals are produced from the mining of theirrespective ores.

Industrial uses of metals and other domestic processes(e.g. burning of fossil fuels, incineration of wastes, automobileexhausts, smelting processes and the use of sewagesludge as landfill material and fertilizer) have introducedsubstantial amounts of potentially toxic heavy metals intothe atmosphere and into the aquatic and terrestrial environments.Discharged toxic metals typically include Cd, Cu, Ni, Cr, Co, Zn and Pb [1].

While many of the heavy metals are needed by plants at the micronutrient level, higher concentrations are known to produce a range of toxic effects. At high exposure levels, lead causes encephalopathy, cognitive impairment, behavioral disturbances, kidney damage, anaemia and toxicity to the reproductive system [2]. Chromium is widely recognized to exert toxic effects in its hexavalent form [3]. Human exposure to Cr(VI) compounds is associated with a higher incidence of respiratory cancers [4]. Cadmium is associated with nephrotoxic effects particularly at high exposure levels; long-term exposure may cause bone damage as well [5]. High concentrations of mercury can lead to neuro-behavioral disorders and developmental disabilities including dyslexia, attention deficit hyperactivity disorder, and intellectual retardation [6]. Excessive copper concentrations can lead to weakness,lethargy and anorexia, as well as damage to the gastrointestinal tract [7]. The toxic effects of nickel and other heavy metalsare discussed in some detail by Nordberg et al. [8].

Pollutants like uranium arise into the wastewaters as a result of different industrial activities like: mining, production of nuclear fuels, laboratory investigations, etc.. Uranium contamination poses a threat in some surface and ground waters.The chemical toxicity of uranium is predominantly caused by the highly reactive hexavalent uranyl ions [9]. Uranium disposed into the environment can reach the top of the food chain and be ingested by humans

[10], causing kidney or liver damage to humans [11-13].Removal of radioactive ions from the wastewaters is a huge problem because these ions are extremely dangerous for the environment and human health by their high toxicity even at very low concentrations and long half lives. Hence, the removal of uranium from waste water is important not only for the nuclear industry,but also for environmental remediation [14].

Presence of metals in water streams and marine water causes a significant health threat to the aquatic community which is most common for the damage of the gill of the fish [15, 16].Consequently, in many countries, more strict legislation has been introduced to control water pollution. Various regulatory bodies have set the maximum prescribed limits for the discharge of toxic heavy metals in the aquatic systems. However, the metal ions are being added to the water stream at a much higher concentration than the prescribed limits by industrial activities, thusleading to the health hazards and environmental degradation. Table 1.1 shows the permissible limits and health effects of various toxic heavy metals [17-20].

Removal of metal ions from wastewater in an effective manner has thus become an important issue today. Various methods exist for the removal of heavy metal ions from wastewater which include chemical precipitation/coagulation, membrane technology, electrolytic reduction, ion exchange and adsorption [21, 22]. The advantages and disadvantages associated with each method are listed in Table 1.2.

The most widely used method of removing heavy metals from solution is to increase the pH of the effluent, thus converting the soluble metal into an insoluble form (i.e. its hydroxide). Ion exchange is the second most widely used method for heavy metal removal from aqueous streams [23]. During removal, recovery, or processing of metals, ion exchange acts as a concentrator of metals. The chemistry of the influent stream becomes very important to the success of the ion exchange application.

Coagulation–flocculation can also be employed to treat wastewater laden with heavy metals wherein the coagulation process destabilises colloidal particles by adding a chemical agent (coagulant) and results in sedimentation [24]. Coagulation is followed by flocculation of the unstable particles in order to increase their size and form into bulky floccules which can be settled out. Flotation is employed to separate solids or dispersed liquids from a liquid phase using bubble attachment [24]. Adsorptive bubble separation employs foaming to separate the metal impurities. Ion flotation, precipitate flotation and sorptive flotation are the main flotation process mechanisms for removal of metal ions from solution. Membrane filtration has received considerable attention for the treatment of inorganic effluent, since it is capable of removing not only suspended solids and organic compounds, but also inorganic contaminants such as heavy metals.

Table 1.1.Permissible limits, source and health effects of various toxic metal ions [88]

Metal	Source	Permissible limits for discharge of industrial effluent to inland surface water (mg/L)		Permissible limits by International bodies for potable water (mg/L)		Health hazards
		Indian Standard	WHO	Indian standard	WHO	
As	Electronics, paints & pigments, metallurgical industries	0.20	-	0.01	0.010	Carcinogenic, producing liver tumors, skin & gastrointestinal effects
Hg	Batteries, manure sewage sludge & electronics	0.01	-	0.001	0.001	Corrosive to skin, eyes and muscle membrane, dermatitis, anorexia, kidney damage & severe muscle pain
Cd	Fertilisers, Manure Sewage sludge, batteries, electronics & Metallurgical industries	2.00	0.10	0.01	0.003	Carcinogenic, causes lung fibrosis, dyspnea & weight loss
Pb		0.10	0.10	0.05	0.010	Suspected carcinogen, loss of appetite, anemia, muscle & joint pains, diminishing IQ, cause sterility, kidney problem &high blood pressure
Cr	Metalliferous mining, Paints & pigments, Electroplating, Electronics	0.10	-	0.05	0.050	Suspected human carcinogen, producing lung tumors, allergic dermatitis
Ni	Metalliferous mining, Electroplating, Electronics, metallurgical industries	3.00	-	0.02	-	Causes chronic bronchitis, reduced lung function, cancer of lungs and nasal sinus
Zn	Metalliferous mining, Paints & pigments, Electroplating, Batteries	5.00	5.0-15.0	5.0	-	Causes short-term illness called metal fume fever & restlessness
Cu	Metalliferous mining, Electroplating, metallurgical industries	3.00	0.05-1.5	1.5	-	Long term exposure causes irritation of nose, mouth, eyes, headache, stomachache, dizziness, diarrhea
Fe	Metallurgical industries	3.00	0.1-1.0	0.30	0.20	Excess amounts cause rapid pulse rates, congestion of blood vessels, hypertension
U	Metallurgical industries	-	-	-	0.03	Dermatitis, renal damage, acute necrotic arterial lesions, respiratory irritants, with coughing, shortness of breath.

Table 1.2. Advantages and disadvantages of different methods used for removal of metal ions

	Physical or Chemical Methods	Advantages	Disadvantages
Conventional Treatment processes	Adsorption	Flexibility and simplicity of design, ease of operation and insensitivity to toxic pollutants	Adsorbent requires regeneration
	Biodegradation	Economically attractive and publically acceptable treatment	Slow, necessary to create an optimal favorable environment, maintenance and nutrition requirements
	Coagulation/ Floculation	Simple and Economicaly feasible	High sludge production and formation of large particles
Established recovery Processes	Oxidation	Rapid and efficient process for toxic pollutants removal	High energy costs and formation of byproducts
	Ion exchange	Effective for a wide range of heavy metals	Adsorbent requires regeneration or disposal
	Membrane filtration technologies	Good removal of heavy metals, produces a high quality treated effluent	High pressures, expensive, incapable of treating large volumes, Concentrated Sludge production
	Electrokinetic Coagulation	Economicaly feasible	High sludge production
	Fentons Reagents	Effective and capable of treating variety of wastes and no energy input necessary to activate hydrogen peroxide	Sludge generation
	Electrochemical treatment	Rapid process and effective for certain metal ions	High energy costs and formation of byproducts
Emerging removal processes	Advanced Oxidation processes (Ozonation, Photochemical, Irradiation)	No sludge production, little or no consumption of chemicals, high efficiency, Effective at lab scale	Economically unfeasible, formation of by-products, technical constraints
	Biological Treatment	Feasible in removing some metals	Technology yet to be established and commercialised
	Selective bioadsorbents	Economically attractive, regeneration is not necessary, high selectivity	Requires chemical modification, non-destructive process
	Biomass	Low operating cost, good efficiency and selectivity, no toxic effect on microorganisms	Slow process, performance depends on some external factors (pH, salts)

In accordance with the very abundant literature data, liquid-phase adsorption is one of the most popular methods for the removal of toxic pollutants from wastewater, since proper design of the adsorption process will produce a high quality treated effluent [25]. This process provides an attractive alternativefor the treatment of contaminated water, especially if the adsorbent isinexpensive and does not require an additional pre-treatment stepbefore its application. Adsorption has been found to be superiorcompared to the other techniques for water re-use in terms of initialcost, flexibility and simplicity of design, ease of operation and insensitivityto toxic pollutants. Adsorption also does not result in theformation of harmful substances.

A number of materials have been extensively investigated as adsorbents in water pollution control. Some of the important onesinclude silica gel, activated alumina, zeolites, activated carbon and clays.

Activated Carbon

Activated carbon(AC) has undoubtedly been the most popular and widely used adsorbent in wastewater treatment throughout theworld.There are different physical forms by which AC can be found, including: (i) granular activated carbon (GAC); (ii) powdered activated carbon (PAC); (iii) activatedcarbon fibers (ACF); and (iv)activated carbon cloths (ACC). GAC can be prepared from hard material, such as coconut shells, and normally includes particles retained in an 80-mesh sieve (0.177 mm); it is commonly used as column filler for gas or liquid treatments and can be regenerated after use. When small particles compose the raw material, like wood sawdust, PAC is obtained (includes particles of 0.177 mm); PAC is normally mixed with the liquid to be treated and afterwards disposed of. Due to its small particles, PAC adsorption is normally very effective, however, and for the same reasons, settling and removal tend to be slower than when using GAC. ACF canbe prepared from homogeneous polymeric raw materials and, as opposed to GAC and PAC, show a mono dispersed pore size distribution [26]. Their thin fiber shape enhances intra-particle adsorption and therefore improved contact efficiencies between the aqueous media and the adsorbent can be achieved [27].

ACC were initially developed in the early 1970s, using as precursors phenolic or viscose rayon [28] and are considered to be excellent adsorbents due to their low-pressure drop during process, high contact efficiency and flexibility [29]. Although many kinds of adsorbents were already prepared and tested in aqueous-phase treatments, GAC and PAC are still themost widely used.

However, activated carbon is expensive which limits its large scale application. According to Bailey and Wan Ngah, an adsorbent can be considered as cheap or low-cost if it is abundant in nature, requires little processing and is a byproduct of waste material from waste industry [30, 31].

A potential method to reduce the cost of activated carbon production is to use low-cost materials as precursors for the production of activated carbon.AC can be prepared from a wide variety of raw materials [32], which should be abundant and cheap, with high carbon content and low inorganic content; rawmaterials should be easily activated and should have low degradation by aging [33].Coal is the most commonly used precursor, mainly due to its low cost and large supply [34]. The adsorption properties of each type of coal are determined by the nature of the vegetable materialand the extent of the physical–chemical changes occurring during coal formation and after its deposition [35].

The preparation of AC from waste materials has several advantages, mainly of economic and environmental nature.A wide variety of ACshave been prepared from different waste materials; conventional wastes (from agriculture and wood industry) as well as non-conventional wastes (from municipal and industrial activities) have been used.

Non-conventional wastes (from municipal and industrial activities)

The economical activities in the modern society gradually created a pattern of mass production, mass consumption as well as mass deposition [36]. As aconsequence, there is an accumulation of several industrial and post-consumer waste products, which by their nature are difficult or poorly effective to be regenerated into other materials and that more currently end up in incineration plants or landfills. Due to the more restricted environmental standards, limitations on the application of such alternatives are increasing.

The discharge of plastic wastes, such as polyethylene terephthalate (PET) and polyvinyl chloride (PVC), industrial wastes, such as oil combustion residues and fabrics, aswell as the discharge of tires, sewage sludges, and fertilizers, represents a serious challenge for waste management strategies. It is therefore of main relevance to findalternatives by which such materials can be reused or recycled according to environmentally acceptable procedures [37].

The use of such non-conventional wastes as carbon source for the production of AC might be an efficient alternative for both, adoption of effective waste managementpractices, and production of low-cost AC. A review of the literature showed that there are a considerable amount of studies dedicated to the valorization of such wastes, namely for the production of AC. Plastic wastes, various industrial wastes like fly ashes, pitch, and polymeric residues from factories as well as other wastes such as tires and sewage sludge have been used as raw material for AC production. For instances, a waste commercial ion-exchange resin might be used to prepare AC with values of specific surface area and pore volume suggesting its application in different purposes, that might include aqueous-phase treatments [38].

Also, AC can be successfully prepared from both old newspaper and paper prepared from simulated paper sludge [39, 40]. Naturally, studies show that raw materials with higher carbon content lead to the achievement of a better AC. Generally, AC show good texture and potential to compete with commercial ones.

Conventional wastes (from agriculture and wood industry)

Due to their abundance, agricultural wastes have low economic value; additionally, their current deposition creates significant environmental degradation. Agriculturalwaste is a rich source for AC production due to its low ash content and reasonable hardness [35]; therefore, conversion of agricultural wastes into AC is a promising alternative to solve environmental problems and also to reduce the costs of AC preparation.

There are currently a large number of studies regarding the use of several agricultural wastes to produce AC. Most of them focus on the use of waste materials of considerable rigidity, such as the shells and/or stones of fruits like nuts, peanuts, olives, dates, almonds, apricots and cherries; however, wastes resulting from the production of cereals such as rice, coffee, soybean, maize and corn as well as olive cakes, sugar cane and sugar beat bagasse, coirpith, oil-palm shell (from oil-palm processing mills) and various seed wastes were already used.

Most of the reviewed studies show that these materials can compete with the commercial AC, and some of them have even better behavior than the commercial ones. Somerelevant issues concerning different recent studies on the application of these materials in aqueous phase were summarized.

Due to their particular porous characteristics, woody materials are very relevant and challenging raw materials to prepare AC, namely for the adsorption of solutes in theliquid phase [41]. The wood industry is responsible to produce great amounts of woody waste materials that might be recycled to produce AC. Also,several forest residues can be used, additionally contributing to a better forest management and conservation. Many studies were made concerning the recycling of these materials for the production of AC. Woody materials of different types such as cedar, fir, oak, as well as from tropical trees have already been used.

The application of AC prepared from woody materials has been made for the removal ofcontaminants such as organic compounds, dyes, and heavy metals, from aqueous phase. These materials seem to be very effective in adsorbing heavy metals such as chromium and copper, being considered potentially good substitutes of the commercial ones. The adsorption rate is normally influenced by the proportion of AC used. On the other hand, PAC obtained from sawdust might be used to prepare GAC with the addition of a proper binder and a reinforcer; such GAC seems to have a very good behavior in adsorbing phenol, namely through physisorption mechanisms [42]. It was concluded that woody materials lead to AC showing good adsorption behaviour for adsorbates of various molecular forms.

When using activated carbon, the adsorption process results from interactions between the carbon surface and the adsorbate. These interactions can be electrostatic or non-electrostatic. When the adsorbate is an electrolyte that dissociates in aqueous solution, electrostatic interactions occur; the nature of these interactions, that can be attractive or repulsive, depends on the: (i) charge density of the carbon surface; (ii) chemical characteristics of the adsorbate; and(iii) ionic strength of the solution. Non-electrostatic interactions are always attractive and can include: (i) van der Waals forces; (ii) hydrophobic interactions; and (iii) hydrogen bonding.

According to Moreno-Castilla [43], the properties of the adsorbate that mainly influence the adsorption process in AC are: (1) molecular size; (2) solubility; (3) pK_a; and (4) nature of the substituents (in the case of aromatic adsorbates). The molecular size determines the accessibility of the adsorbate to the pores of the carbon, the solubility determines the degree of hydrophobic interactions between the adsorbate and the carbon surface and pK_a controls the dissociation of the adsorbate (if it is an electrolyte). When the adsorbate is aromatic, the substituents of the aromaticring have the ability to withdraw or release electrons, which therefore affects the non-electrostatic interactions between the adsorbate and the AC surface.When the AC is in contact with an aqueous solution, an electric charge is generated. This charge results from either the dissociation of the surface functional groups of thecarbon or the adsorption of ions from the solution, and strongly depends on the solution pH and on the surface characteristics of the adsorbent [44]. The centralissue for ion adsorption from an aqueous medium is the understanding of the mechanisms by which ionic species become attached to the carbon surface. There are three different mechanisms by which metallic ions (or other ions) are removed from an aqueous solution. The first states that the process is based on electrostatic adsorbate–adsorbent interactions being totally dependent on the existence of carbon surfaces functionality, especially oxygen surfaces complexes (ion-exchange process). The second one suggests that enhanced adsorption potentials, as occurs in the narrowest of microporosity, may be strong enough to adsorb and retain ions. The third mechanism is based on the hard and soft acids and bases concept, a consequence of the amphoteric nature of carbon surfaces.

Variable amounts of atoms, known as heteroatoms, can be found in AC (e.g. oxygen, hydrogen, nitrogen and sulphur). These atoms, which might have origin in the raw material or could be introduced during preparation or further treatments [45], deeply influence the charge, hydrophobicity and electronic density of the AC surface. The carbon surface chemistry is, therefore, influenced by the presence of hetero atoms [46] and has a great influence on both, electrostatic and non-electrostatic interactions. Additional information regarding the surface characteristics of AC which determine the removal of pollutants from the aqueous phase can be found in a review by Moreno- Castilla and Rivera-Utrilla[33].AC texture includes a wide range of pores that can be classified according to their width as: micropores (2 nm),mesopores (2–50 nm) and macropores (450nm) [43].

Natural materials

Because of their low cost and local availability, natural materials such as chitosan, zeolites, clay, or certain waste products from industrial operations and plant wastes are classified as low-cost adsorbents.

Chitosan has received considerable interest for heavy metals removal due to its excellent metal-binding capacities and low cost. Fishery wastes such as shrimp, lobster, and crab shells have been developed into one of the promising options to produce chitosan. These wastes could be obtained for free from local fishery industries. Since such wastes are abundantly available, chitosan may be produced at low cost. Consequently, chitosan offers a lot of promising benefits for wastewater treatment applications today. The discussion on chitosan as an adsorbent is taken up in chapter 7.

Zeolites are aluminosilicates with Si/Al ratios between 1 and infinity. There are 40 natural and over 100 synthetic zeolites. Natural zeolites also gained a significant interest among scientist, mainly due to their valuable properties such as ion exchange capability, cost efficiency since they are able to treat wastewater contaminated with heavy metal at low cost. Various zeolites have been employed for the removal of pollutants [47-50]. Recently, Wang and Peng[51]discussed the role of natural zeolites as effective adsorbents in water and wastewater treatment [52].

Clay is one of potential alternatives to activated carbon as well. Similar to zeolites, clayminerals are also important inorganic components in soil. Their adsorption capabilities comefrom their high surface area and exchange capacities. The negative charge on the structureof clay minerals gives clay the capability to attract metal ions [53].

Industrial wastes as an adsorbent for removal of heavy metals

Industrial waste is also one of the potentially low-cost adsorbent for heavy metal removal.It requires little processing to increase its adsorptive capacity. Generally industrial wastes are generated as by-products. Since these materials are locally available in large quantities, they are inexpensive. In India, various types of industrial wastes such as waste slurry, lignin, iron(III) hydroxide, and red mud, have been explored for their technical feasibility to remove heavy metals from contaminated water [53]. Low rank coal, such as lignite, is capable of having ion exchange with heavy metals due to its carboxylic acid and phenolic hydroxyl functional groups.

Industrial waste is also one of the potentially low-cost adsorbent for the removal of heavy metals from wastewaters. It requires little processing to increase its adsorptive capacity. Generally industrial wastes are generated as by-products. Since these materials are locally available in large quantities, they are inexpensive. Various types of industrial wastes such as fly ash, blast furnace sludge, waste slurry, lignin, iron (III) hydroxide, and red mud, have been explored for their technical feasibility to remove toxic heavy metals from contaminated water. Other industrial wastes, coffee husks, Areca waste, tea factory waste, sugar beet pulp, waste pomace of olive oil factory waste, battery industry waste, waste biogas residual slurry, sea nodule residue, and grape stalk wastes have been utilized as low-cost adsorbents for the removal of toxic heavy metals from wastewater [54].

Agricultural materials particularly those containing cellulose shows potential metal biosorption capacity. The basic components of the agricultural waste materials biomass include hemicellulose, lignin, extractives, lipids, proteins, simple sugars, water hydrocarbons, starch containing variety of functional groups that facilitates metal complexation which helps for the sequestering of heavy metals [55-58]. Plant wastes are inexpensive as they have no or very low economic value. Most of the adsorption studies have been focused on untreated plant wastes such as papaya wood [59], maize leaf [60], teak leaf powder [61], lalang (*Imperata Cylindrica*) leaf powder [62], rubber (*Heveabra Siliensis*) leaf powder [63, 64], *Coriandrum Sativum* [65], peanut hull pellets [66], sago waste[67], saltbush (*Atriplexcanescens*) leaves [68, 69], tree fern [70-72], rice husk ash and neem bark [73], grape stalk wastes [74], etc. Some of the advantages of using plant wastes for wastewater treatment include simple technique, requires little processing, good adsorption capacity, selective adsorption of heavy metal ions, low cost, easy availability and easy regeneration.

However, the application of untreated plant wastes as adsorbents can also bring several problems such as low adsorption capacity, high chemical oxygen demand (COD) and biological chemical demand (BOD) as well as total organic carbon (TOC) due to release of soluble organic compounds contained in the plant materials [75, 76]. The increase of the COD, BOD and TOC can cause depletion of oxygen content in water and can threaten the aquatic life. Therefore, plant wastes need to be modified or treated before being applied for the decontamination of heavy metals.

Wan Ngah and Hanafiah[31] in their review have compiled an extensive list of adsorbents obtained from plant wastes and their methods of modification are discussed. A comparison of adsorption efficiency between chemically modified and unmodified adsorbents is also reported. The most common chemicals used for treatment of plant wastes are acids and bases. Chemically modified plant wastes vary greatly in their ability to adsorb heavy metal ions from solution. Chemical modification in general improved the adsorption capacity of adsorbents probably due to higher number of active binding sites after modification, better ion-exchange properties and formation of new functional groups that favors metal uptake.

Although chemically modified plant wastes can enhance the adsorption of heavy metal ions, the cost of chemicals used and methods of modification also have to be taken into consideration in order to produce ‘low-cost’ adsorbents. Many reviews are available in literature focusing on the low cost adsorbent from the natural resources [31, 77-89].Table1.3 shown below includes the agro-based adsorbents studied for Cu, Cd, Zn, Hg, Cr and U in the last five years and which have not been included in reviews yet.

Table 1.3. Agro-based adsorbents with their maximum adsorption capacities

Adsorbent	q_{max} (mg g^{-1})						References
	Cu	Cd	Zn	Hg	Cr	U	
Sawdust (Poplar tree)	12.7	-	15.8	-	-	-	[90]
Cassava tuber bark waste	90.9	26.3	83.3	-	-	-	[91]
Jute fibres	8.40	-	8.02	-	-	-	[92]
Azollafiliculoides (aquatic fern)	62	86	48	-	-	-	[93]
Carrot residues	32.74	-	29.61	-	45.09	-	[94]
Sugarcane bagasse	313	139	-	-	23	-	[95, 96]
Sugarbeet pulp	0.15	-	0.18	-	-	-	[97]
Rice husk	2.48	8.82	-	-	-	-	[98]
Modified rice husk	9.36	11.03	-	-	-	-	

Adsorbent	q_{max} (mg g^{-1})						References
	Cu	Cd	Zn	Hg	Cr	U	
Caulerpalentillifera	42.37	4.69	2.66	-	-	-	[99]
Dried non-living biomass (NB) of different *Pseudomonas* strains	-	-	19.6	84.25	-	-	[100]
Lignin	22.87	25.40	11.25	-	-	-	[101]
Lignocellulosic substrate (Wheat bran extract)	10.61	-	16.02	-	-	-	[102]
Neem oil cake	0.157 mmol/g	0.133 mmol/g	-	-	-	-	[103]
Olive pomace	0.480 mmol/g	0.100 mmol/g	-	-	-	-	[104]
Rice husk	0.2175 mmol/g	-	-	0.2114 mmol/g	-	-	[105]
Wheat bran	0.199 mmol/g	-	-	0.239 mmol/g	-	-	[106]
rice husk	-	3.04	14.30	9.32	-	-	[107-109]
Sulfuric acid treated rice husk (wet sorbent)	-	41.15	19.38	384.62	-	-	[110, 111]
Tea industry waste	-	0.45	0.59	-	-	-	[112]
Maize husk (unmodified)	-	4×10^{-6}	0.49	-	-	-	[113]
Maize husk (EDTA modified)	-	114.1	614.11	-	-	-	
Magnetically modified brewer's yeast	-	-	-	30.40	-	-	[114]
Sugarcane bagasse	-	38.03	31.11	-	-	-	[115]
Bacillus jeotgali	-	57.90	222.2	-	-	-	[116]
Dried non-living biomass (NB) of different *Pseudomonas* strains	-	-	19.06	84.25	-	-	[117]
*Cupriavidustaiwanensis*TJ208	19	19.6	-	-	-	-	[118]
Mimosa pudica inoculated with TJ208	25.4	42.9	-	-	-	-	
*Mimosa pudica*without inoculation	22.7	25.30	-	-	-	-	
P. chrysosporium	26.5	27.8	-	-	-	-	[119]
Trametesversicolor	116.9	109.2	-	-	-	-	[120]
Sawdust	8.07	-	17.09	-	-	-	[92]
Almond shell	-	-	-	-	0.580 mmol/g	-	[121]
AzadirachtaIndica (Neem) leaf Powder	-	1.404 mmol/g	-	-	1.211 mmol/g	-	[122, 123]
Green coconut shell powder	-	2.541 mmol/g	-	-	1.412 mmol/g	-	[124]
Waste slurry	20.97	15.73	-	560	640	-	[125, 126]
Gelidium	-	-	13	-	18	-	[127]
Algal waste	-	-	7.1	-	11.8	-	

Adsorbent	$q_{max\ (mg\ g^{-1})}$						References
	Cu	Cd	Zn	Hg	Cr	U	
Carboxymethyl water-insoluble dietary fiber	-	623.5 µmol/g	-	-	615.6 µmol/g	-	[128]
Terminaliaarjuna nuts Coirpith	39.7	-	-	154	28.43	-	[129]
Blast furnace sludge	16.1	-	10.15	4.3	9.55	-	
Blend coffee	2.0	2.0	-	-	-	-	[130]
Mango peel	46.09	68.92	28.21	-	-	-	[131, 132]
Red mud	19.72	10.57	12.59	-	-	-	[133]
Biogas residual slurry	-	-	-	-	7.8	-	[134]
Waste slurry	20.97	15.73	-	560	640	-	[135, 136]
ACC	-	3.75	2	65	-	-	[137]
As-received ACF	9	146	-	-	40	-	[138, 139]
Chlorella vulgaris	1.290	0.609–0.770	-	-	0.356–0.492	-	[140-142]
Risk husk ash	-	25.27	26.10	46.14	26.31	-	[143-145]
Coir pith	39.7	93.4	-	-	138.04–317.65	-	[146-148]
Chitosan coated ACSC	-	-	60.41	-	-	-	[149]
PGCP-COOH	-	-	-	4.99–31.15	-	-	[150]
TARH	29	-	-	-	-	-	[151]
RHC	-	-	-	48.31	-	-	[152]
Activated carbon	-	-	-	-	-	28.49	[153]
CR-azole	-	-	-	-	-	1.60 mol/g	[154]
CR-amine	-	-	-	-	-	1.90mol/g	
Aspergillusniger	5	-	-	-	-	29	[155]
Penicilliumchrysogenum	9	56	6.5	-	-	70	
Rhizopusnigricans	-	19	14	-	47	-	
R. arrhizus	9.5	27	14	-	36	220	
Date pits	-	-	-	-	-	10	[156]
Catenellarepens-red alga	-	-	-	-	-	303.0	[157]
Cross-linked chitosan	-	-	-	-	-	72.46	[158]
ACs-benzoylthiourea-anchored anchored	-	-	-	-	-	113.76	[159]
chitosan/clinoptilolite composite	-	-	-	-	-	562.58	[160]
Chitosan	-	-	-	-	-	482.66	
Chitosan/cotton fibers	24.78	15.74	-	104.31	-	-	[161]
Chitosan/cellulose	26.50	-	19.81	-	13.05	-	
Penicilliumcitrinum	-	-	-	-	-	274.73	[162]
Bi-functionalized biocomposite	-	-	-	-	-	43.2	[163]

Although the amount of available literature data on the use of low-cost adsorbents in water and wastewater treatment is increasing at a tremendous pace, some important issues need to be considered during the consideration of a material as a potential low cost adsorbent:

(1) Selection and identification of an appropriate low-cost adsorbent is one of the key issues to achieve the maximum removal/adsorption of specific type of pollutant depending upon the adsorbent–adsorbate characteristics.

(2) The conditions for the production of low-cost adsorbents after surface modification for higher uptake of pollutants need to be optimized.

(3) Low production cost with higher removal efficiency of adsorbents would make the processeconomical and efficient.

(4) Mechanistic studies need to be performed in detail to propose a correct binding mechanism of aquatic pollutants with low cost adsorbents.

(5) Regeneration studies need to be performed in detail with the pollutants-laden adsorbent to recover the adsorbate as well as adsorbent. It will enhance the economic feasibility of theprocess.

(6) The potential of low-cost adsorbents under multi-component pollutants needs to be assessed. This would make a significant impact on the potential commercial application of low-costadsorbents to industrial systems.

(7) The effectiveness of the treatment depends not only on the properties of the adsorbent and adsorbate, but also on various environmental conditions and variables used for the adsorptionprocess, e.g. pH, ionic strength, temperature, existence of competing organic or inorganic compounds in solution, initial adsorbate/adsorbent concentration, contact time and speedof rotation, particle size of adsorbent, etc. These parameters should also be taken into account while examining the potential of low-cost adsorbents.

(8) The development in the field of adsorption process using low cost adsorbents essentially requires further investigation of testing these materials with real industrial effluents.

(9) Because various heavy metal ions are often present in industrial effluents or other water resources, there issignificant research and practical interest to develop the methods that can effectively remove the heavy metals and, at the same time, recover them in their individual pure form for potential reuse to avoid the second pollution problems of these heavy metals (in a more concentrated form) after they are removed from the water to a certain regulated level. A possible solution to achieve this target is to use adsorbents modified with selective ligands or ion imprinting polymers that have selectivity toward the metals to be separated and recovered.

(10) Last but not the least, environmentally safe disposal of pollutants-laden adsorbents is another important topic of concern which should not be overlooked.

If it is possible to develop such adsorbents having all the above-mentioned characteristics, then these adsorbents may offer significant advantages over currently available expensive commercially activated carbons and, in addition contribute to an overall waste minimization strategy.

A detailed critical investigation into literature and the above deliberations paved the way for us to explore the potential of palm shell (*Borassus Flabellifer*) as an adsorbent. *Borassusflabellifer* is a robust tree and can live 100 years or more and reach a height of 30 m, with a canopy of leaves several dozen fronds spreading 3 meters across. The large trunk resembles that of the coconut tree and is ringed with leaf scars. There are approximately 8.59 crores of palm trees all over world which produces around 80 pieces of fruits per tree per year [164].

Trees are economically useful, and widely cultivated in tropical regions. The *Borassus flabellifer* has long been one of the most important trees of India, where it has number of uses. The leaves are used for thatching, mats, baskets, fans, hats, umbrellas, and as writing material. The stalks are used to make fences and to make a strong, wiry fiber suitable for cordage and brushes. The black timber is hard, heavy, and durable and is highly valued for construction, such as for wharf pilings.

The tree also yields many types of food. The young plants are cooked as a vegetable or roasted and pounded to make meal. The fruits are eaten roasted or raw, and the young, jellylike seeds are also eaten. A sugary sap, called toddy, can be obtained from the young inflorescence, either male or female ones. The toddy is fermented to make a beverage called arrack, or it is concentrated to a crude sugar called jaggery/palm sugar. The roots can be dried to form Odiyal, a hard chewable snack. In addition, the tree sap is taken as a laxative, and medicinal values have been ascribed to other parts of the plant [164].

The recently germinated seeds form fleshy sprouts below the surface which can be boiled and eaten as a fibrous, nutritious food. The germinated seed's hard shell is also cut open to take out the crunchy kernel which tastes like awater chestnut but is sweeter. The ripe fibrous outer layer of the fruits is edible after boiling or roasting. When the fruit is tender, the kernel inside the hard shell is an edible jelly that is refreshing and rich in minerals. When the crown of the tree from which the leaves sprout is cut we get an edible cake [164].

Only the outer hard shell of the kernel has not been used and usually thrown as waste or used as fuel.We thus felt that we could study the potential of shell of kernel of *Borassus flabellifer* as adsorbent and as precursor for the development of a range of adsorbents which may provide an alternative for the commercially available expensive adsorbents.

Furthemore, chitosan is another natural material which can form chelates with a number of metals, can be derivatized because of its amino groups and can also be cross-linked to increase its rigidity.Based on the above deliberations our broad objectives were:

- To prepare low cost adsorbents using palm shell as precursor
- To evaluate the potential of these adsorbents for the removal of Hg^{2+}, Cu^{2+}, Cd^{2+}, Zn^{2+}, Cr^{6+} and U^{6+}
- Application of the materials to synthetic multi-component mixturesand effluents
- To explore the possibility of preparing adsorbents selective for mercury using barbituric acid and chitosan
- Make an attempt to prepare ion imprinting polymer for uranium

Literature Cited.

1. H. Babich, M.A. Devanas, G. Stotzky**.** *Environmental Research* **1985**, *37*, 253.
2. A. Pagliuca, G. J. Mufti. Lead Poisoning: an age-old problem. *British Medical Journal***1990**, *300*, 830.
3. A.L. Rowbotham, L.S. Levy, L.K. Shuker. *Journal of Toxicology and Environmental Health B 3*, **2000**, 145.
4. IARC. Monograph on the Evaluation of Carcinogenic Risk to Humans, Chromium, Nickel and Welding. International Agency for Research on Cancer, Lyon, **1990**, *49*.
5. L.I. Friberg. *American Industrial Hygiene Association Journal***1985**, *46*, 633.
6. B. Weiss, P.J. Landrigan, *Environmental Health Perspectives* **2000**, *108*, 373.
7. T. Theophanides, J. Anastassopoulou. *Critical reviews. Oncology/Haematology***2002**, *42*, 57.
8. G. Nordberg, B. Fowler, M.Nordberg, L.F.Friberg, **2007**. Handbook on the Toxicity of Metals, third ed. Elsevier, Amsterdam, 743.
9. H. Vandenhovea, A. Cuypersb, M.V. Heesa, G. Koppenc, J. Wannijna. *Plant Physiol. Bioch***2006**, *44*, 795.
10. M. Anke. *Chem.Erde-Geochem***2009**, *69*, 75.
11. E.S. Craft. *J. Toxicol. Environ. Health B***2004**, *7*, 297.
12. N.D. Priest. *Lancet***2001**, *357*, 244.
13. S.B. Xie. *J. Environ. Radioact***2008**,*99*, 126.
14. C. Gok, S. Aytas, *J. Hazard. Mater***2009**, *168*, 369.
15. R.A. Corbitt. Standard hand book of environmental engineering2nd ed. McGraw Hill; **1999**.
16. S. Tunali, A. Cabuk, T. *Akar. ChemEngJ***2006**, *115*, 203.
17. http://www.gemswater.org.
18. http://www.lenntech.com.
19. General standards for discharge of environment pollutants: effluent. Gazette Notification of MoEF; May **1993**.
20. Indian standard drinking water — specification (First Revision) IS-10500. New Delhi, India: BIS; **1991**.

21. T.A. Kurniawan, G.Y.S. Chan, W.H. Lo, S. Babel. *Chemical Engineering Journal***2006**, *118*, 83.
22. Y.H. Wang, S.H. Lin, R.S. Juang. *Journal of Hazardous Materials***2003**, *102*, 291.
23. A. Shukla, Y.H. Zhang, P. Dubey, J.L.Margrave, S.S. Shukla. *Journal of Hazardous Materials***2002**, *95*, 137.
24. L.K. Wang, N.K. Hung, N.K. Shammas. Physiochemical Treatment Processes, Human Press, New Jersey, **2004,** ***3***, 103.
25. M. Ahmaruzzaman.*Energy & Fuels* **2009**, *23,* 1494.
26. S. Kasaoka, Y. Sakata, E.Tanaka, R. Naitoh. *International Chemical Engineering***1989**, *29*, 101.
27. J.J. Yu, S.Y. Chou. *Chemosphere***2000**, *41*, 371.
28. A. Bailey, P. Arthur, P. Maggs. In. *British Patent***1971**, 1301101.
29. A.C. Pastor, F. Rodrıguez-Reinoso, H. Marsh, M.A. Martinez. *Carbon***1999**, *37*, 1275.
30. S.E. Bailey, T.J. Olin, R.M. Bricka, D.D. Adrian. *Water Res*. **1999**, *33*, 2469.
31. W.S. Wan Ngah, M.A.K.M. Hanafiah. *Bioresource Technology***2008**, *99*, 3935.
32. A. Dabrowski. *Advances in Colloid and Interface Science***2001**, *93*, 135.
33. C. Moreno-Castilla, J. Rivera-Utrilla. *Materials Research Society Bulletin***2001**, *26*, 890.
34. A. Ahmadpour, D.D. Do. *Carbon***1996**, *34*, 471.
35. M. Ahmedna, W.E. Marshall, R.M. Rao. *Bioresource Technology***2000**, *71*, 113.
36. N.F. Gao, S. Kume, K. Watari. *Materials Science and Engineering: A* **2005**, *399*, 216.
37. J. Hayashi, N. Yamamoto, T. Horikawa, K. Muroyama, V.G. Gomes. *Journalof Colloid and Interface Science***2005**, *281*, 437.
38. V.M. Gunko, R. Leboda, J. Skubiszewska-Zieba, B. Charmas, P. Oleszczuk. *Carbon***2005**, *43*, 1143.
39. K. Okada, N. Yamamoto, Y. Kameshima, A. Yasumori. *Journal of Colloid and Interface Science***2003**, *262*, 179.
40. K. Okada, N. Yamamoto, Y. Kameshima, A. Yasumori. *Journal of Colloid and Interface Science***2003**, *262*, 194.
41. F.C.Wu, R.L. Tseng. *Journal of Colloid and Interface Science***2006**, *294*, 21.
42. N. Tancredi, N. Medero, F. Moller, J. Pıriz, C. Plada, T. Cordero. *Journal of Colloid and Interface Science***2004**, *279*, 357.

43. C. Moreno-Castilla. *Carbon***2004**, *42*, 83.
44. Li, Quinlivan, P.A., Knappe, D.R.U. *Carbon***2002**, *40*, 2085.
45. L.R. Radovic, C. Moreno-Castilla, J. Rivera-Utrilla. Carbon materials as adsorbents in aqueous solutions. Marcel Dekker, New York, **2000**.
46. Y. El-Sayed, T.J. Bandosz. *Journal of Colloid and Interface Science***2004**, *273*, 64.
47. J. Ellis, W. Korth. *Water Res***1993**, *27*, 535.
48. B. Okolo, C. Park, M.A. Keane. *J. Colloid Interface Sci***2000**, 226, 308.
49. A. Metes, D. Kovacevic, D. Vujevic, S. Papic. *Water Res***2004**, 38, 3373.
50. T. Motsi, N.A. Rowson, M.J.H. Simmons. *Int. J. Miner. Process* **2009**, 92, 42.
51. S. Wang, Y. Peng. *Chem. Eng. J.*, in press, **doi:10.1016/j.cej.2009.10.029.**
52. A. Bhatnagar, M. Sillanpaa. *Chemical Engineering Journal***2010**, *157*, 277.
53. S. Babel, T.A. Kurniawan. *Journal of Hazardous Materials***2003**, *B97*, 219.
54. M. Ahmaruzzaman. *Advances in Colloid and Interface Science***2011**,*166*, 36.
55. V.M. Nurchia, G.G. Crisponi, I. Villaescusa. *Coordination Chemistry Reviews***2010**, *254*, 2181.
56. A. Hashem, E.S. Abdel-Halim, K.F. El-Tahlawy, A. Hebeish. *Adsorp. Sci. Technol***2005**, *23*, 367.
57. A. Hashem, R.A. Akasha, A. Ghith, D.A. Hussein. *Energy Edu. Sci. Technol***2005**, *19*, 69.
58. D. Sud, G. Mahajan, M.P. Kaur. *Bioresource Technology***2008**, *99*, 6017.
59. A. Saeed, M.W. Akhter, M. Iqbal. *Sep. Purif. Technol*. **2005**, *45*, 25.
60. N.A.A. Babarinde, J. O. Babalola, R. A. Sanni. *Int. J. Phys. Sci***2006**, *1*, 23.
61. P. King, P. Srivinas, Y. Prasanna Kumar, V.S.R.K. Prasad. *J. Hazard. Mater. B***2006**, *136*, 560.
62. M.A.K. Hanafiah, W.S.W. Ngah, H. Zakaria, S.C. Ibrahim. *J. Biol. Sci***2007**, *7*, 222.
63. M.A.K.M. Hanafiah, W.S.W. Ngah, S.C. Ibrahim, H. Zakaria, W.A.H.W. Ilias. *J. Appl. Sci***2006**, *6*, 2762.
64. M.A.K.H. Hanafiah, S. Shafiei, M.K. Harun, M.Z.A. Yahya. *Mater. Sci. Forum***2006**, *517*, 217.
65. D. Karunasagar, M.V. Balarama Krishna, S.V. Rao, J. Arunachalam. *J. Hazard. Mater. B***2005**, *118*, 133.
66. P.D. Johnson, M.A. Watson, J. Brown, I.A. Jefcoat. *Waste Manage***2002**, *22*, 471.

67. S.Y. Quek, D.A.J. Wase, C.F. Forster. *Water SA***1998**, *24*, 251.
68. M.F. Sawalha, J.R. Peralta-Videa, J. Romero-Gonza´lez, M. Duarte-Gardea, J.L. Gardea-Torresdey. *J. Chem. Thermodyn***2007**, *39*, 488.
69. M.F. Sawalha, J.R. Peralta-Videa, J. Romero-Gonzalez, J.L. Gardea-Torresdey. *J. Colloid Interface Sci***2007**, *300*, 100.
70. Y.S. Ho, C.C. Wang. *Process Biochem***2004**, *39*, 759.
71. Y.S. Ho, W.T. Chiu, C.S. Hsu, C.T. Huang. *Hydrometallurgy***2004**, *73*, 55.
72. Y.S. Ho. *Water Res***2003**, *37*, 2323.
73. A.K. Bhattacharya, S.N. Mandal, S.K. Das. *Chem. Eng. J***2006**, *123*, 43.
74. I. Villaescusa, N. Fiol, M. Martınez, N. Miralles, J. Pocj, J.Serarols. *Water Res* **2004**, *38*, 992.
75. I. Gaballah, D. Goy, E. Allain, G. Kilbertus, J. Thauront. *Met. Metall. Trans. B***1997**, *28*, 13.
76. A. Nakajima, T. Sakaguchi. *Biomass***1990**, *21*, 55.
77. J. Febrianto, A. N. Kosasih, J. Sunarso, Y.H. Ju, N. Indraswati, S. Ismadji. *J. Hazard. Mat.***2009**, *162*, 616.
78. A. Bhatnagar, V.J.P. Vilar, C.M.S. Botelho, R.A.R. Boaventura. *Advances in Colloid and Interface Science*. **2010**. doi:10.1016/j.cis.2010.06.011.
79. S. O. Lesmanaa, N. Febrianaa, F. E. Soetaredjoa, J. Sunarsob, S. Ismadjia. *Biochemical Engineering Journal* **2009**, *44*, 19.
80. Y. Chen, Y. Zhu, Z. Wang, Y. Li, L. Wang, L. Ding, X. Gao, Y. Ma, Y. Guo. *Advances in Colloid and Interface Science.* doi:10.1016/j.cis.2011.01.006.
81. W.S. Wan Ngah, L.C. Teong, M.A.K.M. Hanafiah. *Carbohydrate Polymers***2011**, *83*, 1446.
82. E.M. Saada, R.A. Mansourb, A. El-Asmyb, M.S. El-Shahawic. *Talanta***2008**, *76*, 1041.
83. S. S. Ahluwalia, D. Goyal. *Bioresource Technology***2007**, *98*, 2243.
84. A. A. Atia. *Hydrometallurgy***2005**, *80*, 13.
85. C. Kütahyalı, M. Eral. *Separation and Purification Technology***2004**, *40*, 109.
86. K.K. Krishnani, X. Meng, C. Christodoulatos, V.M. Boddu. *Journal of Hazardous Materials* **2008**, *153*, 1222.
87. P. Miretzky, A. F. Cirelli. *Journal of Hazardous Materials***2010**, *180*, 1.

88. D. W.O’Connell, C. Birkinshaw, T. F. O’Dwyer. *Bioresource Technology* **2008**, *99*, 6709.
89. K.Y. Foo, B.H. Hameed. *Adv. Colloids. Interface Sci.* **2009**, *152*, 39.
90. M. Sciban, M. Klasnja, S B. Krbic. *J. Hazard. Mater. B* **2006**, *136*, 266.
91. M. Horsfall Jr., A.A. Abia, A.I. Spiff. *Bioresour. Technol* **2006**, *97*, 283.
92. S.R. Shukla, R.S. Pai. *Bioresour. Technol* **2005**, *96*, 1430.
93. M.T. Ganji, M. Khosravi, R. Rakhsaee. *Int. J. Environ. Sci. Technol* **2005**, *1*, 265.
94. B. Nasernejad, T.E. Zadeh, B.B. Pour, M.E. Bygi, A. Zamani. *Process Biochem* **2005**, *40*, 1319.
95. O.K. Junior, L.V.A. Gurgel, J.C.P. de Melo, V.R. Botaro, T.M.S. Melo, R.P. de Freitas Gil, L.F. Gil. *Bioresour. Technol* **2006**, *98*, 1291.
96. K.K. Krishnani, X. Meng, L. Dupont, *J. Environ. Sci. Health: A* **2009**, *44*, 688.
97. E. Pehlivan, S. Cetin, B.H. Yanik. *J. Hazard. Mater. B* **2006**, *135*, 193.
98. S.A. Ong, C.E. Seng, P.L. Lim. *J. Environ. Agric. Food Chem* **2007**, *6*, 1764.
99. P. Pasavant, R. Apiratikul, V. Sungkhum, P. Suthiparinyanont, S.Wattanachira, T.F. Marhaba. *Bioresource Technology* **2006**, *97*, 2321.
100. M.A. Shaker. *American Journal of Applied Sciences* **2007**, *4*, 605.
101. X.Y. Guo, A.Z. Zhang, X.Q. Shan. *Journal of Hazardous Material* **2008**, *151*, 134.
102. L. Dupont, J. Bounanda, J. Dumonceau, M. Aplincourt. *Environment Chemistry Letters* **2005**, *2*, 165.
103. R.A.K. Rao, N.A. Khan. *Sep. Purif. Technol* **2007**, *57* 394.
104. H. Gao, Y.G. Liu, G.M. Zeng,W.H. Xu, T. Li,W.B. Xia. *J. Hazard. Mater* **2008**, *150*, 446.
105. S. Mohan, G. Sreelakshmi. *J. Hazard. Mater* **2008**,*153*, 75.
106. D. Dupont, J. Bouanda, J. Dumonceau, M. Aplincourt. *Environ. Chem. Lett* **2005**, *2*, 165.
107. Q. Feng, Q. Lin, F. Gong, S Sugita, M. Shoya. *J Colloid InterfSci* **2004**, *274*, 1.
108. A.K. Bhattacharya, S.N. Mandal, S.K. Das. *ChemEng J* **2006**, *123*, 43.
109. V.C. Srivastava, I.D. Mall, I.M. Mishra. *ChemEng Process* **2009**, *48*, 370.
110. E.I. EI-Shafey. *J Hazard Mater* **2010**, *175*, 319
111. E.I. El-Shafey. J *Hazard Mater* **2007**, *147*, 546.

112. S. Cay, A. Uyanik, A. Ozasik. *Separation and Purification Technology* **2004**, *38*, 273.

113. J.C. Igwe, A.A. Abia. *Electronic Journal of Biotechnology* **2007**, *10*, 536.

114. H. Yavuz, A. Denizli, H. Gungunes, M. Safarikova, I. Safarik. *Separation and Purification Technology* **2006**, *52*, 253.

115. D. Mohan, K.P. Singh. *Water Res*. **2002**, *36*, 2304.

116. C. Green-Ruiz, V. Rodriguez-Tirado, B. Gomez-Gil. *Bioresource Technology* **2008**, *99*, 3864.

117. M.A. Shaker. *American Journal of Applied Sciences* **2007**, *4*, 605.

118. W. Chen, C. Wu, E.K. James, J. Chang. *Journal of Hazardous Materials* **2008**, *151*, 364.

119. R. Say, A. Denizli, M.Y. Arica. *Bioresource Technology* **2001**, *76*, 67.

120. G. Bayramoglu, S. Bektas, M.Y. Arica. *Journal of Hazardous Materials*. **2003**, *101*, 285.

121. E. Pehlivan, T. Altun. *J. Hazard. Mater*. **2008**,*155*, 378.

122. A. Sharma, K.G. Bhattacharyya. *J. Hazard. Mater. B.* **2005**,*125*, 102.

123. B.V. Babu, S. Gupta. *Adsorption* **2008**, *14*, 85.

124. G.H. Pino, L.M.S. de Mesquita, M.L. Torem. *Sep. Sci. Technol* **2006**, *41*, 3141.

125. S.K. Srivastava, R. Tyagi, N. Pant, *Water Res* **1989**, *23*, 1161.

126. S.M. Lee, A.P. Davis, *Water Res* **2001**, *35*, 534.

127. V.J.P. Vilar, C.M.S. Botelho, R.A.R. Boaventura. *Journal of Hazardous Materials* **2007**, *149*, 643.

128. S. Ou, K. Gao, Y. Li. *J. Agric. Food Chem* **1999**, *47*, 4714.

129. A. Lopez-Delgado, C. Perez, F.A. Lopez. *Water Res* **1998**, *32*, 989.

130. M. Minamisawa, S. Nakajima, H. Minamisawa, S. Yoshida, N. Takai. Removal of copper (II) and cadmium(II) from water using roasted coffee beans, in: Eric Lichtfouse, Jan Schwarzbauer, Didier Robert (Eds.), Environmental Chemistry Green Chemistry and Pollutants in Ecosystems, Springer, Berlin Heidelberg, **2005**, 259.

131. M. Iqbal, A. Saeed, S.I. Zafar. *J. Hazard. Mater* **2009**, *164*, 161.

132. M. Iqbal, A. Saeed, I. Kalim. *Sep. Sci.Technol* **2009**, *44*, 3770.

133. E. López, B. Soto, M. Arias, A. Nunez, D. Rubinos, M.T. Barral. *Water Res* **1998**, *32*, 1314.

134. C. Namasivayam, R.T. Yamuna, *Water Air Soil Pollut***1999**, *113*, 371.

135. S.K. Srivastava, R. Tyagi, N. Pant, *Water Res***1989**, *23*, 1161.

136. S.M. Lee, A.P. Davis, *Water Res***2001**, *35*, 534.

137. B.M. Babi, S.K. Milonji, M.J. Plovina, S. Upi, B.V. Kaludjerovi, *Carbon***2002**, *40*, 1109.

138. J.R. Rangel-Mendez, M. Streat, *Water Res***2002**, *36*, 1244.

139. J.-W. Shim, S.-J. Park, S.-K. Ryu, *Carbon***2001**, *39*, 1635.

140. Z. Aksu, U. Acikel. *Biochem. Eng. J* **2000**, *4*, 229.

141. F.A.A. Al-Rub, M.H. El-Naas, I. Ashour, M. Al-Marzouqi, *Process Biochem* **2006**, *41*, 457.

142. Z. Aksu, G. Dönmez, *Process Biochem***2006**, *41*, 860.

143. V.C. Srivastava, I. D. Mall, I.M. Mishra. *ChemEng J***2007**, *132*, 267.

144. A.K. Bhattacharya, T.K. Naiya, S.N. Mandal, S.K. Das. *ChemEng J* **2008**, *137*, 529.

145. D. P. Tiwari, D. K. Singh, D.N. Saksena. *J Environ Eng***1995**, *121*, 479.

146. P. Suksabye, P. Thiravetyan, W. Nakbanpote, S. Chayabutra. *J Hazard Mater* **2007,** *141*, 637.

147. K. Kadirvelu, C.Namasivayam. *Adv Environ Res***2003**, *7*, 471.

148. C. Namasivayam, K. Kadirvelu. *Chemosphere***1997**, *34*, 377.

149. O.S. Amuda, A.A. Giwa, I.A. Bello. *BiochemEng J***2007**, *36*, 174

150. T.S. Anirudhan, L. Divya, M. Ramachandran. *J Hazard Mater***2008**, *157*, 620

151. K.K. Wong, C.K. Lee, K.S. Low, M.J. Haron. *Chemosphere***2003**, *50*, 23.

152. M. Bansal, D. Singh, V.K. Garg. *J Hazard Mater***2009**, *171*, 83.

153. C. Kutahyali, M. Eral. *Separation and Purification Technology***2004**, *40*, 109.

154. A. A. Asem. *Hydrometallurgy***2005**, *80*, 13.

155. S. S. Ahluwalia, D. Goyal. *Bioresource Technology***2007**, *98*, 2243.

156. E.M. Saad, R.A. Mansour, A. El-Asmy, M.S. El-Shahawi. *Talanta***2008**, *76*, 1041.

157. S. VikasBhat, J.S. Melo, B.B. Chaugule , S.F. D'Souza. *Journal of Hazardous Materials***2008**, *158*, 628.

158. G. Wang, J. Liu, X. Wang, Z. Xie, N. Deng; *Journal of Hazardous Materials* **2009**, *168* 1053.

159. Y. Zhao, C. Liu, M. Feng, Z. Chen, S. Li, G. Tian, L. Wang, J. Huang, S. Li. *Journal of Hazardous Materials***2010**, 176, 119.

160. M. Humelnicu, V. Dinu, E. Dragan. *Journal of Hazardous Materials***2011**, *185*, 447.

161. W.S. Wan Ngah, L.C. Teong, M.A.K.M. Hanafiah; *Carbohydrate Polymers***2011**, *83*, 1446.

162. C. Pang, Y.H. Liu, X.H. Cao, M. Li, G.L. Huang, R. Hu, C.X. Wang, X.F. Ya. Liu. *Chemical Engineering Journal***2011**, *170*, 1.

163. S. Aytas, D.A. Turkozu, C. Gok. *Desalination,* in press doi:10.1016/j.desal.2011.07.023.

164. Linnaeus, Species Plantarum 1187. 1753. Type:*B. flabellifer*.

165. http://en.wikipedia.org/wiki/Borassus.

Chapter 2

Preparation and Characterization of modified forms of Palm Shell Powder

Outline:

2.1. Introduction

Activated carbon has undoubtedly been the most popular and widely used adsorbent in wastewater treatment throughout the world.Activated carbon is well known as an efficient adsorbent because of its porosity and large surface area. It has thus been widely used in the sorption of gases and chemical species from aqueous solution. Precursors to activated carbons are either of botanical origin (e.g. wood, coconut shells and nut shells) or of degraded and coalified plant matter (e.g. peat, lignite and all ranks of coal). Agricultural by-products are considered as very important feedstock as they are renewable and low-cost materials [1, 2].Agricultural materials particularly those containing cellulose shows potential sorption capacity for various pollutants. The basic components of the agricultural waste materials include hemicellulose, lignin, lipids, proteins, simple sugars, water, hydrocarbons, and starch, containing variety of functional groups.

Agricultural waste materials being economic and eco-friendly due to their unique chemical composition, availability in abundance, renewable nature and low cost are viable option for water and wastewater remediation. Agricultural waste is a rich source for activated carbon production due to its low ash content and reasonable hardness [3]. Therefore, conversion of agricultural wastes into low-cost adsorbents is a promising alternative to solve environmental problems and also to reduce the preparation costs.In the last several decades, various agricultural wastes have been explored as low-cost adsorbents[4].Cost effective activated carbons can be prepared from a variety of agricultural wastes. Some of the most commonly used precursors have been given in Table 1.3 of chapter 1 which include nutshells, fruit stones, rice bran rice husk , coconut shell and oil palm shell due to ecological and economic significance [5-8].

Heavy metal adsorption onto activated carbons generallydepends on their physical and chemical properties.Physical properties of carbons include their specific surfacearea, size, and porosity, whereas chemical properties aremainly determined by their surface functional groups,including carboxyls, carboxylic anhydrides, phenols, lactones, lactols, carbonyls, quinones, and quinone-like structures [9].Activation of carbon surfaces by physicochemical methods has been studied so that metal removal can be enhanced to meet increasingly stringent environmentalregulations[10, 11].

During the activation process, partial oxidation takesplace and a pore structure develops.Generally activated carbons are produced by carbonizing the raw material prior to activation. Carbonization is necessary to increase the carbon content and for the development of porous material. During carbonisation, pyrolytic decomposition of the precursor occurs [12] together with the concurrent elimination of many of the non-carbon elemental species (H, N, O and S). Low molecular weightvolatiles are first released, followed by light aromatics and finally, hydrogen gas [13], the resultant product being a fixed carbonaceous char [14]. The pores formed during carbonisation are filled with tarrypyrolysis residues and require activation in order to develop the internal surface of the char[15]. During the activation process, the spaces between the elementary crystallites are cleared by removal of less organizedloosely bound carbonaceous material. The resulting channels through the graphitic regions, the spaces between the elementary crystallites, together with fissures within and parallel to the graphite planes constitute the porous structure, with a large internal surface area[16]. Two types of activation, thermal/physical or chemical activation, impart a porous structure within a starting material of relatively low surface area[17].

Carbonization temperature affects the shapes of pores in the carbon. High temperature char samples have higher micro-pore volume [18,19]. To prepare mesoporous carbons activation to high burn off degrees, physical and chemical activation [20-25], catalytic activation in the presence of transition metals [26, 27] and template carbonization [28-31] have been used.

2.1.1. Activation Approaches.

Carbon surface can be activated to develop desirable physicochemical properties by adequate choice of activation procedures (Figure 2.1). It is even possible to prepare carbons with designated proportions of micro-, meso-, and macropores.

2.1.1.1. ***Chemical Approaches.*** Chemical activation employs a catalyst, metallic chlorides or acid impregnation into the raw material to influence the pyrolysis such that tar formation and volatilization are kept to minimum [32]. The most widely used chemical activants are $ZnCl_2$, H_3PO_4, H_2SO_4, KOH, K_2S,oxidizing agents and KCNS [33].The feedstock is impregnated with the catalyst, often as a near saturated solution, dried and then carbonised and activated in a single action although two separate temperatures are often used. Post activation treatment is required to remove residual catalyst which may be reclaimed for subsequent reuse. Chemical activation is performed at temperatures of between 400-800°C and used industrially for wood-based carbons.

The pore size distribution of the final product is largely a function of the degree of initial impregnation [34].

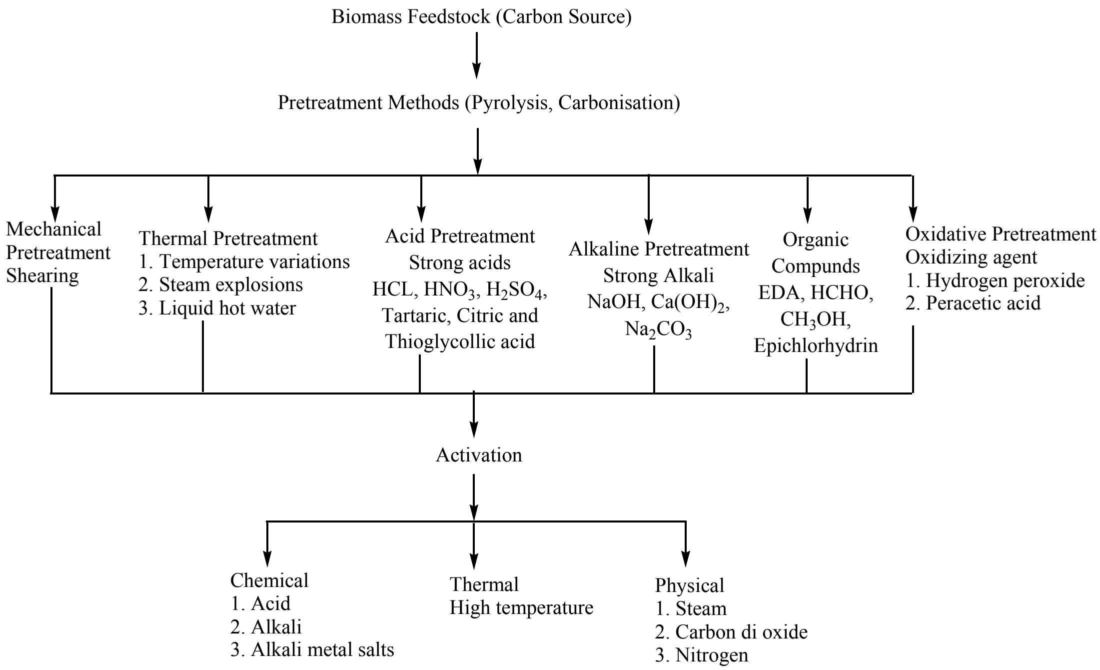

Figure 2.1. Methods of activation

Treatment by acids, bases, or oxidizing agents produces favorable chemical and physical properties for different applications (e.g. separation and catalysis). Gas phase oxidation mainly increases the content of hydroxyl and carbonyl surface groups, while liquid phase oxidation enhances especially that of carboxylic groups[35].

The modification by inorganic acids mainly changes the surface chemistry of the carbons and sometimes alters their specific surface area and porosity. For example, treatment of carbon by phosphoric acid can cause a high surface area and high degree of porosity[36-38]. Both strongly and weakly acidic oxygen functional groups can be introduced by acid modification[39].

Oxidation of activated carbons by H_2O_2increases hydroxide groups in the oxidized products when the solution pH is not controlled. However, when the solution pH is fixed at 2.5 or 11.5, the hydroxide groups decrease while other oxygen groups (e.g., carbonyl andcarboxyl) increase[40].

HNO_3 treatment increases the quantity of acidic surface functional groups[41]. Various surface oxygen groups and structures containing N-O bonds (nitro groups and nitrate complexes) are developed [42]. Mazet et al. showed a significant increase in the surface area, while Gomez-Serrano et al. observed a slight variation [43].

Carbons with well-developed meso- and microporous structure have been produced by $ZnCl_2$ incorporation. KOH activation successfully increased active carbon surface area and pore volume [44]. Ammonium salts, borates, calcium oxide, ferric and ferrous compounds, manganese dioxide, nickel salts, hydrochloricacid, nitric acid and sulfuric acid have also been used for activation.Polymers and chelating agents have been selected to modify activated carbons. The density of positive surface charges on the carbons can be increased after they are grafted by cationic polymers [45, 46]. The quantity of surface functional groups is also changed [47].

2.1.1.2. ***Physical Approaches.*** Carbons can be treated physically for improvement of their properties for different applications.It is reported that heat treatment in an inert atmosphere can selectively remove some functional groups.Partial gasification refers to the direct reaction between the carbonized char and an activant in its gaseous or vapor state. As in chemical activation, the principle objective is the removal of tarry amorphous carbon from the interstitial layers of the structure in order to develop the porosity and make accessible the internal surface area. Porosity develops with increased burn-off of disorganized carbon [48]. Steam, carbon dioxide and air are the most common activants, the kinetics and mechanisms of these reactions being well known for many years [49-52].

Surface carboxylic acid groups of carbons disappear after treatment in H2 at 723 K [39]. De la Puente et al. observed the removal of carboxylic acid groups at the temperature of 400-623 K [53].The elimination of stable ether groups was found at temperatures above 823 K. At higher temperatures, the concentrations of carboxylic acid groups decrease and, subsequently, ketone and quinone groups disappear [54]. With a further increase in the temperature, elimination of both the ether groups and the aliphatic structures occurs [55].

Menendez et al. modified an activated carbon by a microwave device under nitrogen flow [56]. Most acidic oxygen groups are removed from the carbon surface, resulting in a significant increase in the carbon pH. The basic differences between physical and chemical activationis the number of stages required for activation andthe activation temperature. Chemical activation occurs inone step while physical activation employs two steps, carbonizationand activation.

Physical activation temperatures (800–1000 ^{0}C) are higher than those of chemical activation (200–800 ^{0}C).

According to Steenberg's classification [57], acidic and basic activated carbons exist: Depending on the extent of the oxidizing reaction, two forms of activated carbons can be produced [58, 59].

(a) Carbon activated at 200–400 ^{0}C, called L carbons, generally develop acidic surface oxides and lower solution pH values.They adsorb bases, are hydrophilic, and exhibit a negative zeta potential.

(b) The carbons activated at 800–1000 ^{0}C, termed H carbons,develop basic surface oxides are hydrophobic and raise solution pH. They adsorb acids and exhibit a positive zeta potential. However, cooling H carbons in contact with air changes the zeta potential to a negative value due to the formation of acidic surface oxides.

The acidic groups on activated carbons adsorb metalions [60]. The L carbons are stronger solid acids than the H carbons and more efficiently adsorb metal ions. Garten *et al.* have suggested carboxyl, phenolic hydroxyl, carbonyl (quinone type), carboxylic acid, anhydrides, lactone, and cyclic peroxide as the predominant surface functional groups of L-carbons[61].

Surfacearea may not be a primary factor for adsorption onactivated carbon. High surface area does not necessarilymean high adsorption capacity [62]due to the followingfactors:

(a) Only the wetted surface adsorbs ions. The total surface areais seldom wetted.

(b) Sometimes the material to be adsorbed is too large to enterthe smallest pores where the bulk of the surface area mayexist.

(c) Surface area, pore volume and surface chemistry are notusually correlated with species adsorbed.

The adsorption of metal ions on carbon is more complexthan uptake of organic compounds because ionic charges affectremoval kinetics from solution. Adsorption capacity dependson activated carbon properties, adsorbate chemical properties, temperature, pH, ionic strength, etc. Many activated carbons areavailable commercially but few are selective for heavy metals. As they are expensive improved and tailor-made materials are sought. Substitutesshould be easily available, cheap and, above all, be readily regenerated,providing quantitative recovery.Industrial or agricultural by-products can be converted intoactivated carbons or low cost adsorbents.

The raw ligno-cellulosic biosorbents are modified by various chemical methods either to increase the metal adsorption capacity or to prevent leaching [63-66]. However, typically almost all carbonizations are conducted at high temperatures (300–800 ˚C) [67].

To the best of our knowledge very few reports are available in the literature on the combined treatment of agrowaste with combined acid (H_2SO_4) and chemical activation (persulfate or hydrogen peroxide) at temperatures as low as 140˚C [68]. As the effect of this treatment on palm shell (*BorassusFlabellifer*), which is available throughout coastal Asia has not been reported, it was decided to explore the potential of palm shell as raw material to prepare various adsorbents. Thus, the possibility of preparing adsorbents from palm shell powder (PSP) using concentrated sulfuric acid for charring and charring in the presence of oxidizing chemicals like $K_2S_20_8$ have been explored. Adsorbent was also prepared by thermal activation to 900˚C for comparison.

2.1.2. **Metal Adsorption onto Modified Activated Carbon.**

Heavy metal adsorption onto activated carbons is due to a series of adsorption reactions between the metal ions and the organic functional groups in the carbons. The adsorptive behaviors maybe significantly altered after the surfaces of carbons are modified [69-72].

Heat-treated activated carbons can significantly improve the adsorption capacity [42]. Anodic oxidation of carbon results in enhancement of both uptake capacity and kinetics for Cr^{6+}. Air oxidation can cause an improvement in copper adsorption [70]. In the copper adsorption ontoa sulfuric acid-modified carbon, it was observed that the concentration of acidic surface oxides on the carbon surfaces increased and cation exchange reactions occurred[71]. On the other hand, the copper adsorption onto a carbon treated in an ammonia atmosphere is due to theformation of surface complexes with the nitrogen- and oxygen-containing functional groups[72].

Since modification of adsorbent surface might change the properties of adsorbent, it is recommended that for any work on chemically modified plant wastes, characterization studies involving surface area, pore size, porosity, pH_{ZPC}, etc. are also carried out. Spectroscopic analyses involving Fourier transform infrared (FTIR), Nuclear Magnetic Resonance Spectroscopy(NMR), X-ray photoelectron spectroscopy (XPS) were also done to have a better understanding on the mechanism of metal adsorption on modified plant wastes.

Outer shell of palm fruit (*Borassus Flabellifer*) is a cheap and abundant agricultural by-product in tropical countries. Hence objective of this work was:

i) To study the feasibility of the use of palm shell powder as a precursor for the preparation of different adsorbents by charring using H_2SO_4 (APSP) at 140^0C, steam treatment of APSP (SAPSP), persulfate treatment of APSP (PAPSP), activation to higher temperatures of APSP (3AAC, 6AAC, 7AAC and 9AAC) and formaldehyde treatment of PSP, APSP, SAPSP and PAPSP (MPSP, MAPSP, MSAPSP and MPAPSP)
ii) To characterize all the prepared materials as well as palm shell powder for their physicochemical characteristics and compare the surface area, porosity and surface chemistry of the prepared materials.

2.1.3. Preparation of *Borassus Flabellifer* (PSP) based adsorbents

The shells of palm fruit (*Borassus Flabellifer*) were collected from coastal Andhra Pradesh, India, and were cut into small pieces. The pieces were extensively washed with running tap water for 30 to 40 minutes to remove dirt and other particulate matter followed by double distilled water. The pieces were dried in an oven at 70^0C, ground in a laboratory blender and sorted using standard test sieves. The sample used was of particle size passing 40 micron sieve and is henceforth termed as palm shell powder (PSP).

The PSP was modified by using different techniques (Scheme 2.2). PSP was treated with conc. H_2SO_4 in a ratio of 1:1.5 weight/volume with continuous stirring. The charred substance was then heated in an air oven at 140^0C for 24h. The sample was then extensively washed with a solution of 2% $NaHCO_3$ until the effervescence ceased, and further kept soaked in 2% $NaHCO_3$ overnight. After washing with distilled water 2-3 times, the sample was then kept in an air oven for 4 hrs at 105^0C. The prepared acid treated palm shell powder is termed as APSP.

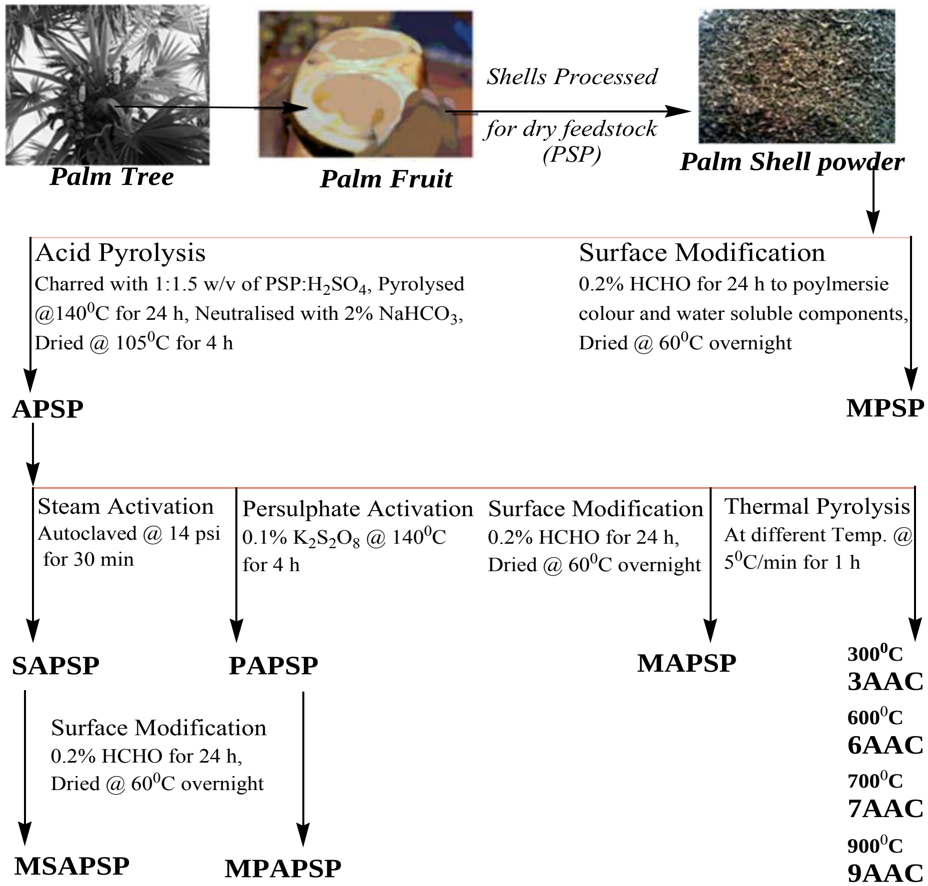

Scheme 2. Different methods of modification of palm shell powder

APSP was modified by different methods- i) APSP was treated with steam in an electric autoclave for 30 minutes at 14psi pressure and the product obtained was termed as SAPSP. ii) PAPSP was obtained by treating APSP with conc. H_2SO_4 in the ratio of 1: 1.5 wt/volume in presence of 0.1% $K_2S_2O_8$ and was kept in an air oven for 4 hrs at 140^{0}C. Subsequently it was washed extensively with 2% $NaHCO_3$ until effervescence ceased and left overnight, soaked in 2% $NaHCO_3$. Finally it was washed 2-3 times with distilled water and then again dried in an air oven at 105^{0}C for 4hrs.

Modification of PSP, APSP, SAPSP and PAPSP with formaldehyde was done in order to polymerize and immobilize the color and water soluble substances. One gram each of PSP, APSP, SAPSP and PAPSP were soaked in 100 mL of 0.2% formaldehyde solution for 24 h. The resulting MPSP, MAPSP, MSAPSP and MPAPSP were then filtered, washed with 300 mL of distilled water several times, and dried overnight in an oven at 60°C.

To see the effect of temperature on surface area of APSP, thermal activation was done at four different temperatures 300^{0}C (3AAC), 600^{0}C (6AAC), 700^{0}C (7AAC), 900^{0}C (9AAC). The heating was carried out with a programmable muffle furnace at a rate of 5^0C/min until the desired temperatures were reached and then kept at that temperature for one hour. The samples 3AAC, 6AAC, 7AAC and 9AAC were then washed with 2% $NaHCO_3$ until effervescence ceased, and were left soaked in 2% $NaHCO_3$ overnight. Finally they were washed 2-3 times with distilled water and then again dried in an air oven at 105^0C for 4hrs.

2.2.Characterization techniques and methods of analysis

The surface chemistry of adsorbents has been indicated to have a significant effect on the uptake of various adsorbate molecules. The changes in the surface chemistry of the adsorbents under study were followed by potentiometric titrations and data analysis, Solid state ^{13}C NMR, X-ray photoelectron spectroscopy, X-ray powder diffraction (XRD), Braunett-Emett-Teller (BET), Scanning Electron Microscopy (SEM), Thermo-gravimetric analysis (TGA) and Fourier transform infrared spectroscopy. The specific surface area of the adsorbent, pore volume and pore size can be measured by the BET method (N_2 adsorption–desorption). The surface images of samples were obtained using SEM. DTA–TGA was employed to analyze the population of surface functional groups on the basis of thermal stability. Fourier transform infrared (FTIR) analysis was applied to determine the surface functional groups. XPS helps in interpreting the surface features of the adsorbents.

2.2.1.Methods of Analysis

Physical properties (bulk density, moisture content, solubility in water and acid) and chemical properties (pH, ion exchange capacity) of the prepared adsorbents were investigated. **Bulk density** measurements were done using a previously weighed 100mL graduated cylinder and filling it up to 50 mL mark with the adsorbent under study. The cylinder with the carbon was weighed accurately. The apparent density was calculated by dividing the difference in weight by 50. **Moisture content** was found out by heating a known weight of the sample in an air oven maintained at 105 ± 5^0C for about 4 hr. Heating, cooling and weighing were repeated at 30 min time interval till the difference between two consecutive weighings was less than 5 mg. **Solubility in water and acid** was determined by taking ten gram of adsorbent under study into a one litre beaker and boiling with 300 mL distilled water and 0.25 N HCl respectively followed by digestion for around 30 min. The material was washed thoroughly with distilled water and washings were collected along with the filtrate. The filtrate was concentrated on a water bath, cooled and made up to 100 mL in a volumetric flask. Exactly 50 mL of the concentrate was transferred to a china dish, evaporated to almost dryness on a water bath and finally dried in an electric oven maintained at105 ± 5^0C, cooled and weighed. The weight of the residue represents the matter soluble in water and acid. The **pH** was measured by heating a suspension of ten gram adsorbent in 300 mL distilled water to boiling with constant stirring. The solution was then digested for around 30 minutes. The material was filtered, cooled and pH of the solution was measured. For measuring the **ion exchange capacity**, 0.5 g of adsorbent under study was added to 100 mL solution of 0.25M sodium sulphate in a stoppered conical flask and kept for shaking in a temperature controlled shaking bath for 5 hours. The contents were filtered and the filtrate was titrated against 0.1N NaOH using phenolphthalein indicator. The ion exchange capacity of the adsorbent in meq/g was calculated from the following equation.

$$\text{Ion exchange capacity}\left(\frac{\text{meq}}{\text{g}}\right)=\frac{aW}{V}$$

Where, a = Normality of NaOH

V = Volume of NaOH

W = Weight of the adsorbent in g

Iodine Value was calculated by means of adsorption of iodine from aqueous solution which can be used to compare adsorbent surface areas and is a relative indicator of porosity [73]. A sample of 0.2 g of adsorbent under study was equilibrated with iodine/iodide solution and the iodine residual concentration was determined by titrating with sodium thiosulphate solution.

Iodine Value = (Blank-Burette reading for sample) x Conversion factor; mg/g.

$$\text{Conversion factor}=\frac{\text{Mol. Wt. of Iodine (127) x 40}}{\text{Wt. of Carbon x Blank Reading}}$$

Blank Reading: Burette reading for iodine concentration without adding the carbon sample. Burette reading for sample: Burette reading for iodine remaining unadsorbed in solution after adding the carbon sample.

The iodine number is a relative indicator of porosity in a carbonaceous material and may be used as an approximation of surface area for some types of carbons [73]. Correlation between the Braunett-Emett-Teller surface area and the iodine number is established and well documented [8,74, 75]. As iodine number gives an indication on micro-porosity (pores less than

1 nm in diameter), higher iodine numbers reflect better development of the micro-porous structure and higher adsorption abilities for low-molar-mass solutes [74, 76, 77].All the experiments were carried out in triplicate and the average results are provided.

Potentiometric experiments were carried out usingan adsorbent mass of 0.1 g suspended in 50 mL of 0.01 M KNO_3 solution, and the suspension was left for 24 h in contact with the electrolyte. The suspensions were acidified to pH 3.0 using 0.1 M HNO_3 and then titrated to pH 11 using 0.1 M NaOH. All experiments were conducted in triplicate in a glass vessel with a lid as part of a Spectralab AT-38C automatic potentiometric titrator. The temperature was recorded with a temperature sensor; the error of the temperature probe was 0.1 ^{0}C. The pH electrode was three-point calibrated with buffers (pH 4, 7, and 10) before each experiment, and the slope did not deviate more than 1 % from the Nernst value. The titrator unit was programmed with a step volume dose mode for the titration, which adds 0.001 mL of titration solution according to the pH changes.

Data Analysis. The titration data were analyzed using the linear programming method (LPM) approach or so called pK_a spectrum method as proposed by Brassard [78]. Proton dissociation from the surface ligands can be described by the following equation:

$$\mathrm{HL^0} \leftrightarrow \mathrm{H^+} + \mathrm{L^-}$$

Where L^- is the proton binding site on the surface and H^+ is the protons in solution. The concentration of protonated and deprotonated surface sites can be quantified with the corresponding mass action equation.

$$K_\mathrm{a} = \frac{[\mathrm{H^+}][\mathrm{L^-}]}{[\mathrm{HL^0}]}$$

Where K_a is the acidity constant.

The titration data are expressed in the form of charge excess versus $-\log[H^+]$. Where charge excess ($\mathrm{b} = C_b - C_a + [H^+] - K_w/[H^+]$) for the known concentration of acid (C_a) and base (C_b) was calculated for the jth addition of acid and base, the charge balance expression can be written as

$$b_j = \sum_{i=1}^{n} [\mathrm{L}_i^-] + S = \sum_{i=1}^{n} \left(\frac{\mathrm{L}_{Ti} K_{ai}}{K_{ai} + [\mathrm{H^+}]_j} \right) + S$$

S is a constant term analogous to the acid neutralizing capacity (ANC) as in Brassard. This equation could be solved by setting the number of sites (n) and varying$L_{Ti}$and K_i. This is essentially what FITEQL does, where n is increased until the fit is good enough. To avoid selecting n and to prevent convergence problems caused by the correlation of L_{Ti} *and* K_i, it is preferable to fix the pK_a values as a grid from a minimum to a maximum value at fixed step sizes. The ligand concentration associated with each pK_a is assigned a positive value where zero is a possible result; the result is the so called pK_a spectrum. For the data here the minimum and maximum pK_a values corresponds to the measured minimum and maximum pH, respectively, and the step size is fixed at 0.2. The pH range was selected because Smith (http://info.wlu.ca/wwwchem/faculty/Smith/Research/research.shtml) demonstrates the errors for acid base titrations outside this range are very large. The pK_a spectrum approach is used here to determine the best fit of K_{ai}/L_{Ti} pairs, with pK_a values fixed as a grid from 4 to 10 at fixed step sizes (0.2). Once the pK_a values are selected, the matrix version of eq 3 is set up as $Ax = b$. The entry α_{ij}in the $m \times n$ matrix A for n proposed sites and m additions of titrant is

$$\alpha_{ij} = \frac{K_{ai}}{K_{ai} + [H^+]j}$$

The matrices used to solve the linear programming problem were set up as in Brassard and solved using Matlab linear programming routine.

The thermal behavior of the adsorbents was evaluated by using thermo-gravimetric analyzer (TG-DTA 32, SEIKO Thermal Analysis System SS 5100), under air at a heating rate of 10°C min^{-1}.

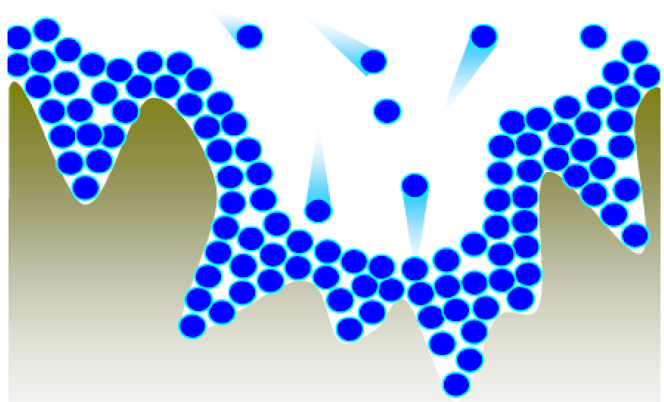

The porous structure of the adsorbents was determined by nitrogen adsorption at 77.37K (Surface Area Analyser Micromeritics, ASAP 2020 V3.03H). Nitrogen adsorption isothermwas measured over a relative pressure (P/P0) range from approximately 0.03 to 1.The specific surface areas were determined from the isotherms using the Brunauer–Emmett–Teller equation. BET isotherm is an extension of the Langmuir theory, which explains monolayer molecular adsorption capacity, to multilayer adsorption with the following hypotheses: (a) gas molecules physically adsorb on a solid in layers infinitely; (b) there is no interaction between each adsorption layer; and (c) the Langmuir theory can be applied to each layer. The resulting **BET equation** is expressed by:

$$\frac{1}{v\left[\left(\frac{P_0}{P}\right)-1\right]}=\frac{c-1}{v_m c}\left(\frac{P}{P_0}\right)+\frac{1}{v_m c}$$

P and P_0 are the equilibrium and the saturation pressure of adsorbates at the temperature of adsorption, v is the adsorbed gas quantity (for example, in volume units), and v_m is the monolayer adsorbed gas quantity. c is the BET constant, which is expressed by:

$$c = exp\left(\frac{E_1 - E_L}{RT}\right)$$

E_1 is the heat of adsorption for the first layer, and E_L is that for the second and higher layers and is equal to the heat of liquefaction.

Nitrogen adsorption results can be plotted using $1/v[(P_0 / P) - 1]$ on the y-axis and relative pressure P/P_0 on the x-axis. This plot is called a **BET plot**. The linear relationship of this equation is maintained only in the range of $0.05 < P/P_0 < 0.35$. The value of the slope A and the y-intercept I of the line are used to calculate the monolayer adsorbed gas quantity v_m and the BET constant c. The following equations can be used:

$$v_m = \frac{1}{A+I}$$

$$c = 1 + \frac{A}{I}$$

BET method is widely used in surface science for the calculation of surface areas of solids by physical adsorption of gas molecules. A total surface area S_{total} and a specific surface area S are evaluated by the following equations:

$$S_{BET,total} = \frac{(v_m N_s)}{V}$$

$$S_{BET} = \frac{S_{total}}{a}$$

N: Avogadro's number, v_m: molar volume of the adsorbate gas in terms of volume, s: adsorption cross section of the adsorbing species, V: molar volume of adsorbate gas, a: mass of adsorbent (g) [79].

The cross-sectional area of a nitrogen molecule was assumed to be 0.162 nm^2.The *t*-plot and DR plot methods were applied to calculate the pore volume and the BJH method was used for pore size distribution determination [7, 80].

Multi-layer formation is modeled mathematically to calculate a layer “thickness, t” as a function of increasing relative pressure (P/P_o). The resulting t-curve is compared with the experimental isotherm in the form of a t-plot. That is, experimental quantity adsorbed is plotted versus statistical thickness for each experimental P/P_o value. The linear range lies between monolayer and capillary condensation. The slope of the t-plot (V/t) is equal to the “external area”, i.e. the area of those pores that are not micropores. Mesopores, macropores and the outside surface are able to form a multilayer, whereas micropores, which have already been filled, cannot contribute further to the adsorption process. Harkins and Jura equation was employed to interpret the t-plot micropore area and external surface area.

$$t = \left[\frac{13.99}{\left(0.034 - log\left(\frac{P}{P_0}\right)\right)}\right]^{0.5}$$

BJH method was used for describing pore volume and pore size using Halsey equation with Faas correction. Condensation occurs in pores that already have some multilayers on the walls. Severely underestimates size of small to medium mesopores and acceptable for broad size distributions of medium to large mesopores.

$$t = 3.54 \times \left[\frac{-5}{\left(ln\left(\frac{P}{P_0}\right)\right)}\right]^{0.33}$$

Dubinin-Radushkevich (DR) analysis has been devoted to elucidating the micropore structures of various solids regardless of insufficient understanding of the basis of the DR equation. In particular, activated carbon whose micropore structure cannot be determined by other characterization techniques has been analyzed by the DR equation.

$$W = W_0 e^{\left[-\left(\frac{A}{E}\right)^n\right]}$$

$$n=2,\ E=\beta E_0,\ A=RT\ln(P_0/P)$$

W and W_0 are the amount of adsorption at the relative pressure $P/P0$ and the micropore volume, respectively. A is the adsorption potential. β and E_0 are the affinity coefficient and characteristic adsorption energy, respectively. Plot of $\ln W$ versus A^2 relationship which linearizes the isotherm based on micropore filling principle. Best fit is extrapolated to A^2 to find the micropore volume. Useful to find micropore volume when chosen analysis conditions do not aloe complete filling.

The surface morphology and topographic analysis of the adsorbent samples was examined by Scanning Electron Microscope (JEOL, Model JSM-5610LV). Samples were mounted onto metal holders using a conducting substrate.

Powder-XRD of the ingredients was taken by holding the samples in place on quartz plate for exposure to CuKα radiation of wavelength 1.5406 Å. The sample was analyzed at room temperature over a range of 10-70^0 2θ with sampling intervals of 0.02^0 2θ and scanning rate of 6^0 /min.

FT-IR-The functional groups in the materials under study were characterized by infrared spectroscopy (Fourier Transform Infra Red spectra were collected by a Perkin Elmer RX1 model within the wave number range of 400-4000cm^{-1}. Specimens of samples were first mixed with KBr and then ground in an agate mortar at an appropriate ratio of 1/100 for the preparation of the pellets. Resulting mixture was pressed at 10 tons for 5 min. sixteen scans and 8cm^{-1} resolution were applied in recording spectra. The background obtained from the scan of pure KBr was automatically subtracted from the sample spectra.

XPS is a surface technique which will provide an estimate of the chemical composition of the few uppermost layers of the material. The materials under study were analyzed by XPS to determine thechemical states of the surface functional groups. The surface of the samples was analyzed using a KRATOS AXIS 165 X-ray Photoelectron spectrometer equipped with dual aluminum–magnesium anodes using Mg Kα radiation. The X-ray power supply was run at 15 kV and 5 mA. The pressure of the analysis chamber during the scan was 10^9 Torr. Peak fitting and presentation output are produced by an integrated VISION control and information system. The deconvolution process of C 1s spectra as well as the elemental composition evaluation may result in an error of up to 5%. All spectra are presented charge balanced and energy referenced to C 1s at 284.6 eV[81]. Chemical states of O, N and C species were determined from the charge corrected hi-resolution scans. The atomic concentrations wereestimated based on comparisons of integrated peak intensities normalized by the atomic sensitivity factors.

Solid state ^{13}C NMR describes the detailed components present in the adsorbents.The study of the structure and properties of carbon materials by nuclear magnetic resonance (NMR) has been a subject of increasing interest in recent years. ^{13}C nuclei belonging to aromatic carbons resonate at a frequency range readily separated from the aliphatic ones, providing important information about the structure of these materials. Applications in the study of coals, cokes, charcoals, chars, polymeric carbons, amorphous carbons and new carbon forms have been reported [82-90].The ^{13}C-NMR experiments were performed with a BrukerAvance (300 MHz) spectrometer.The chemical shifts δ, expressed in parts per million [ppm], were referenced relative to the signal of tetramethylsilane (TMS) at $\delta c = 0$ ppm.

2.3. Result and Discussion

2.3.1. Physical characterization of adsorbents.

The series of adsorbents namely APSP, SAPSP, PAPSP, MAPSP, MSAPSP, MPAPSP, 3AAC, 6AAC, 7AAC and 9AAC prepared from PSP by different routes and different activating agents were characterized for various characteristics like bulk density, solubility in water, solubility in acid, ash content, moisture content and ion exchange capacity and are tabulated in Table 2.1.

Table 2.1. Physical characterization of sorbents

Sample	Bulk density	Moisture Content	pH	Solubility in H_2O	Solubility in acid	Ion exchange capacity	Ash content
	gm/cm^3	%		%	%	meq/gm	%
PS	0.351	8.37	6.00	3.44	4.04	0.004	0.897
APSP	0.550	2.60	8.05	12.33	15.61	0.125	6.653
SAPSP	0.576	14.58	7.75	53.40	51.20	0.110	6.893
PAPSP	0.626	16.34	8.00	25.30	27.70	0.071	6.783
MPSP	0.362	9.34	7.10	2.50	3.91	0.500	1.098
MAPSP	0.553	15.32	6.80	10.00	13.06	0.250	5.470
MSAPSP	0.578	19.14	6.41	36.50	38.10	0.124	5.230
MPAPSP	0.551	17.62	6.32	6.00	8.10	0.125	6.980
3AAC	0.648	11.56	7.60	3.50	4.20	0.014	1.409
6AAC	0.549	9.32	6.99	3.50	4.71	0.250	4.678
7AAC	0.448	9.08	6.95	0.01	0.04	0.167	9.532
9AAC	0.539	15.90	6.90	0.50	0.92	0.167	10.989

It can be observed from the table that bulk density of activated carbons in each case is higher than PSP. Moisture content was in the range of 2.6–19.1%. The moisture content detected was due to the contact of moisture from atmosphere after activation. Solubility in water and acid is negligible for PSP, MPSP, 3AAC, 6AAC, 7AAC and 9AAC. All the adsorbents prepared have pH in the range (6.0-8.0) which is appropriate for water treatment purpose. APSP, SAPSP, PAPSP, 3AAC have a pH of ~7.5–8.0 while the others have a neutral to near neutral pH of 6.0-7.1. pH values of the adsorbents under study are lower than reported pH values of commercial activated carbons. Ion exchange capacity is significantly increased and was found to be the highest for MPSP (0.5) followed by MAPSP and 6AAC (0.25), 7AAC and 9AAC (0.167), APSP (0.125) and SAPSP (0.110). The other modified forms had comparatively low ion exchange capacity.

Adsorbents that can remove a high percentage of iodine normally have a high surface area and also largely a micro- and mesoporous structure [91]. It can be seen from the Figure 2.2 that on modification with formaldehyde the iodine value was higher (312.41 mg/g) as compared to PSP (146.82 mg/g) but was slightly lower to that of APSP (342.47 mg/g). Temperature variation from 300°C to 900°C during thermal activation of APSP resulted in an increase in iodine value from 436.82 to 990.44 mg/g which is comparable with reported values.

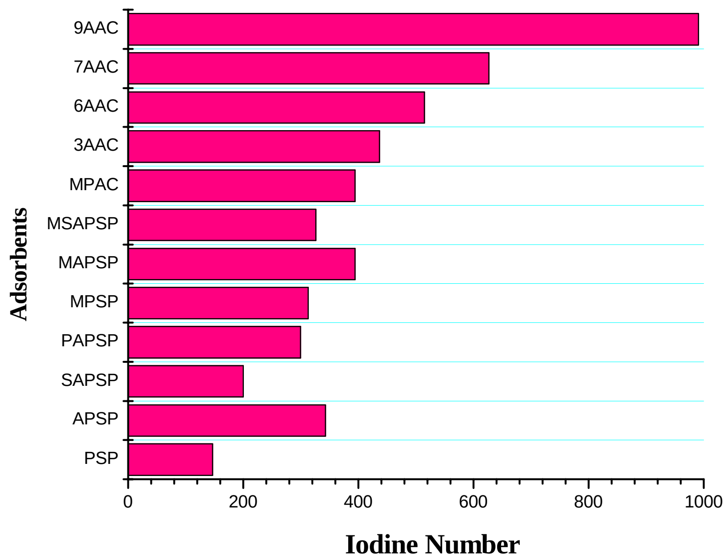

Figure 2.2. Iodine Number of the adsorbents under study

2.3.2.Thermal characterization of adsorbents.

Thermal analysis curves (DTG, DTA and TGA) are shown (Figure 2.3). The weight loss during thermo-gravimetric decomposition of the adsorbents can be divided into different stages and tabulated in Table 2.2.

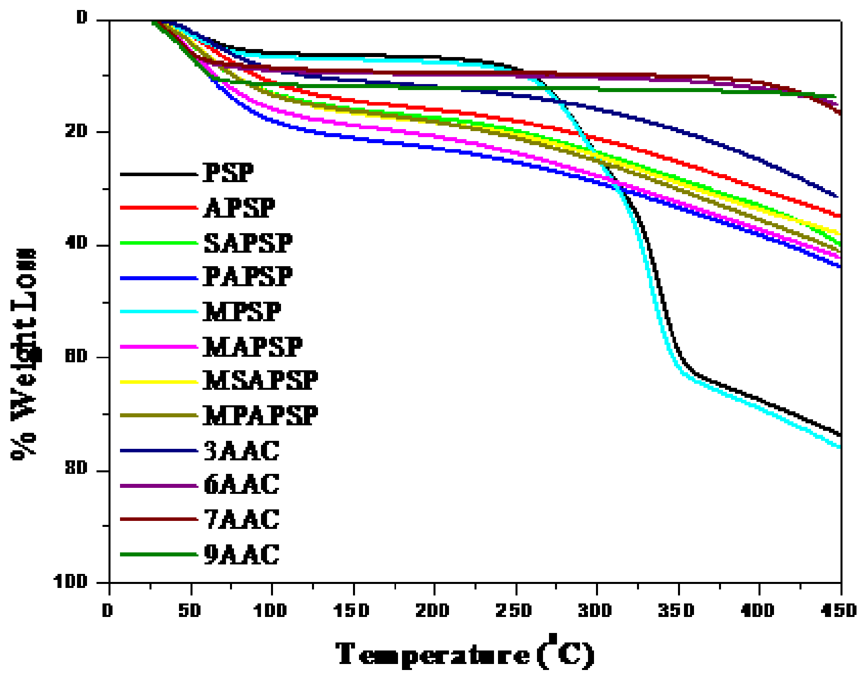

Figure 2.3. Thermal Analysis of Activated Carbons

Table 2.2. Thermal analysis

Sample	Weight loss (%)							
	1st stage	Temperature range (°C)	2nd Stage	Temperature range (°C)	3rd Stage	Temperature range (°C)	4th Stage	Temperature range (°C)
PSP	5.610	26.1 – 99.9	89.21	207.3 – 493.7	-	-	1.91	493.7 – 858.3
APSP	10.480	30.5 – 99.9	36.00	99.9- 478.0	8.20	478.0 - 746.4	31.6	746.4 - 829.2
SAPSP	13.900	28.3 – 124.5	-	-	38.59	124.5 – 750.9	33.54	750.9 – 858.3
PAPSP	14.570	30.5 – 129.0	61.71	129.0 – 578.7	1.92	578.7 – 748.7	9.60	748.7 – 860.5
MPSP	6.059	30.5 – 205.1	90.50	205.1 – 495.9	-	-	2.10	495.9 – 858.3
MAPSP	16.596	30.6 – 135.7	54.60	135.7 – 585.4	-	-	19.90	585.4 – 860.6
MSAPSP	11.040	26.1 – 102.2	-	-	40.08	102.2 – 717.4	33.29	717.4 – 858.3
MPAPSP	15.199	30.5 – 144.6	62.50	144.6 – 558.5	-	-	10.10	708.4 – 858.3
3AAC	12.745	28.3 – 135.7	83.60	135.7 – 486.9	-	-	1.30	486.9 – 858.3
6AAC	7.147	30.6 – 102.1	2.10	102.1- 305.7	86.10	305.7 – 560.8	-	-
7AAC	4.560	30.5 – 95.4	33.50	95.4 – 372.8	80.00	372.8 – 547.3	-	-
9AAC	4.326	32.8 – 84.3	4.25	84.3 – 406.4	80.40	406.4 – 623.4	-	-

The TGA curves of the adsorbents showed a first stage weight loss of about 4-16% in the region below 145°C corresponding to the loss of water molecules. The second stage (145°C< T<600°C), which corresponds to the primary carbonization, is seen as a large weight loss for the adsorbents, suggesting the elimination of volatile matters and tars. Above 600°C, SAPSP, PAPSP, MAPSP, MPAPSP and 3AAC showed very little weight loss indicating their decomposition to a structure with higher stability while APSP and MAPSP showed a higher weight loss, indicating that more surface functional groups are created on APSP and MAPSP [92]. The TGA curves indicate that thermal stability is greater for 9AAC. Gergova [93] and Krisztina [94] have also reported three stages in the carbonization process and the formation of basic structure at 800-900^{0}C in ligno-cellulosic materials.

2.3.3.BET surface area measurements/ N_2 adsorption isotherms.

Adsorption isotherms of nitrogen for the adsorbents are shown in Figure 2.4. N_2 uptake was found to be very less in PSP, APSP, SAPSP, PAPSP, MPSP, MAPSP, MSAPSP, MPAPSP and 3AAC. The shapes of the isotherms are different as a result of different porosities. The porosities seem to be same for MPSP, MAAC, MSAPSP and 3AAC and similar for APSP, PSP and PAPSP. Predominant adsorption finishes at a very low relative pressure and the amount of nitrogen adsorbed decreased for 3AAC, MAPSP, MPSP, PSP indicating that pore cavities are micro-porous/ blocked. The nitrogen adsorption isotherms of 9AAC, 7AAC and 6AAC show increase in amount of nitrogen adsorbed with relative pressure which reflect a certain amount of meso-pore volume. It is observed that the carbons 6AAC and 7AAC exhibit type II isotherms, indicating an indefinite multi-layer formation after completion of the monolayer and is found in adsorbents with a wide distribution of pore sizes. Near to the first point of inflexion a monolayer is completed, following which adsorption occurs in successive layers, while 9AAC exhibits type IV adsorption curve with a hysteresis loop (in the relative pressure range of 0.8-1), which is associated with capillary condensation in meso-pores.

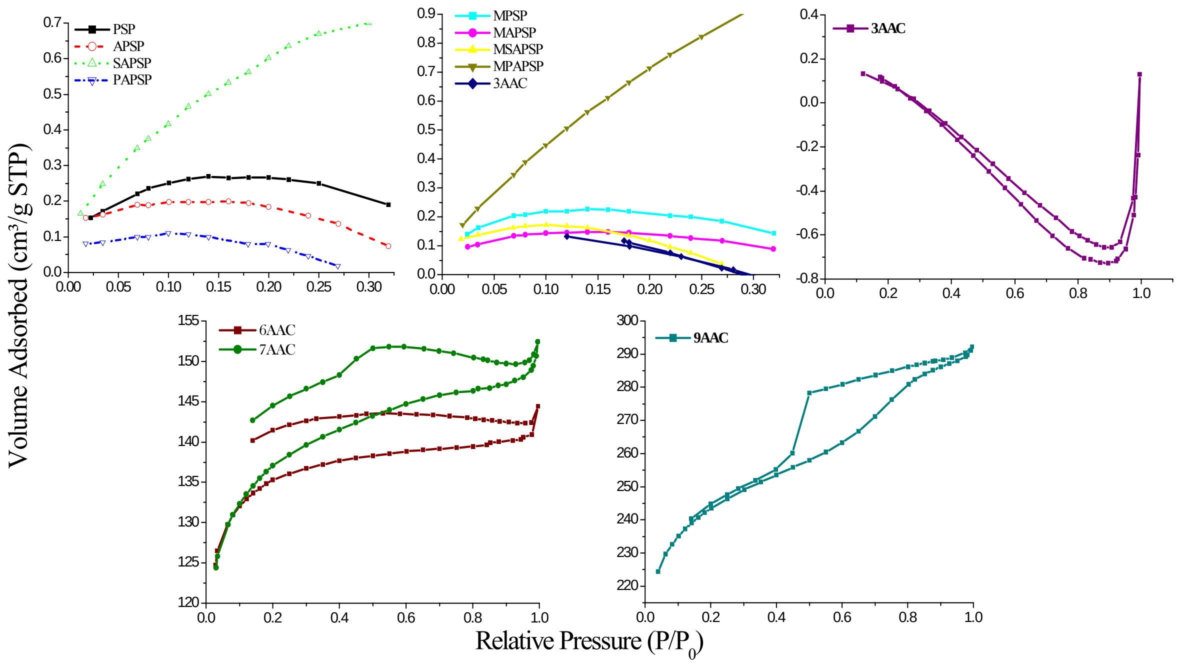

Figure 2.4. Adsorption isotherms of nitrogen for the adsorbents

The hysteresis loops are different in 6AAC, 7AAC suggesting the presence of pores with different shapes. The nitrogen adsorption isotherm of 9AAC shows a tremendous increase in N_2 uptake compared to 6AAC and 7AAC.The adsorption was found to be higher at low relative pressure for 6AAC, 7AAC and 9AAC suggesting the presence of relatively larger number of micro-pores. Type III isotherm is obtained for 3AAC which occurs when affinity between adsorbent and adsorbate is less than adsorbate-adsorbate interactions. BET isotherm is not applicable for calculation of surface area in such adsorbents.

PSP, APSP, SAPSP, PAPSP, MPSP, MAPSP, MSAPSP, MPAPSP show type I isotherm according to BET classification indicating monolayer adsorption and are typical of micro-porous samples and hence not amenable to BET analysis [95].

Table 2.3. Surface Area Analysis

Adsorbent	Single point SA	BET SA	Langmuir SA	BJH Pore SA	BJH Pore Volume	BET Av. Pore dia.
Unit	m^2/g	m^2/g	m^2/g	m^2/g	cm^3/g	Å
PSP	0.562	0.673	0.965	-	0.004	237.984
APSP	0.217	0.297	0.408	-	0.003	422.652
SAPSP	2.134	2.419	3.894	-	0.005	81.244
PAPSP	0.056	0.090	0.115	-	0.022	9829.990
MPSP	0.424	0.504	0.714	-	0.004	301.040
MAPSP	0.260	0.314	0.442	-	0.0016	201.730
MSAPSP	2.810	3.405	6.344	-	0.0055	64.240
MPAPSP	0.121	0.176	0.225	-	0.001	243.823
3AAC	0.254	0.113	0.132	-	0.001	-
6AAC	470.793	469.586	596.925	50.481	0.218	18.569
7AAC	477.179	476.194	606.997	79.780	0.230	19.349
9AAC	846.334	834.874	1083.357	162.848	0.447	21.436

BET surface area measured for different activated carbons is presented in Table 2.3. The carbons APSP, SAPSP, PAPSP, MAPSP, MSAPSP and MPAPSP do not show high BET surface area but adsorption property as seen by iodine value is higher. They may contain a number of narrow micropores inaccessible (within reasonable time) to N_2 at 77 K [96]. The iodine number is considered as a simple method to evaluate the surface area of activated carbons associated with pores with d>1nm. The carbons prepared at higher carbonization temperatures (6AAC, 7AAC and 9AAC) have significantly increased pore volume (~0.218, 0.23 and 0.447 cm^3/g) and BET surface area (~469.586, 476.194 and 834.874 m^2/g); with supportive evidence from iodine values. BET surface area is higher than BJH surface area, which agrees well with observations made by Gregg and Sough[97]. Complete decomposition of PSP could not be achieved even at 700^0C. Thus the low surface area of 3AAC, 6AAC and 7AAC are due to the presence of non decomposed or partially decomposed products in the pores of the carbon. On heating to 900^0C the decomposition of these products was also complete and pores were liberated and surface area increased to $846m^2/g$. BET surface area is highest for 9AAC forming mainly micro-pores. A comparison has been made for the surface area of different activated carbons and presented in

Table2.4. It is evident that the surface area of 9AAC is comparable to that of other activated carbons prepared from agro-wastes reported in literature.

Table 2.4. Comparison of surface area of adsorbents

Raw material	Carbonisation conditions ^0C/hr	Activation conditions ^0C/hr	Chemical Treatment	BET Surface aream^2/g	Ref.
Grape seeds	800/1 hr (15^0C/min)	800/1 hr	Steam activation, one step pyrolysis/ activation	497	[18]
Nut shells	800/1 hr (15^0C/min)	800/1 hr	Steam activation, one step pyrolysis/ activation	743	[18]
Pistachio-nut shells	500/ 2hr (10^0C/min)	900/ 30min (10^0C/min)	Physical activation, CO_2	778	[30]
Macadamia nut shells	1 hr	500^0C	Chemical activation with both $ZnCl_2$ and KOH	1718	[31]
Peanut hulls	500/2 hr	700-900^0C	Physical activation, two step	80.8-97.1 420	[29]
Almond shells	800/1 hr (15^0C/min)	800/1 hr	Steam activation, One step pyrolysis/ activation	998	[18]
Oat hulls	500^0C/ (1.5sec residence)	800/ 30 min	Steam activation	625	[7]
Cotton stalk	400-700^0C with 7^0C/min	-	-	3.14 37.28	[5]
Oak	700-800^0C	-	Residence time 1-2 hr	985	[28]
Corn hulls	700-800^0C	-	Residence time 1-2 hr	1010	[28]
Corn Stover	700-800^0C	-	Residence time 1-2 hr	660	[28]
Olive seed	800/ 1hr	800-900^0C	Residence time 1-2 hr, Chemical activation, KOH	1550	[105]
Rice straw	700-1000/ 1hr (10^0C/min)	900^0C	Chemical activation, KOH, Two step method	2410	[106]
Rice husk	-	600^0C/ 3hr	Chemical activation, one step, $ZnCl_2$/ CO_2	480	[107]
Pecan shell	-	-	Chemical activation, (H_3PO_4),	724	[108]
Cassava peel	650/ 3hr	750^0C	Chemical activation, KOH	1183	[109]
9AAC	105^0C/ 1hr	900^0C	Carbonization using H_2SO_4	834	This study

2.3.4. Pore structure and pore size distribution.

The extent of the microporosity and the development of the pore structure under different conditions used were evaluated by identifying the micro- and mesopore volumes and pore size distributions presented in Figure2.5.

Micropore volumes were analyzed by DR and t-plots as shown in Table 2.5. The *t*-plot [29] estimates the pore volume by assuming that layers build up on the wall of the pores until the pore is completely filled. The DR method [98] describes the adsorption according to the mechanism of volume filling.It can be seen from Table2.5 that the *t*-plot slightly underestimates the micropore volume showing values lower than those from DR. This feature is probably due to the high values of the surface area. Remy and Poncelet [99]suggested that the DR equation overestimated $W_{0,DR}$, with respect to $W_{0,t}$, when a solid presents an high surface area. The micro-pore volumes determined from the DR plot (Figure2.6) increase with increase in temperature of APSP.

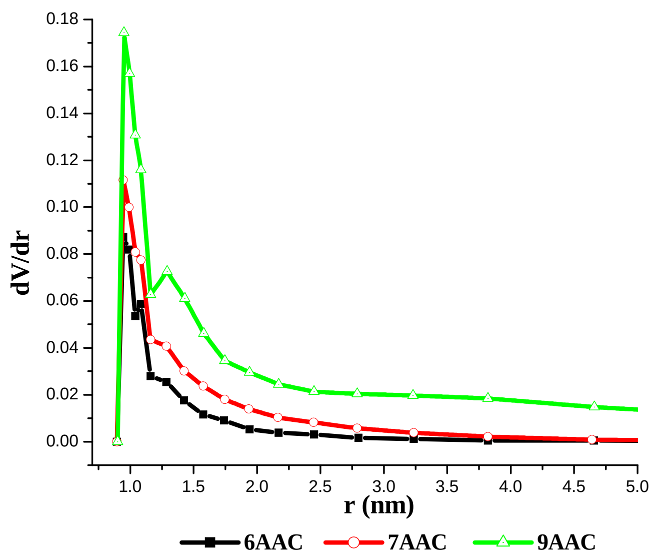

Figure 2.5. Pore size distribution graph

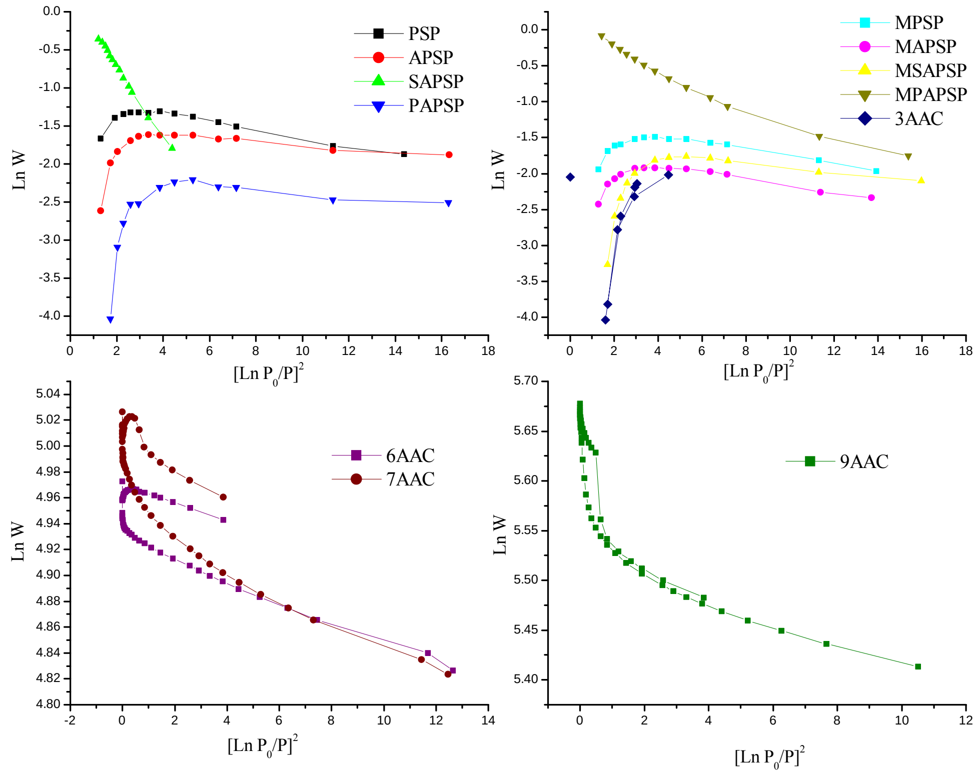

Figure 2.6. DR Plot for the adsorbents

For 6AAC, 7AAC and 9AAC, DR plots exhibited a brief linear range and then deviated upward indicating formation of multilayer and capillary condensation in the mesopores. Furthermore the mesopores (2-50 nm) increased with increase in temperature of activation i.e. increasing the extent of burn off (6AAC, 7AAC and 9AAC) as a consequence of enhanced pore formation and pore widening effect. Micro-pore volumes for 6AAC, 7AAC and 9AAC are in the range of 0.18-0.30 which is comparable to those reported in literature [7]. Thus increase of carbonization temperature resulted in creation of micropore structure and widening of micro-pores to mesopores and an increase in the total pore volume of carbons as seen in Table 2.5. Similar observations were made by D. Adinata et al. and Ismadji and Bhatia [100-102].

Table 2.5. Constants from DR Plot for the adsorbents

Adsorbent	E	E_0	W_0	Micropore volume (t-plot)	Mesopore volume
Unit	$KJmol^{-1}$	$KJmol^{-1}$	cm^3/g	cm^3/g	cm^3/g
PSP	4.227	12.432	0.00052	-	-
APSP	6.456	18.988	0.00034	-	-
SAPSP	1.456	4.2823	0.00195	-	-
PAPSP	6.153	18.097	0.00019	-	-
MPSP	4.567	13.432	0.00042	-	-
MAPSP	4.654	13.689	0.00028	-	-
MSAPSP	5.489	16.144	0.00032	-	-
MPAPSP	2.872	8.198	0.00146	-	-
3AAC	0.906	2.665	0.0000005	-	-
6AAC	11.070	32.559	0.21387	0.179	0.034
7AAC	9.027	26.55	0.22088	0.168	0.062
9AAC	7.925	23.309	0.39874	0.295	0.152

gas volumes were multiplied by 0.001547 to get liquid volumes

The pores of the carbons 6AAC, 7AAC and 9AAC are mostly located in the range of micropores with a peak at 1.2 nm. It is seen from Tables2.3 and 2.5 that BET surface area as well as micropore volume were highest for 9AAC suggesting that micropores make the largest contribution to the surface area. At high carbonization temperatures more ordered structure is likely to be developed in the carbon that leads to a lower rate of gasification in the interior of the particles [103]. Thus activated carbon high in microporosity is produced. PSP, APSP, SAPSP, PAPSP showed small BET surface area and small pore volume suggesting the entry of the gas molecules was partially restricted.

The value of E_o provides a first indication for the presence or absence of microporosity in carbons. Typical micropores correspond to E_o>18–20 kJ mol^{-1} (APSP, PAPSP, 6AAC, 7AAC and 9AAC), whereas values below 14–15 kJ mol^{-1} reflect either variable degrees of surface heterogeneity, or the presence of super micropores (1.5–2.5 nm)(PSP, SAPSP, formaldehyde treated adsorbents, 3AAC)[104].

2.3.5. Scanning electron micrographs.

The micrographs in Figure 2.7 show the surface morphologies of PSP and the prepared adsorbents. The activated and modified adsorbents are having large particle size which is developed like a coral shell. A channel of tubes passing through can be observed. Cross section of some particles has been taken showing distorted pores. Porosity can be seen but not homogeneous, and some pores are broken also which may not support adsorption, in SAPSP and MSAPSP. The pores are superficial and bulk of the sample does not seem to have any porosity, resulting in less surface area. In 6AAC, 7AAC and 9AAC defined surface porosity is seen to develop with temperature. Bulk porosity distributed in an even manner can be observed in some of the cross sections suggesting possible higher adsorption capacity as supported by iodine number and BET surface area parameters.

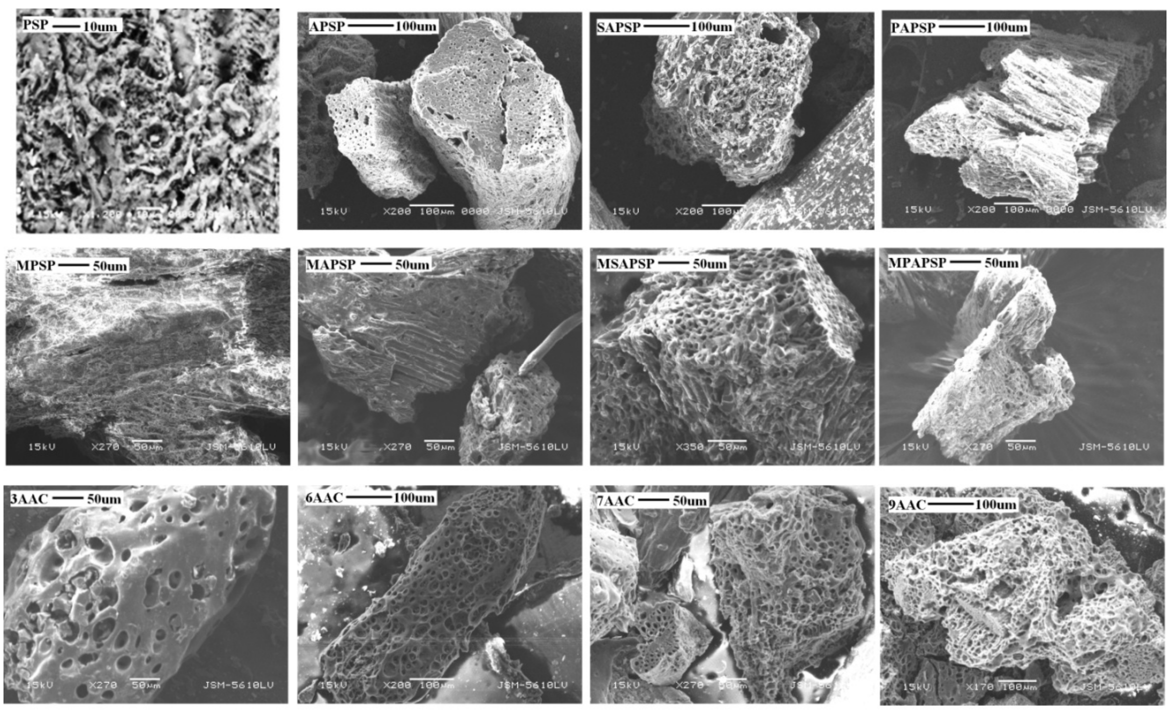

Figure 2.7. Scanning Electron Micrographs

2.3.6. X-ray Diffraction studies of carbons.

The X-ray diffraction patterns of PSP and the other adsorbents under study are presented in Figure 2.8 with the major peaks and their respective 2θ values tabulated in Table 2.6.XRD shows no characteristic peaks after activation at higher temperature. (6AAC, &7AAC and 9 AAC) suggesting turbostratic structure of disordered carbon materials. There is a broad peak at

2θ value of 25^0 for all the materials under study. Sharp non-labelled peaks in PSP, APSP, SAPSP, PAPSP, and MPSP show miscellaneous inorganic components.Peak spacings of PSP and APSP at 0.430 and 0.281nm are assigned to nkl 200 and 004 crystallographic planes of completely ordered regions of cellulose respectively, if a monoclinic unit cell is assumed with C as the fiber axis [110]. It is observed that in MSAPSP, MPAPSP the strong peaks are progressively losing intensity and becoming broader indicating a gradual decrease in cellulose crystallinity. A complete loss of crystal structure in cellulose is indicated by disappearance of 0.160 nm signals and shift of ~0.420 nm signal to higher angles in 3AAC, 6AAC, 7AAC and 9AAC. Similar observations were reported by Marko Kleber during activation at different temperatures[111].

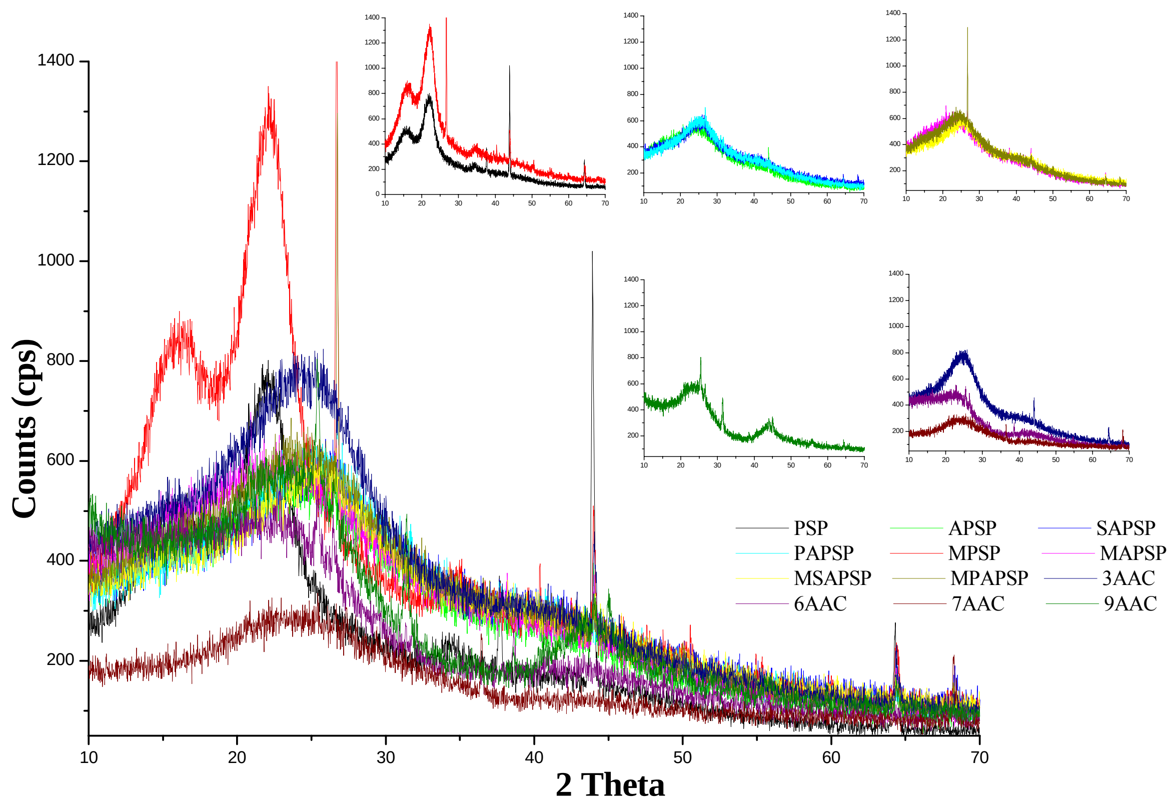

Figure 2.8. X-Ray Diffraction analysis

Peak spacings at ~0.60, ~0.53nm in MPSP and PSP can be assigned to101, 110 crystallographic planes of cellulose. Increased intensity of the 101 and 100 planes at 0.220nm in MPSP indicates lateral growth of graphene planes. Broadening of XRD signal with increasing temperature at ~0.37nm (23^0) in 7AAC suggests the dominance of small aromatic units arranged in random order which may be attributed to the (002) reflection of a graphitic-type lattice. A weak reflection centered around 43˚ corresponds to a superposition of the (100) and (101) reflections of a graphitic-type carbon structure, indicating a limited degree of graphitization in this material [112].Narrowing of peak ~0.4nm with increasing temperature indicates developing atomic order in 9AAC and is attributed to the formation of turbostatic crystallites, i.e. progressive stacking of graphene sheets [113, 114].

Table 2.6.XRD analysis

Sr. No.	Sample	Peak
1	PSP	10^0, 23^0, 27^0 and 34^0
2	APSP	9.22^0, 20.55^0, 20.0865^0, 26.827^0 and 31.8145^0
3	SAPSP	10^0, 27^0 and 32^0
4	PAPSP	10^0 and 27^0
5	MPSP	17^0, 23^0 and 25^0
6	MAPSP	25^0
7	MSAPSP	25^0
8	MPAPSP	25^0
9	3AAC	
10	6AAC	-
11	7AAC	-
12	9AAC	-

NOTE: From the above studies it is seen that no observable advantageous difference in properties were seen for MAPSP, MSAPSP, MPAPSP as compared to MPSP and similarly in 3AAC, 6AAC and 7AAC. Based on the characteristics of the prepared materials we decided to restrict further detailed characterization only for PSP, APSP, SAPSP, PAPSP, 9AAC and MPSP and their use as adsorbents in our further studies.

2.3.7. Potentiometric titrations.

The surface acidity of the carbons studied was estimated using potentiometric titration experiments. The pK_a distribution curves (Figure 2.9) show differences in surface groups of the adsorbents under study.

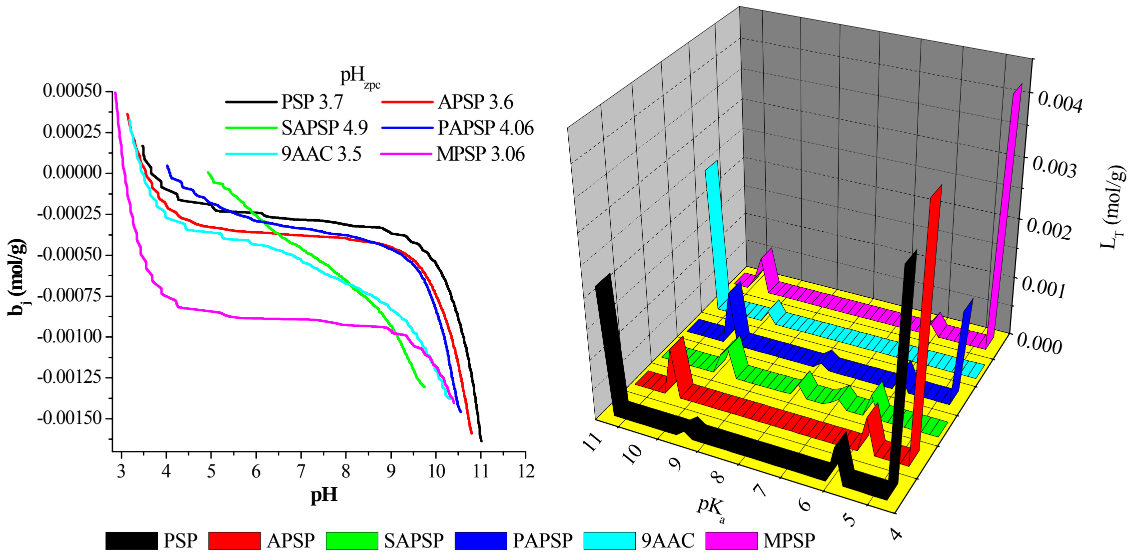

Figure 2.9. Potentiometric titrations and data analysis

Carboxyl groups are considered to havepK_a values <8 and those groups with pK_a>8 are classified as phenols and quinines [115]. However presence of adjacent electron-withdrawing groups increase acidity and decrease basicity. Thus the presence of greater number of acidic groups in APSP and MPSP could be due to the treatment favoring the fixation of carboxyl groups adjacent to acid enhancing groups [116]. In the case of PAPSP and SAPSP very little proton uptake is noticed. Treatment of APSP with steam results in a heterogeneous surface with pK_a at about 5.6, 6.4, 7.4, 9.2 and 9.5. This broad distribution indicates the existence of a wide spectrum of organic acidic groups covering the range of pK_a associated with both carboxylic and phenolic groups. On heating APSP to 900˚C (9AAC) the concentration of surface groups at pK_a 11slightly increased. Phenolic compounds were created in PSP, SAPSP and 9AAC.The number of acidic groups with pK_a 4 increased in MPSP and APSP while in 9AAC the number of acidic groups decreased significantly. Weaker acidic groups of pK_a in the range 5-6 are present in all the adsorbents under study (Table 2.7).Figure 2.9 shows the proton isotherms and zero point of charge (pH$_{ZPC}$) values of the adsorbents under study. The pH$_{ZPC}$ values increase in the order

MPSP(3.06)>9AAC(3.5)> APSP(3.6)> PSP(3.7)> PAPSP(4.06) >SAPSP(4.9). MPSP, 9AAC, APSP and PSP were found to exhibit low pH_{ZPC} values. The surface is positively charged at pH values below the pH_{ZPC}, since the oxygen-containing groups are undissociated and the adsorbent will remove anionic species from solution under these conditions. On the other hand, at solution pH values greater than the pH_{ZPC}, the adsorbent surface becomes more negative due to dissociation of weakly acidic oxygen-containing groups. Thus, the adsorbent surface has the possibility to attract and exchange cations in solution.

Table 2.7. Three-site model from pK_a analysis for titration data of adsorbents under study by linear programming

Ligand Class	1	2	3	4	Total Conc. (mol/g)
Range of pK_a	4.0– 5.0	5.0-7.0	7.0 - 9.0	9.0 – 11.0	
Functional Group	Carboxyl	Lactone	Amine	Hydroxyl/ Phenol	
Adsorbents	pK_a (L_T mol/g)				
PSP	4.0 (0.0036)	5.4 (0.0006)	9.0 (0.0001)	11.0 (0.021)	0.00633
APSP	4.0 (0.0041)	5.2 (0.0006)	-	10.0 (0.001)	0.00480
SAPSP	-	6.2 (0.0002)	7.5 (0.0001)	9.3 (0.0004)	0.00060
PAPSP	4.0 (0.0016)	5.4 (0.0003)	7.4 (0.0001)	9.8 (0.0009)	0.00290
9AAC	-	-	-	10.2 (0.0013)	0.00130
MPSP	4.0 (0.0042)	5.6 (0.0002)	-	10.3 (0.0004)	0.00480

2.3.8. Functional group analysis using FTIR.

The possible modifications in the functional groups of palm shell upon charring and activation were studied by infrared spectroscopy (Table 2.8 and Figure 2.10).

The presence of absorption bands characteristic of $–CH_3$ or $–CH_2$ symmetric stretching vibrations in the spectra of all the adsorbents suggests the existence of some aliphatic species on all the adsorbents under study. For PSP, APSP, PAPSP and SAPSP the bands in the frequency range 1723 to 1732 cm^{-1} indicate the presence of carboxylic acid groups as shown in Table 2.8. On charring with sulphuric acid (APSP) a new band at 1770 cm^{-1} appears which is characteristic of carbonyl moieties in carboxylic anhydrides [117-125]. The band at ~1348 to 1373 cm^{-1} for the adsorbents under study corresponds to vibrations in alkanes and alkyl groups, whereas the band near 1589-1597cm^{-1} is attributed to aromatic ring stretching coupled to highly conjugated carbonyl groups. The presence of bands at 1101 to 1180cm^{-1} in 3AAC, PSP and MPSP can be attributed to stretching frequency of the bonds in ester, ether and the phenol groups. 1348-

1373cm^{-1} is the characteristic peak of carbohydrates seen in PSP, APSP, SAPSP, PAPSP and MPSP. After formaldehyde treatment there seems to be a slight change in morphology probably due to the reaction of hydroxyl groups of cellulose with formaldehyde which is indicated by the absence of bands in the frequency range 1723-1732 cm^{-1}[125].

Table 2.8. FTIR Analysis

PSP	MPSP	APSP	SAPSP	PAPSP	9AAC	Assignment
3361	3389	3584	3489	3597	-	-N-H, -O-H stretching
-	-	-	-	-	2100	$-CH_3$, $-CH_2$ symmetric stretch
2959, 2895	2891	3036, 2876	2887	3078, 2887	3009, 2875	Free CO_2
1732	1727	1720	1723	1723	-	-C=O stretch for acids or aldehyde
1648	1666	-	-	-	-	-C=O stretch of Enolic group, nonconjugated lignin, amide/ -C=C- Aromatic stretch
1597	1597	1596	1597	1597	1589	-C=O stretch cellulose/ C=C Aromatic stretch (skeletal vibration)/ N-H bending of amide
1454	1477	1484	1488	1484	1484	$-CH_2$- stretching
1430	1436	1438	1430	1433	1436	-C=C- Aromatic stretching
1373	1354	1344	1350	1356	1348	-C-H stretch/ N-H bending
1250	1238	1229	1229	1256	1208	-C-O bending of carboxylic acids/ phenolic O-H stretch/ N-H bending
1101	1161	-	-	-	-	-O-H stretch (2^0 Alcohol), -C-O-C- stretching
1049	1051	1044	1052	1035	-	-C-H stretch, -C-O stretch (1^0 Alcohol)
893	897	-	-	-	-	Anomeric C-H bending of cellulose
809	837	842	-	800	846	-C-H out of plane bending

The bands at 1079.82, 835.91 cm^{-1} are characteristic of carbohydrate units [126]. The bands for 3AAC at 1592cm^{-1}, MPSP at 1512 and 1387cm^{-1}, MSAPSP at 1578 and 1375cm^{-1}and APSP at 1378cm^{-1} suggests that lignin present in palm shell is still not completely depolymerised. The presence of bands at 1725cm^{-1} in the case of PAPSP, and at 1734cm^{-1} in PSP & MPSP is indicative of –C=O stretching of aromatic esters, aldehydes, ketones and acetyl derivatives.

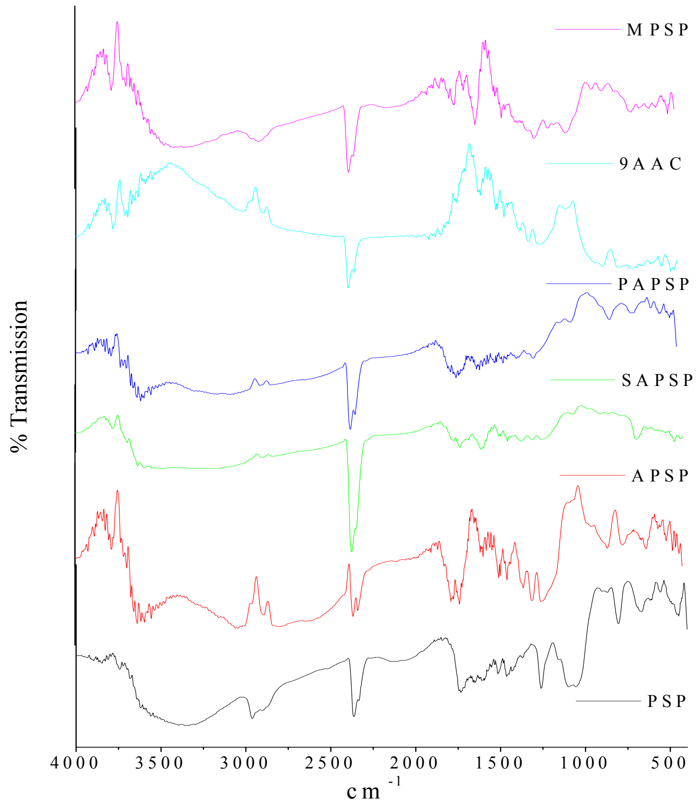

Figure 2.10. Functional group analysis using FTIR

Cyclic compounds containing conjugated C=C and C=N may be responsible for the absorption bands observed at 846 to 809 cm^{-1} except for SAPSP [117-119]. Absorption band in the region 666 to 750 cm^{-1} can be assigned to out-of-plane deformation vibrations of C-H groups located at the edges of aromatic planes [117-127, 128].The changes observed in FTIR spectra of APSP at 300^0C, 600^0C, 700^0C and 900^0C are an evidence for the formation of structures containing multiple carbon-carbon bonds as well as the elimination of originally present hydrogen and oxygen atom. The frequencies between 3200 and 3500cm^{-1} may contain stretching of both amine ($-NH_2$) and alcoholic groups (-OH) which disappears on activation to 300^0C and higher temperatures suggesting dehydration of cellulosic and ligneous components. Lignin substances in APSP, SAPSP and PAPSP show strong absorption (1510, 1460 and 1379 cm^{-1}) till a temperature of 300^0C. As the activation temperature increases from 140 to 300 to 900^0C, the peak around 1600cm^{-1} disappears showing the absence of carboxylic acid group as activation temperature increases. A similar phenomenon is seen after acid, persulphate and steam treatment.

The peak intensity of –O–H, –C=O and –C–H becomes weak or disappear with the increase of activation temperature of APSP. The results prove that the structure of activated carbons (6AAC, 7AAC and 9AAC) becomes stable due to the decomposition of functional groups with increasing activation temperature.

2.3.9. X-Ray Photoelectron Spectroscopic Analysis.

The wide scan XPS spectra of adsorbents are presented in Figure 2.11 and the corresponding binding energies with relative content of species studied are listed in Table 2.9.

Table 2.9. Summary of binding energy and area ratios of carbons

Sample Surface	Proposed components	Binding Energy(eV)	FWHM(eV)	Relative Quantity
C1s Valence State				
PSP	C-(C, H) graphitic C	284.661	2.310	0.6906
	C-(O, N, H) phenolic, alcoholic, etheric	285.984	1.774	0.1871
	C=O, O-C-O, COOR -carbonyl or quinine	287.200	2.495	0.1223
APSP	C-(C, H)	284.647	2.462	0.6716
	C-(OH, OR)	286.599	2.074	0.2112
	O=C-O	288.577	2.605	0.1172
SAPSP	C- (C, H)	284.524	2.264	0.5272
	C-(OH, OR)	286.342	1.894	0.2499
	O=C-O	288.073, 289.791	1.973, 2.181	0.1471, 0.0758
PAPSP	C-(C, H)	284.590	2.051	0.6297
	C-(OH, OR)	286.071	2.204	0.2552
	C=O, O-C-O, COOR	287.979	1.527	0.0817
	O=C-O	289.308	1.424	0.0334
9AAC	C-(C, H)	284.507	2.336	0.5552
	C-(OH, OR)	286.511	2.284	0.2822
	C=O, O-C-O, COOR	288.384	2.572	0.1155
	C=C, occluded CO, π electrons in aromatic ring, CO_2	290.295	3.464	0.0471
MPSP	C-(C, H, R), C-(C, H)	284.624	2.460	0.5456
	C-(OH, OR)	286.116, 286.346	1.718, 2.120	0.2137, 0.1311
	C=O, O-C-O, COOR O=C-O	288.517	2.491	0.1095

O1s Valence State				
PSP	C=O, C-O (Lactones, phenolic and etheric)	531.400	2.050	0.4424
	Singly bonded oxygen C-O	532.846	2.072	0.5576
APSP	C=O, C-O (Lactones, phenolic and etheric)	531.770	2.606	0.8160
	Singly bonded oxygen C-O	533.570	2.394	0.4796
SAPSP	C=O (Carboxylic acid)	532.209, 534.596	3.492, 3.517	0.8032, 0.1968
PAPSP	C=O, C-O (Carboxylic acid, etheric, lactonic, anhydrides, pyrones and phenols)	531.656 533.388	2.449 3.347	0.4576 0.5424
9AAC	C=O, C-O (Carboxylic acid, etheric, lactonic, anhydrides, pyrones and phenols)	533.080	3.389	0.8437
	Occluded CO, chemisorbed CO_2, O_2 and H_2O	535.638	3.618	0.1563
MPSP	C=O, C-O (Carboxylic acid, etheric, lactonic, anhydrides, pyrones and phenols)	531.367 532.931	2.440 2.978	0.3795 0.6205
N1S				
PSP	C-N-C (pyrrolic nitrogen, pyridines)	399.839, 398.597, 400.846	1.492, 1.512, 1.258	0.6129, 0.2141, 0.1729
APSP	C-N-C (pyrrolic nitrogen, pyridones)	399.98, 400.075	1.228, 1.468	0.3556, 0.2780
	Quartenary nitrogen, protonated pyridinic ammonium ions, nitrogen atoms replacing carbon in graphene	401.278	1.908	0.3664
SAPSP	C-N-C (pyrrolic nitrogen, pyridones)	399.797	1.366	0.3883
	Quartenary nitrogen, protonated pyridinic ammonium ions, nitrogen atoms replacing carbon in graphene	401.477	1.941	0.6118
PAPSP	C-N-C (pyrrolic nitrogen, pyridones)	398.584, 399.774	1.097, 1.319	0.2677, 0.4869
	Quartenary nitrogen, protonated pyridinic ammonium ions, nitrogen atoms replacing carbon in graphene	401.074	1.032	0.2454
9AAC	C-N-C (pyrrolic nitrogen, pyridones)	397.686, 400.803	1.516, 1.596	0.3000, 0.3745
	Oxidised nitrogen functionalities or NO_2 groups	402.300	1.639	0.3255
MPSP	C-N-C (pyrrolic nitrogen, pyridones)	398.703, 400.000	1.889, 1.679	0.2787, 0.5613
	Quartenary nitrogen, protonated pyridinic ammonium ions, nitrogen atoms replacing carbon in graphene	401.606	1.570	0.1599

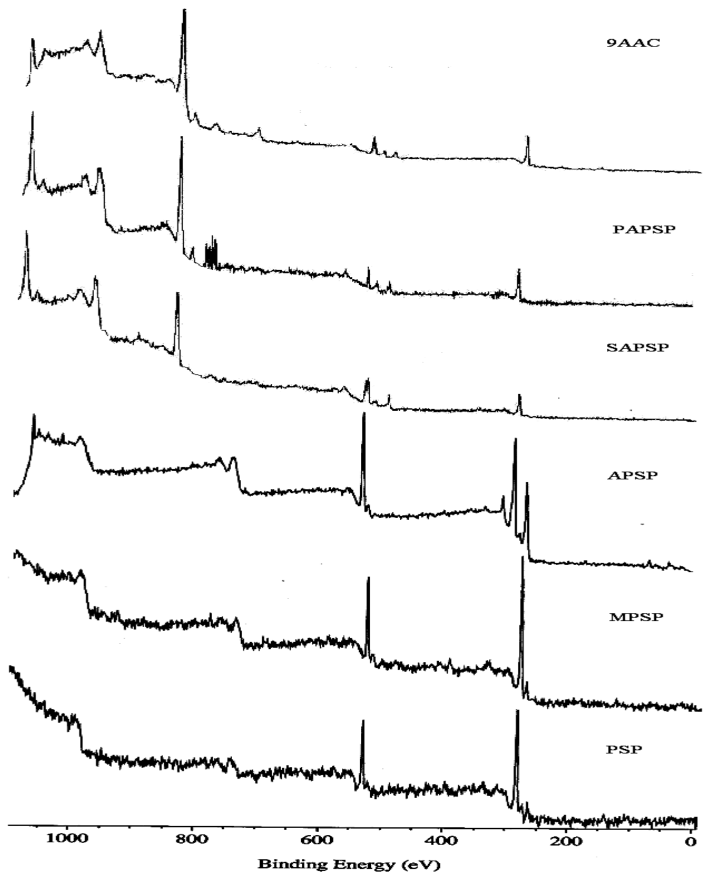

Figure 2.11. Wide scan XPS spectra of adsorbents

C1s spectra (Figure 2.12) can be deconvoluted into six components corresponding to graphitic carbon in PSP, MPSP, APSP, SAPSP, PAPSP, 9AAC (peak 1, ~284.6 eV), aliphatic or defect carbon in PSP (peak 2, ~285.1 eV), carbon in single C-O bonds as ether, alcohol, phenol in MPSP, APSP, SAPSP, PAPSP, 9AAC (peak 3, ~286.6 eV), carbon in carbonyl groups of PSP, MPSP, SAPSP, PAPSP, 9AAC (peak4,~ 287.5 eV), carbon in carboxyl or ester groups of MPSP, APSP, SAPSP, PAPSP (peak 5, ~289.3 eV) and the π-π* shake-up peak in 9AAC (peak 6, 290.6 eV). Comparison of XPS spectra with those of pure lignin and pure cellulose coupled with pyrolysis studies[127-129] have previously shown that the relatively high content of peak 1 can be attributed to the presence of fatty acid.

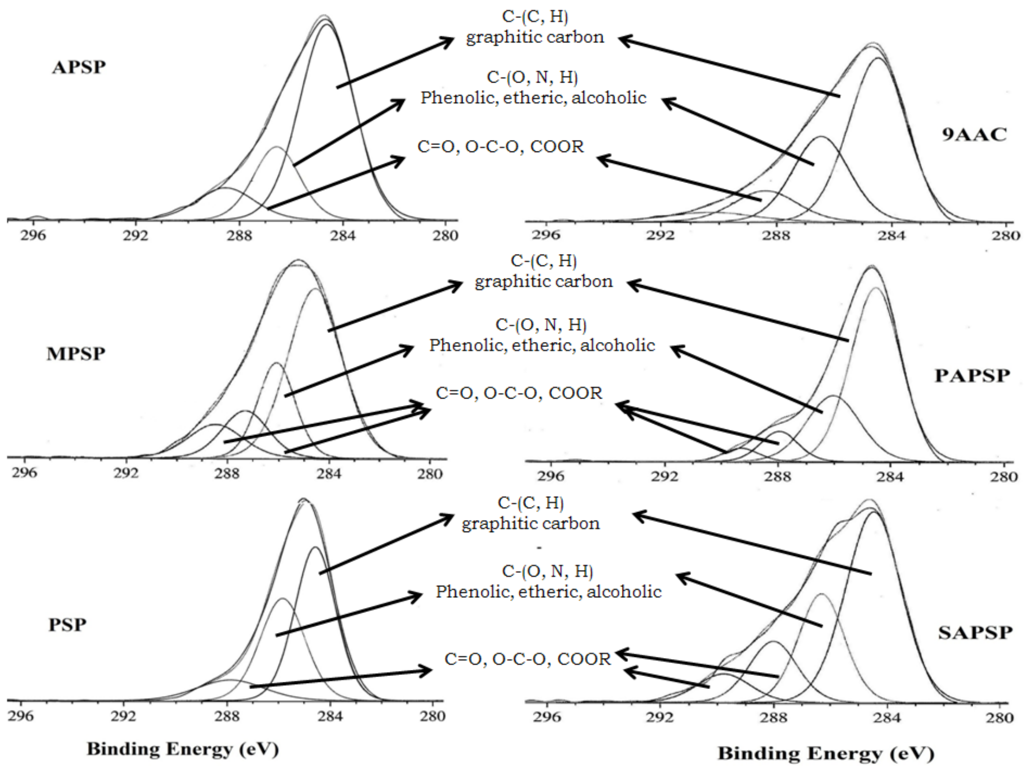

Figure 2.12. C1s XPS deconvolution spectra of adsorbents

The O1S peaks indicate two different chemical states of oxygen (Figure 2.13). The C=O and carboxyl increased for APSP, SAPSP, PAPSP, 9AAC and MPSP as compared to PSP with the maximum increase being observed for 9AAC and SAPSP. This suggested that a more stable structure was formed after modification. Peak I (531.3–531.6 eV) corresponds to C=O groups (ketone, lactone, carbonyl) MPSP, APSP, peak II (532.2– 533.0 eV) to carbonyl oxygen atoms in esters, amides, carboxylic anhydrides which is consistent with the carbon being acidic in nature and oxygen atoms in hydroxyls or ethers PSP, MPSP, SAPSP and peak III (533.9–534.5 eV) to the oxygen atoms in carboxyl groups SAPSP [130-138]. The peak for 9AAC at BE = 535.6 eV is ascribed to chemisorbed oxygen and water [130, 139].

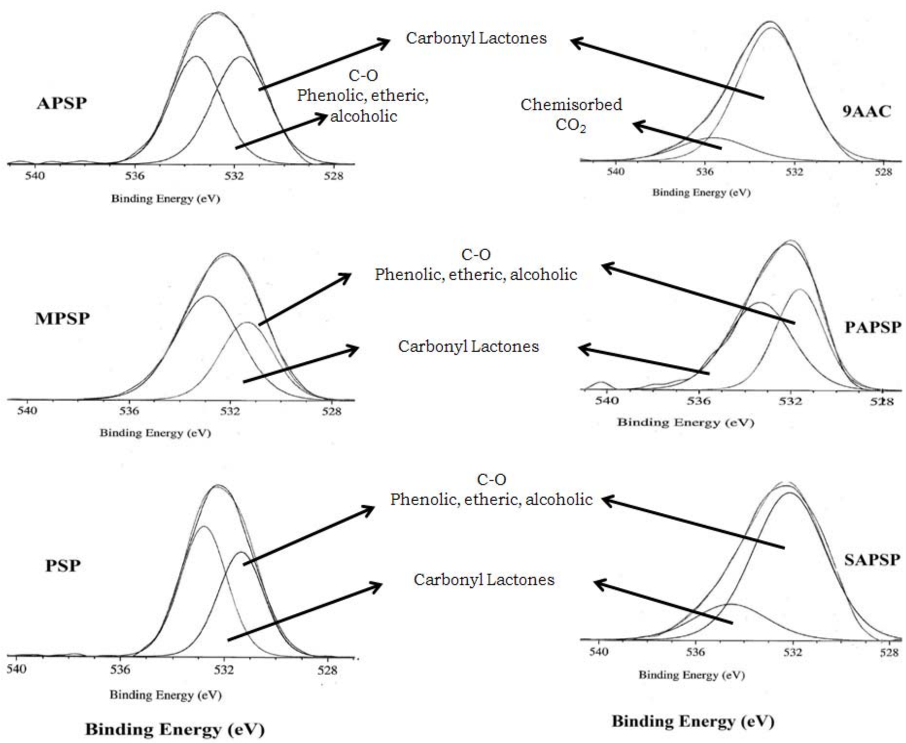

Figure 13. O1s XPS deconvolution spectra of adsorbents

The analysis of N 1S peaks for PSP, MPSP, APSP, SAPSP, PAPSP, 9AAC reveals two peaks at 400.4 and 401.0 eV which can be regarded as characteristic of pyrrolic nitrogen, pyrridones, or a mixture of both. After modification with sulphuric acid the peak becomes characteristic of quaternary nitrogen or protonated pyridinic ammonium ion [140].It was observed (Table 2.10) that PSP found possess the highest amount of phenolic or etheric group. Acid treatment leads to decreased number of phenolic groups but increased graphitic content than PSP. Further treatment with steam, persulphate and heat resulted in increased amount of oxygen containing groups which resulted due to oxidation of cellulosic ether linkages and aldehydic groups to hemicelluloses and carboxylic acid groups. The O/C ratios are seen to be in the order SAPSP~PAPSP~APSP<MPSP<PSP<9AAC.

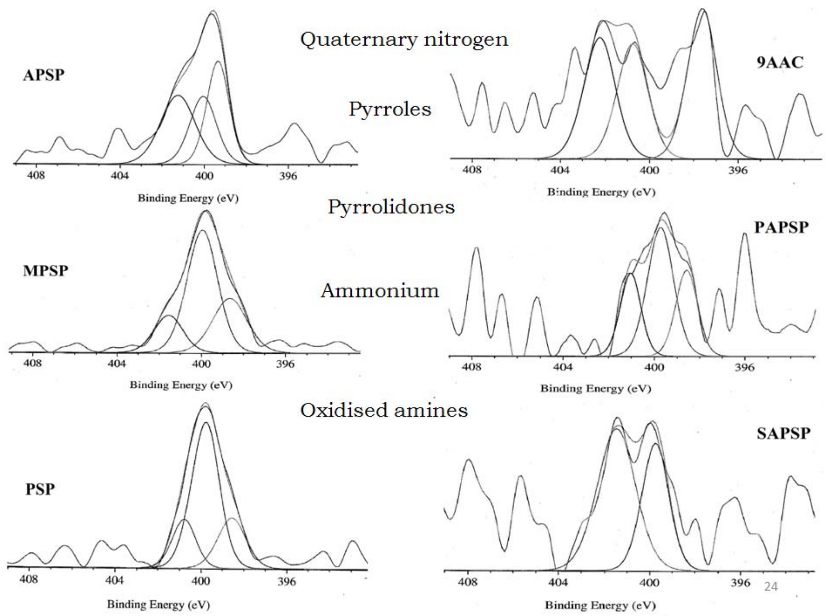

Figure 2.14. N1s XPS deconvolution spectra of adsorbents

Table 2.10. Surface concentration of C, N, O in the adsorbents

Samples	Cox/Cg	Surface concentration (from C 1s peak)%				
Native		C in graphite	Phenol-ether	Carbonyl-quinone	Carboxyl	Others
PSP	0.951	51.20	37.40	11.41	-	-
APSP	0.489	67.16	21.12	-	11.72	-
SAPSP	0.896	52.72	24.99	14.71	7.58	-
PAPSP	0.587	62.97	25.52	8.17	3.34	-
9AAC	0.801	55.52	28.22	-	11.55	4.71
MPSP	0.832	54.56	21.37	13.11	10.95	-
Native	**XPS (C, N, O)**			**O/ C ratio**		
PSP	58.00, 2.16, 39.84			0.687		
APSP	49.16, 1.17, 49.67			1.011		
SAPSP	43.79, 0.55, 55.66			1.273		
PAPSP	45.01, 0.65, 54.34			1.201		
9AAC	61.57, 0.68, 37.76			0.612		
MPSP	53.03, 1.94, 45.04			0.849		

2.3.10.Solid state-NMR Spectroscopic Analysis.

^{13}C solid state NMR spectra of free and metal loaded adsorbents was done and presented in Figure 2.15, the peaks assigned to different carbons are shown in Table 2.11.

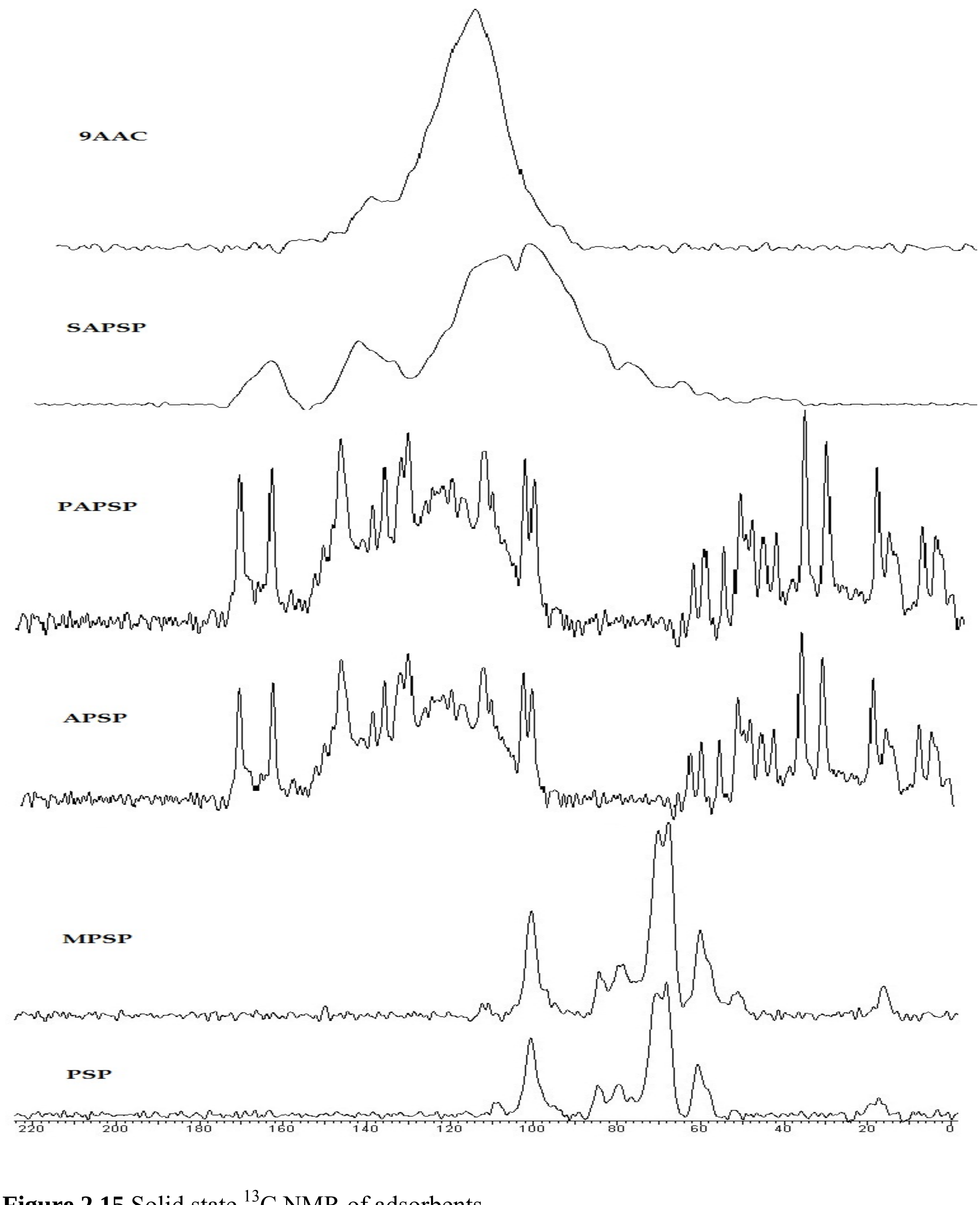

Figure 2.15. Solid state ^{13}C NMR of adsorbents

Relatively sharp signals are assigned to ordered cellulose or hemicelluloses, while broader background signals are assigned to lignin and disordered hemicelluloses [143]. For lignin, we can identify the resonance lines near 50-55 ppm associated with methoxyl groups in PSP, APSP, SAPSP, PAPSP and MPSP [135] and between 115 and 150 ppm for aromatic carbons [141, 142]; the resonance lines due to aliphatic side chains in lignin are concealed by the stronger cellulose and hemicellulose peaks.The bands due to aliphatic carbon show weak resonance in PSP and MPSP and are absent in SAPSP and 9AAC. However these bands are more pronounced in APSP and PAPSP. In particular, the peaks around 17 ppm and 172 ppm in APSP, SAPSP and PAPSP can be attributed to methyl C and carbonyl C in acetyl groups of hemicelluloses, respectively[139].

Table 2.11. Assignments to the NMR peaks

PSP	**APSP**	**SAPSP**	**PAPSP**	**9AAC**	**MPSP**	**Range**	**Assignment**
-	171	**170**	171	-		195-165	RCOO-RH (Standard oxidized cellulose) Carboxyl carbon of acetate group of hemicelluloses
-	164	**-**	163/146	-		169-140	C_6H_5O-RH Phenolic carbon
-	-	**147**	-	-		150-140	Subsituted oxygenated aromatic carbon
-	130	**-**	130	123		135-120	Non oxygenated Aromatic carbons, Aromatic acids and anhydrides
100	101	**111**	101	-	112, 101	102-108	Anomeric carbon (Anhydroglucose) C1
82	-	**-**	-	-	84, 79	81-93	Anomeric carbon (Anhydroglucose) C4 amorphous cellulose~84
60, 70	62	**-**	61, 55	-	72, 61, 52	50-70	1^0 Alcohol of (Anhydroglucose) Aliphatic C-O C2, C3, C5(~70) C6 (~60) amorphous cellulose ~62
17	48, 36, 30, 18, 6	**-**	48, 35, 31, 16, 6	-	17	5-50	Aliphatic C-C possibly of polymethylene type

The signals located at 82-85 ppm in PSP and MPSP can be attributed to C-4 in amorphous cellulose. The peaks between 71 ppm and 74 ppm in PSP and MPSP can be assigned to C-2, C-3, and C-5 in cellulose, whereas the strong peak at 102-110 ppm in PSP, APSP, SAPSP, PAPSP and MPSP can be attributed to anomeric carbon (C-1). The peaks in the region of 130–138 ppm were assigned to the ring carbons in which the ring was not substituted by strong electron donors such as oxygen and nitrogen [142]. The multiple peaks in the range of 147 ppm in SAPSP and PAPSP are due to the carbons of phenolic components, mainly the syringyl and guaiacyl units in lignin. The peak at 146 ppm can be attributed to C-4 in guaiacyl unit with free phenolic OH at C-4 [143] whose signal is strong in SAPSP and moderately strong in PAPSP [139, 144].

When thermal treatment at 900˚C is applied, the corresponding spectrum (Figure 2.15) shows a single main peak at 123 ppm with a clear loss of all aliphatic and carbonyl groups. This behaviour is rather typical for a strong aromatization/pseudo-graphitization of the material. 9AAC shows (Figure 2.15) bands from carbonyl or carboxyl carbon (190 ppm), sp^2-hybridized carbon in condensed aromatic rings in all carbons (125–143 ppm), alcohol carbon in all carbons except for 9AAC (C-O, 55–70 ppm)and aliphatic carbon in all carbons except for 9AAC (9–44 ppm). Aromatic carbon dominates the spectra for all adsorbents indicating that carbons are composed of condensed aromatic ring system. Overall, the NMR results demonstrate that while lignocellulosic structure is retained in PSP, APSP, MPSP, SAPSP and PAPSP, on the other hand 9AAC has a highly aromatic structure[145]. The changes incurred on the surface of the palm shell powder due to the various treatments are summarized in scheme 2.3.

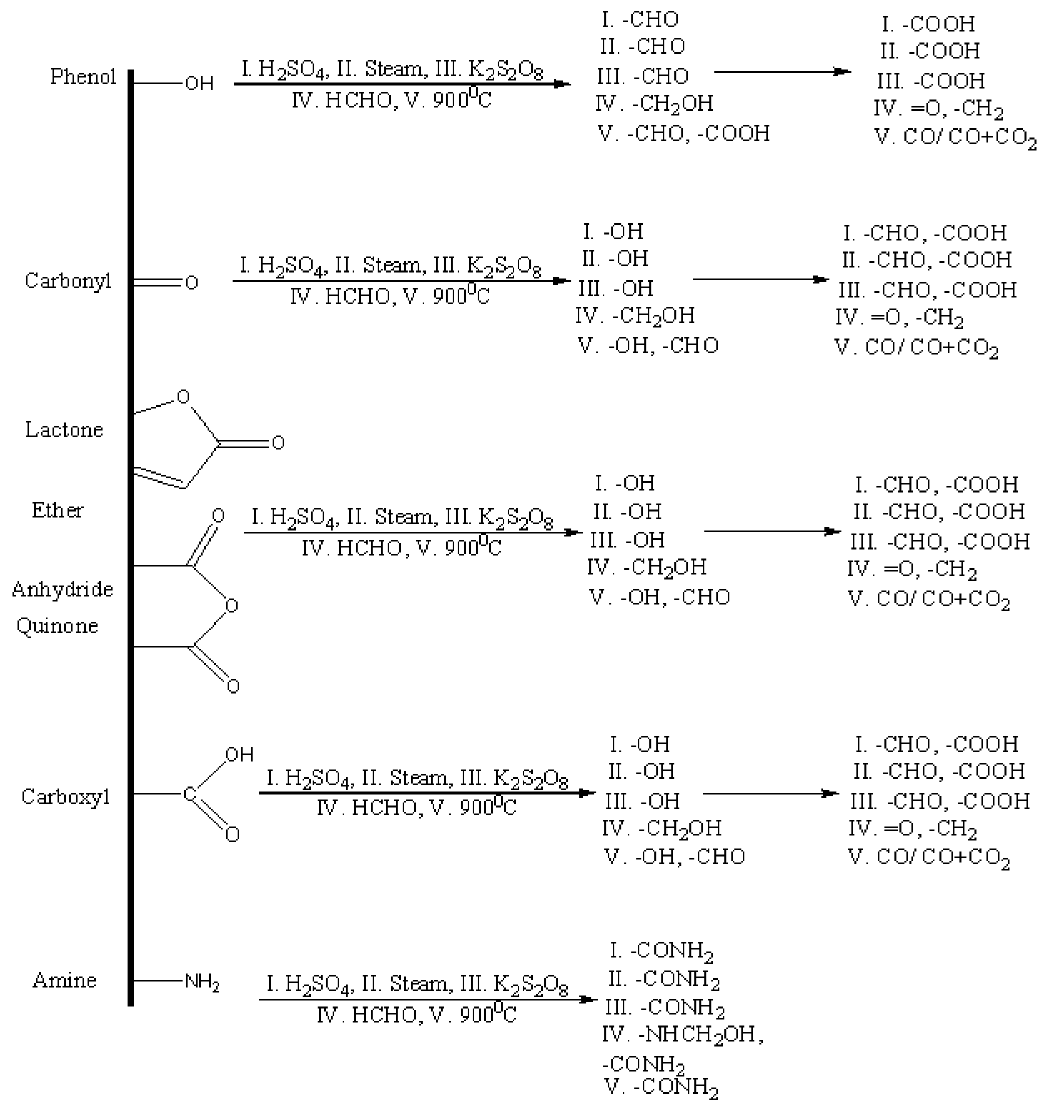

Scheme 2.3. Functional groups of virgin palm shell powder and on modification

2.4. CONCLUSIONS

A series of adsorbents were prepared (PSP, ASPS,SAPSP,PAPSP,MPSP and 9AAC) by giving mild physicochemical treatments as well as thermal activation and their physicochemical properties were compared. Evidence for the change in functional groups produced on treatment of palm shell powder using different physicochemical treatments was provided by FT-IR, XPS and NMR spectroscopic techniques as well as by potentiometric titrations. The prepared adsorbents were also characterized using thermal analysis, X-ray diffraction, nitrogen isotherms and scanning electron microscopic techniques. Potentiometric titrations suggested that all the prepared adsorbents were acidic in nature and also indicated the presence of acid groups with a wide range of pK_a values. All the materials had reasonable iodine values, with 9AAC having an iodine value of about 990 mg/g which is comparable with reported values suggesting reasonable surface areas and micro and mesoporous structures. Though the presence of micro and mesoporous structures were further evidenced by nitrogen isotherms, except for 9AAC, none of the other materials showed good surface areas. This could be probably due to condensation occurring in micropores and capillaries of mesopores which results in underestimation of surface areas. FTIR, XPS and ^{13}CNMR analyses revealed the presence of aldehydic groups along with etheric linkages of lignocellulosic moiety in higher numbers in PSP and MPSP. A small number of amino groups were present in all the adsorbents under study. Furthermore the number of oxygen containing functional groups were also found to increase with acid treatment and oxidation, the order being SAPSP>PAPSP>APSP> MPSP>PSP>9AAC. The prepared materials were found to possess interesting properties. This made us curious to study their adsorption potential for copper, cadmium, zinc, mercury, chromium and uranyl ions, the results of which are shown in chapters 3,4 and 5.

Literature Cited.

1. O. Ioannidou, A. Zabaniotou. *Renewable and Sustainable Energy Reviews.***2007**, *11*, 1966.
2. B. Corcho-Corral, M. Olivares-Marin, C. Fernandez-Gonzalez, V. Gomez Serrano, A. Macias Garcia. *Applied Surface Science.***2006,***252*, 5961.
3. M. Ahmedna, W.E. Marshall, R.M. Rao. *Bioresour. Technol.***2000,** *71*, 113.
4. A. Bhatnagar, M. Sillanpaa. *Chemical Engineering Journal.***2010,** *157*, 277.
5. F.R. Reinoso, M.M. Sabio. *Carbon.***1992,** *30*, 1111.
6. A.A. El-Hendawy, *Carbon.***2003**, *41*, 713.
7. R.M. Suzuki, A.D. Andrade, J.C. Sousa, M.C. Rollemberg. *Biores. Technol.***2007,** *98*, 1985.
8. A.A. El-Hendawy, A.J. Alexander, R.J. Andrews, G. Forrest, *J. Anal. Appl. Pyrolysis.***2008,** *82,* 272.
9. H.P. Boehm, *Carbon.* **1994**, *32*, 759.
10. J. P. Chen, S. N. Wu, K. H. Chong. *Carbon.* **2003**, *41*, 1979.
11. J. Paul Chen, W. Shunnian.*Langmuir.* **2004,** *20,* 2233.
12. E. Fitzer, K. Mueller, W. Schaefer. The chemistry of the pyrolytic conversion of organic compounds to carbon. In: P. L. Walker (Ed.), Marcel Dekker, New York. *The Chemistry and Physics of Carbon.***1971,***7*, 237.
13. Hucknall, D.J. Chemistry of Hydrocarbon Combustion, Ch. 6: Coke and Carbon Formation. *Chapman and Hall, London*. **1985,** 348.
14. I.C. Lewis.*Carbon.* **1982**,*20*, 519.
15. S.J.T. Pollard, G.D. Fowler, C.J. Sollars, R. Perry. *The Science of the Total Environment.***1992,** *116*, 31.
16. R.F. Rodriguez-Reinoso, A.L. Solano. Microporous structure of activated carbons as revealed by adsorption methods, in: P.A. Thrower (Ed.). *Chemistry and Physics of Carbon*, Marcel Dekker, New York, **1989,***116*.
17. D. Mohan, C.U. Pittman Jr. *Journal of Hazardous Materials.***2006,** *B137*, 762.
18. F. Rodriguez-Reinoso, J. Lahaye, P. Ehrburger, Editors. *Fundamental issue in control of carbon gasification reactivity, Netherland, Kluwer Academic***1991**, 533.
19. K. Tomkow, A. Jankowska, F. Chechowsk, T. Siemieniewska, *Fuel.***1977,** *56,* 266.
20. C.T. Hsieh, H. Teng, *Carbon*. **2000,** *38*, 863.

21. I. Martin-Gullon, R. Font. *Water Res*. **2001**, *35*, 516.
22. Q. Li, V.L. Snoeyink, B.J. Marinas, C. Campos. *Water Res*. **2003,** *37*, 773.
23. K. Nakagawa, A. Namba, S.R. Mukai, H. Tamon, P. Ariyadejwanich. *Water Res*. **2004,** *37*, 1791.
24. Z. Yue, J. Economy, K. Rajagopalan, G. Bordson, M. Piwoni, L. Ding, V.L. Snoeyink, B.J. Marinas. *J. Mater. Chem.***2006,** *37*, 3375.
25. S. Han, K. Sohn, T. Hyeon. *Chem. Mater.***2000,** *37*, 3337.
26. H. Tamai, T. Kakii, Y. Hirota, T. Kumamoto, H. Yasuda, *Chem. Mater*. **1996**, *8*,454.
27. A. Oya, S. Yoshida, J. Alcaniz-Monge, A. Linares-Solano. *Carbon.***1995,** *33*, 1085.
28. T. Kyotani, T. Nagai, S. Inoue, A. Tomita, *Chem. Mater.***1997**, *9*, 609.
29. S. Han, T. Hyeon. *Chem. Commun.***1999,** *19*, 1955.
30. Z. Li, M. Jaroniec. *J. Am. Chem. Soc.***2001,** *123*, 9208.
31. L. Lee, S. Yoon, S.M. Oh, C. Shin, T. Hyeon. *Adv. Mater.***2000**, *123*, 359.
32. M. Smisek, S. Cerny. *Active Carbon: Manufacture, Properties and Applications*. *Elsevier, London* **1970.**
33. T. Wigmans. *Carbon***1989**, *27(1)*, 13.
34. R.P. Bansal, J. P. Donner, F. Stoeckli. *Active Carbon. Marcel Dekker, New York***1988**.
35. J. L. Figueiredo, M. F. R. Pereira, M. M. A. Freitas, J. J. M. Orfao. *Carbon.* **1999**, *37*, 1379.
36. C. A. Toles, S. Rimmer, J. C. Hower. *Carbon.* **1996**, *34*, 1419.
37. C. A. Toles, W. E. Marshall, M. M. Johns. *Carbon.* **1997**, *35*, 1407.
38. B. S. Girgis, M. F. Ishak, *Mater. Lett.* **1999**, *39*, 107.
39. A. Dandekar, R. T. K. Baker, M. A. Vannice. *Carbon.***1998**, *36*, 1821.
40. V. Gomez-Serrano, M. Acedo-Ramos, A. J. Lopez-Peinado, C. Valenzuela-Calahorro. *Fuel* **1994**, *73*, 387.
41. J. S. Noh, J. A. Scharwz. *Carbon.* **1990**, *28*, 675.
42. V. Gomez-Serrano, M. Acedo-Ramos, A. J. Jopez-Peinado, C. Valenzuela-Calahorrro. *Thermochim. Acta.* **1997**, *291*, 109.
43. M. Mazet, B. Farkhani, M. Bauhu. *Water Res*. **1994**, *28*, 1609.
44. T. Otowa, Y. Nojima, T. Miyazaki. *Carbon.***1997,** *35 (9)*, 1315.
45. D. R. Preston, G. Bitton, S. R. Farrah. *Appl. Environ. Microb.* **1990**, *56*, 295.
46. R. Gajardo, J. Diezs, J. Jofre, A. Bosch. *J. Virol. Methods.* **1991**, *31*, 345.

47. F. Julien, M. Baudu, M. Mazet. *Water Res*. **1998**, *32*, 3414.
48. F. Rodriguez-Reinoso. Preparation and characterisation of activated carbons. In: Proceedings of the NATO Advanced Study Institute on Carbon and Coal Gasification. *NATO ASI Series E, MartinusNijhoff Publishers, Netherlands*, **1986**,*105*, 603.
49. H. Marsh, B. Rand. *Carbon*. **1971**,*9*, 47.
50. F. Kapteijn, J.A. Moulijn. Kinetics of catalysed and uncatalysed coal gasification. *In: Proceedings of the NATO Advanced Study Institute on Carbon and Coal Gasification, NATO ASI Series E, MartinusNijhoff Publishers, Netherlands*, **1986**, *105*, 291.
51. P.L. Walker, Carbon gasification- A ubiquitous reaction of great importance to mankind. *In: Proceedings of the NATO Advanced Study Institute on Carbon and Coal Gasification, NATO ASI Series E, MartinusNijhoff Publishers, Netherlands*, **1986**, *105*, 3.
52. A. A. Lizzio, H. Jiang, L. R. Radovic. *Carbon.***1990**, *28(1)* 97.
53. G. De la Puente, J. J. Pis, J. A. Menendez, P. Grange. *J. Anal. Appl. Pyrolysis.* **1997**, *43*, 125.
54. S. Shin, J. Jang, S. H. Yoon, I. Mochida. *Carbon.* **1997**, *35*, 1739.
55. J. Pastor-Villegas, V. Gomez-Serrano, C. J. Duran-Valle, F. J. Higes- Rolando. *J. Anal. Appl. Pyrolysis.* **1999**, *50*, 1.
56. J. A. Menendez, E. M. Menendez, M. J. Iglesias, A. Garcia, J. J. Pis. *Carbon.* **1999**, *37*, 1115.
57. J.S. Mattson, H.B. Mark Jr., *Activated Carbon, Marcel Dekker,NewYork*, 1971.
58. T. Van der Plas. The Texture and the Surface Chemistry of Carbons. *Physical and Chemical Aspects of Adsorbents and Catalysis* (B. G. Linsen, Ed.), Academic Press, London, **1970.**
59. J. S. Mattson, H. B. Mark, Acfivared Carbon: Surface Chemistry and Adsorption from Solufion*. Marcel Dekker, Inc., New York,* **1971**.
60. M.O. Corapcioglu, C.P. Huang. *Water Res.***1987**, *21*, 1031.
61. V. A. Garten, D. E. Weiss, J. B. Willis. *Au&. J. Chem.***1957**,*10*, 285.
62. J.R. Perrich. Activated Carbon Adsorption for Wastewater Treatment. *CRC Press*, **1981**.
63. N.R. Bishnoi, M. Bajaj, N. Sharma, A. Gupta. *Biores. Technol.***2004**, *91*, 305.
64. V.K. Garg, R. Gupta, R. Kumar, R.K. Gupta. *Biores. Technol.* **2004**, *92*, 79.
65. A. Dhaouadi, L. Monser, N. Adhoum. *J. Hazard. Mat.***2010**, *181*, 692.
66. A. Ozer, H.B. Pirinc. *J. Hazard. Mat.***2006**, *B137*, 849.
67. Suhas, P.J.M. Carrott, M.M.L. RibeiroCarrott. *Bioresour. Technol.***2007**, *98*, 2301.
68. A. Arulanantham, N. Balasubramaniam, T.V. Ramakrishna. *Metal Finishing.* **1989**, *87*, 51.

69. S. J. Park, B. J. Park, S. K. Ryu. *Carbon.* **1999**, *37*, 1223.
70. C. A. Toles, W. E. Marshall, M. M. Johns. *Carbon.* **1999**, *37*, 1207.
71. M. R. Mostafa. *Adsorpt. Sci. Technol*. **1997**, *15*, 551.
72. S. Biniak, M Pakula, G. S. Szymanski, A. Swiatkowski. *Langmuir.* **1999**, *15*, 6117.
73. ASTM, Standard Test Method for Determination of Iodine Number of Activated Carbon. *ASTM Committee on Standards, ASTM: Philadelphia, PA, USA*, **2006,** 4607.
74. A. Aziz, M.S. Ouali, E.H. Elandaloussi. J. Hazard. Mater. **2009**, *163*, 441.
75. P. Galiatsatou, M. Metaxas, V. Kasselouri-Rigopoulou J. Hazard. Mater. **2002**, *B91*, 187.
76. R. Baccar, J. Bouzid, M. Feki, A. Montiel. J. Hazard. Mater. **2009**, *162*, 1522.
77. P.R.F. Campos, M.Sc. Dissertation. *Departamento de EngenhariaQuimica, UEM*. **1996**, 1.
78. P. Brassard, J.R. Kramer, P.V. Collins.*Environ. Sci. Technol.***1990**, *24*, 195-201.
79. S. Brunauer, P. H. Emmett, E. Teller. *J. Am. Chem. Soc.***1938**, *60*, 309.
80. C. Naizhen, H. Darmstadt, R. Christian. *Energy & Fuels.***2001**, *15*, 1263.
81. D.K. Chattopadhyay, B. Sreedhar, V.S.N. KothapalliRaju. *Ind. Eng. Chem. Res.***2005**, *44*, 1772.
82. V. H. Pan, G. E. Maciel. *Fuel.***1993**, *72*, 451.
83. K. Kidena, s. Murata, M. Nomura. *Energy fuels.***1996,** *10*, 672.
84. M. M. Maroo-valer, J. M. Rocha, C. E. Snape. *Fuel*. **1996**, *75*, 1721.
85. J. M. Andresen, Y. Martin, S. R. Moinelo, M. M. Maroto-Valer, C. E. Snape. *Carbon.***1998**, 36, 1043.
86. H. A. Resing, D. K. C. Hodgeman, J. A.Baker, E. J. Poziomek. *Carbon*. **1985**, *23*, 395.
87. J. C. C. Freitas, T. J. Bonagamba, F. G. Emmerich. *Energy fuels.***1999**, *11*, 53.
88. H. Eckert, Y. A. Levendis, R. C. Flagan. *J Phys. Chem.* **1988**, *92*, 5011.
89. H. Pan, M. Pruski, B. C. Gemstein, F. Li, J. S. Lanin. *Phys. Rev. B.***1991**, *44*, 6741.
90. Y. Maniwa, M. Sato, K. Kume, M. E. Kozlov, M. Tokumoto. *Carbon*. **1996**, *34*, 1287.
91. K. Gergova, N. Petrov, V. Minkova, *J. Chem. Technol. Biotechnol.***1993**, *56*, 77.
92. P.A. Bazuła, A.H. Lu, J.J. Nitz, F. Schuth. *Microporous and Mesoporous Materials.***2008**, *108*, 266.
93. K. Gergova, N. Petrov, S. Eser. *Carbon.***1994**, *32*, 693.
94. L. Krisztina, B. Attila, G.N. Lajos, *Carbon.***2000**, 38, 1965.

95. J.P. Fraissard. Physical adsorption: experiment, theory, and applications, NATO ASI series *Kluwer Academic Publishers***1996**, 9.
96. F.R. Reinoso, A.L. Solano. Chemistry and Physics of Carbon, *P.A. Thrower, Marcel Dekker, New York*, **1989**, *21,* 1.
97. S.J. Gregg, K.S.W. Singh. Adsorption surface area and porosity. *New York: Academic press***1982**, 303.
98. T. Ohba, K. Kaneko. *Langmuir.***2001**, *17*, 3666.
99. M.J. Remy, G. Poncelet. *J. Phys. Chem.* **1995**, *99*, 773.
100. D. Adinata, M.A.W.D. Wan, M.K. Aroua. *Biores. Technol.***2007**, *98*, 145.
101. S. Ismadji, S.K. Bhatia. *Langmuir.***2000**, *16*,9303.
102. S. Ismadji, S.K. Bhatia. *Langmuir.***2001**, *17*, 1488.
103. P.T. Williams, A.R. Reed. *J. Anal. Appl. Pyroly*. 2003, *70,* 563.
104. F. Stoeckli, A. Guillot, A. M. Slasli, D. Hugi-Cleary. *Carbon.***2002**, *40*, 211.
105. N.A. Khan, S. Ibrahim, P. Subramaniam. *Malaysian J. Sci.***2004**, *23*, 43.
106. K. Kadirvelu, M. Kavipriya, C. Karthika, M. Radhika, N. Vennilamani, S. Pattabhi. *Bioresource Technol.***2003**, *87*, 129.
107. H. Demiral, I. Demiral, F. Tümsek, B. Karabacakoglu. *Chem. Eng. J.***2008**, *144*, 188.
108. D. Mohan, K.P. Singh, *Wat. Res.***2002**, *36*, 2304.
109. A.A. Abia, M. Horsfall Jr., O. Didi. *Bioresour. Technol*. **2003**, *90*, 345
110. M. Koyama, W. Helbert, T. Imai, J. Sugiyama, B. Henrissat. *Proc. Natl. Acad. Sci. U.S.A*. **1997**, *94*, 9091.
111. K. Marco, S.N. Peter, G.J. Mark, K. Markus. *Environ. Sci. Technol.***2010**, *44*, 1247.
112. Wentao Huang, Hao Zhang, Yaqin Huang, Weikun Wang, Shaochen Wei, *Carbon.***2011**, *49*, 838.
113. A.K. Kercher, D.C. Nagle, *Carbon.***2003**, *41*, 15.
114. O. Paris, C. Zollfrank, G.A. Zickler, *Carbon.***2005**, *43*, 53.
115. T.J. Bandosz, J. Jagiello, C. Contescu, J.A. Schwarz. *Carbon.* **1993**, *31*, 1193.
116. C.M. Castilla, M.V. Lopez-Ramon, F. Carrasco-Marin.*Carbon.* **2000**, *38*,1995.
117. B.J. Meldrum, C.H. Rochester. *J. Chem. Soc. Faraday Trans.***1990**, *86*, 1881.
118. B.J. Meldrum, C.H. Rochester, J. Chem. Soc. *Faraday Trans.***1990**, *86*, 861.

119. G. Socrates. Infrared Characteristic Group Frequencies, 2nd Edn. *John Wiley and Sons,* Chichester**1994**,50.
120. P.E. Fanning, M.A. Vannice. *Carbon.* **1993**, *31*, 721.
121. B.J. Meldrum, C.H. Rochester. *J. Chem. Soc. Faraday Trans*. **1990**, *86*, 2997.
122. B.J. Meldrum, C.H. Rochester. *J. Chem. Soc. Faraday Trans*. **1990**, *86*, 3647.
123. M. Nakahara, S. Asai, Y. Sanada, T. Ueda. *J. Mater. Sci.*, **1995**, *30*,5667.
124. M. Nakahara, Y. Sanada. *J. Mater. Sci.* **1995**, 30 4363.
125. J. Zawadzki. Chemistry and Physics of Carbon. Ed. P. A. Thrower. *'Marcel Dekker, New York*. **1989**, *21*, 147.
126. L. Dupont, E. Guillon. *Environ. Sci. Technol*. **2003**, *37*, 235.
127. S. Biniak, G. Szymanski, J. Siedlewski, A. Swiatkowski. *Carbon.***1997**, *35*, 1799.
128. A. Gauthier, S. Derenne, L. Dupont, E. Guillon, C. Largeau, J. Dumonceau, M. Aplincourt. *Anal. Bioanal. Chem*. **2002**, *373*, 830.
129. H. Darmstadt, C.Roy. *Carbon.* **2003**, *41*, 2653.
130. H. Chen, A. Wang. *J. Hazard. Mater.***2009**, *165*, 223.
131. S. Qaiser, A. R. Saleemi, M. Umar. *J. Hazard. Mater.***2009**, *166*, 998.
132. G. Gilardi, L. Abis, A. E. G. Cass. *Enzyme Microb. Technol.***1995**, *17*, 286.
133. K. Laszlo, E. Tombacz, K. Josepovits. *Carbon.***2001**, *39*, 1217.
134. K. K. Pandey. *J. Appl. Polym. Sci.* **1999**, *71*, 1969.
135. W. L. Earl, D. L. VanderHart. *J. Am. Chem. Soc.***1980**, *102*, 3251.
136. P. T. Larsson, K. Wickholm, T. Iversen. *Carbohydrate Res.***1997**, *302*, 19.
137. L. Huang, T. Boving, B. S. Xing. *Environ. Sci. Technol.* **2006**, *40*, 3279.
138. C. M. Popescu, P. T. Larsson, C.Vasile. *Carbohyd. Polym.***2011**, *83*, 808.
139. J. C. C. Freitas, T. J. Bonagamba, F. G. Emmericha. *Carbon.***2001**, *39*, 535.
140. W. S. Wan Ngah, M. A. K. M. Hanafiah. *J. Environ. Sci.* **2008**, *20*, 1168.
141. A. E. Ofomaja, E. B. Naidoo, S. J. Modise. *J. Hazard. Mater.***2009**, *168*, 909.
142. V. K. Gupta, A. Rastogi. *J. Hazard. Mater.***2008**, *152*, 407.
143. L. Huang, Z. Ou, T. B. Boving, J. Tyson, B. Xing. *Chemosphere.***2009**, *76*, 1056.
144. K. Srividya, K. Mohanty. *Chem. Eng. J.* **2009**, 155, 666.
145. M. Schnitzer, C. M. Preston. *Plant Soil.***1983**, *75*, 201.

Chapter 3

Mechanistic and Spectroscopic study for adsorption of Cd^{+2}, Zn^{+2}, Cu^{+2} and Hg^{+2} onto the adsorbents prepared from Palm Shell Powder

Outline:

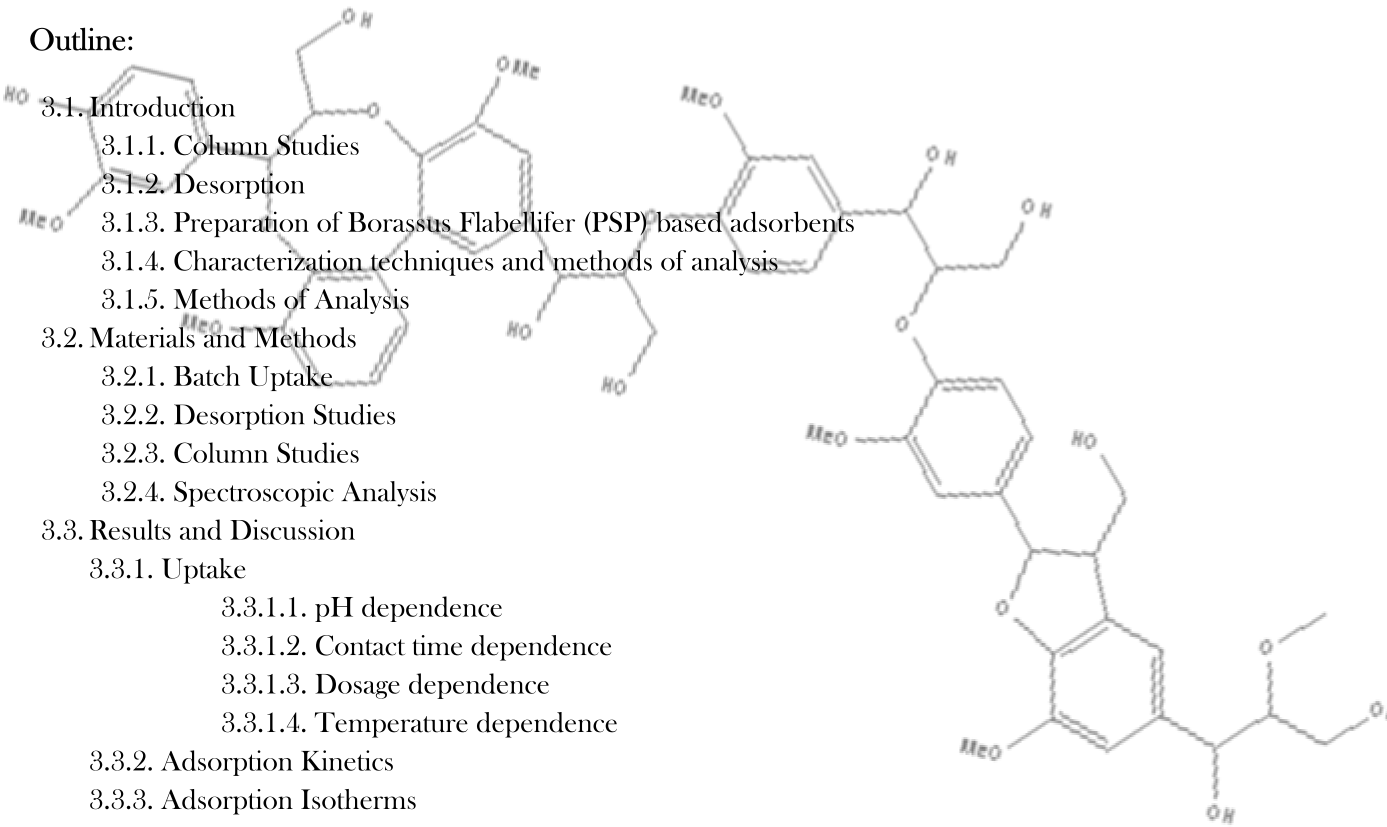

3.1.Introduction

The utilization of agro waste based adsorbents for the removal of Cu, Cd, Zn and Hg from industrial waste waters and polluted waters has been already recognized (Chapter 1). The biomass has to satisfy the following requirements to be considered as an adsorbent [1]: (1) the efficient and rapid uptake and release of metals, (2) the low production cost of the biosorbent and possibility of its reutilization, (3) the efficient, rapid, and cheap separation of the biosorbent from the solution, and (4) a high selectivity of metal adsorption and desorption. If they are fulfilled, the utilization of the material under study would make the adsorbent more attractive compared to other available adsorbents.

Agricultural by-products usually are composed of lignin and cellulose as major constituents and may also include other polar functional groups of lignin, which includes alcohols, aldehydes, ketones, carboxylic, phenolic and ether groups. These groups have the ability to bind heavy metals by the replacement of hydrogen ions for metal ions in solution or by donation of an electron pair from these groups to form complexes with the metal ions in solution.

Spectroscopic techniques have been a valuable aid in determining functional groups that are responsible for metal binding to *adsorbents.* FT-IR and XPS provide good insight into adsorption process at the molecular level as reported in the literature [2-5]. They have been adopted to identify the major functional groups of adsorbents and elucidate their interactions with metal ions. Both techniques,however, cannot provide a quantitative description of the sorption process, which is important in the design and engineering of treatment systems. Nonetheless, they are essential to provide evidence to further support the formation of mathematical models[6].

Although a considerable amount of research has been carried out on the adsorption of a range of metals bymany materials, studies that have focused upon most of the toxic metals using a single adsorbent are rare.Despite the extensive range of materials that have been shown to exhibit adsorptive ability for a range of sorbates, there is still comparatively little understanding of the mechanisms of adsorption.Previous studies have revealed that biosorption of metals is a complex process that is based upon a range of mechanisms that differ both quantitatively and qualitatively according to the type of biosorbent, the degree of processing it has undergone, and also the targeted metal ion. These different mechanisms caninclude ion exchange, chelation, adsorption by physical forces, and intraparticle diffusion [7].A different retention mechanism investigated recently is the amalgamationof Hg(II) on mossy tin filters [8].

Proper analysis and design of adsorption/biosorption separation processes requires relevant adsorption/biosorption equilibria as one of the vital information. In equilibrium, a certain relationship prevails between solute concentration in solution and adsorbed state (i.e., the amount of solute adsorbed per unit mass of adsorbent). Their equilibrium concentrations are a function oftemperature. Therefore, the adsorption equilibrium relationship at a given temperature is referred as adsorption isotherm. Several adsorption isotherms originally used for gas phase adsorption areavailable and readily adopted to correlate adsorption equilibria in heavy metals biosorption. Some well-known two parameter models are summarized in Table 3.1.

Predicting the rate at which adsorption takes place for a given system is probably the most important factor in adsorption system design, with adsorbate residence time and the reactor dimensions controlled by the system's kinetics. A number of adsorption processes for pollutants have been studied in an attempt to find a suitable explanation for the mechanisms and kinetics for sorting out environment solutions. In order to investigatethe mechanisms of adsorption, various kinetic models have been suggested. In recent years, adsorption mechanisms involving kinetics-based models have been reported [9]. Numerous kinetic models have described the reaction order of adsorption systems based on solution concentration.

Table 3.1. Common isotherm and kinetics models

Model	Assumptions/comments	Ref.
ISOTHERMS		
Two parameter models		
Langmuir $$\frac{q_e}{q_m} = \frac{K_L C_e}{1 + K_L C_e}$$	The Langmuir theory is valid for monolayer adsorption onto a surface containing a finite number of identical sites. Langmuir model for isotherm modeling were unsuccessful in the low concentration. Q_m and K_L represent maximum adsorption capacity and energy of adsorption; $0<R_L$ (separation factor)<1 implies favorable adsorption; R_L values indicate the type of isotherm to be irreversible ($R_L = 0$), favorable ($0 < R_L < 1$), linear ($R_L = 1$) or unfavorable ($R_L>1$). Represents boundary layer diffusion of solute molecules; Uniform energies of adsorption onto the surface and no transmigration of the adsorbate in the plane of the surface. Based on the film resistance and homogeneous solid phase. Two site Langmuir - Presence of two different types of sites (hydrophobic and hydrophillic) on adsorbent favors the applicability of two site model.	[15, 16]

Freundlich $$q_e = K_f C_e^{1/n}$$	High values for K_f shows high adsorption capacity; Heterogeneous adsorbent and multilayer adsorption and the adsorption capacity is related to the concentration of adsorbate at equilibrium. The constant n is the empirical parameter related to the intensity of adsorption, which varies with the heterogeneity of the material. To describe heterogeneous systems 1/n values indicate the type of isotherm to be irreversible (1/n = 0), favorable (0 < 1/n < 1) and unfavorable (1/n>1) shows the adsorption capacity of an adsorbent, The adsorption process occurs on the heterogeneous surfaces. If the n is below one, then the adsorption is chemical process; otherwise, the adsorption is physical process.	[17]
Temkin $$\frac{q_e}{q_m} = \frac{R_T}{\Delta Q}\mathrm{Ln}(K_T C_e)$$	Parameters from Temkin model describes The heat of adsorption of all the molecules in the layer decreases linearly with coverage due to adsorbent–adsorbate interactions, and that the adsorption is characterized by a uniform distribution of binding energies, up to some maximum binding energy; K_T equilibrium constant corresponds to maximum binding energy and B1 is related to heat of adsorption.	[18]
Flory Huggins $$\mathrm{Log}\frac{\theta}{C_0} = \mathrm{Log}K_{FH} + n_{FH}\mathrm{Log}(1-\theta)$$	Account for the degree of surface coverage characteristics of the sorbate on the sorbent.	[19-21]
Elovich $$\frac{q_e}{q_m} = K_E C_e exp^{-\left(\frac{q_e}{q_m}\right)}$$	The Elovich model is based on a kinetic development according to the hypothesis that the adsorption sites increase exponentially with adsorption, involving multi-layered adsorption.	[22]
Dubinin-Radushkevich $$\frac{q_e}{q_m} = \exp(-\beta\varepsilon^2)$$ With $\beta = \frac{1}{E^2}$ and $\varepsilon = RT\mathrm{Ln}\frac{C_s}{C_e}$	Dubinin and his co-workers conceived this equation for subcritical vapors in micropore solids where the adsorption process follows a pore filling mechanism onto energetically non-uniform surface.	[23]
Halsey $$q_e = K_H / C_e^{1/n_H}$$	Halsey proposed an expression for condensation of a multilayer at a relatively large distance from the surface.	[24]
KINETICS		
Pseudo 1st order $$\frac{dq}{dt} = K_i(q_e - q_t)$$	Generally do not fit well in whole range of contact time, only follows in initial stage of sorption. The adsorbate uptake, *q*, increases with increasing the initial concentration.	[25]
Pseudo 2nd order $$q_t = \frac{q_e^2 K_2 t}{1 + q_e K t}$$	The adsorption rate of adsorbate depends on the concentration of adsorbate at the absorbent surface. Mechanism being the rate controlling step, involve valency forces through sharing or exchange of electrons between adsorbate and adsorbent. Kinetic performance is proportional to the adsorption rate. Based on the sorption equilibrium capacity. The adsorption process and the overall rate of the adsorption process appears to be controlled by the chemical reaction. Chemisorption significantly contribute to the adsorption process	[26]
Intraparticle $$q_t = K_i t^{0.5}$$	Commonly used to identify the steps involved in adsorption. If it passes through origin it infers the applicability of intraparticle diffusion whereas presence of intercept shows the surface adsorption/ boundary layer effects. Adsorption is said to be intra-particle diffusion controlled if the reaction sites are internally located in the porous adsorbents and the external resistance to diffusive transport process is much less than the internal resistance.The term k_{dif} calculated from the slope is indicative of an enhancement in the rate of adsorption. The value of *C* from intercept gives an idea about the boundary layer thickness. Adsorption is said to be intra-particle diffusion controlled if the reaction sites are internally located in the porous adsorbents and the external resistance to diffusive transport process is much less than the internal resistance.	[27-29]
Elovich model	Considers that the rate-controlling step is the diffusion of the	[30-32]

$$q_t = \frac{1}{\beta}\mathrm{Ln}(\alpha\beta) + \frac{1}{\beta}\mathrm{Ln}t$$	adsorbate molecules. The Elovich equation describes chemisorption.	
Liquid film diffusion model $$\frac{q_t}{q_e} = 1 - \frac{6}{\pi^2}\exp(-Bt)$$ $$\mathrm{Ln}(1-F) = -K_{fd}t$$	Determines whether the main resistance to mass transfer is in the thin film (boundary layer) surrounding the adsorbent particle, or in the resistance to diffusion inside the pores. Applicable when flow of the reaction from the bulk liquid to the surface of the adsorbent determines the rate constant.	[33]
Bangham $$\mathrm{LogLog}\left(\frac{C_0}{C_0 - q_t m}\right) = \mathrm{Log}\left(\frac{K_m}{2.303V} + \propto \mathrm{Log}t\right)$$	Applicability of the Bangham equation indicates that diffusion of adsorbate into the pores of adsorbent is importantly controls the adsorption process. It is a pore diffusion controlled process.	[34]
Column Models		
Thomas Model $$ln\left(\frac{C_0}{C} - 1\right) = \frac{K_T q_0 m}{Q}$$	This model assumes plug-flow behaviour in the bed and uses the Langmuir isotherm for equilibrium and second-order reversible reaction kinetics. It assumes a constant separation factor but is applicable to both favorable and unfavorable sorption conditions. This model is suitable for sorption processes in which external and internal diffusion limitations are absent.	[11]
Yoon and Nelson Model $$\ln\left(\frac{C}{C_0 - C}\right) = k_{YN}t - t_{0.5}k_{YN}$$	Relatively simple model based on the assumption that the rate of decrease in the probability of sorption for each sorbate molecule is proportional to the probability of sorbate sorption and sorbate breakthrough on the sorbent.	[12]
Wolborska Model $$\ln\frac{C}{C_0} = \frac{\beta C_0}{N_0}t - \frac{\beta Z}{U}$$	Wolborska deduced the following relationship for describing the concentration distribution in a bed for the low-concentration range of the breakthrough curve.	[14]

3.1.1.Column studies.

Batch operations are very easy to apply in the laboratory study, but less convenient forfield applications. The sorption capacity of the sorbent, obtainedfrom batch equilibrium experiments, is useful in providing fundamentalinformation about the effectiveness of metal–sorbentsystem. However, this data may not be practically applicable tomost of the treatment systems (such as continuous modes) wherecontact time is not sufficient for the attainment of equilibrium.Thus, it is necessary to ascertain the practical applicability of the adsorbent in fixed bed column modes. Fixed-bed adsorption isused to determine the experimental breakthrough curve. Several models have been reportedfor predicting the breakthrough performance in fixed-bed sorption[10-14].

3.1.2.Desorption.

Desorption studies are important to investigate the possibility for the recovery of metals adsorbed on the adsorbent surface, as well as for the regeneration of the adsorbent for subsequent reuse. It also gives a hint about the mechanism of ineraction between the adsorbent and adsorbate. For instance, if acid medium employed for recovery, protons appear to compete with the metal ions and displace them from the adsorbent's surface, suggesting that adsorption of metal ions involve mainly ion-exchange mechanisms. On the other hand if a complexing agent like EDTA is effective, it suggests a complexation mechanism of interaction between adsorbent and adsorbate. The main objective will be:

i) To investigate the copper,cadmium, zinc and mercury removal efficiency and adsorption capacity of the adsorbents which had been prepared and characterized as described in chapter 2 (PSP,APSP,SAPSP,PAPSP,9AAC and MPSP).

ii) To study the effects of adsorbent dosage, pH, contact time, adsorbate concentration, and solution temperature.

iii) To determine and discuss the thermodynamic parameters and kinetic data, equilibrium isotherms by using the models described in Table 3.1.

iv) To obtainstructural as well as analytical information about the metalbiomass interactions, through Fourier transform infrared (FTIR)and the X-ray photoelectron (XPS) spectroscopic techniques

v) To perform desorption experiments to determine the feasibility of reusing the adsorbents under study vi) study the performance of the adsorbents in flow through columns experiments

3.2. Materials and Methods

3.2.1. Batch Uptake.

Stock solutions of Cu^{2+}, Cd^{2+}, Zn^{2+} and Hg^{2+} was prepared by dissolving 3.84, 2.77, 4.59 and 1.36 g of copper nitrate, cadmium nitrate, zinc nitrate and mercuric chloride (E-Merck) in slightly acidified double distilled water and making upto 1L to give 1000 mg/L of Cu^{2+}, Cd^{2+}, Zn^{2+} and Hg^{2+} solutions respectively. Working standards were prepared by diluting different volumes of the stock solution to obtain the desired concentration.

Batch adsorption experiments were conducted at 30°C by agitating 0.1 g of adsorbent with 25mL of respective metal ion solution of desired concentration maintained at pH 6.0 (except for pH experiments) in 100mL stoppered conical flasks in a thermostated rotary mechanical shaker at 180 rpm for 4 hours (except for the contact time experiments) at 30 °C. Experiments were done to determine the pH range at which the maximum metal uptake would take place on the adsorbents under study by varying the initial pH of the solution in the range 1 to 10 (except copper i.e. pH 1-5) using 0.1 N NaOH and/or HCl. The effect of the initial concentration (1 to 1000 mg/L) was also studied in order to determine the effect of the parameter on the adsorption of metal from the solution. The optimum equilibrium time was determined as the contact time required for the concentration of metal in the solution to reach equilibrium and was obtained by varying the contact time in the range 30 to 240 minutes.

At the end of the predetermined time intervals, the suspensions were filtered and the Cu^{2+}, Cd^{2+}, Zn^{2+} and Hg^{2+}content in the filterate was analysed by using AAnalyst 200 Perkin-Elmer atomic absorption spectrophotometer. The uptake of Cu^{2+}, Cd^{2+}, Zn^{2+} and Hg^{2+} by the adsorbents under study (q_e) was calculated from the difference between the initial and final concentration as follows:

$$q_e = (C_i - C_e)/m; \qquad (1)$$

Where, C_i-initial concentration of metal ion mg/L; C_e – Equilibrium concentration of metal ion mg/L; m – Mass of adsorbent g/L; q_e – Amount of metal ion adsorbed per gram of adsorbent. Each experimental result was obtained by averaging the data from three parallel experiments.

Adsorption isotherm experiments were also performed by agitating 0.1 g of the adsorbent under study with a series of 25 mL solutions at optimum pH,containing different initial concentrations of (1 to 1000 mg/L) at 30 °C. After the established contact time was attained, the suspension was filtered, and supernatant was analyzed for the metal concentration. The adherence of the equilibrium isotherm and data obtained to different adsorption isotherms models as given in Table 3.1 was tested.

Similarly the Cu^{2+}, Cd^{2+}, Zn^{2+} and Hg^{2+} adsorption data obtained after agitating solutioncontaining 10 mg/L of Cu^{2+}, Cd^{2+}, Zn^{2+} and $Hg^{2+}$for various contact times with the adsorbents under study at optimum pH obtained and were modeled to determine the order of reaction rate and the adherence to different kinetic models as given in Table 3.1 was tested.

Thermodynamic parameters of the adsorption process (ΔG^0, ΔH^0 and ΔS^0) could be determined from the experimental data obtained at various temperatures using following equations:

$$ln\frac{q_e}{C_e} = \frac{\Delta S^0}{R} - \frac{\Delta H^0}{RT} \quad (2)$$

$$\Delta G^0 = \Delta H^0 - T\Delta S^0 \quad (3)$$

where R is the gas constant (8.314 $Jmol^{-1}K^{-1}$) and T is the absolute temperature (K). Values of correlation coefficients and standard deviation were used to compare the models. SD was calculated using the equation.

$$\mathrm{SD} = \sqrt{\frac{1}{\mathrm{N}}\sum_{\mathrm{i}=1}^{\mathrm{N}}(\mathrm{x_i} - \bar{\mathrm{x}})^2} \quad (4)$$

3.2.2. Desorption Studies.

0.1 g of metal loaded adsorbents under study was treated with 10 mL of 0.1 M EDTA, 0.1M NH_3 and 0.1M HCl for a period of 60 min in a thermostated rotary mechanical shaker. After 60 min the amount of metal desorbed from the adsorbents under study wasdetermined by AAS. The adsorption-desorption experiments were repeated for three cycles.

3.2.3. Column Studies.

Column experiments were conducted in a glass column with an internal diameter of 1 cm and a length of 30 cm packed with the adsorbent under study. Cu^{2+}, Cd^{2+}, Zn^{2+} and Hg^{2+}solution of known concentration (1000 mg/L) at optimum pHwas passed through the column of adsorbent at a flow rate of 1 mL/min. Samples from the column effluent were collected at regular intervals and analyzed by atomic absorption spectrometry. The break-through time has been chosen when the concentration of the effluent is 1 mg/L.

3.2.4. Spectroscopic Analysis.

FT-IRspectra for biosorbent and the metal-loaded biosorbents were obtained using a Perkin Elmer RX1 model within the wave number range of (400 to 4000) cm^{-1}.

The surface of the Cu and Hg–loaded samples was analyzed using a KRATOS AXIS 165 X-ray Photoelectron spectrometer. Peak fitting and presentation output are produced by an integrated VISION control and information system. The deconvolution process of C 1s spectra as well as the elemental composition evaluation may result in an error of up to 5%. All spectra are presented charge balanced and energy referenced to C 1s at 284.6 eV[35].

The ^{13}C-NMR experiments were performed with a BrukerAvance (300 MHz) spectrometer for Cu–loaded samples.The chemical shifts δ, expressed in parts per million [ppm], were referenced relative to the signal of tetramethylsilane (TMS) at $\delta c = 0$ ppm.

3.3. Results and Discussion

3.3.1. Uptake studies.

3.3.1.1. *pH Dependence*.The pH of the medium from which adsorption is taking place is an important controlling parameter in heavy metal adsorption process. Hence uptake of Cd^{2+}, Zn^{2+} and Hg^{2+} has been studied with respect to pH (1-10) whereas uptake of Cu^{2+} was studied within pH (1-5) as shown in Figure 3.1. pH of the solution remains unchanged after the adsorption experiment.

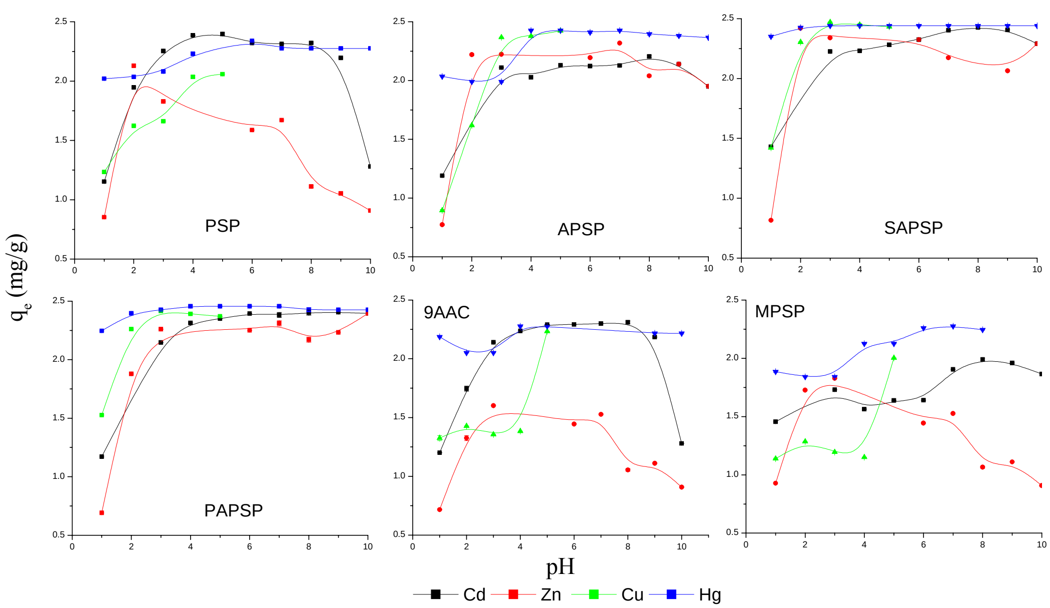

Operating parameters: 180 rpm, 10ppm of M^{2+}, 0.1g adsorbent, time 240 min, temperature 30 ^{0}C

Figure 3.1. Effect of pH on adsorption of metal ions

Cd^{2+} and Zn^{2+}: As all the metal exists as ions at a low pH (<4.0), the sharp increase observed in the adsorption of Cd^{2+} and $Zn^{2+}$from pH 1 to 3(more prominent in the case of PSP, APSP, SAPSP and PAPSP) cannot be attributed to the presence of different forms of metal species [36]. This implies that the functional groups on the adsorbents and their ionized forms under these pH conditions determine the extent of adsorption.

It can be presumed that the mechanism for removal of M^{2+}can be by ion-exchange and electrostatic interaction depending on the solution pH. At pH<pK_a of carboxylic groups, the removal could be due to ion-exchange process, as the binding sites are protonated. However, at

pH >pK_a, the carboxyl groups are negatively charged, the metal ions may bind to the binding sites by electrostatic attraction [41]. The hydroxyl groups can also become negatively charged at high pH, thereby contributing to metal removal at high pH (7 to 10).

Specific interactions of metal ion species with adsorbent surface and/or the existence of preferential adsorption sites may also affect the metal adsorption and could be responsible for the slight differences found in the adsorptive behavior of M^{2+} ions with pH variation [37]. Optimum adsorption above pH 3 has been reported for M^{2+} uptake on some other agro based activated carbons [38, 39].

Cu^{2+}: In case of PSP, APSP, SAPSP and PAPSP adsorption increased with increase in pH till pH 4, 3.5, and 2.9 respectively for $Cu^{2+}$and then remained constant. Compared to other adsorbents APSP showed a sharp increase in adsorption of copper between pH 1 to 3.5 probably due to the presence of more number of carboxyl groups as evidenced by FT-IR, NMR and XPS. On the other hand, for MPSP and 9AAC adsorption remained constant till pH 3.5 and 4 and then increased giving maximum adsorption at pH 5. The possible reason could be that 9AAC and MPSP had lesser number of carboxyl groups and more of phenolic groups and metal ions mainly exchanged with –COOH groups of natural biomass between pH 1.5 and 5, while at higher pH, phenol groups might become more active Cu^{2+} sorption sites. Above pH_{Zpc}(PSP 3.298; APSP3.719; SAPSP 3.718; PAPSP 4.21; 9AAC 3.085; MPSP 3.155) the surface is negatively charged and hence attracts copper cations.

Hg^{2+}: Figure 3.1 shows that adsorption of mercury reaches maximum at ~pH 3.5 and is constant for the entire range of pH studied for all the adsorbents . This high adsorption is believed to be associated with the formation of positively charged metal hydroxy species having strong affinity for surface functional groups. The observed reduced adsorption at low pH value (2.0) may be attributed to (i) higher hydrated species [Hg^{2+} (aq) species] having low mobility and (ii) protonation of the surface functional groups as well as the competition between mercuric ions and H^+ or H_3O^+ ions present in the solution. At higher pH values (3.0), more functional groups are available for metal ion binding due to deprotonation, resulting in high adsorption. Thereby, maximum adsorption of mercury from pH 3.0 may be due to partial hydrolysis forming $HgCl^+$, $HgClOH^+$, and $Hg(OH)_2$ species, having strong affinity for the negatively charged functional groups of the adsorbents under study.(need to give references which were given in paper)

However adsorption capacity for mercury is still > 90% in acidic pH conditions. This implies that an acidic group is responsible for mercury binding at low pH, while a weak acidic group such as carboxyl group is dominant at neutral pH *(15)*. The initial rapid uptake of Hg (II) from solution may likely be due to binding of adsorbate ions on the surface of the adsorbents through ion-exchange process. This instantaneous surface adsorption causes a rapid increase in Hg (II) uptake. Later on slower adsorption might be due to intraparticle diffusion, and diffusion of mercury from the aqueous phase to the adsorbents under study.

At pH values above 8.3, 7.1, 4.6 and 8.5; Cd, Zn, Cu and Hg respectively precipitates in the form of metal oxides or hydroxides are formed [40].It was decided to perform all the adsorption studies at pH of 6 for Cd^{2+}, Zn^{2+}, Hg^{2+}; whereas Cu^{2+} was studied at pH 4.5.

3.3.1.2.*Contact Time Dependence*. The effect of contact time variation on adsorption of Cd^{2+}, Zn^{2+}, Cu^{2+} and $Hg^{2+}$was studied and the results are shown in Figure 3.2.

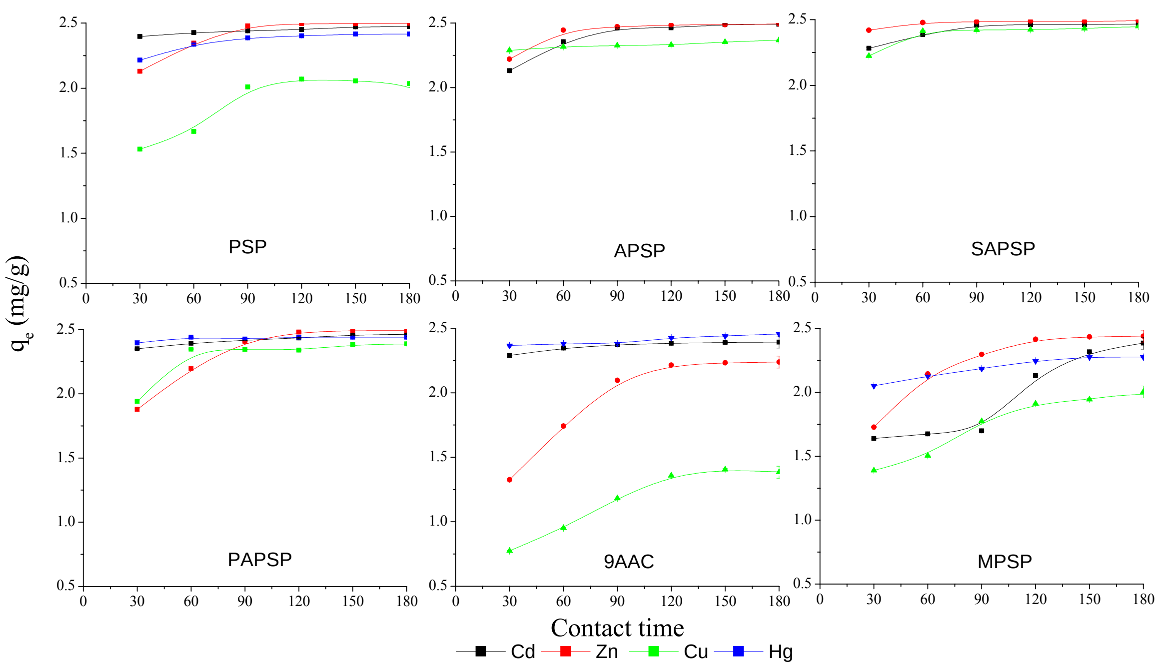

Operating parameters: 180 rpm, 10ppm of M^{2+}, 0.1g adsorbent, temperature 30 ^{0}C, optimum pH

Figure 3.2. Effect of contact time of M^{2+}

It is seen that more than 50% of M^{2+} was adsorbed within 60 min and equilibrium adsorption was attained in 1590 min for all the adsorbents but optimum time for adsorption equilibrium was fixed as 180 min.The rate of adsorption is very fast initially followed by a decreased rate with the approach of equilibrium. The removal rate is high initially due to the presence of free binding sites which gradually become saturated with time resulting in decreased rate of adsorption as equilibrium approaches. This indicates that the adsorption is mainly through surface binding. Similar observations were made by Das et al [42].

3.3.1.3.*Dosage dependence*. The effect of variation in dose of the adsorbent was studied to obtain the saturation limit of the adsorbent to adsorbate ratio (Figure 3.3).

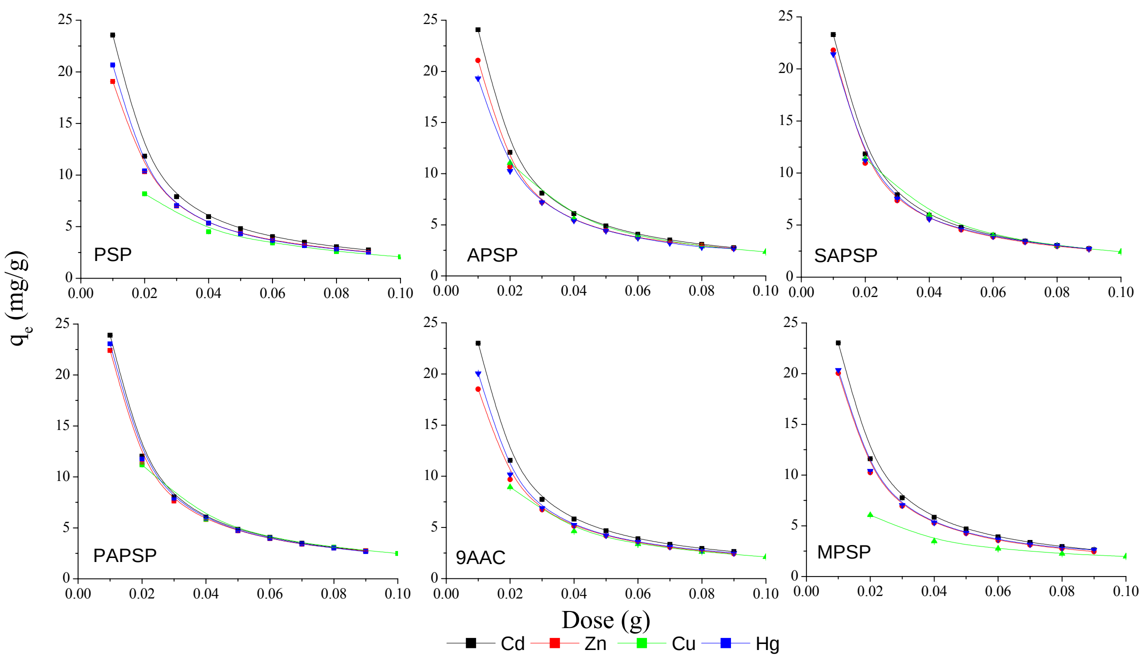

Operating parameters: 180 rpm, time 240 min, temperature 30 ^{0}C, optimum pH

Figure 3.3. Effect of initial concentration of M^{2+}

It was observed that when the adsorbent dose was higher than 0.06 g the metal ion uptake remained almost constant. Increase in the percentage uptake of metal ions with adsorbent dosage could be attributed to increase in the adsorbent surface area and hence the adsorption sites available for adsorption. On the other hand, it is also seen that the increase in the adsorbent dosage leads to a decrease in the q_e. The decrease in $q_e$value may be due to the concentration gradient between adsorbate and adsorbent with increasing adsorbent concentration causing a decrease in amount of metallic ion adsorbed per gram of adsorbent under study [43].

3.3.1.4.*Temperature Dependence*. The effect of temperature variation (Figure 3.4) showed almost same trend for the adsorbents under study. The uptake was found to decrease with increase in temperature indicating that the mechanism of adsorption is exothermic in nature.

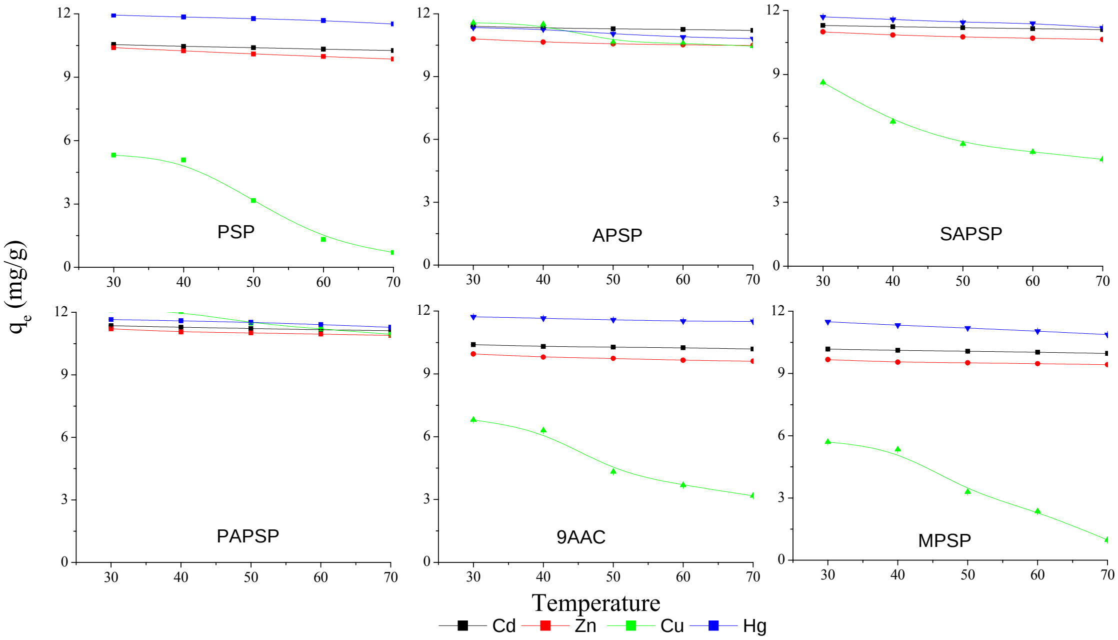

Operating parameters: 180 rpm, 10 ppm of M^{2+}, 0.1g adsorbent, time 240 min, optimum pH

Figure 3.4. Effect of temperature on uptake of M^{2+} ions by PSP, MPSP, APSP, SAPSP, PAPSP and 9AAC

3.3.2. Adsorption Kinetics.

The kinetics of adsorption process describes the solute uptake, which, in turn governs the residence time of the adsorption reaction. The kinetic models of pseudo first order, pseudo second order, intra-particle diffusion, Bangham, Elovich and Liquid film diffusion models were studied. Adsorption kinetics for Cd^{2+}, Zn^{2+}, Cu^{2+} and Hg^{2+}removal by each of the adsorbents under study was conducted at optimum pH and the kinetic constants for the adsorption kinetics are presented in Table 3.2.

Table 3.2. Adsorption kinetic parameters for Cd^{2+}, Zn^{2+}, Cu^{2+} and Hg^{2+} adsorption

Cd^{2+}/ Zn^{2+}						
	PSP	**APSP**	**SAPSP**	**PAPSP**	**9AAC**	**MPSP**
q_e(exp)(mg.g^{-1})	2.573/ 2.591	1.632/ 2.668	2.514/ 2.794	1.594/ 2.804	1.061/ 2.927	2.376/ 2.636
Pseudo 2nd Order						
q_e (mg.g^{-1})	2.492/ 1.605	2.792/ 1.593	2.577/ 2.336	2.501/ 2.448	2.493/ 2.447	1.424/ 2.427
K_2 (g.mgmin^{-1})	0.254/ 0.062	0.009/ 0.060	0.070/ 0.106	0.148/ 0.047	0.174/ 0.049	0.702/ 0.113
r^2	0.999/ 0.997	0.953/ 0.996	0.998/ 0.999	0.999/ 0.999	0.999/ 0.997	1.000/ 0.999
SD	0.056/ 0.088	0.099/ 0.59	0.034/ 0.054	0.022/ 0.066	0.083/ 0.060	0.032/ 0.058
Lagergren						
q_e (mg.g^{-1})	0.219/ 2.453	14.39/ 1.877	6.800/ 1.184	0.718/ 11.26	0.765/ 0.502	0.610/ 1.853
K_1 (min^{-1})	-0.03/ -0.04	-0.05/ -0.04	-0.06/ -0.04	-0.05/ -0.06	-0.04/ -0.03	-0.04/ -0.03
r^2	0.821/ 0.799	0.671/ 0.807	0.855/ 0.858	0.836/ 0.778	0.821/ 0.878	0.901/ 0.684
SD	0.074/ 0.058	0.096/ 0.087	0.079/ 0.027	0.039/ 0.071	0.073/ 0.037	0.069/ 0.033
Intraparticle Diffusion						
K_{ip} (mg.gmin$^{-0.5}$)	0.024/ 0.029	0.018/ 0.029	0.005/ 0.021	0.012/ 0.042	0.030/ 0.020	0.025/ 0.039
r^2	0.917/ 0.938	0.976/ 0.917	0.765/ 0.979	0.948/ 0.934	0.985/ 0.957	0.879/ 0.972
SD	0.034/ 0.025	0.007/ 0.029	0.013/ 0.010	0.013/ 0.041	0.018/ 0.014	0.045/ 0.021
Elovich						
β (g.mg^{-1})	23.13/ 8.00	2.21/ 8.00	4.98/ 10.72	9.437/ 4.674	15.58/ 11.43	18.23/ 5.74
α (mg.g^{-1}min^{-1})	4.478E+50/ 1100001	0.329/ 825703	5641180/ 1.981E+18	2.289E+17/ 137142	9.771E+31/ 9.283E+20	8.388E+36/ 452
r^2	0.983/ 0.882	0.765/ 0.855	0.887/ 0.961	0.892/ 0.949	0.995/ 0.926	0.954/ 0.979
SD	0.004/ 0.034	0.085/ 0.038	0.050/ 0.014	0.027/ 0.036	0.004/ 0.018	0.009/ 0.018
Liquid film diffusion model						
K_{FD}	0.025/ 0.043	0.047/ 0.031	0.063/ 0.056	0.04/ 0.062	0.037/ 0.033	0.049/ 0.027
r^2	0.815/ 0.799	0.671/ 0.659	0.854/ 0.789	0.927/ 0.777	0.821/ 0.684	0.902/ 0.878
SD	0.063/ 0.041	0.065/ 0.033	0.064/ 0.082	0.073/ 0.088	0.090/ 0.089	0.089/ 0.054
Bangham						
K_{BM}	0.569/ 0.218	-0.021/ 0.214	0.376/ 0.455	0.491/ 0.311	0.538/ 0.487	0.126/ 0.149
α	4E-04/ 0.002	0.005/ 0.002	0.002/ 9E-04	0.001/ 0.022	7E-04/ 9E-04	6E-04/ 0.01
r^2	0.984/ 0.882	0.765/ 0.855	0.889/ 0.961	0.900/ 0.949	0.754/ 0.926	0.955/ 0.979
SD	0.001/ 0.001	0.001/ 0.001	0.001/ 0.001	0.001/ 0.001	0.001/ 0.001	0.001/ 0.001
Cu^{2+}/ Hg^{2+}						
q_e (exp) (mg/g)	1.662/ 2.178	1.956/ 2.105	2.332/ 2.482	2.712/ 2.455	2.429/ 2.079	1.615/ 1.923
Pseudo 2nd order						
q_e (mg/g)	1.492/ 2.462	1.560/ 2.448	2.406/ 2.449	2.482/ 2.479	2.455/ 2.346	1.742/ 2.173
k_2(g/mgmin)	0.496/ 0.129	0.001/ 0.783	0.079/ 0.777	0.309/ 0.168	0.158/ 0.079	0.015/ 0.124
r^2	0.993/ 0.999	0.971/ 0.999	0.999/ 0.999	0.999/ 0.999	0.999/ 0.999	0.978/ 0.999
SD	0.054/ 0.115	0.048/ 0.089	0.077/ 0.104	0.023/ 0.061	0.059/ 0.019	0.972/ 0.289
Lagergren						
q_e (mg/g)	0.427/ 0.479	0.733/ 0.106	0.315/ 0.045	0.166/ 0.142	0.384/ 0.503	1.202/ 0.318
k_1(min^{-1})	0.012/ 0.030	0.005/ 0.030	0.012/ 0.045	0.022/ 0.011	0.027/ 0.022	0.007/ 0.022
r^2	0.903/ 0.998	0.827/ 0.991	0.887/ 0.529	0.913/ 0.858	0.941/ 0.971	0.928/ 0.916
SD	0.027/ 0.037	0.088/ 0.028	0.097/ 0.042	0.034/ 0.035	0.033/ 0.011	0.087/ 0.023
Intra Particle Diffusion						
k_i(mg/gmin$^{0.5}$)	0.043/ 0.024	0.000/ 0.005	0.182/ 0.018	0.128/ 0.012	0.056/ 0.030	0.162/ 0.025
r^2	0.996/ 0.918	0.000/ 0.976	0.972/ 0.765	0.991/ 0.949	0.968/ 0.985	0.929/ 0.879
SD	0.008/ 0.034	0.000/ 0.008	0.092/ 0.013	0.040/ 0.013	0.029/ 0.018	0.019/ 0.045
Elovich						
β (g.mg^{-1})	12.55/ 8.92	3.953/ 22.472	6.83/ 44.44	17.09/ 19.53	8.514/ 7.353	3.953/ 8.375
α (mg.g^{-1}min^{-1})	0.969/ 4.153E+15	0.119/ 9.57E+48	0.916/ 8.09E+101	0.606/ 1.938E+41	0.391/ 7.911E+10	0.514/ 8.032E+11

r^2	0.824/ 0.962	0.872/ 0.951	0.949/ 0.819	0.845/ 0.911	0.826/ 0.991	0.872/ 0.930
SD	0.099/ 0.024	0.108/ 0.010	0.037/ 0.012	0.028/ 0.017	0.061/ 0.014	0.108/ 0.035
Liquid film diffusion model						
k_{fd}(min^{-1})	-0.01/ -0.07	0.009/ -0.153	-0.013/ -0.03	-0.022/ -0.04	-0.027/ -0.06	-0.01/ -0.06
r^2	0.903/ 0.919	0.954/ 0.874	0.887/ 0.656	0.913/ 0.814	0.941/ 0.992	0.928/ 0.904
SD	0.092/ 0.076	0.072/ 0.079	0.053/ 0.086	0.038/ 0.099	0.036/ 0.083	0.101/ 0.093
Bangham						
K_{BM}(mL.g^{-1}.L^{-1})	-119/ -130	-115/ -142	-114/ -114	-116/ -135	-123/ -131	-124/ -139
α	0.049/ 0.098	0.019/ 0.182	0.009/ 0.009	0.022/ 0.160	0.063/ 0.132	0.059/ 0.160
r2	0.959/ 0.813	0.953/ 0.937	0.819/ 0.891	0.912/ 0.904	0.992/ 0.938	0.926/ 0.937
SD	0.005/ 0.023	0.002/ 0.022	0.002/ 0.001	0.003/ 0.025	0.003/ 0.016	0.008/ 0.019

APSP, SAPSP and PAPSP showed better kinetics attaining equilibrium in ~60 min. followed by PSP attaining equilibrium in 90 min. 9AAC and MPSP attained equilibrium for all the four metal ions in 120 and 150 min respectively. Adsorption capacity at equilibrium was found to be in following order Cu^{2+}<Cd^{2+}~Zn^{2+}~Hg^{2+}.The pseudo second order kinetics provided the best fit for the kinetic data. The q_e values were very close to the experimental q_e values and correlation coefficient values were ~0.99 for PSP, APSP, SAPSP, PAPSP, 9AAC and MPSPfor all the metal ions under study suggesting that the rate limiting step in adsorption of metal is chemisorption involving valence forces through the exchange of electrons between adsorbent and adsorbate, complexation, coordination and/or chelation. In pseudo first order the $q_{e(exp)}$ values were much higher than q_e fitted values suggesting that the reaction cannot be classified as first order although this plot has reasonably good correlation coefficient from the fitting process.

The kinetic constants obtained from the Elovich equation are presented in Table 3.2. The results demonstrate a significant relationship between the metal ion adsorbed, q_t, and in these studies with regression coefficients >0.98 and low standard deviation values. Therefore, the kinetic data of the metal ions for all the adsorbents under study showed satisfactory compliance with the Elovich equation. The Liquid film diffusion model is applicable when flow of the reaction from the bulk liquid to the surface of the adsorbent determines the rate constant. The applicability of the model is found to be good as inferred from the values of r^2. The curves did not pass though origin as required by the model but very small intercepts indicates that diffusion of metal from the liquid phase to the adsorbent surface might be having some role in deciding the rate processes.

The Weber and Morris adsorption kinetic model was plotted using equation given in Table 3.1.The plots obtained for PSP, APSP, SAPSP, PAPSP, 9AAC and MPSP do not pass through origin implying that the intra-particle diffusion is not the only operative mechanism.

Bangham equation was applied to the adsorption data with reasonable correlation coefficients confirming the applicability of Bangham equation, thus indicating that diffusion of metal into the pores of adsorbent correlates the adsorption process. However the not so linear curves indicate that the diffusion of adsorbate into pores of the sorbent is not the only rate controlling step.

The study of the various kinetic models reveals that the rate limiting step is chemisorptions and diffusion of adsorbate from the liquid phase to the adsorbent surface and into the pores of the adsorbent might be having some role in deciding the rate processes.

3.3.3. Adsorption Isotherms.

For modeling of cadmium uptake Freundlich, Langmuir, Temkin, Dubinin-Radushkevich (DR), Flory-Huggins, Elovich and Halsey isotherm models (Table 3.1) were employed. The values of fitted model constants for adsorption of M^{2+} on PSP, APSP, SAPSP, PAPSP, 9AAC and MPSPalong with their correlation coefficients, r^2 and SD values for all the system studied arepresented in Table 3.3.

Table 3.3. Adsorption isotherm parameters for Cd^{2+}, Zn^{2+}, Cu^{2+} and Hg^{2+}

Cd^{2+}/ Zn^{2+}						
	PSP	**APSP**	**SAPSP**	**PAPSP**	**9AAC**	**MPSP**
q_e (exp) (mg.g^{-1})	226/ 203	233/ 202	230/ 215	232/ 216	223/ 219	217/ 204
Freundlich						
K_f(mg.g^{-1})(dm^3/mg)$^{1/n}$	1.45/ 1.20	1.28/ 1.05	1.98/ 1.23	1.62/ 1.39	1.69/ 1.61	1.13/ 0.882
N	1.08/ 1.06	1.05/ 01.01	1.38/ 1.01	1.15/ 1.08	1.22/ 1.15	0.982/0.911
r^2	0.994/0.999	0.997/0.997	0.995/0.999	0.999/0.999	0.999/0.999	0.994/0.998
SD	0.044/0.038	0.017/0.075	0.044/0.021	0.067/0.019	0.066/0.055	0.043/0.059
Langmuir						
K_L (dm^3.mg^{-1})	0.004/0.009	0.008/0.005	0.006/0.007	0.005/0.008	0.005/0.009	0.005/0.010
q_m (mg.g^{-1})	282/ 204	187/ 230	298/ 228	364/ 238	347/ 193	154/ 243
ΔG (kJ.mol^{-1})	-14.0/-12.2	-12.5/ -13.6	-13.2/ -12.9	-13.9/ -12.6	-13.9/ -11.9	-13.6/ -11.6
r^2	0.961/0.982	0.915/0.999	0.926/0.997	0.890/0.964	0.949/0.990	0.998/0.979
SD	0.063/0.054	0.043/0.002	0.058/0.004	0.065/0.071	0.049/0.003	0.024/0.097
Temkin						
-ΔH (kJ.mol^{-1})	14.91/11.62	8.90/ 11.79	17.13/13.51	20.87/14.24	21.77/12.08	8.49/7.82
K_T (dm^3.mg^{-1})	0.146/0.126	0.118/0.100	0.227/0.162	0.214/0.178	0.222/0.198	0.115/0.105
r^2	0.996/0.981	0.994/0.995	0.956/0.986	0.964/0.981	0.961/0.973	0.939/0.989
SD	0.037/0.023	0.069/0.071	0.054/0.062	0.071/0.072	0.025/0.047	0.069/0.056
DR						
q_m (mg.g^{-1})	166/ 155	165/ 127	178/113	174/159	173/ 164	179/ 154
E^0 (KJ)	2.56/ 9.03	2.16/6.25	2.75/2.17	2.66/5.29	2.59/ 4.73	1.42/ 1.05
r^2	0.957/0.968	0.967/0.943	0.960/0.882	0.960/0.964	0.954/0.964	0.966/0.978
SD	0.092/0.043	0.093/0.068	0.074/0.079	0.077/0.059	0.051/0.044	0.050/0.077
Halsey						
K_H(mg/g)(dm^3/mg)$^{1/n}$	0.751/0.639	0.778/0.734	0.388/0.224	0.416/0.163	0.332/0.285	0.359/0.974
n_H	-0.94/-1.06	-0.95/-1.06	-1.03/-1.25	-1.04/-1.31	-1.11/-1.15	-0.69/-0.98
r^2	0.994/0.999	0.999/0.995	0.994/0.995	0.999/0.967	0.996/0.999	0.997/0.999
SD	0.090/0.088	0.047/0.022	0.079/0.071	0.032/0.048	0.052/0.027	0.029/0.084

Flori-Huggins						
K_{FH}(mg/g)(dm^3/mg)$^{1/n}$	1.174/ 1.6E-29	3.871/ 1.945E-12	1.426/ 4.197E-37	1.374/ 6.531E-16	1.384/ 2.884E+34	1.143/ 4.092E+18
N_{FH}	2.31/ -39.41	2.53/-19.18	2.56/-27.79	2.64/-14.57	2.61/-34.58	3.28/28.39
r^2	0.999/0.985	1.000/0.989	0.991/0.958	0.986/0.997	0.992/0.894	0.999/0.998
SD	0.025/0.025	0.002/0.071	0.099/0.011	0.061/0.049	0.072/0.025	0.087/0.042
Elovich						
q_m (mg.g^{-1})	1.286/1.244	1.516/1.206	1.813/1.613	1.743/1.844	0.6340.466	0.891/0.954
K_E (dm^3.mg^{-1})	9.23E+125/ 7.249E+85	8.959E+55/ 6.848E+85	5.195E+89/ 3.247E+80	7.443E+95/ 3.658E+46	1.37E+236/ 8.69E+190	7.89E+125/ 1.69E+54
r^2	0.994/0.932	0.924/0.999	0.985/0.997	0.967/0.991	0.911/0.950	0.989/0.945
SD	0.046/0.018	0.068/0.002	0.071/0.005	0.089/0.016	0.020/0.047	0.084/0.026
Cu^{2+}/ Hg^{2+}						
q_e (exp) (mg.g^{-1})	36/239	42/218	125/220	88/217	117/206	33/230
Freundlich						
K_f (L.g^{-1})	1.380/2.230	1.413/1.928	2.41/2.139	1.62/1.935	2.76/1.499	1.142/1.79
N	2.311/0.991	2.267/1.242	2.40/1.344	1.99/1.265	2.67/1.287	2.241/1.03
r^2	0.863/0.984	0.874/0.994	0.97/0.989	0.95/0.995	0.997/0.97	0.950/0.98
SD	0.023/0.040	0.023/0.034	0.013/0.03	0.02/0.017	0.004/0.01	0.013/0.02
Langmuir						
K_L (L.mmol^{-1})	0.008/0.06	0.011/0.16	0.012/0.27	0.006/0.18	0.019/0.16	0.003/0.07
q_m (mg.g^{-1})	40/105	45/ 35	119/30	99/34	120/23	40/60
ΔG (kJ.mol^{-1})	-12.6/-7.22	-11.9/-4.68	-11.5/-3.4	-13.4/-4.5	-10.4/0.963	-14.7/-7.1
r^2	0.989/0.88	0.98/0.997	0.865/0.97	0.91/0.999	0.96/0.986	0.90/0.65
SD	0.078/0.02	0.02/0.015	0.415/0.06	0.069/0.01	0.07/0.11	0.672/0.09
Temkin						
-ΔH (kJ.mol^{-1})	13.519/2.82	17.71/1.17	15.98/0.932	14.44/1.12	18.10/0.66	14.72/1.75
K_T (L.mmol^{-1})	0.130/0.301	3.11/0.123	0.394/0.122	0.119/0.12	0.81/0.040	0.068/0.19
r^2	0.956/0.997	0.997/0.996	0.893/0.994	0.931/0.99	0.951/0.91	0.905/0.99
SD	0.087/0.037	0.065/0.097	0.074/0.085	0.039/0.08	0.021/0.04	0.065/0.09
DR						
q_m (mg.g^{-1})	34/218	37/ 172	65/ 174	64/ 169	60/ 152	17/ 211
E_0 (KJ.mol^{-1})	0.125/19.33	0.133/9.55	0.811/9.64	0.206/9.18	1.77/3.59	0.198/11.9
r^2	0.944/0.993	0.925/0.975	0.847/0.974	0.963/0.98	0.789/0.96	0.625/0.99
SD	0.047/0.090	0.048/0.066	0.081/0.071	0.033/0.09	0.077/0.08	0.045/0.07
Halsey						
k_H (L.g^{-1})	0.182/0.16	0.165/0.152	0.01/0.09	0.108/0.15	0.002/0.30	0.505/0.25
n_H	-2.31/-0.99	-2.27/-1.25	-2.40/-1.34	-1.20/-1.27	-2.67/-1.29	-2.24/-1.03
r^2	0.863/0.984	0.874/0.994	0.971/0.99	0.947/0.81	0.997/0.97	0.95/0.98
SD	0.053/0.07	0.052/0.015	0.036/0.01	0.096/0.08	0.10/0.083	0.097/0.03
Flori-Huggins						
k_{fh}(L.g^{-1})	0.001/ 1.380E-14	0.033/ 1.940E-05	0.024/ 0.0002	0.036/ 3.419E-05	0.009/ 1.370	0.01/ 3.97
n_{fh}	-3.86/-8.92	-1.416/-2.62	-2.34/-1.63	-1.09/-2.41	-15.45/4.38	-3.46/ 2.31
r^2	0.981/0.98	0.989/0.97	0.978/0.99	0.996/0.96	0.983/0.88	0.981/0.99
SD	0.023/0.06	0.038/0.08	0.092/0.02	0.079/0.02	0.078/0.03	0.063/0.08
Elovich						
q_m (mg.g^{-1})	0.47/6.56	0.504/6.46	2.836/10.8	0.831/6.74	7.29/0.612	0.214/2.32
K_E (L.mmol^{-1})	2644/ 5.5E+258	17703/ 2.3E+58	2.90E+53/ 5.54E+61	4.29E+15/ 3.29E+56	3.07E+94/ 2.96E+89	38.53/ 3.53E+116
r^2	0.756/0.88	0.768/0.999	0.817/0.96	0.812/0.99	0.939/0.99	0.775/0.99
SD	0.052/0.09	0.083/0.006	0.019/0.02	0.071/0.04	0.075/0.05	0.074/0.072

The Freundlich isotherm model fits the experimental data very well due to the heterogeneous distribution of non identical and energetically non uniform sites on the adsorbents under study. According to Treybal[44], an *n* value between 1 and 10 represents beneficial adsorption. The value of n, for the Freundlich model falling in the range of 0.98 to 1.34 for Cd^{2+}, Zn^{2+} and Hg^{2+}, 1.9 to 2.6 for Cu^{2+},indicates favorable adsorption. Langmuir equation relates the coverage of molecules on a solid surface to concentration of a medium above the solid surface at a fixed temperature. For the Langmuir model, the parameters K_L (equilibrium adsorption constant) and q_{max} were calculated from the intercept and slope of the plot of C_e/q_e versus C_e. For the Langmuir model r^2 varied from 0.86 to 0.998. In the present work although both the equations are obeyed, Freundlich isotherm model has a slightly better correlation coefficient and SD value indicating that surface of the adsorbents is heterogeneous in the long range but may have short range uniformity [45]. The comparative adsorption capacities were found in the order of $Cu^{2+}<Cd^{2+}\sim Zn^{2+}\sim Hg^{2+}$, adsorption capacity for Cu^{2+} was found to be lowest among the metal ions studied.

In case of Cd^{2+}, Cu^{2+} and Zn^{2+}, SAPSP, PAPSP was found to have better adsorption capacities, whereas for Hg^{2+} it was PSP. 9AAC showed higher adsorption capacities in case of Cu^{2+} and Zn^{2+}as compared to Cd^{2+} and Hg^{2+} due to the affinity of the hard copper and zinc to the hard basic ligands present in 9AAC. Higher adsorption of Hg^{2+} onto PSP as compared to other adsorbents may be due to the reduction of mercury to elemental mercury and creation of more carboxyl groups as seen from XPS studies in section3.3.8.The correlation coefficients of Temkin model (0.893 to 0.996) indicate a satisfactory fit of the model to the experimental data. The variation of adsorption energy, ΔQ was found to be positive for all the metal ions adsorbed onto PSP, APSP, SAPSP, PAPSP, 9AAC and PAPSP, indicating the adsorption to be exothermic.

The Dubinin–Radushkevich model does not assume a homogeneous surface, like the Langmuir model. Its theory of filling the micro-pore volume is based on the fact that the adsorption potential is variable and that the free adsorption enthalpy is linked to the degree of pore filling. The values of correlation coefficients obtained from D-R model are lower than other isotherm values representing poor fit to experimental data and hence further analysis of D-R model was not done.

In all cases, though the Elovich isotherm exhibited good coefficients of correlation for the adsorbents under study, the values of maximum adsorption capacity determined (Table 3.3) are lower than the experimental adsorbed amounts at equilibrium. Therefore, the Elovich model is unable to describe the adsorption isotherms of the metal ions onto all the adsorbents under study.

Multilayer adsorption is generally discussed by the Halsey equation and is found to fit well with the experimental data having r^2 ($\geq$ 0.865)[46] indicating that the mechanism may be multilayer adsorption for PSP, APSP, SAPSP, PAPSP, 9AAC and MPSP. However, the values of K_H suggest that multilayer adsorption might be playing only a small role.

The Flory-Huggins model was used to assess the isotherm data (Table 3.3). Thoughthe correlation coefficients seem to be high, the negative value of n and low values of k_{FH} imply that the model cannot be used to describe the adsorption data.Thus it can be concluded that the Freundlich and Langmuir isotherm model fits best with low SD values followed by Halsey and Temkin. The adherence to these models suggests that these adsorbents might have homogeneous and heterogeneous surface energy distributions which would induce single and multilayer adsorption occurring either simultaneously or one after another.

3.3.4. Thermodynamic Parameters.

The negative value of ΔH^0 indicates that the adsorption of M^{2+} on PSP, APSP, SAPSP, PAPSP,9AAC and MPSP is exothermic. The negative values of ΔG^0 in Table 3.4 indicate that the adsorption of M^{2+} by the adsorbents under study is by physisorption and is spontaneous and thermodynamically favorable [47]. The negative values of ΔS^0 are indicative of decrease in randomness during adsorption and a high affinity of the adsorbent towards the adsorbate.

Table 3.4. Thermodynamic Parameters for Cd^{2+}, Zn^{2+}, Cu^{2+} and Hg^{2+}

	Cd	**Zn**	**Cu**	**Hg**
		ΔG (KJ/mol)		
PSP	-1.849	-3.664	-0.612	-34.184
APSP	-3.124	-2.12	-8.583	-6.871
SAPSP	-2.304	-3.272	-4.571	-5.233
PAPSP	-3.001	-3.36	-3.152	-5.82
9AAC	-1.844	-2.814	-0.495	-9.765
MPSP	-2.451	-2.707	-0.632	-16.157
		ΔS (KJ/molK)		
PSP	0.0001	0.006	0.841	0.049
APSP	0.0009	0.002	13.302	0.009
SAPSP	0.0002	0.004	6.983	0.005
PAPSP	0.0019	0.003	4.714	0.008
9AAC	0.0001	0.004	0.665	0.015
MPSP	0.0019	0.004	0.829	0.022
		ΔH (KJ/mol)		
PSP	-1.818	-1.922	-0.358	-19.241

APSP	-3.097	-1.601	-4.553	-4.1
SAPSP	-2.248	-2.206	-2.455	-3.663
PAPSP	-2.419	-2.38	-1.724	-3.533
9AAC	-1.812	-1.506	-0.294	-5.079
MPSP	-1.852	-1.415	-0.381	-9.395

3.3.5. Fourier Transform Infrared Spectroscopy.

Infrared spectra of the pristine and metal-loaded sorbents are shown in Figure 3.5. From figure 3.5 it is evident that there is shift in wave number and decrease in intensity of certain bands. Similarity in FTIR spectra of PSP with APSP and PAPSP suggests that a large proportion of the organic functional groups are retained on chemical or physical treatment of palm shell powder at 150^0C (Figure 3.5).

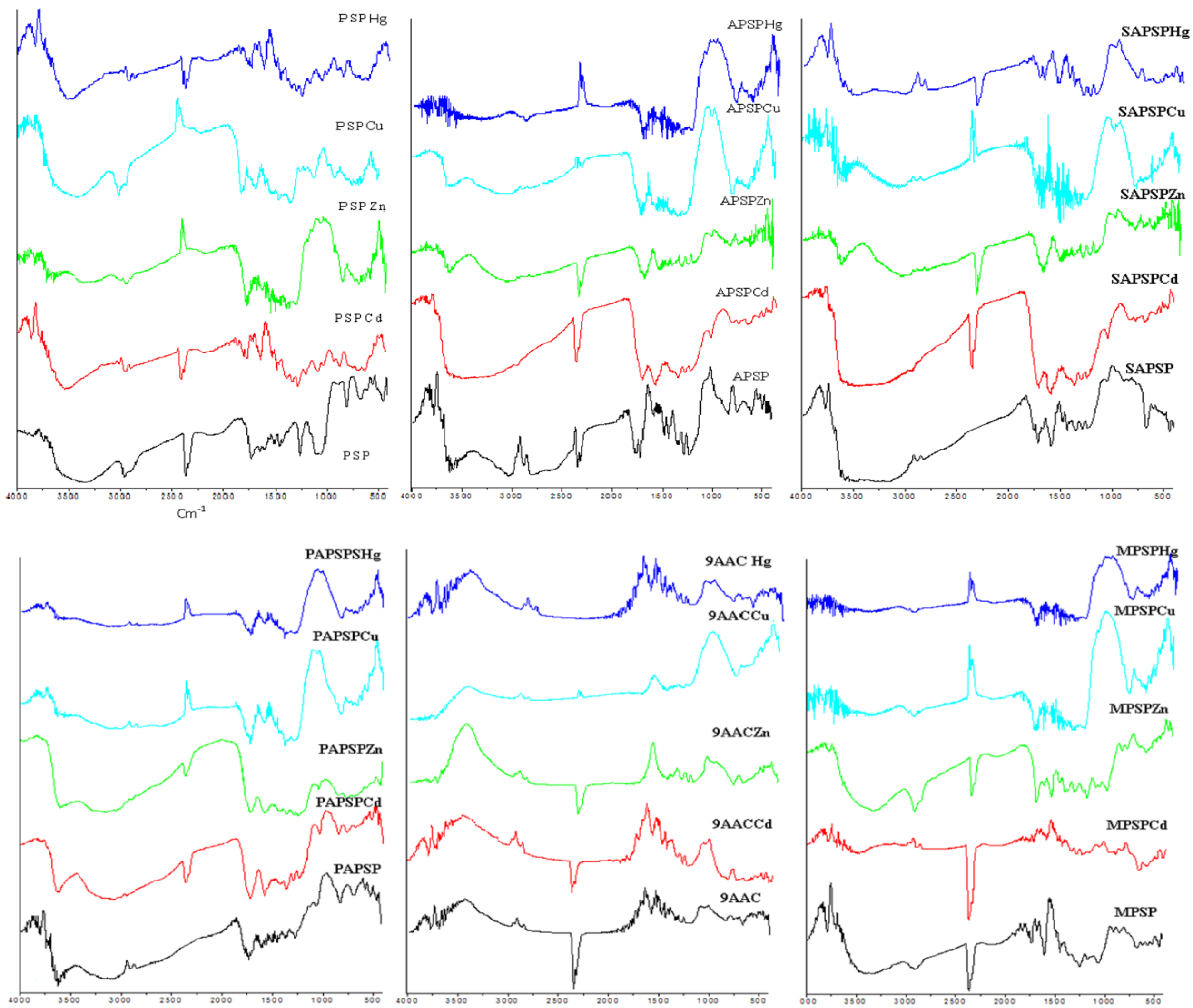

Figure 3.5. FTIR of native and metal loaded samples

Table 3.5. Typical Absorption frequencies and Carbonyl stretching frequencies of Infra red

spectra for free and metal loaded adsorbents

PSP-Cd/Zn	APSP-Cd/Zn	SAPSP-Cd/Zn	PAPSP-Cd/Zn	9AAC-Cd/Zn	MPSP-Cd/Zn	Assignment
3451/3561	3450/3633	3478/ 3606	3621/3601	-	3496/ 3331	-N-H, -O-H stretching
2887, 2830/ 3244, 2889	2923/3002, 2896	3040, 2877/ 3074, 2896	3067, 2935/ 3153, 2894	2995, 2882/ 2995, 2870	2995, 2879/ 2923, 2855	$-CH_3$, $-CH_2$ symmetric stretch
2347/2131	2357/2353	2357/ 2359	2349/ 2357	2366/2357	2361/ 2369, 2119	Free CO_2
1717/1735	1709/1719	1716/ 1723	1716/ 1709	-	1716/ 1731	-C=O stretch for acids or aldehyde
1594/ 1599, 1520	1584/1572	1589/ 1580	1580/ 1573	1572/ 1574	1584/ 1585	-C=O stretch cellulose/ C=C Aromatic stretch (skeletal vibration)/ N-H bending of amide
1436/ 1460, 1416	1440/1433	1479, 1433/ 1433	1433/ 1433	1486, 1433/ 1486, 1433	1433/ 1452	$-CH_2$- stretch/ -C=C- Aromatic stretching
1346/1368	1361/1354	1347/ 1354	1354/ 1354	1342/ 1347	1347/ 1361	-C-H stretch/ N-H bending
1238/1263	1229/1229	1229/ 1237	1229/ 1229	1215/ 1227	1237/ 1229	-C-O bending of carboxylic acids/ phenolic O-H stretch/ N-H bending
1166/1118	-	-	-	-	1157/ 1162	-O-H stretch (2^0 Alcohol), -C-O-C- stretching
1049/1033	1042/1033	1045/ 1037	1033/ 1033	1064/ 1037	1052/1045	-C-H stretch, -C-O stretch (1^0 Alcohol)
893/893	-	-	-	-	894/ 894	Anomeric C-H bending of cellulose
845/845	826/853	841/ 834	-/ 834	841/ 841	841/ 841	-C-H out of plane bending
768, 549, 404/ 771, 512, 423	768, 572, 404/772, 526, 418	755, 549, 437, 409/ 764, 518, 423	762, 516, 404/ 778, 510, 422	750, 558, 493, 418/ 777, 512, 426	750, 535, 420/ 769, 516, 419	Cd/ Zn -O bending vibrations
PSP-Cu/Hg	**APSP-Cu/Hg**	**SAPSP-Cu/Hg**	**PAPSP-Cu/Hg**	**9AAC-Cu/Hg**	**MPSP-Cu/Hg**	**Assignment**
3352/3456	3606/ 3569	3645/ 3788, 3501	3612/ 3584	-/-	3304/3343	-N-H, -O-H stretching
2930/ 2943, 2875	3067/ 2920, 2875	3050/ 3056, 2867	3055/ 3079, 2883	3055/ -	2889/ 2953, 2880	$-CH_3$, $-CH_2$ symmetric stretch
1738/ 1758, 1713	1728/ 1728	1731/ 1766, 1728	1723/ 1728	-/-	1738/ 1735	-C=O stretch for acids or aldehyde
1603/ 1600	1589/ 1600	1556/ 1592	1528/ 1584	1587/ 1584	1644/ 1652, 1600	-C=O stretch cellulose/ C=C Aromatic stretch (skeletal vibration)/ N-H bending of amide
1428/ 1479, 1433	1436/ 1449	1436/ 1472, 1423	1428/ 1471	1428/ 1486, 1449	1450/ 1449	$-CH_2$- stretch/ -C=C- Aromatic stretching
1368/ 1335	1361/ 1366	1361/ 1350	1376/ 1373	1373/ 1350	1366/ 1350	-C-H stretch/ N-H bending
1261/ 1283	1294/ 1260	1289/ 1290	1285/ 1285	-/-	1268/ 1260	-C-O bending of carboxylic acids/ phenolic O-H stretch/ N-H bending
1040/ 1049	-/-	1021/ 1041	1028/ 1026	-/ 1049	-	-C-H stretch, -C-O stretch (1^0 Alcohol)
826/ 845	819/ 822	817/ 837	826/ 822	834/ 845	826/ 822	-C-H out of plane bending
797, 533, 425/ 790, 527	790, 536, 428/ 787, 524	789, 533, 427/ 792, 525	794, 530, 422/ 789, 527	780, 526, 420/ 793, 531	791, 528, 421/ 796, 530, 418	Cu/ Hg -O bending vibrations

The band at 3300- 3600 cm^{-1} represents -OH and -NH groups in the adsorbents under study (Table 3.5). The shift in the band to 3400-3650 cm^{-1} indicates M^{2+}–OH and –NH interaction during metal sorption onto the adsorbents under study. Carboxylate groups exhibit bands in the range 1700-1732 and ~1200 cm^{-1} for the adsorbents under study. The bands were shifted to 1710-1735 and 1215-1265 cm^{-1} respectively in metal loaded adsorbents. This shift could be due to the association of the carbonyl group with metal ions [37]. The bands at 1125 cm^{-1}-1127 cm^{-1} could be due to the –C–O stretching of ether groups while the bands at 1030 cm^{-1}-1065 cm^{-1} could be assigned to the –C–O stretching of alcoholic groups. The difference between C=O and C-O bond stretching has been related to the relative symmetry of these two carbon-oxygen bonds and is reported to reflect the nature of carboxyl group binding status [48].

Adsorbents were found to have much larger Δ values than the metal loaded adsorbents (Table 3.6). The lower values of Δ in the presence of metal ions indicate the involvement of carboxylate groups in forming complexes with metal ions.

Table 3.6.Δ values for virgin and metal loaded adsorbents

Biosorbent	$\upsilon_{C=O}$	υ_{C-O}	$\Delta = \upsilon_{C=O} – \upsilon_{C-O}$	**Biosorbent**	$\upsilon_{C=O}$	υ_{C-O}	$\Delta = \upsilon_{C=O} – \upsilon_{C-O}$
PSP	1732	1250	482	PAPSP	1723	1235	488
APSP	1720	1229	491	MPSP	1727	1238	489
SAPSP	1723	1229	494				
PSP-Cd	1717	1238	479	PSP-Zn	1735	1263	472
APSP-Cd	1709	1229	480	APSP-Zn	1719	1229	490
SAPSP-Cd	1716	1229	487	SAPSP-Zn	1723	1237	486
PAPSP-Cd	1716	1229	487	PAPSP-Zn	1709	1229	480
MPSP-Cd	1716	1237	479	MPSP-Zn	1731	1229	502
PSP-Cu	1738	1261	477	PSP-Hg	1758	1283	475
APSP-Cu	1728	1294	434	APSP-Hg	1728	1260	468
SAPSP-Cu	1731	1289	442	SAPSP-Hg	1766	1290	476
PAPSP-Cu	1723	1285	438	PAPSP-Hg	1728	1285	443
MPSP-Cu	1738	1268	470	MPSP-Hg	1735	1260	475

It is clear from the FT-IR analysis that the possible mechanism of adsorption of Cd^{2+}, Zn^{2+}, Cu^{2+} and Hg^{2+} on the adsorbents may be physical adsorption, ion exchange, surface precipitation, complexation with functional groups and chemical reactions with surface sites [49, 50].

3.3.6. Column Studies.

The column breakthrough curves for Cd^{2+}, Zn^{2+}, Cu^{2+} and Hg^{2+} are shown in Figure 3.6. The effluent concentration is seen to have the typical ‘S’ shape.

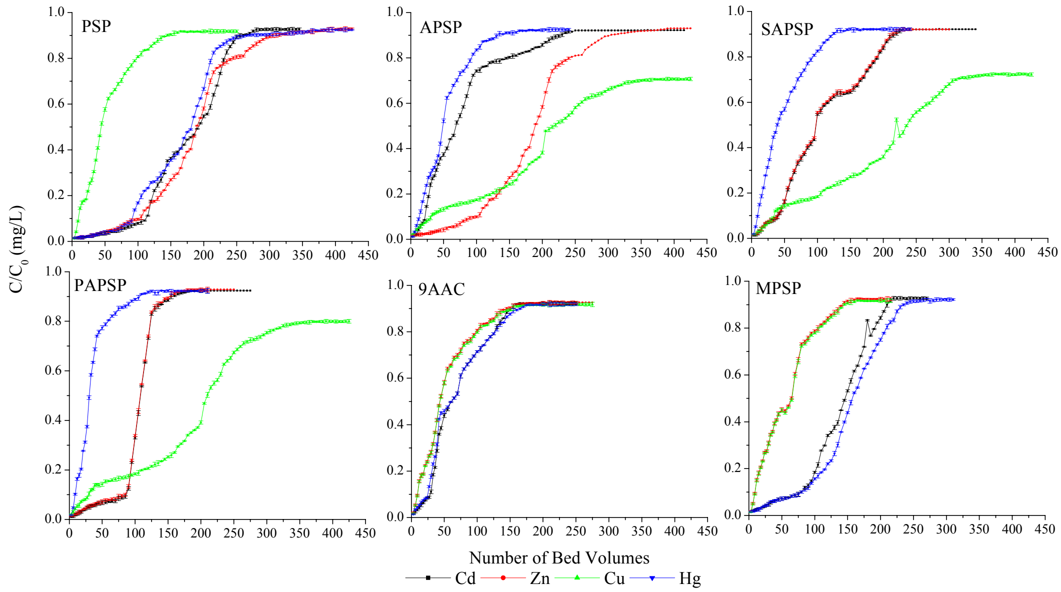

Figure 3.6. Column breakthrough studies

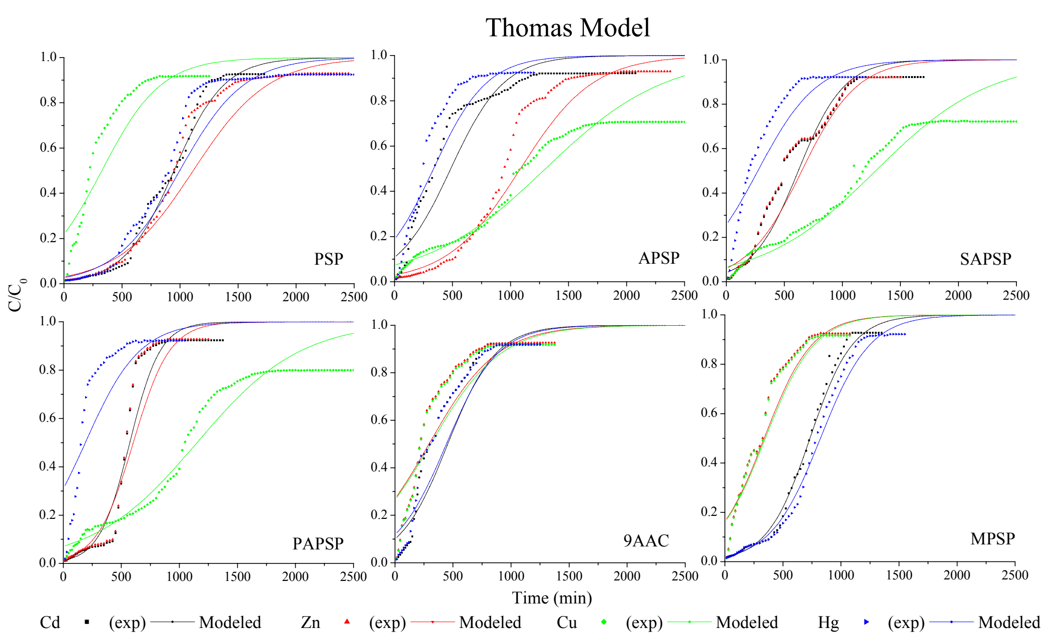

Figure 3.7. Thomas Model for forCu^{2+}, Cd^{2+}, Zn^{2+} and Hg^{2+}

Thomas and Yoon–Nelson models were also applied to the column adsorption data at a flow rate of 1mL/min at an initial metal ion concentration of 1g/L and bed height 5cm for M^{2+} with all the adsorbents under study. The respective values of Thomas rate constant (k_{Th}) and bed capacity (q_{Th}) were calculated from the linear plots of $\ln[(C_o/C_t)-1]$ versus V_{eff}. The theoretical predictions based on the model parameters are compared in Figure 3.7with the observed data. The well fit of the experimental data on to the Thomas model indicate that external and internal diffusion will not be the limiting step.

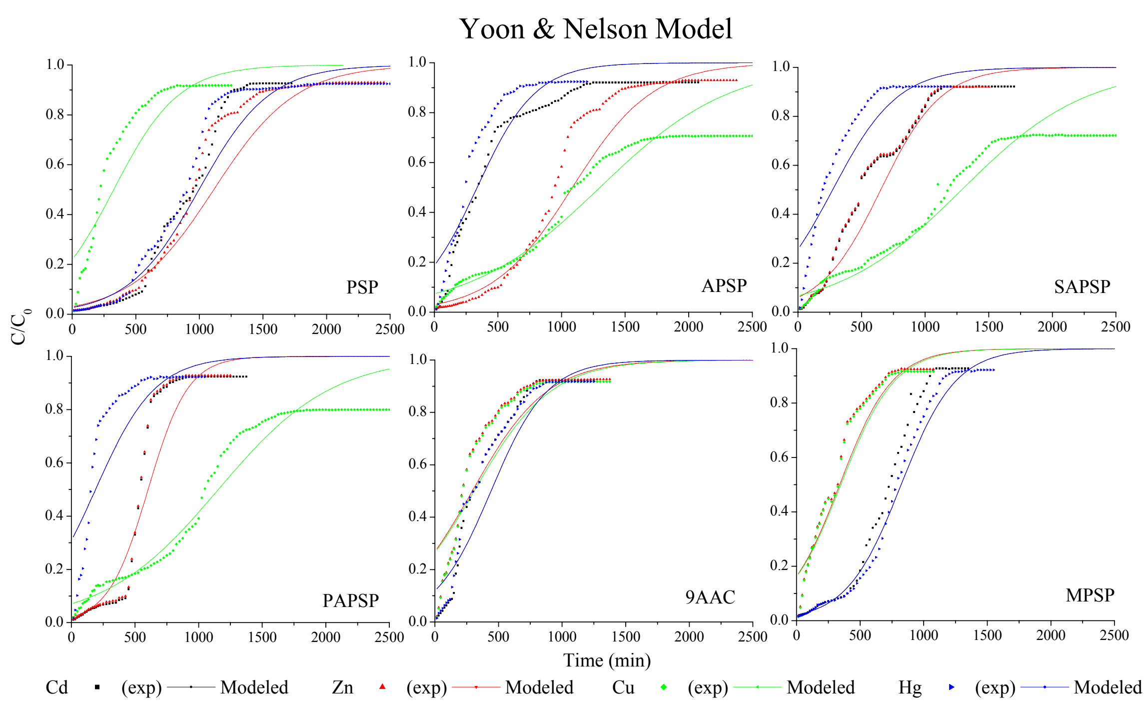

Figure 3.8. Yoon & Nelson Model for Cu^{2+}, Cd^{2+}, Zn^{2+} and Hg^{2+}

It can be seen that the less stirred property in column mode reduces the M^{2+}adsorption capacity of PSP, APSP, SAPSP, PAPSP, 9AAC and MPSP. The trend observed in maximum adsorption capacity measured in batch system is different from that measured in columns as the diffusion coefficient is different in batch and column reactors and is also dependent on flow rate in column [51].From the equations in Table 3.1 it is evident that the characteristic parameter associated with Thomas and Yoon and Nelson models (Figure 3.8) vary but both the models predict essentially same uptake capacity and C/C_0 values for a particular experimental set of data. Hence same r^2 and SD values were obtained as also suggested by Baral et al. [52].

3.3.7. Desorption studies.

Solutions of 0.1 N HCl, 0.1 N EDTA and 0.1 N NH_3 have been studied as eluents for desorption of M^{2+}.

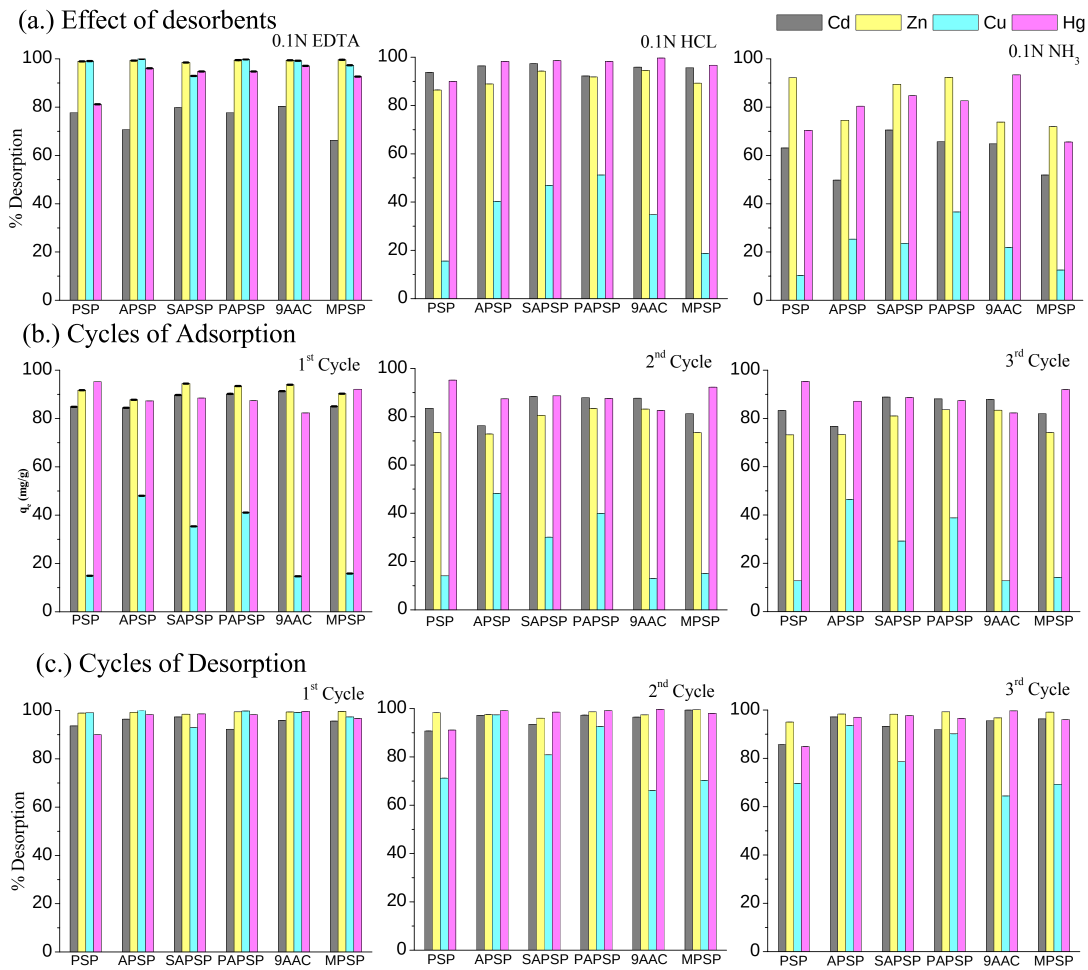

Operating parameters: Adsorption: 30 ^{0}C, 180 min, optimum pH, 1000 ppm, 0.1 g adsorbent, 180 rpm. Desorption: 0.1 N eluent, 30 ^{0}C.

Figure 3.9. Desorption and cycles of adsorption: a)Effect of desorbents, b) Cycles of adsorption, c) Cycles of desorption for Cu^{2+}, Cd^{2+}, Zn^{2+} and Hg^{2+}

From Figure 3.9 it is evident that desorption of Cd^{2+} and Zn^{2+} from the metal-loaded adsorbents with 0.1M HCl and 0.1M EDTA resulted in greater than 92 and 99% recovery of these metals, respectively. It was observed that Cd(II) and Zn(II) were easily desorbed within 30 min, which would prove highly advantageous for metal recovery. It is also seen that the removal capacity of adsorbents decreased only by ~6% in the second cycle, and by ~6.5% in the third cycle. Quantitative desorption of Cd(II) and ~86% desorption of Zn(II) with HCl suggests that the metal ions are adsorbed to the functional groups of the adsorbents under study by electrostatic attraction while ~79% desorption of Cd(II) and quantitative desorption of Zn(II) with 0.1N EDTA could be due to the stability of Cd-EDTA ($2.9x10^{16}$) and Zn-EDTA ($3.2x10^{16}$) chelates.

HCl desorbed 16-42% of Cu^{2+} from the adsorbents under study while NH_3 desorbed 10-38% of Cu^{2+}. On the other hand EDTA was found to be effective in desorbing >95% of copper from all the adsorbents under study.The adsorbents exhibited highest copper uptake capacities for PAPSP (48, 48 and 47 mg/g in first, second and third cycles, respectively). In the case of APSP and PAPSP 0.1M EDTA maintained a consistent elution efficiency of around 100, 98, 97% in the first second and third desorption cycle respectively. Such high elution efficiency with EDTA could be due to high stability constants of Cu-EDTA complexes.

From Figure 3.9 it is evident that desorption of Hg^{2+} from the metal-loaded PSP with 0.1M HCl resulted with ~90% recovery. However, the use of 0.1M EDTA and 0.1 M NH_3 resulted in 81.2 and 70.2 % recovery of Hg^{2+} respectively. It was observed that mercury was easily desorbed within 30 min, which would prove highly advantageous for metal recovery. This indicates that ion exchange is involved in the adsorption process [53].

It was observed that all the metal ions were easily desorbed within 30 min, which would prove highly advantageous for metal recovery. Thus regeneration and reuse of the adsorbents under studywas checked for 3 cycles and found to be an economical and efficient method for removal of M^{2+} from water.

3.3.8. X-ray Photoelectron Spectroscopy.

The wide scan XPS spectra of adsorbents (native and metal-loaded adsorbents) are presented in Figure 3.10,deconvoluted spectra in Figures 3.11 and 3.12 and the corresponding binding energies with relative content of species studied are listed in Table 3.7. X-ray photoelectron spectroscopy was employed to study the binding energy (BE) of oxygen (O1s), carbon (C1s), nitrogen (N1S) in adsorbents under study and to study the shift in binding energy after mercury and copper adsorption.

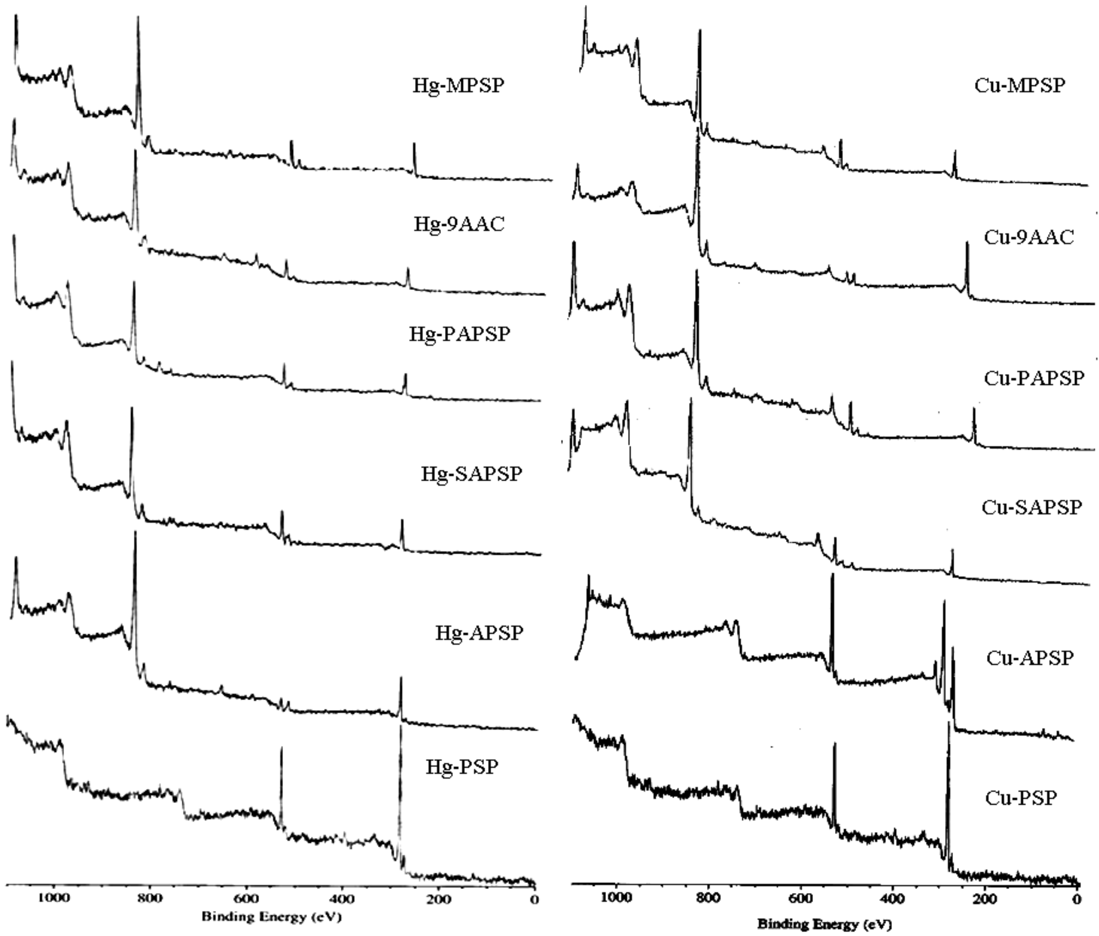

Figure 3.10. Wide scan spectra for $Cu^{2+}$and Hg^{2+}

The changes in the contents of C=O and C-O after metaladsorption indicate that, these groups are involved in the adsorption of metal onto the adsorbents, which is consonant with the FT-IR analysis

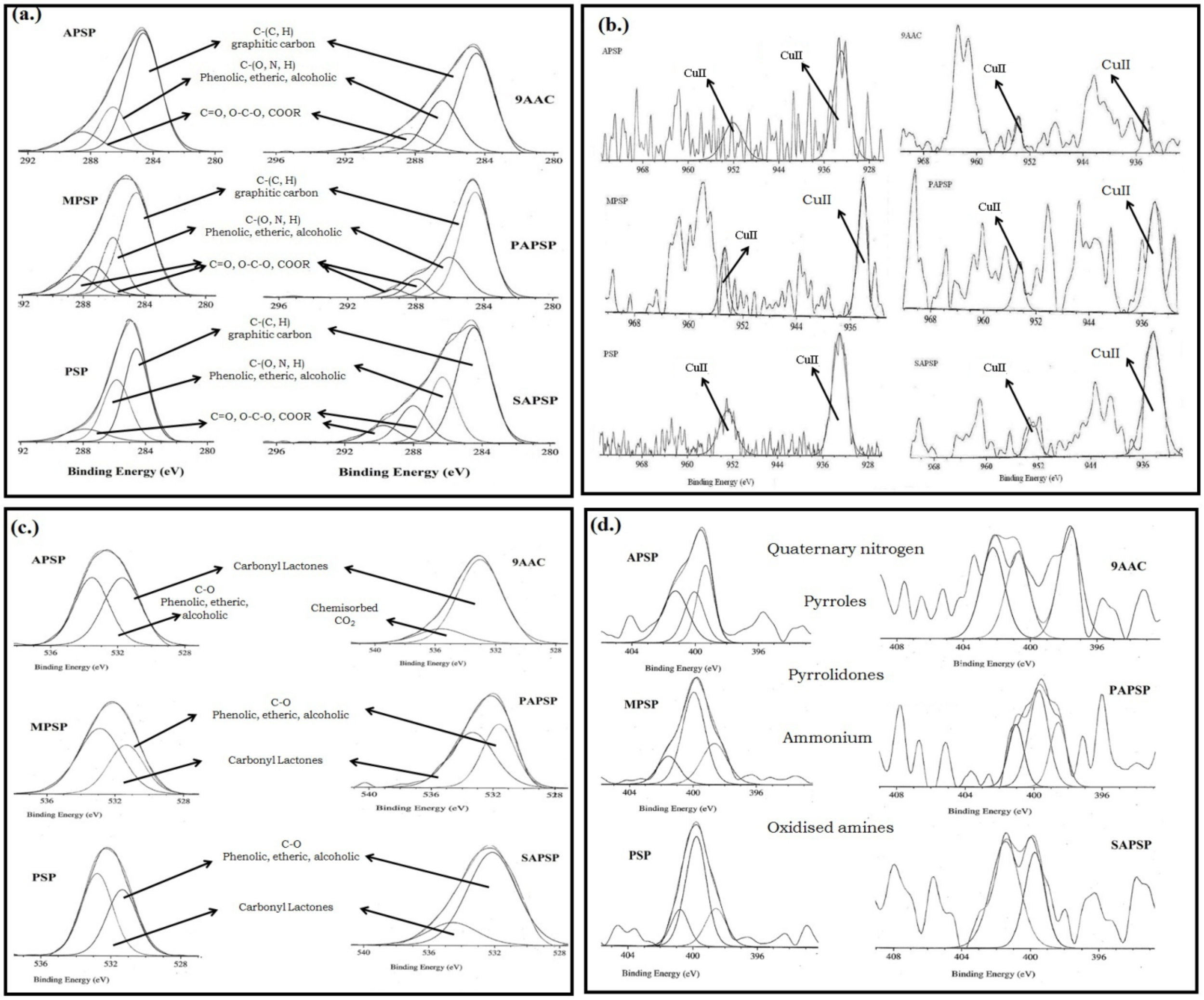

Figure 3.11. Deconvoluted(a.) C1s spectra (b.)Cu2p spectra (c.)O1s spectra and (d.) N1s spectra for the Cu-loaded adsorbents

.

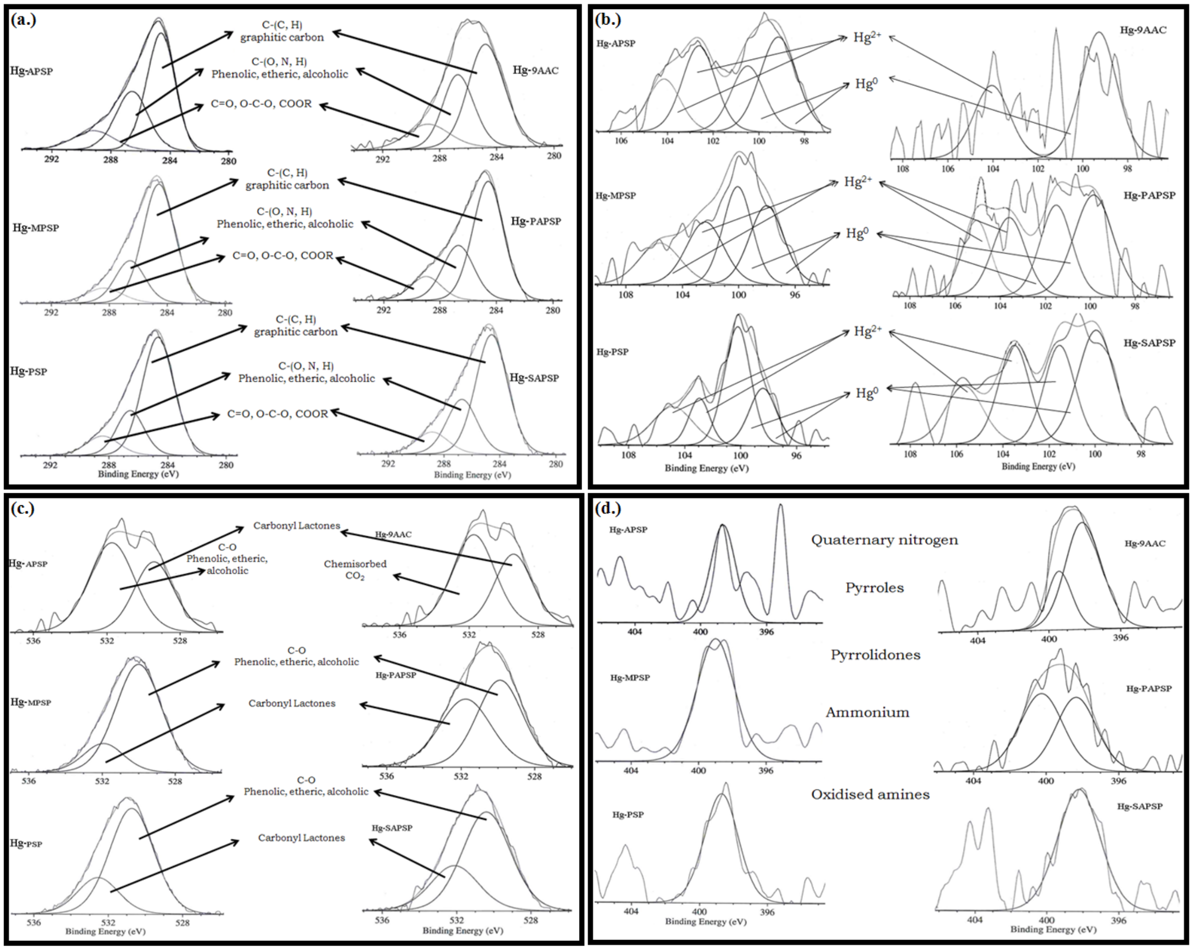

Figure 3.12. Deconvoluted (a.) C1s spectra (b.)Cu2p spectra (c.)O1s spectra and (d.) N1s spectra for the Hg-loaded adsorbents

Table 3.7. Summary of binding energy and area ratios of pristine and Cu^{2+}& Hg^{2+}-loaded sorbents

Sample Surface	Proposed components	Binding Energy(eV)	FWHM	Relative Quantity
C1s Valence State				
PSP	C-(C, H) graphitic C	284.661	2.310	0.6906
	C-(O, N, H) phenolic, alcoholic, etheric	285.984	1.774	0.1871
	C=O, O-C-O, COOR -carbonyl or quinine	287.200	2.495	0.1223
Hg-PSP	C-(C, H)	284.642	2.504	0.6639
	C-(OH, OR)	286.569	2.196	0.2209
	O=C-O carboxyl or ester	288.442	2.624	0.1152
Cu-PSP	C-(C, H)	284.570	1.899	0.6685
	C-(OH, OR)	286.183	1.663	0.2264
	O=C-O carboxyl or ester	287.881	2.186	0.1051
APSP	C-(C, H)	284.647	2.462	0.6716
	C-(OH, OR)	286.599	2.074	0.2112
	O=C-O	288.577	2.605	0.1172
Hg-APSP	C-(C, H)	284.696	2.206	0.5529
	C-(OH, OR)	286.605	2.550	0.3179
	O=C-O	289.188	3.139	0.1291
Cu-APSP	C-(C, H)	284.590	2.118	0.5491
	C-(OH, OR)	286.321	2.562	0.3086

	O=C-O	288.894	3.896	0.1263
SAPSP	C- (C, H)	284.524	2.264	0.5272
	C-(OH, OR)	286.342	1.894	0.2499
	O=C-O	288.073, 289.791	1.973, 2.181	0.1471, 0.0758
Hg-SAPSP	C- (C, H)	284.645	2.634	0.6139
	C-(OH, OR)	286.762	2.543	0.2700
	O=C-O	288.874	2.706	0.1151
Cu-SAPSP	C-(C, H)	284.682	2.374	0.4528
	C-(OH, OR)	286.275	2.331	0.3219
	O=C-O	288.115, 289.936	2.180, 2.467	0.1537, 0.0717
PAPSP	C-(C, H)	284.590	2.051	0.6297
	C-(OH, OR)	286.071	2.204	0.2552
	C=O, O-C-O, COOR	287.979	1.527	0.0817
	O=C-O	289.308	1.424	0.0334
Hg-PAPSP	C-(C, H)	284.620	2.510	0.5989
	C-(OH, OR)	286.738	2.576	0.2819
	O=C-O	289.023	2.515	0.1191
Cu-PAPSP	C-(C, H)	284.581	2.367	0.4962
	C-(OH, OR)	286.119	2.337	0.2895
	C=O, O-C-O, COOR	287.957	2.502	0.1621
	O=C-O	289.802	2.602	0.0521
9AAC	C-(C, H)	284.507	2.336	0.5552
	C-(OH, OR)	286.511	2.284	0.2822
	C=O, O-C-O, COOR	288.384	2.572	0.1155
	C=C, occluded CO, π electrons in aromatic ring, CO_2	290.295	3.464	0.0471
Hg-9AAC	C-(C, H)	284.665	2.935	0.5300
	C-(OH, OR)	286.660	2.513	0.3209
	C=O, O-C-O, COOR	288.806	3.483	0.1481
Cu-9AAC	C-(C, H)	284.566	2.507	0.6918
	C-(OH, OR)	286.472	2.352	0.1744
	O=C-O	288.556	2.360	0.0829
	C=C, occluded CO, π electrons in aromatic ring, CO_2	290.939	3.606	0.0509
MPSP	C-(C, H, R), C-(C, H)	284.624	2.460	0.5456
	C-(OH, OR)	286.116, 286.346	1.718, 2.120	0.2137, 0.1311
	C=O, O-C-O, COOR O=C-O	288.517	2.491	0.1095
Hg-MPSP	C-(C, H, R), C-(C, H)	284.621	2.528	0.6759
	C-(OH, OR)	286.573	2.380	0.2260
	C=O, O-C-O, COOR O=C-O	288.391	2.907	0.9801
Cu-MPSP	C-(C, H, R), C-(C, H)	284.634	2.606	0.4712
	C-(OH, OR)	286.237	2.208	0.3381
	C=O, O-C-O COOR	287.650	1.517	0.1122
	O=C-O	289.142	1.897	0.0785
O1s Valence State				
PSP	C=O, C-O (Lactones, phenolic and etheric)	531.400	2.050	0.4424
	Singly bonded oxygen C-O	532.846	2.072	0.5576
Hg-PSP	C=O, C-O(Lactones, phenolic and etheric)	530.749	2.751	0.7579
	Singly bonded oxygen C-O	532.546	2.563	0.2521
Cu-PSP	C=O, C-O(Lactones, phenolic and etheric)	531.416	2.137	0.4460
	Singly bonded oxygen C-O	532.843	2.023	0.5539
APSP	C=O, C-O (Lactones, phenolic and etheric)	531.770	2.606	0.8160
	Singly bonded oxygen C-O	533.570	2.394	0.4796
Hg-APSP	C=O, C-O (Carboxylic acid, etheric, lactonic, anhydrides,	530.216	3.481	0.7579

	pyrones and phenols)	532.568	2.929	0.2421
Cu-APSP	C=O, C-O(Lactones, phenolic and etheric)	531.417	2.315	0.4934
	Singly bonded oxygen C-O	533.252	2.402	0.5067
SAPSP	C=O (Carboxylic acid)	532.209, 534.596	3.492, 3.517	0.8032, 0.1968
Hg-SAPSP	C=O, C-O (Carboxylic acid, etheric, lactonic, anhydrides, pyrones and phenols)	530.410, 532.119	2.987, 2.988	0.6869 0.3130
Cu-SAPSP	C=O, C-O (Carboxylic acid, etheric, lactonic, anhydrides, pyrones and phenols)	531.859 533.815	3.167 3.150	0.6953 0.3047
PAPSP	C=O, C-O (Carboxylic acid, etheric, lactonic, anhydrides, pyrones and phenols)	531.656 533.388	2.449 3.347	0.4576 0.5424
Hg-PAPSP	C=O, C-O (Carboxylic acid, etheric, lactonic, anhydrides, pyrones and phenols)	529.915 531.754	2.888 3.263	0.5321 0.4680
Cu-PAPSP	C=O, C-O (Carboxylic acid, etheric, lactonic, anhydrides, pyrones and phenols)	531.935 533.832	2.771 2.781	0.6274 0.3726
9AAC	C=O, C-O (Carboxylic acid, etheric, lactonic, anhydrides, pyrones and phenols)	533.080	3.389	0.8437
	Occluded CO, chemisorbed CO_2, O_2 and H_2O	535.638	3.618	0.1563
Hg-9AAC	C=O, C-O (Carboxylic acid, etheric, lactonic, anhydrides, pyrones and phenols)	529.434 531.736	2.518 2.851	0.4085 0.5910
Cu-9AAC	C=O, C-O (Carboxylic acid, etheric, lactonic, anhydrides, pyrones and phenols)	531.586 533.576	3.039 3.071	0.6443 0.3557
MPSP	C=O, C-O (Carboxylic acid, etheric, lactonic, anhydrides, pyrones and phenols)	531.367 532.931	2.440 2.978	0.3795 0.6205
Hg-MPSP	C=O, C-O (Carboxylic acid, etheric, lactonic, anhydrides, pyrones and phenols)	530.044 532.934	2.893 2.577	0.8089 0.1911
Cu-MPSP	C=O, C-O (Carboxylic acid, etheric, lactonic, anhydrides, pyrones and phenols)	531.497 533.075	2.757 2.798	0.5732 0.4268
N1S				
PSP	C-N-C (pyrrolic nitrogen, pyridines)	399.839, 398.597, 400.846	1.492, 1.512, 1.258	0.6129, 0.2141, 0.1729
Hg-PSP	C-N-C (pyrrolic nitrogen, pyridones)	398.759	2.317	1.000
Cu-PSP	C-N-C (pyrrolic nitrogen, pyridones)	399.182, 400.207	1.578, 2.038	0.3922, 0.6078
APSP	C-N-C (pyrrolic nitrogen, pyridones)	399.98, 400.075	1.228, 1.468	0.3556, 0.2780
	Quartenary nitrogen, protonated pyridinic ammonium ions, nitrogen atoms replacing carbon in graphene	401.278	1.908	0.3664
Hg-APSP	C-N-C (pyrrolic nitrogen, pyridones)	398.658	1.734	1.000
	Quartenary nitrogen, protonated pyridinic ammonium ions, nitrogen atoms replacing carbon in graphene	401.278	1.908	0.3664
Cu-APSP	C-N-C (pyrrolic nitrogen, pyridones)	400.028	1.824	0.6157
	Oxidised nitrogen functionalities or NO_2 groups	402.307	1.486	0.3843
SAPSP	C-N-C (pyrrolic nitrogen, pyridones)	399.797	1.366	0.3883
	Quartenary nitrogen, protonated pyridinic ammonium ions, nitrogen atoms replacing carbon in graphene	401.477	1.941	0.6118
Hg-SAPSP	C-N-C (pyrrolic nitrogen, pyridones)	398.237	2.747	1.000
Cu-SAPSP	C-N-C (pyrrolic nitrogen, pyridones)	400.073	1.753	0.7105
	Quartenary nitrogen, protonated pyridinic ammonium ions, nitrogen atoms replacing carbon in graphene	401.567	1.403	0.2895
PAPSP	C-N-C (pyrrolic nitrogen, pyridones)	398.584, 399.774	1.097, 1.319	0.2677, 0.4869

	Quartenary nitrogen, protonated pyridinic ammonium ions, nitrogen atoms replacing carbon in graphene	401.074	1.032	0.2454
Hg-PAPSP	C-N-C (pyrrolic nitrogen, pyridones)	398.348, 400.289	2.603, 2.781	0.4710, 0.5291
Cu-PAPSP	C-N-C (pyrrolic nitrogen, pyridones)	399.928	1.824	0.6157
	Oxidised nitrogen functionalities or NO_2 groups	402.207	1.486	0.3843
9AAC	C-N-C (pyrrolic nitrogen, pyridones)	397.686, 400.803	1.516, 1.596	0.3000, 0.3745
	Oxidised nitrogen functionalities or NO_2 groups	402.300	1.639	0.3255
Hg-9AAC	C-N-C (pyrrolic nitrogen, pyridones)	398.022, 399.356	1.516, 1.596	0.7319, 0.2681
Cu-9AAC	C-N-C (pyrrolic nitrogen, pyridones)	397.100, 399.700	1.326, 1.342	0.4173, 0.3199
	Quartenary nitrogen, protonated pyridinic ammonium ions, nitrogen atoms replacing carbon in graphene	401.400	1.199	0.2627
MPSP	C-N-C (pyrrolic nitrogen, pyridones)	398.703, 400.000	1.889, 1.679	0.2787, 0.5613
	Quartenary nitrogen, protonated pyridinic ammonium ions, nitrogen atoms replacing carbon in graphene	401.606	1.570	0.1599
Hg-MPSP	C-N-C (pyrrolic nitrogen, pyridones)	398.999	2.583	1.000
Cu-MPSP	Quartenary nitrogen, protonated pyridinic ammonium ions, nitrogen atoms replacing carbon in graphene	401.191	1.587	0.1034
	C-N-C (pyrrolic nitrogen, pyridones)	398.641, 399.939	2.160, 1.332	0.5294, 0.3672
Hg-PSP	Hg-4f 5/2 (Hg^0) Hg-4f 5/2 (Hg^0) Hg-4f 7/2 (Hg^{+2}) Hg-4f 7/2 (Hg^{+2})	98.460 102.985 100.303 104.878	2.279 1.733 2.155 3.366	0.2169 0.1359 0.4310 0.2170
Cu-PSP	Cu-2p3/2 (Cu^{+2}) Cu-2p1/2 (Cu^{+2})	933.100 952.991	2.200 1.578	0.8685 0.1324
Hg-APSP	Hg-4f 5/2 (Hg^0) Hg-4f 5/2 (Hg^0) Hg-4f 7/2 (Hg^{+2}) Hg-4f 7/2 (Hg^{+2})	99.191 102.626 100.499 104.153	1.859 1.680 1.688 1.665	0.3399 0.2780 0.2130 0.1681
Cu-APSP	Cu-2p3/2 (Cu^{+2}) Cu-2p1/2 (Cu^{+2})	932.982 952.160	3.181 3.982	0.7000 0.2999
Hg-SAPSP	Hg-4f 5/2 (Hg^0) Hg-4f 5/2 (Hg^0) Hg-4f 7/2 (Hg^{+2}) Hg-4f 7/2 (Hg^{+2})	99.950 103.531 101.533 105.678	1.858 1.564 1.539 1.909	0.3359 0.2457 0.2422 0.1761
Cu-SAPSP	Cu-2p3/2 (Cu^{+2}) Cu-2p1/2 (Cu^{+2})	934.419 952.875	3.020 1.981	0.8431 0.1569
Hg-PAPSP	Hg-4f 5/2 (Hg^0) Hg-4f 5/2 (Hg^0) Hg-4f 7/2 (Hg^{+2}) Hg-4f 7/2 (Hg^{+2})	99.899 103.653 101.547 105.092	2.011 1.691 1.633 1.441	0.3429 0.2230 0.2501 0.1839
Cu-PAPSP	Cu-2p3/2 (Cu^{+2}) Cu-2p1/2 (Cu^{+2})	934.441 954.836	2.216 1.694	0.7536 0.2473
Hg-9AAC	Hg-4f 5/2 (Hg^0) Hg-4f 7/2 (Hg^{+2})	99.273 104.068	1.842 1.854	0.6319 0.3680
Cu-9AAC	Cu-2p3/2 (Cu^{+2}) Cu-2p1/2 (Cu^{+2})	934.521 953.845	1.106 1.193	0.5370 0.4629
Hg-MPSP	Hg-4f 5/2 (Hg^0) Hg-4f 5/2 (Hg^0) Hg-4f 7/2 (Hg^{+2}) Hg-4f 7/2 (Hg^{+2})	98.088 102.420 100.122 105.610	2.816 3.084 2.385 3.419	0.2809 0.2440 0.2959 0.1791
Cu-MPSP	Cu-2p3/2 (Cu^{+2}) Cu-2p1/2 (Cu^{+2})	934.400 954.849	1.582 1.405	0.6949 0.3050

Table 3.8. Surface concentration of oxygen containing carbon and graphitic carbon, % content of C, N and O

Samples	Cox/Cg	Surface concentration (from C 1s peak)%				
Native		C in graphite	Phenol-ether	Carbonyl-quinone	Carboxyl	Others
Hg-PSP	0.506	66.39	22.09	-	11.52	-
Hg-APSP	0.808	55.29	31.79	-	12.91	-
Hg-SAPSP	0.627	61.39	27.00	-	11.51	-
Hg-PAPSP	0.669	59.89	28.19	-	11.91	-
Hg-MPSP	0.479	67.59	22.60	-	9.80	-
Hg-9AAC	0.884	53.00	32.09	-	14.81	-
Cu-PSP	0.234	81.1	14.9	4.0	-	-
Cu-APSP	0.959	54.91	30.86	-	12.63	-
Cu-SAPSP	1.208	45.28	32.19	15.37	7.17	-
Cu-PAPSP	1.015	49.62	28.95	16.21	5.21	-
Cu-MPSP	1.122	47.12	33.81	11.22	7.85	-
Cu-9AAC	0.446	69.18	17.44	-	8.29	5.09
Native	**XPS (C, N, O)**	**O/ C ratio**	**Cu-Loaded**	**XPS (C, N, O)**		**O/ C ratio**
Hg-PSP	49.43, 1.39, 49.18	0.995	**Cu-PSP**	54.48, 1.74, 43.79		0.804
Hg-MPSP	54.54, 1.07, 44.39	0.814	**Cu-MPSP**	50.07, 1.62, 48.30		0.965
Hg-APSP	68.82, 0.39, 30.79	0.448	**Cu-APSP**	50.58, 0.49, 48.93		0.967
Hg-SAPSP	46.44, 1.58, 51.98	1.119	**Cu-SAPSP**	49.64, 0.58, 49.79		1.003
Hg-PAPSP	43.46, 3.18, 53.36	1.228	**Cu-PAPSP**	51.03, 0.49, 48.48		0.950
Hg-9AAC	53.89, 1.10, 45.00	0.835	**Cu-9AAC**	61.57, 0.68, 37.75		0.613

Table 3.8 shows changes in the contents of C=O and C-O after copper and mercury adsorption suggesting that these groups are involved in the adsorption of the metal ions onto the adsorbents, which is in consonance with the FT-IR results. The 2*p*3/2 peak of copper was fitted by binding energies corresponding to 933.1, 932.982, 934.419, 934.441,934.521 and 934.400 for PSP, APSP,SAPSP, PAPSP, 9AAC and MPSP. The peaks for Cu^{2+} in Cu-PSP and Cu-APSP could be characterized as the Cu^{2+} that has relatively higher electron density in its valence shell, and the corresponding peaks in Cu-SAPSP, Cu-PAPSP, Cu-9AAC and Cu-MPSP as the Cu^{2+} ion with lower electron density in its valence shell. Cu^{2+} can gain electrons from the ligands (hydroxyl and ether) via covalent bonding while Cu^{2+} located in the ionic bonding environment (carboxylate) has less electron density. As a result, the Cu^{2+} ions in the former environment gave rise to a peak around ~933 eV and those in the latter one the peak about 934.0 eV. These observations suggested that the adsorption interactions of copper species might involve not only the cation exchange interaction resulted from the oxygen containing functional groups, there should be other interactions like complex formation.Thus the influence of the chemical

interaction of copper with surface functional groups in different environments has resulted in different binding energies for Cu^{2+} on the adsorbents under study.A corresponding shift in C1S peaks and O1S peaks is also observed

The XPS spectrum of copper treated adsorbents under study does not indicate any reduction whereas in case of mercury it showed reduction of Hg^{+2} to metallic mercury simultaneously oxidizing the adsorbent surface. The surface groups were divided for the adsorbents under study by taking their percentage in the surface layer from XPS data (C 1s peak was taken into account, following the procedure presented in [54]), as shown in Table 3.8. A relatively stronger intense peak at a BE of 398.759 eVindicates that the N-atoms existed in a more reduced state on the surfaces of adsorption due to mercury adsorption. This may be due to the formation of the covalent bond of N-Hg in which, Hg shared electrons with the N-atom, which increased the electron cloud density of the nitrogen atom and resulted in a lower BE peak observed.Deconvoluted XPS spectra of mercury in the Hg 4f region and the peaks at 99.779 and 103.949 eV correspond to the binding energies (4f7/2 and 4f 5/2) of elemental mercury [55]. On the other hand, the peaks at 100.303 and 104.878 eV correspond to the binding energies (4f7/2 and 4f 5/2) of Hg(II) in HgO[56] suggesting that part of the mercury on PSP is present in elemental form and partly in +2 state.An increase in the O/C ratio is observed which can be attributed to the oxidation of lignin aromatic carbons (aldehydic groups) by Hg(II) and formation of alcoholic sites, carboxylic sites and elemental mercury. Similar observation has been made by Dupont et al. during their studies on the removal of hexavalent chromium with a lignocellulosic substrate extracted from wheat bran [57]which could be related to the abundance of lignin and fatty acid moieties, which allow the reduction of Hg(II) into Hg(0) on carboxylic moieties [58].Earlier studies reflected the binding of mercury on the biomass occurs through electrostatic and complexation reactions[59, 60].

3.3.9. Solid state-^{13}CNMR Spectroscopic Analysis.

^{13}C NMR spectral analysis was done only for copper loaded samples as a representative to see the changes occurring in the adsorbents after metal adsorption.^{13}C solid state NMR spectra of Cu-loaded adsorbents is presented in Figure 3.13, the peaks assigned to different carbons are shown in Table 3.9.

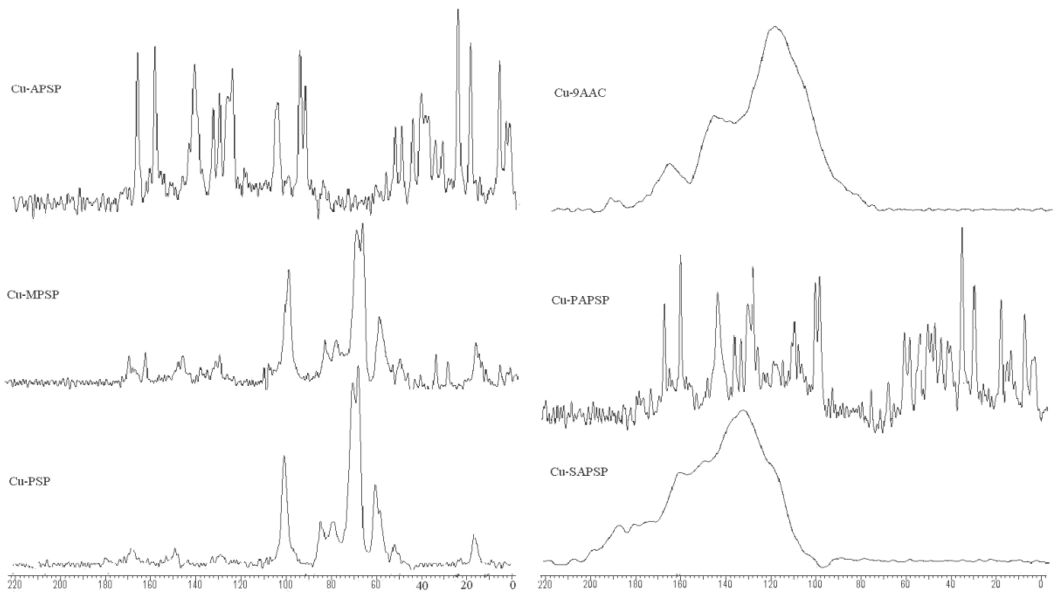

Figure 3.13. NMR spectra for the Cu-loaded adsorbents

Table 3.9. Assignments to the NMR peaks

PSP	Cu-PSP	APSP	Cu-APSP	MPSP	Cu-MPSP	Range	Assignment
-	168	171	171		171	195-165	RCOO-RH (Standard oxidized cellulose) Carboxyl carbon of acetate group of hemicelluloses
-	-	164	164		164	169-140	C_6H_5O-RH Phenolic carbon
-	-	-	148		148	150-140	Subsituted oxygenated aromatic carbon
-	138, 129	130	138		131	135-120	Non oxygenated Aromatic carbons, Aromatic acids and anhydrides
100	101	101	112, 102	112, 101	101	102-108	Anomeric carbon (Anhydroglucose)C1
82	82	-		84, 79	85, 81	81-93	Anomeric carbon (Anhydroglucose)C4 amorphous cellulose~84
60, 70	70, 60, 52	62	61, 57	72, 61, 52	70, 61, 52	50-70	1^0 Alcohol of (Anhydroglucose) Aliphatic C-O C2,C3,C5(~70)C6(~60) amorphous cellulose~62
17	16	48, 36, 30, 18, 6	49, 36, 30, 16, 6	17	36, 30, 18, 8	5-50	Aliphatic C-C possibly of polymethylene type
SAPSP	Cu-SAPSP	PAPSP	Cu-PAPSP	9AAC	Cu-9AAC	Range	Assignment
170	-	171	167	-	192	195-165	RCOO-RH (Standard oxidized cellulose) Carboxyl carbon
-	-	163/146	146	-	-	169-140	C_6H_5O-RH Phenolic carbon
147	-	-	-	-	-	150-140	Subsituted aromatic carbon
-	122	130	138, 132	123	121	135-120	Aromatic carbons, Aromatic acids and anhydrides
111	-	101	116, 101	-	-	102-108	Anomeric carbon (Anhydroglucose)
-	-	-	-	-	-	81-93	Anomeric carbon (Anhydroglucose)
-	-	61, 55	61, 55	-	-	50-70	1^0 Alcohol of (Anhydroglucose) Aliphatic C-O
-	-	48, 35, 31, 16, 6	48,36, 30, 19, 14, 5	-	-	5-50	Aliphatic C-C

Cu-APSP and Cu- PSP showed a peak at 171ppm and 168 ppm respectivelysimilar to thepeak observed at 171 ppm in APSP and PAPSP which can be attributed to the carboxyl carbon (C-6), in the oxidized anhydroglucose unit of the cellulose chain formed after treatment with acid and persulfate respectively This peak is not seen in PSP and is of higher intensity in Cu-APSP than APSP indicating that adsorption of copper has caused changes in the c=o and c-o content as evidenced by XPS spectra. Similarly the peak at 93 ppm in Cu-APSP is attributed to C-1 of the terminal α-D-glucose unit that is usually present in oxidized cellulose .Moreover the peaks are seen to be sharper in Cu-PSP, APSP, Cu-APSP, PAPSP, Cu-PAPSP probably due to binding of Cu(II), and oxidation by acid and persulfate respectively which result in more ordered structures.

3.4. Mechanism.

In this work, several different modifications have been applied to improve/ modify the functional groups of palm shell powder and enhance the uptakes of metal ions. On the basis of FT-IR spectra as well as kinetic and isotherm modeling, the adsorption of Cd^{2+}, Zn^{2+}, Cu^{2+} and Hg^{2+} on the adsorbents could be considered to be via (1) Surface active functional groups like amine and carboxyl involving valence forces through the exchange of electrons, complexation, coordination and/or chelation and (2) Intraparticle diffusion into the micropores. The first step dominates at low concentrations while the latter step at high concentrations of Cd^{2+}, Zn^{2+}, Cu^{2+} and Hg^{2+}. These speculations are in agreement with the reported mechanisms [61-63].

Valeria et al. have reported that cadmium and zinc in aqueous solutions exist as Cd^{2+} and Zn^{2+}in solution till pH 8 and 7 respectively, beyond which the metal hydroxides starts precipitating in [64].

Hence, the probable mechanism by which $M^{2+}$are bound to carboxyl groups is:

$$2(-\mathrm{COOH}) + \mathrm{M}^{2+} \leftrightarrow (-\mathrm{COO})_2 - \mathrm{M} + 2\mathrm{H}^+$$

$$2(-\mathrm{COOH}) + \mathrm{M(OH)}_2 \leftrightarrow (-\mathrm{COO})_2 - \mathrm{M(OH)} + \mathrm{H}^+ + \mathrm{H_2O}$$

$$(-\mathrm{COOH}) + \mathrm{M(OH)}^+ \leftrightarrow (-\mathrm{COO}) - \mathrm{M(OH)} + \mathrm{H}^+$$

The binding mechanism of M^{2+} with phenolic groups could be:

$$2(-\mathrm{C_6H_5} - \mathrm{OH}) + \mathrm{M}^{2+} \leftrightarrow (-\mathrm{C_6H_5} - \mathrm{O})_2 - \mathrm{M} + 2\mathrm{H}^+$$

$$(-\mathrm{C_6H_5} - \mathrm{OH}) + \mathrm{M(OH)}^+ \leftrightarrow (-\mathrm{C_6H_5} - \mathrm{O}) - \mathrm{M(OH)} + \mathrm{H}^+$$

A similar type of mechanism has been proposed for chromium adsorption onto agro-waste materials by Bernardo et al. [65]. Cd^{2+}, Zn^{2+}, Cu^{2+} and Hg^{2+}were considered to be adsorbed due to binding with amino groups by electrostatic interaction as follows:

$$2(-NH_2) + M^{2+} \leftrightarrow (-NH)_2 - M + 2H^+$$

$$(-NH_2) + M^{2+} \leftrightarrow \equiv (-N - M) + 2H^+$$

$$(-NH_2) + M(OH)^+ \leftrightarrow (-NH) - M(OH) + H^+$$

$$(-NH_2) + M(OH)_2 \leftrightarrow (-NH)_2 - M(OH) + H^+ + H_2O$$

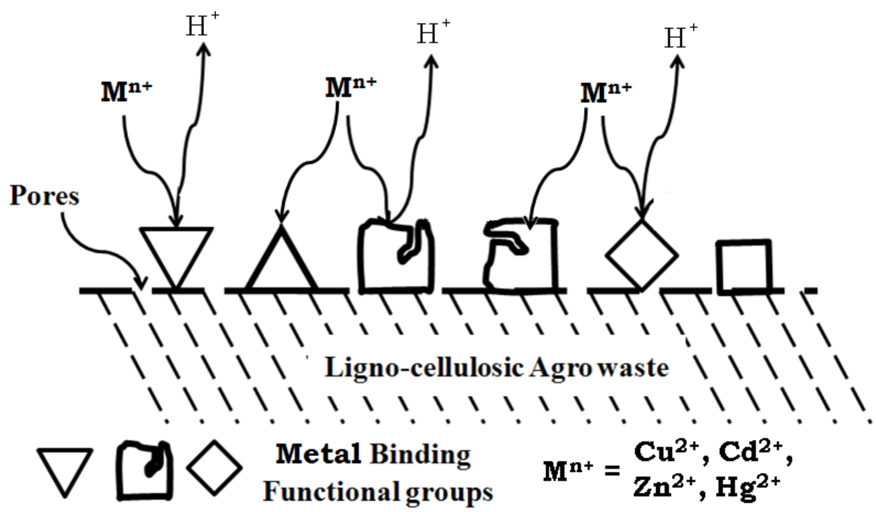

Scheme 3.1. Mechanism for binding of divalent metal ion

The XPS spectra confirmed the presence of Hg^0 and Hg^{2+} on the surface of PSP after mercury adsorption suggesting that reduction of Hg^{2+} to Hg^0 took place on PSP surface. This could be due to the oxidation of lignin aromatic carbons (aldehydic, phenolic and carboxyl groups) by Hg(II) and formation of alcoholic sites, carboxylic sites, CO_2 and elemental mercury.

$$Hg^{2+} + 2e^- \rightarrow Hg^0 \quad E^0 = +0.85\ V$$

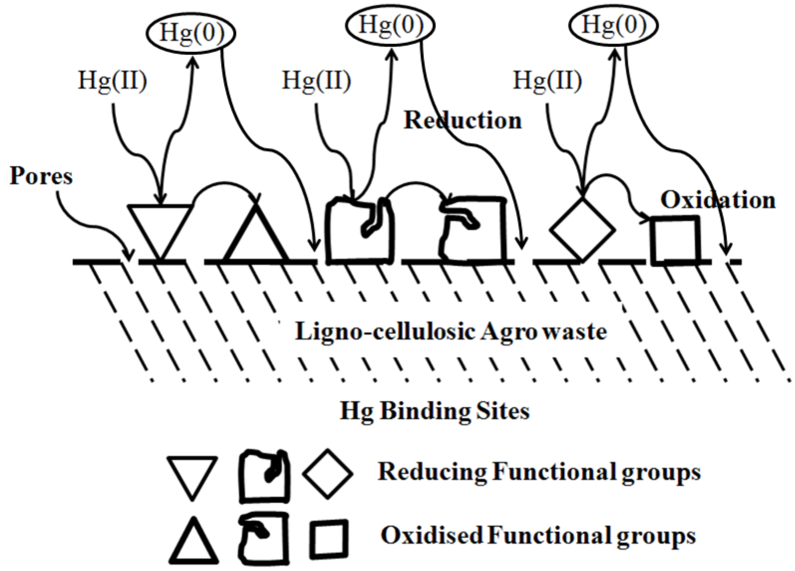

Scheme 3.2. Redox mechanism for mercury

E.I. El-Shafey reported reduction of Hg(II) to Hg(I) using sulfuric acid treated rice husk while M.Cox et al. reported reduction of Hg(II) to Hg(I) and Hg(0) using sulfuric acid treated flax shive[59, 60]. However there have been no literature reports on reduction of Hg(II) using virgin lignocellulosic materials though there have been reports on reduction of Cu(II) to Cu(0) and Cr(VI) to Cr(III) [57, 66]. Xin Huang et al have studied the adsorption of Hg(II) onto bayberry tannin-immobilised collagen fiber wherein they have reported the adsorption mechanism to be only chelation of Hg(II) [67]. Reduction of Hg(II) to Hg(0) has been reported on organic matter present in soil, fungi and other microorganisms [68-72].

3.5. Conclusions.

The prepared adsorbents show potential as effective systems for the removal of trace levels of metal ions from aqueous systems. Potentiometric, FT-IR and XPS studies reveal that carboxyl, amino, hydroxyl, lactonic and phenolic groups on PSP seem to be responsible for mercury adsorption. XPS studies showed different binding energies for Hg^{2+} and Cu^{2+} on the adsorbents under study indicating different types and degrees of chemical interaction of mercury and copper with surface functional groups. XPS studies also indicate that Hg(II) was reduced to Hg(0) on PSP surface and was adsorbed onto it by physisorption.

Sorption isotherms of the metal ions on the adsorbents were studied and modeled using Freundlich, Langmuir, Temkin, Dubinin-Radushkevich (DR), Elovich,Flory-Huggins, and Halsey isotherms.The adsorption data of the metal ions were best fit by Langmuir and Freundlich models.

Pseudo second order kinetics describes the overall sorption preocess well while intraparticle diffusion of the metal ion from the liquid phase to the adsorbent surface might be having some role up to variable extents in deciding the rate processes. The sorption process is exothermic, spontaneous and accompanied by decrease in entropy.

Adsorption of metals is thus a complex process that is based upon a range of mechanisms which differ according to the type of adsorbent, the degree of processing it has undergone and also the adsorbate. The different mechanisms which play a role include ion exchange, chelation and physisorption.In the case of mercury reduction of divalent mercury to elemental mercury also seems to play a role in the case of PSP.

The data obtained from column studies have shown good agreement with the predicted results obtained by application of Thomas model and Yoon and Nelson model as evident from the low value of standard deviation.

Adsorbent regeneration and metal recovery indicate the advantage of not producing any sludge. Thus based on the good uptake capacity, rapid kinetics, regenerability and low cost, the adsorbents under study prepared from palm shell appear to be promising for the removal of cadmium and zinc from aqueous solutions. Interestingly the adsorption capacity of 9AAC and PAPSP were found to be almost similar or sometimes lesser for 9AAC, thus proving that PAPSP is a more economical and efficient adsorbent as compared to 9AAC.

Literature Cited.

1. B. Volesky. *Trends Biotechnol***1987**, *5*, 96.
2. L. Dambies, C. Guimon, S.Yiacoumi, E. Guibal. *Colloid Surf. A***2001**, *17*, 203.
3. M.M. Figueira, B. Volesky, H.J. Mathieu. *Environ. Sci. Technol***1999**, *33*, 1840.
4. E. Fourest, B. Volesky. *Environ. Sci. Technol.***1996**, *30*, 277.
5. J. Buschmann, L. Sigg. *Environ. Sci. Technol.***2004**, *38*, 4535.
6. S.F. Lim, Y.M. Zheng, S.W. Zou and J. Paul Chen. *Environ. Sci. Technol***2008**, *42*, 2551.
7. B. Volesky, Z.R. Holen. *Biotech.Progress***1995**, *11*, 235-250.
8. H. Biester, P. Schuhmacher, G. Muller. *Water Res.***2000**, *34*, 2031.
9. Y.S. Ho. *Water Res.***2006**, *40*, 119.
10. G. Bohart, E. Q. Adams. *J. Am. Chem. Soc.* **1920**, *42*, 523.
11. H. C. Thomas. *J. Am. Chem. Soc.* **1944**, *66*, 1664.
12. Y. H.Yoon, J. H. Nelson. *Am. Indian Hygiene Assoc. J.* **1984**, *45*, 509.
13. R. M. Clark. *EnViron. Sci. Technol.* **1987**, *21*, 573.
14. A. Wolborska. *Water Res.* **1989**, *23*, 85.
15. C. Hepplewhite, G. Newcombe, D.R.U. Knappe. *Water Sci. Technol.***2004,** *49*, 257–265.
16. Langmuir. *J. Am. Chem. Soc.***1916**, *38*, 2221–2295.
17. H.M.F. Freundlich. *Z. Phys. Chem.* **1906**, *57*, 385–470.
18. M.J. Temkin, V. Pyzhev. *ActaPhysiochim***1940**, *12*, 327.
19. P.J. Flory. *J. Chem. Phys***1942**, *10*, 51.
20. M.L. Huggins. *Amt, N.Y. Acad, Sci***1942**, *43*, 1.
21. P.J. Flory. *Discuss. Faraday Soc***1970**, *49*, 7.
22. S.Y. Elovich, O.G. Larinov. *J.Physical Chemistry***1962**, *2*, 209.
23. M.M. Dubinin, L.V. Radushkevich. *ProcAcadSci USSR PhysChem Sect***1947**, *55*, 331.
24. G. Halsey. *J. Chem. Phys.* **1948**, *16*, 931.
25. S. Lagergren, K. Sven, *VetenskapsakadHandlingar***1898**, *24*, 1.
26. Y.S. Ho. Adsorption of heavy metals from waste streams by peat. Ph.D. thesis, University of Birmingham, Birmingham, UK, **1995.**
27. W.J. Weber Jr., J.C. Morris. *J. SanitaryEng. Div. Proceed. Am. Soc. Civil Eng***1963**, *89*, 31.
28. W.J. Weber, J.C.S. Morris, Proceedings of International Conference on Water Pollution Symposium. Oxford **1962**, *2*, 231.

29. W.J. Weber, J.C. Morris. Advances in water pollution research: removal of biologically resistant pollutants from waste waters by adsorption, in: International Conference on Water Pollution Symposium, Pergamon, Oxford **1962**, *2*, 231.
30. W. Rudzinsk, D.H. Everett. Adsorption of gases on heterogeneous surfaces. London: Academic Press; **1992**.
31. Y.S. Ho, G. McKay. *Ads SciTechnol***2002**, *20*,797.
32. W. Rudzinski, T. Panczyk. *Adsorption***2002**, *8*, 23.
33. G.E. Boyd, A.W. Adamson, L.S. Myers. *J. Am. Chem. Soc*. **1947**, *69*, 2836.
34. V.K. Gupta, I. Ali, Suhas, V.K. Saini, *J. Colloid Interface Sci***2006**, *299*, 556.
35. P.X. Sheng, Y.P. Ting, J.P. Chen, L. Hong, *J. Colloid and Interface Sci***2004**,*275*, 131.
36. D.K. Chattopadhyay, B. Sreedhar, V.S.N. Kothapalli, Raju.*Ind. Eng. Chem. Res.* **2005,** *44,* 1772-1779.
37. A. Seco, P. Marzal, C. Gabaldon , J. Ferrer. *J. Chem. Technol. Biotechnol***1997**, *68*, 23.
38. T.K. Budinova, K.M. Gergova, N.V. Petrov, V.N. Minkova. *J. Chem. Technol. Biotechnol***1994**, *60*, 177.
39. P. Marzal, A. Seco, C. Gabaldon, J. Ferrer. *J. Chem. Technol. Biotechnol***1996**, *66*, 279.
40. J.P. Chen, L.Yang, *Ind. Eng. Chem. Res***2005**, *44*, 9931.
41. S.B. Choi, Y.S. Yun. *J. Hazard. Mater* **2006**, *B138*, 378.
42. S.K. Das, A.R. Das, A.K. Guha. *Environ. Sci. Technol***2007**,*41*, 8281.
43. K.V. Kumar, K. Porkodi. *J. Hazard. Mater***2007**, *146*, 214.
44. R.E. Treybal. Mass Transfer Operations, third ed., McGraw-Hill, New York, **1980**.
45. G.S. ElShafei, I. N. Nasr, A.S.M. Hassan, S.G.M. Mohammad. *J. Hazard. Mater* **2009**, *172*, 1608.
46. J. Febrianto, A.N. Kosasih, J. Sunarso, Y.H. Ju, N. Indraswati, S. Ismadji. *J. Hazard. Mater* **2009**, *162*,616.
47. G.J.L. Torresdey, K. Dokken, K.J. Tiemann, J.G. Parsons, J. Ramos, N.E. Pingitore, G. Gamez. *Microchem. J***2002**, *71*, 157.
48. J.P. Chen. L. Yang.*Langmuir* **2006**,*22*,8906.
49. V.K. Gupta, A. Rastogi. *J. Hazard. Mater***2008**, *152***,** 407.
50. K. Srividya, K. Mohanty. *Chem. Eng. J***2009**, *155*, 666.

51. V.J. Inglezakis, S.J. Poulopoulos. Adsorption, ion exchange and catalysis: design of operations and environmental applications, By Elsevier **2006**, 339.
52. S.S. Baral, N. Das, T.S. Ramulu, S.K. Sahoo, S.N. Das, G.R. Chaudhury. *J. Hazard. Mater* **2009**, *161*,1427.
53. L. Xiaomin,Y. Tang, C. Xiuju, L. Dandan, L. Fang, W. Shao. *Colloidsand Surfaces A: Physicochem. Eng. Aspects* **2008**, *317*, 512.
54. F.R. Reinoso, A.L. Solano. Chemistry and Physics of Carbon, by Thrower, P. A.; Marcel Dekker, New York **1989**, *21*, 1.
55. X. Zeng, S. Prasad, S. Bruckenstein. *Langmuir* **1998**, *14*,2535.
56. K.P. Lisha, S.M. Maliyekkal, T. Pradeep. *Chem. Eng. J* **2010**, *160*, 432.
57. L. Dupont, E. Guillon. *Environ. Sci. Technol* **2003**, *37*, 4235.
58. K.K. Krishnani, X. Meng, C. Christodoulatos, V.M. Boddu. *J. Hazard. Mater* **2008**,*153*, 1222.
59. E.I. El-Shafey. *J. Hazard. Mat* **2010**,*175*, 319.
60. M.Cox, E.I. El-Shafey, A.A.Pichugin, Q. Appleton. *J. Chem. Technol. Biotechnol* **1999**, *74*, 1019.
61. Y. Wang, X.W. Tang, Y.M. Chen, L.T. Zhan, Z.Z. Li and Q. Tang. *J. Hazard. Mater.* **2009**, *172*, 30.
62. Z. Li, X. Tang, Y. Chen, L. Wei, Y. Wang. *J. Hazard. Mater.* **2009**,*169*,386.
63. Z. Li, T. Katsumi, S. Imaizumi, T. Xiaowu, T. Inui. *J. Hazard. Mater.* **2010**,*183*, 410.
64. M.N. Valeria, I. Villaescusa. *Coord. Chem. Rev.* **2008**, *252*, 1178.
65. G.R.R. Bernardo, R.M.J. Rene. *J. Hazard. Mater.* **2009**, *170*, 845.
66. J. G. Parsons, M. Hejazi, K. J. Tiemann, J. Henning, J. L.G. Torresdey. *Microchem. J.* **2002**, *71*, 211.
67. X. Huang, X. Liao, B. Shi. *J. Hazard. Mat* **2009**, *170*, 1141.
68. N. Belzile, G.J. Wu, Y.W. Chen, V.D. Appanna. *Science of the Total Environment* **2006**, *367*, 704.
69. B. Allard, I. Arsenie. *Water Air Soil Pollut* **1991**, *56*, 457.
70. C.L. Hansen, G. Zwolinski, D. Martin, J.W. Williams. *Biotechnol. Bioeng.* **1984**, *26*, 1330.
71. K. Schluter. *Environ. Geol.* **2000**, *39*, 249.
72. N.D. Hutson, B.C. Attwood, K.G. Scheckel. *Environ. Sci. Technol.* **2007**, *41*, 1747.

Chapter 4

Mechanistic and Spectroscopic study for adsorption of Cr^{6+} and Cr^{3+} onto the adsorbents prepared from Palm Shell Powder

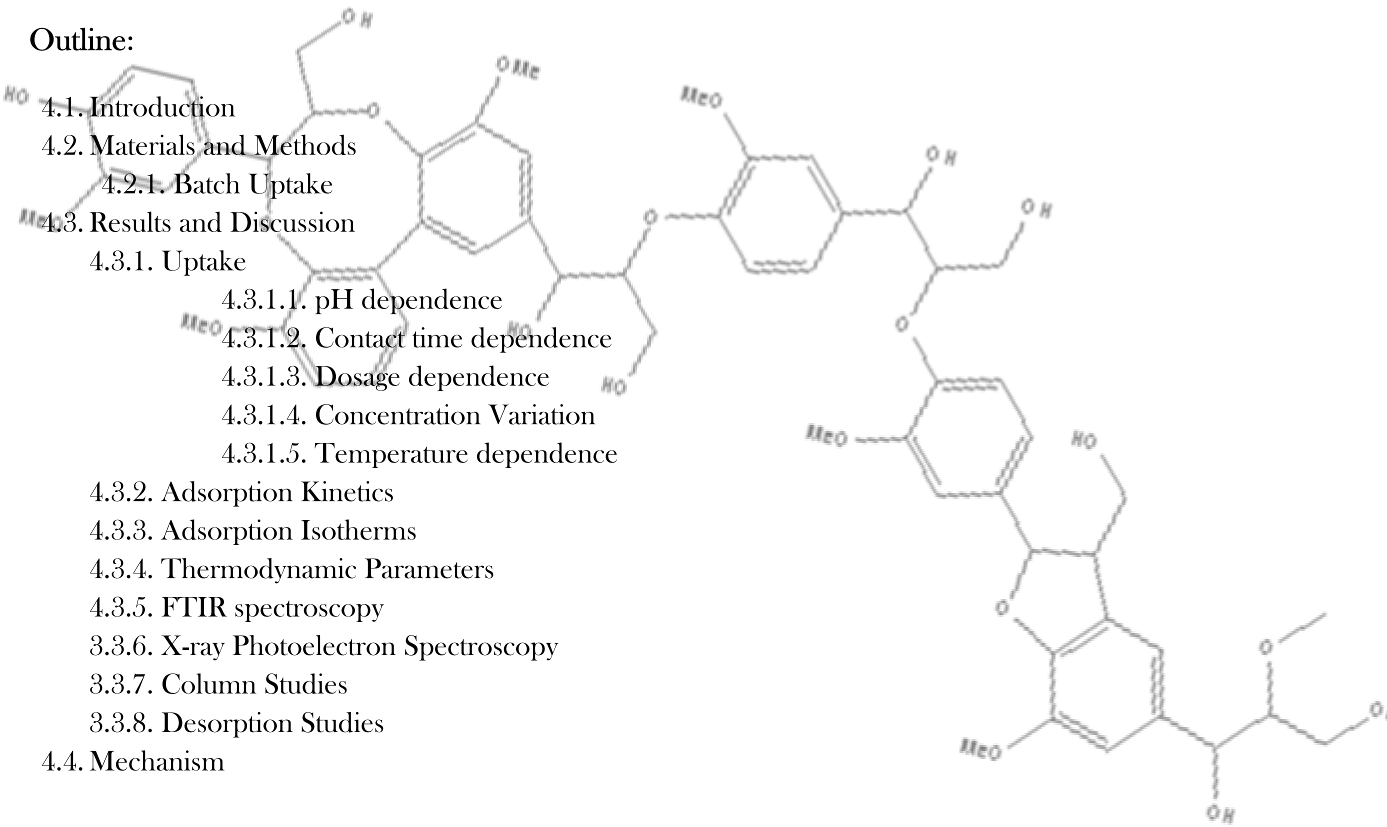

Outline:

4.1. Introduction

Among the several oxidation states(di-, tri-, penta- and hexa-) of chromium, trivalent chromium together with the hexavalent state can be mainly present in the aquaticenvironment [1]. Although trivalent chromium is less toxic than hexavalent chromium, a long-term exposure to trivalent chromium is known to cause allergic skin reactions and cancer [2]. As a result, the total chromium level in the effluent is strictly regulated in many countries.Hexavalent chromium species are strong oxidants that act as carcinogens, mutagens, and teratogens in biologicalsystems. Hexavalent chromium exists in water as oxyanions such as chromate ($HCrO_4^-$) and dichromate ($Cr_2O_7^{2-}$). Itsspeciation is dependent on the pH. It causes diseases such as epigastric pain nausea, vomiting, severe diarrhea, andhemorrhage by ingestion. The maximum allowed contaminant drinking level for the drinking water is 0.05 mg/L [3].

Several inexpensive sorbents have been tested in the removal of hexavalent chromium as given in Table1.3 of chapter 1. Most reports claim that the Cr^{6+} was removed from aqueous systems by anionic adsorption [4-24]but it has been newly explained that these findings were misinterpreted due to errors in measuring chromium species in aqueous phase, insufficient contact time required for equilibrium, and the lack of information about the oxidation state of the chromium bound on the biomaterials [25].Someresearchers have reported that the removal of $Cr^{6+}$was partly through reduction, as well as anionic adsorption,and the partial reduction could take place only under stronglyacidic conditions (pH < 2.5) [26-31].

Therefore the aim of this study is to i) determine the influence of the various parameters on the adsorption of hexavalent and trivalent Cr, ii) Evaluation of the adsorption capacity of the adsorbents by studying the equilibriumadsorption isotherms of Cr^{6+}.iii) Fitthe equilibrium data to five different isotherm models,and obtain the values of parameters of the isotherms. iv) Obtain breakthrough curves using column adsorptionand fit the data to various column models and v) Use XPS and FT-IR spectroscopic techniques to gain insight into the mechanism of adsorption of hexavalent chromium onto the adsorbents under study.

4.2.Material and Methods.

4.2.1. Batch Uptake.

A stock solutions of Cr^{3+} and Cr^{6+} were prepared by dissolving 5.13 and 2.83 g of $CrCl_3.6H_2O$and $K_2Cr_2O_7$(E-Merck) respectively in slightly acidified double distilled water and making upto 1L to give 1000 mg/L of Cr^{3+} and Cr^{6+}solutions. Working standards were prepared by diluting different volumes of the stock solution to obtain the desired concentration. Batch adsorption experiments were conducted as discussed in Chapter 3.

At the end of the predetermined time intervals, the suspensions were filtered and the filterate was analysed to find the uptake of chromium by the adsorbents under study. The Cr^{6+}concentration in the filterate was analysedspectrophotometricallyby UV spectrophotometer (Elico SL177) at 540 nm after usingdiphenylcarbazidecomplexing agent, while the total chromium concentration was determined by ICP analysis (model). The Cr(III) concentration was obtained from the differencebetween the total Cr and Cr(VI) concentrations in the filterate.

4.3.Results and Discussion

4.3.1. Uptake studies.

4.3.1.1. *pH dependence.*

The pH of the medium from which adsorption is taking place is an important controlling parameter in heavy metal adsorption process. Its effect on the removal of Cr^{6+}/ Cr^{3+}ion (initial concentration 100ppm) was studied by varying pH from 1 to10.

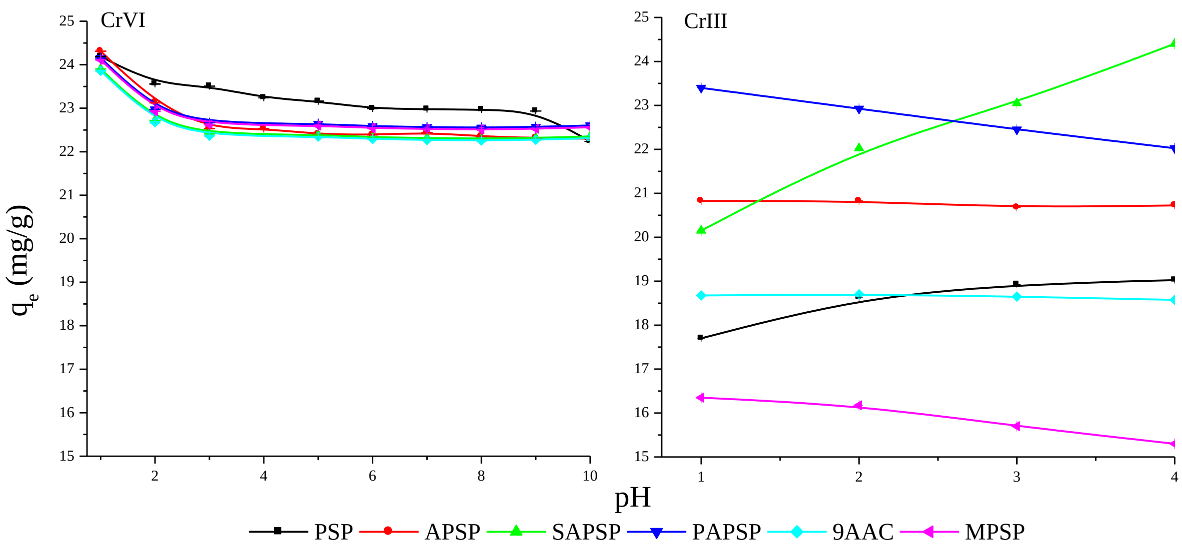

Operating parameters: 180 rpm,100ppm of Cr^{6+}/ Cr^{3+}, 0.1g adsorbent, time 240 min, temperature 30 ^{0}C, pH 1-4

Figure 4.1.Effect of pH, time, dose, initial concentration of Cr^{6+}/ Cr^{3+}

Cr^{3+} predominates at pH<3.0 whereas at pH>3.5, hydrolysis of aqueous Cr^{3+} yields trivalentchromium hydroxy species [$CrOH^{2+}$, $Cr(OH)_2^{+}$, $Cr(OH)_3$and $Cr(OH)_4^{-}$] [32]. Hexavalent chromiumexists primarily as salts of chromic acid (H_2CrO_4), hydrogenchromate ion ($HCrO_4^{-}$) and chromate ion (CrO_4^{2-}),depending on the pH. H_2CrO_4 predominates at pH's less than about 1.0, $HCrO_4^-$at pH's between 1.0 and 6.0, and CrO_4^{2-}at pHs above about 6[33].

Figure 4.1 shows that for all the adsorbents under study adsorption of Cr^{6+} ionwas maximum at ~pH 1, decreased slightly till pH 3 and then remainedconstant for the remaining range of pH studied. In the case of Cr^{3+}maximum adsorption was observed at pH 1 with slight decrease in adsorption till pH4 observed for APSP, PAPSP and MPSP. On the other hand for PSP and 9AAC a slight increase in Cr^{3+}adsorption was observed as pH was increased from 1 to 4,whilethe increase in adsorption was found to be significant for SAPSP.Similar reports of optimum adsorption at pH 4 for trivalent chromium are available in literature[34].

At low pH conditions, the amino (–NH_2) phenolic and carboxyl groups may become protonated, thus making the biomass more positively charged resulting in electrostatic attraction of the Cr^{6+} species.The acid chromate ion species ($HCrO_4^-$) is reported to be the major form of Cr^{6+} at this range of pH value of 1-4[35, 36].The phenolic groups, carboxyl and amino groups may contribute to Cr^{3+} binding at low pH which may be attributed to competition of chromium (III) species with H^+ or H_3O^+ ions for the surface functional groups as evidenced by considerable adsorption of Cr^{3+} at low pH in the case of APSP,PAPSP and MPSP and maximum adsorption in the case of SAPSP,PSP and 9AAC. As pH increases from 1 to 4, deprotonation of these functional groups leads to a slightly increasednegative charge on the biomass resulting in repulsionof anionic Cr^{6+} species, while positively charged Cr^{3+} experiences increasedattraction to the biomass.At higher pH values (>4.0) formation of chromium hydroxide starts, resulting in reduced adsorption.

4.3.1.2. *Contact time dependence*.

Contact time variation shows that equilibrium is achieved faster (80 min) when SAPSP & 9AAC was used as the adsorbent as compared to other adsorbents under study (PSP, SAPSP, PAPSP and MPSP) where equilibrium was achieved in 150 min (Figure 4.2) in case of Cr^{6+} whereas all the adsorbents showed similar trend for Cr^{3+} adsorption and equilibrium was achieved in 120 min.

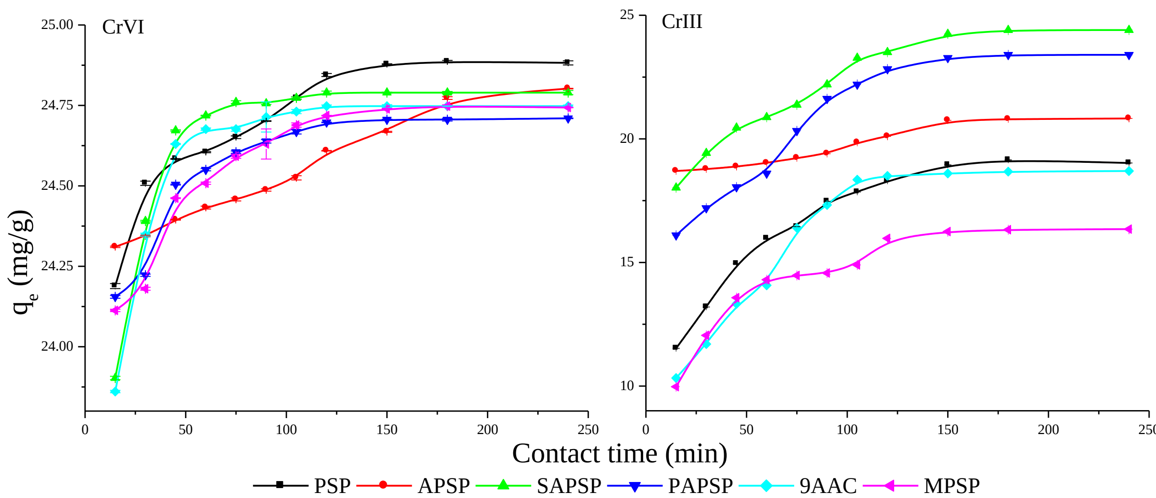

Operating parameters: 180 rpm,100ppm of Cr^{6+}/ Cr^{3+}, 0.1g adsorbent, time 15-240 min, temperature 30 ^{0}C, pH 1

Figure 4.2.Effect of contact time of Cr^{6+}/ Cr^{3+}

The rate of adsorption is very fast initially with about >95% of Cr^{6+} being removed within few minutes followed by a decreased rate with the approach of equilibrium when compared with slow rate of adsorption of Cr^{3+} with 40-90% in 120 min. The removal rate is high initially due to the presence of free binding sites which gradually become saturated with time resulting in decreased rate of adsorption as equilibrium approaches. This indicates that the adsorption is mainly through surface binding. Similar observations were made by Das et al [37].

4.3.1.3. *Dosagedependence.*

The effect of dose of adsorbents under study on the removal of Chromium [Cr^{6+}& Cr^{3+}] is shown in Figure 4.3, which illustrates the adsorption of Chromium ion with change of the adsorbent dose from 0.02 to 0.12g.

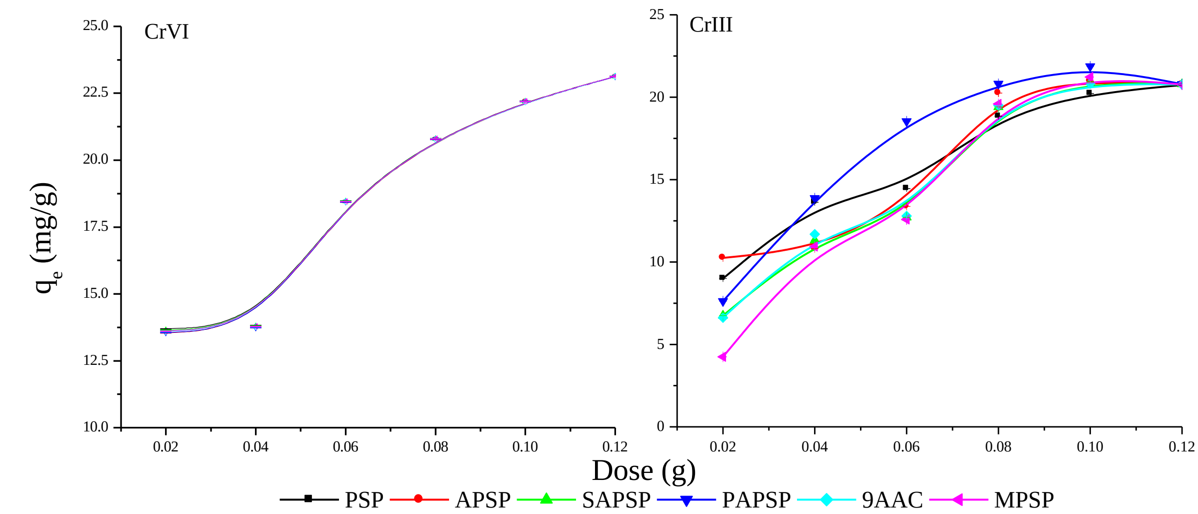

Operating parameters: 180 rpm,100 ppm of Cr^{6+}/ Cr^{3+}, time 240 min, temperature 30 ^{0}C, pH 1

Figure 4.3.Effect of initial concentration of Cr^{6+}/ Cr^{3+}

As inferred from Figure4.3, for a fixed metal initial concentration, increasing the adsorbent dose provided greater surface area and availability of more active sites [38], thus leading to the enhancement of metal ion uptake for both Cr^{6+} and Cr^{3+}.

4.3.1.4. *Concentration Variation*.

Variation in initial concentration of Cr^{6+}/ Cr^{3+}as shown in Figure 4.4 showed similar trend. In case of Cr^{6+} maximum adsorption capacity was found to be higher than for Cr^{3+}.

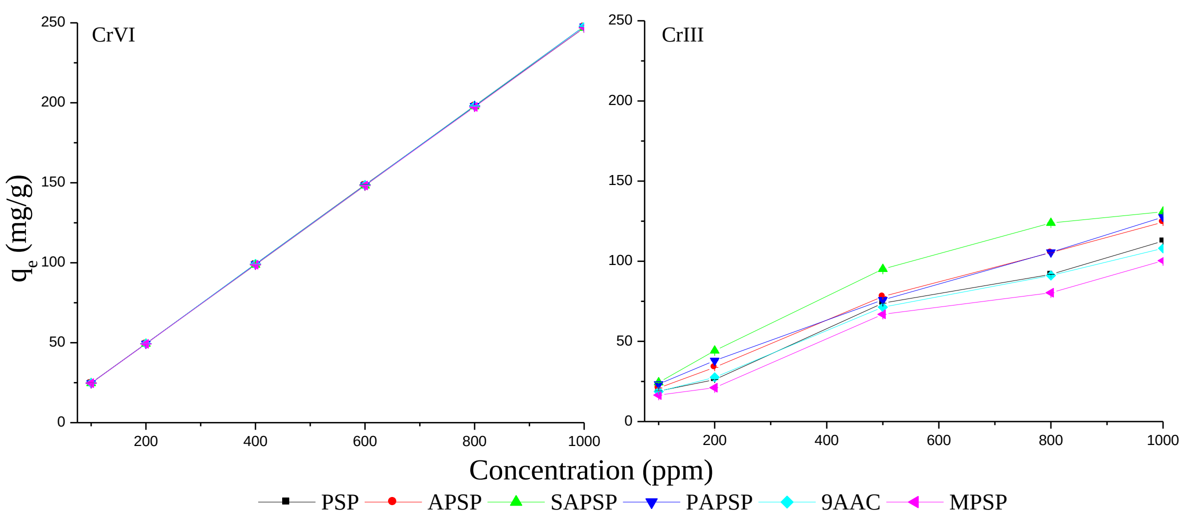

Operating parameters: 180 rpm,0.1g adsorbent, time 240 min, temperature 30 ^{0}C, pH 1

Figure 4.4.Effect of initial concentration of Cr^{6+}/ Cr^{3+}

4.3.1.5. *Temperature variation*.

Temperature studies showed (Figure 4.5) almost the same trend for all the adsorbents under study. From the figure it can be seen that uptake decreases as temperature increases indicating that the mechanism of adsorption is exothermic in nature for both Cr^{6+}/ Cr^{3+}.

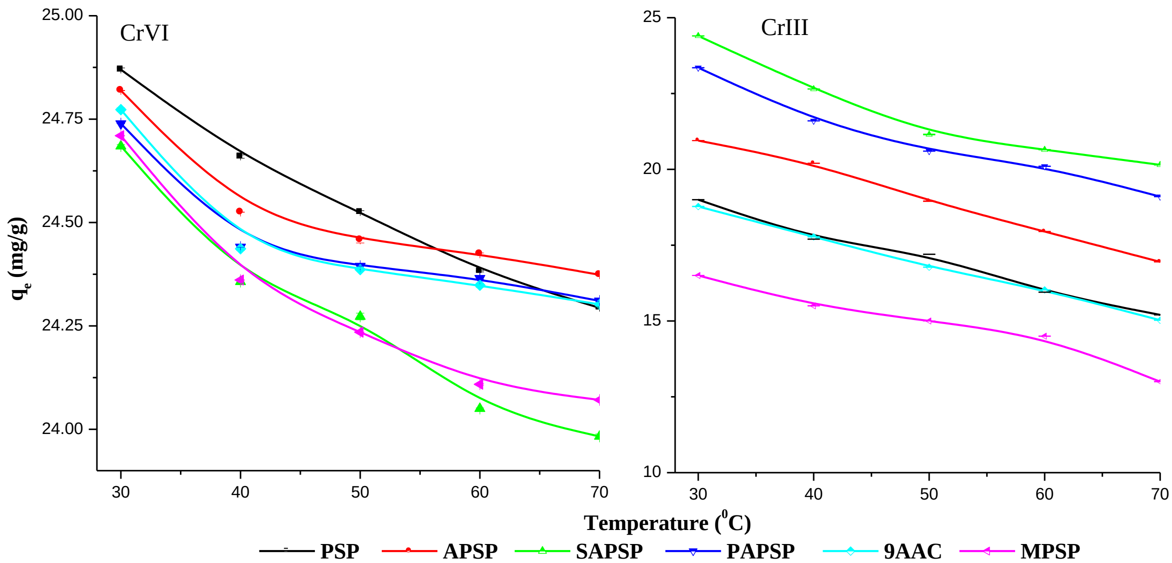

Operating parameters: 180 rpm,1000 ppm of Cr^{6+}/ Cr^{3+}, 0.1g adsorbent, time 240 min, pH 1

Figure 4.5. Effect of temperature on uptake of Cr^{6+}/ Cr^{3+} ions by PSP, MPSP, APSP, SAPSP, PAPSP and 9AAC

4.3.2. Adsorption Kinetics.

Adsorption of Cr^{6+}/Cr^{3+} ions onto PSP, APSP, SAPSP, PAPSP, 9AAC and MPSP was carried out for 240 min to ensure complete attainment of equilibrium. The kinetic models of Pseudo First order, Pseudo Second order, Intraparticle diffusion, Bangham, Elovich and Liquid film diffusion models were studied and the kinetic constants for the adsorption of chromium by all the adsorbents under study are presented in Table 4.1.

Table 4.1. Kinetic parameters

Cr^{6+}/ Cr^{3+}	PSP	APSP	SAPSP	PAPSP	9AAC	MPSP
qe (exp)	24.87/ 19.00	24.82/ 20.95	24.68/ 24.40	24.74/ 23.35	24.77/ 18.78	24.71/ 16.50
Pseudo 2ndorder						
q_e(mg.g^{-1})	24.630/ 18.195	24.845/ 21.263	24.771/ 21.061	24.808/ 25.006	62.112/ 16.667	24.857/ 17.343
K_2 (g.mgmin^{-1})	0.058/ 0.054	0.104/ 0.008	0.082/ 0.005	0.099/ 0.003	0.012/ 0.004	0.042/ 0.004
r^2	1.000/ 0.999	1.000/0.999	1.000/ 0.99	1.000/ 0.999	0.999/ 0.995	0.999/ 0.99
SD	0.007/ 0.013	0.005/ 0.010	0.004/ 0.014	0.005/ 0.015	0.001/ 0.018	0.015/ 0.015
Lagergren						
q_e(mg.g^{-1})	0.754/ 5.879	1.219/ 7.262	0.927/ 10.385	1.219/ 18.892	1.064/ 8.404	1.833/ 15.354
K_1 (min^{-1})	-0.016/ -0.022	-0.043/ -0.026	-0.029/ -0.025	-0.041/ -0.029	-0.027/ -0.34	-0.006/ -0.032
r^2	0.966/ 0.934	0.969/ 0.896	0.991/ 0.941	0.975/ 0.958	0.986/ 0.934	0.997/ 0.955
SD	0.068/ 0.025	0.167/ 0.032	0.062/ 0.087	0.144/ 0.078	0.067/ 0.082	0.007/ 0.041
Intra Particle Diffusion						
K_{ip}(mg/g/min)	0.041/ 0.342	0.012/ 0.230	0.024/ 0.449	0.013/ 0.739	0.034/ 0.874	0.052/ 0.527
r^2	0.927/ 0.847	0.821/ 0.954	0.889/ 0.960	0.859/ 0.946	0.898/ 0.929	0.982/ 0.920
SD	0.049/ 0.087	0.024/ 0.066	0.037/ 0.074	0.023/ 0.092	0.050/ 0.076	0.030/ 0.087
Elovich						
β (g.mg^{-1})	3.983/ 0.637	3.478/ 1.074	4.429/ 0.521	3.475/ 0.312	3.788/ 0.260	5.273/ 0.421
α (mg.g^{-1}min^{-1})	2.562E+93/ 1896285.996	6.800E+80/ 5.368E+16	5.934E+103/ 305002.297	3.945E+80/ 388.126	1.218E+88/ 2.000	1.89E+124/ 124.328
r^2	0.972/ 0.913	0.859/ 0.906	0.941/ 0.963	0.865/ 0.964	0.959/ 0.959	0.933/ 0.977
SD	0.051/ 0.063	0.047/ 0.073	0.069/ 0.056	0.143/ 0.076	0.066/ 0.097	0.062/ 0.044
Liquid film diffusion model						
K_{FD}	0.029/ -0.022	0.043/ -0.026	0.038/ -0.025	0.029/ -0.029	0.036/ -0.033	0.025/ -0.032
r^2	0.892/ 0.934	0.905/ 0.895	0.981/ 0.940	0.904/ 0.958	0.969/ 0.934	0.886/ 0.955
SD	0.074/ 0.073	0.082/ 0.073	0.050/ 0.042	0.094/ 0.041	0.041/ 0.051	0.090/ 0.055
Bangham						
K_{BM}	-113.37/ -126.10	-113.39/ -120.38	-113.46/ -123.75	-113.44/ -122.31	-113.72/ -132.28	-113.72/ -131.44
α	4.660E-05/ 4.41E-04	4.46E-05/ 2.60E-04	3.98E-05/ 5.26E-04	4.51E-05/ 7.70E-04	4.80E-05/ 0.001	4.29E-05/ 7.84E-04
r^2	0.840/ 0.738	0.616/ 0.951	0.768/ 0.907	0.625/ 0.874	0.809/ 0.840	0.983/ 0.808
SD	0.002/ 0.028	0.004/ 0.006	0.002/ 0.017	0.004/ 0.020	0.003/ 0.057	0.001/ 0.040

The pseudo second order kinetics provided the best fit for the kinetic data at optimumpH. The q_e values were very close to the experimental q_e value and correlation coefficient values were 0.995-1.00 for PSP, APSP, SAPSP, PAPSP, 9AAC and MPSP for both Cr^{3+} and Cr^{6+}. This suggests that the rate limiting step in adsorption of chromium is chemisorption involving valence forces through the exchange of electrons between sorbent and sorbate[39, 40], complexation, coordination and/ or chelation.

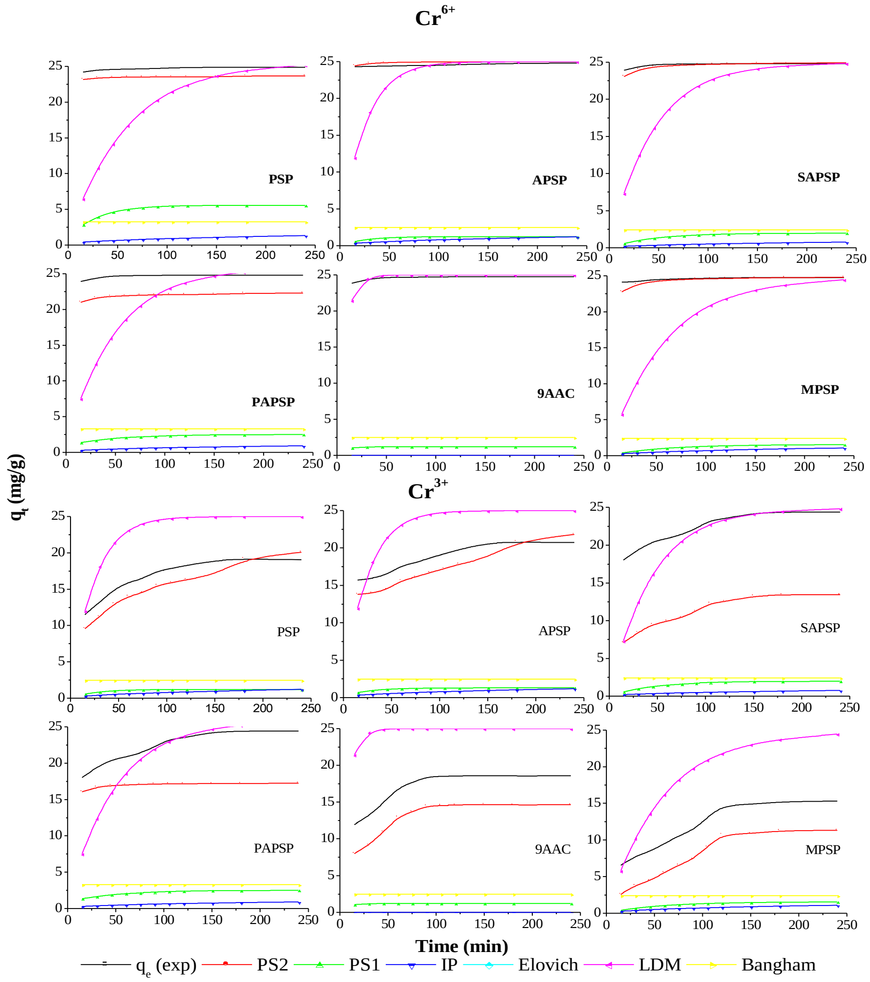

Operating parameters: 180 rpm,100ppm of Cr^{6+}/ Cr^{3+}, 0.1g adsorbent, time 15-240 min, temperature 30 ^{0}C, pH 1

Figure 4.6. Kinetics for Cr^{6+} and Cr^{3+} by PSP, APSP, SAPSP, PAPSP, 9AAC and MPSP

In pseudo first order model the $q_{e(exp)}$ values were much higher than q_e fitted values (Figure 4.6) for both Cr^{3+} and Cr^{6+}. The large discrepancies show that the reaction cannot be classified as pseudo first order although this plot has reasonably good correlation coefficient from the fitting process. This underestimate of the amount of binding sites is probably due to the fact that q_e was determined from the y-intercept (0, 1). This intercept is affected strongly by the short term metal uptake, which is much lower than equilibrium uptake [41]. This has been observed by several other workers [42-44]. This could be due to boundary layer controlling the beginning of the adsorption process [44]. Elovich model's correlation coefficients (0.859-0.977) provided a bad fit to the experimental data and hence we can not predict any meaningful information or any definite mechanism. The Liquid film diffusion model is applicable when flow of the adsorbate from the bulk liquid to the surface of the adsorbent determines the rate constant. The curves did not pass though origin as required by the model but very small intercepts indicates that diffusion of chromium from the liquid phase to the adsorbent surface might be having some role in deciding the rate processes. The Weber and Morris adsorption kinetic model was plotted using the equation given in Chapter 3 Table3.1.

The plots obtained for PSP, APSP, SAPSP, PAPSP, 9AAC and MPSP do not pass through origin implying that intraparticle diffusion is not the only operative mechanism.The intraparticle diffusion rate is fastest in PSP &APSP, the order being APSP~PSP>SAPSP>MPSP>PAPSP>9AAC for Cr^{3+};APSP~PAPSP>SAPSP>9AAC>PSP>MPSPfor Cr^{6+}as evident from intraparticle diffusion rate constants. Finally, in order to further confirm the occurrence of intraparticle diffusion, Bangham equation (Chapter 3 Table3.1) was applied to the adsorption data. The double logarithmic plots obtained with very less correlation coefficients (>0.616) for both Cr^{6+} and Cr^{3+}indicated very less contribution of pore diffusion towards adsorption process. The lowest r^2 value for 9AAC is in agreement with the results of intraparticle diffusion. The not so linear curves indicated the diffusion of adsorbate into pores of the sorbent is not the only rate controlling step.

Adsorption capacity of the adsorbents for Cr^{6+} washighest at pH 1, whereas Cr^{3+}adsorption was highest at pH4 which is consistent with results of others [45].Initial rapid uptake implies the binding of adsorbate ions on the surface of adsorbents under study throughproton exchange at optimum pH(pH 1) as Cr^{6+} occurs in its anionic form and preferably bind at pH1.Later on slower adsorption might be due to intraparticle diffusion, and diffusion of chromium from the aqueous phase to the adsorbent due to weak acidic and basic groups such as carboxyl, hydroxyl, amino groups at pH >1.

4.3.3. Adsorption Isotherms.

For modeling ofchromiumuptake Freundlich, Langmuir, Temkin, Dubinin-Radushkevich (DR), Flory-Huggins, Elovich and Halsey isotherm models were employed. Adsorption isotherms of the type $q_e$vsC_e were also used to verify the isotherm models. The values of model constants along with their correlation coefficients, r^2 and SD values for all the systems studied are presented in Table 4.2.

Table 4.2. Isotherms parameters for different adsorbents Cr^{6+}/ Cr^{3+}

Cr^{6+}/ Cr^{3+}	PSP	APSP	SAPSP	PAPSP	9AAC	MPSP
Freundlich						
$q_{e(exp)}$ (mg/g)	24.87/ 19.00	24.82/ 20.95	24.68/ 24.40	24.74/ 23.35	24.77/ 18.78	24.71/ 16.50
K_F(mg.g^{-1})(dm^3/mg)$^{1/n}$	5.08/ 1.47	3.66/ 1.13	4.36/ 1.88	3.54/ 3.45	3.84/ 2.71	4.31/ 1.49
n	1.37/ 1.00	1.00/ 1.49	1.07/ 1.85	0.96/ 2.98	0.93/ 2.53	1.01/ 1.69
r^2	0.997/ 0.959	0.995/ 0.948	0.991/ 0.989	0.999/ 0.993	0.996/ 0.985	0.995/ 0.976
SD	0.038/ 0.013	0.044/ 0.031	0.056/ 0.054	0.034/ 0.044	0.038/ 0.062	0.046/ 0.083
Langmuir						
K_L (dm^3.mg^{-1})	0.164/ 0.006	0.071/ 0.004	0.075/ 0.008	0.051/ 0.034	0.073/ 0.012	0.107/ 0.006
q_m (mg.g^{-1})	289/ 138	303/ 133	284/ 149	313/ 137	262/ 136	249/ 154
ΔG (kJ.mol^{-1})	-4.71/ -13.32	-6.88/ -14.31	-6.72/ 12.67	-7.73/ -8.79	-6.79/ -11.49	-5.79/ -13.41
r^2	0.993/ 0.985	0.910/ 0.981	0.987/ 0.984	0.994/ 0.996	0.998/ 0.960	0.983/ 0.991
SD	0.002/ 0.054	0.002/ 0.046	0.001/ 0.030	0.006/ 0.057	0.003/ 0.005	0.002/ 0.088
Temkin						
-ΔH (kJ.mol^{-1})	7.346/ 7.633	10.443/ 7.670	10.357/ 8.726	10.983/ 11.741	9.755/ 9.418	8.975/ 9.292
K_T (dm^3.mg^{-1})	0.319/ 0.146	0.333/ 0.072	0.440/ 0.227	0.324/ 0.213	0.391/ 0.22	0.468/ 0.115
r^2	0.995/ 0.995	0.988/ 0.993	0.960/ 0.956	0.982/ 0.963	0.973/ 0.961	0.953/ 0.939
SD	0.077/ 0.036	0.031/ 0.068	0.082/ 0.054	0.023/ 0.071	0.045/ 0.025	0.073/ 0.069
DR						
q_m (mg.g^{-1})	187/ 167	229/ 166	216/ 178	221/ 174	235/ 173	253/ 179
E^0 (KJ)	12.46/ 10.44	10.72/ 11.94	14.85/ 19.92	11.21/ 15.04	1.29/ 1.19	12.82/ 10.75
r^2	0.956/ 0.957	0.972/ 0.967	0.939/ 0.960	0.954/ 0.959	0.971/ 0.954	0.975/ 0.967
SD	0.014/ 0.092	0.072/ 0.093	0.051/ 0.074	0.021/ 0.077	0.075/ 0.051	0.062/ 0.050
Halsey						
K_H (mg.g^{-1})(dm^3/mg)$^{1/n}$	0.823/ 0.751	0.716/ 0.777	0.758/ 0.388	0.699/ 0.416	0.701/ 0.332	0.745/ 0.359
n_H	-0.27/ -0.95	-0.33/ -0.95	-0.29/ -1.03	-0.34/ -1.04	-0.32/ -1.11	-0.29/ -0.69
r^2	0.997/ 0.994	0.995/ 0.999	0.991/ 0.994	0.997/ 0.997	0.996/0.996	0.995/ 0.997
SD	0.087/ 0.090	0.101/ 0.046	0.093/ 0.079	0.078/ 0.032	0.088/ 0.052	0.071/ 0.028
Flory-Huggins						
K_{FH} (mg.g^{-1})(dm^3/mg)$^{1/n}$	1.026/ 1.174	1.040/ 3.871	1.034/ 1.426	1.043/ 1.374	1.042/ 1.384	1.039/ 1.143
N_{FH}	0.998/ 2.307	0.996/ 2.528	0.997/ 2.558	0.996/ 2.634	0.995/ 2.607	0.996/ 3.282
r^2	1.000/ 0.999	1.000/ 1.000	1.000/ 0.990	1.000/ 0.986	1.000/ 0.992	1.000/ 0.998
SD	0.001/ 0.025	0.001/ 0.002	0.001/ 0.099	0.001/ 0.060	0.001/ 0.072	0.001/ 0.087
Elovich						
q_m (mg.g^{-1})	52.01/ 1.29	21.57/ 1.52	21.98/ 1.81	16.45/ 1.74	20.29/ 0.63	18.73/ 0.89
K_E (dm^3.mg^{-1})	1.627/ 9.23E+125	2.113/ 8.96E+55	0.651/ 5.19E+89	1.462/ 7.44E+95	1.006/ 1.37E+236	1.008/ 7.89E+125

r^2	0.994/ 0.994	0.997/ 0.924	0.988/ 0.985	0.995/ 0.967	1.000/ 0.911	0.999/ 0.988
SD	0.043/ 0.046	0.006/ 0.068	0.015/ 0.071	0.012/ 0.089	0.001/ 0.019	0.003/ 0.084

The value of n≈1 for the Freundlich model indicates favorable adsorption for Cr^{6+} whereas in case of adsorption of Cr^{3+} only PSP was having n≈1 others were having higher n values. The parameters K_L (equilibrium sorption constant) and qmax were calculated from the intercept and slope of the plot of C_e/q_e versus $C_e$of Langmuir isotherm model. Based on the correlation coefficient r^2 and standard deviations for Langmuir it varied from 0.910-0.998 for Cr^{6+} and 0.960-0.996 for Cr^{3+} with very less SD values. Langmuir monolayer adsorption capacity was found in good agreement with the experimental adsorption capacities.Adsorption of Cr^{6+} was found to be 2 times higher than adsorption of Cr^{3+} according to Langmuir maximum adsorption capacities on all the adsorbents. The order of preference of adsorbents to metal ion was found to be PAPSP>APSP>SAPSP~PSP>9AAC>MPSP for Cr^{6+} and MPSP~SAPSP>PAPSP~APSP~PSP~9AAC for Cr^{3+}. The maximum adsorption capacities found with these adsorbents were found to be comparable with literature (Chapter 1 Table 1.3) and in some cases higher than reported ones.

The correlation coefficients of Temkin Model (0.953 to 0.995 for Cr^{6+} and 0.939 to 0.995 for Cr^{3+}) indicate a satisfactory fit of the model to the experimental data. The variation of adsorption energy, ΔQ (7.346, 10.443, 10.357, 10.983, 9.755 and 8.975 for PSP, APSP, SAPSP, PAPSP, 9AAC and MPSP respectively in the case of Cr^{6+} and 7.633, 7.670, 8.726, 11.741, 9.418 and 9.292 for PSP, APSP, SAPSP, PAPSP, 9AAC and MPSP respectively in the case of Cr^{3+} is positive for all the sorbents under study, which indicated the adsorption process to be exothermic.

The Dubinin–Radushkevich model is applied in the form of linear equation as given in Chapter 3 Table3.1. The adsorption energy values calculated for $Cr^{6+}$are (12.462,10.715, 14.850, 11.207, 1.286 and 12.820 $KJmol^{-1}$) and for Cr^{3+} (10.438, 11.939, 19.924, 15.044, 1.198 and 10.751$KJmol^{-1}$) on PSP, APSP, SAPSP, PAPSP, 9AAC and MPSP respectively. The magnitude of E is useful for estimating the mechanism of the sorption reaction. In case of E < 8.0 kJ/mol, physical forces may affect the sorption; for E in the range 8–16 kJ/mol, ion exchange is the working mechanism, while for E>16 kJ/mol sorption may be dominated by particle diffusion [44, 46].It is thus evident from D-R model that for 9AAC physisorption is the predominant mechanism, while for PSP, APSP, SAPSP, PAPSP and MPSP ion-exchange is the predominant mechanism.

Multilayer adsorption is generally discussed by the Halsey equation and is found to fit well with the experimental data having r^2 (> 0.991 and 0.994 for Cr^{6+}/ Cr^{3+}) [38] indicating that the mechanism may be multilayer sorption for adsorbents under study while the low values of K_H suggest that multilayer sorption might be playing only a small role.The Flory-Huggins model was used to assess the isotherm data. From the linear plots of log(θ/C_0) versus log(1–θ) for chromium adsorption on the adsorbents under study and the correlation coefficient values (r^2 =1.00), it is apparent that the model shows good fits for the adsorbent under study. However the negative values of n and low values of k_{FH} imply that the model cannot be used to describe the adsorption data.

4.3.4. Thermodynamic Parameters.

The thermodynamic parameters of the sorption process could be determined from the experimental data obtained at various temperatures using the equations:

$$\Delta G^0 = \Delta H^0 - T\Delta S^0$$

The values of ΔH°and ΔS°can be calculated from the slope and intercept of the plots of ΔG° against 1/T (Figure4.7).

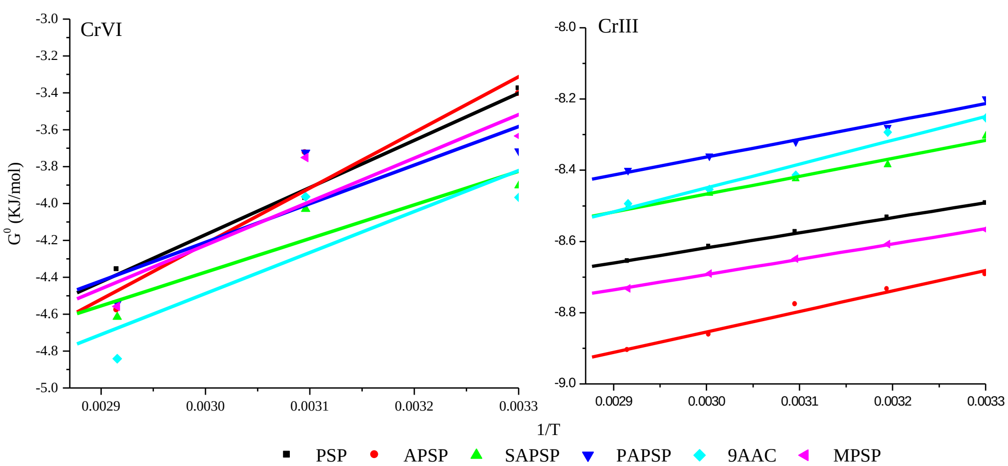

Operating parameters: 30-70 ^{0}C, 240 min, pH 1, 1000 ppm of Cr^{6+}/ Cr^{3+}, 0.1g adsorbent, 180 rpm.

Figure 4.7. Thermodynamic studies

Table 4.3. Thermodynamic Parameters for Chromium ions by PSP, APSP, SAPSP, PAPSP, 9AAC and MPSP

Cr^{3+}/ Cr^{6+}			
	ΔG (KJ/mol)	ΔS (KJ/molK)	ΔH (KJ/mol)
PSP	-28.439/ -48.113	0.082/ 0.094	-3.525/ -19.621
APSP	-31.425/ 58.613	0.088/ 0.110	-4.772/ -25.108
SAPSP	-29.323/ -39.861	0.083/ 0.081	-4.182/ -15.173
PAPSP	-29.029/ -43.819	0.082/ 0.087	-4.165/ -17.392
9AAC	-31.912/ -46.688	0.087/ 0.093	-5.562/ -18.473
MPSP	-28.708/ -48.121	0.083/ 0.094	-3.567/ -19.629

The negative value of ΔH° indicates that the adsorption of Cr^{6+}/ Cr^{3+} on PSP, APSP, SAPSP, PAPSP, 9AAC and MPSP is exothermic. Generally the absolute magnitude of the change in energy for physisorption is between (-20 and 0 KJ/mol); chemisorption has a range of (-400 and -80 KJ/mol). The negative value of ΔG° in Table 4.3 indicates that sorption of Cr^{6+}/ Cr^{3+}ion by PSP, APSP, SAPSP, PAPSP, 9AAC and MPSP to be physisorption and is spontaneous and thermodynamically favorable [47]. Also the ΔG° values become less negative with increase in temperature suggesting that adsorption is favored at lower temperatures and hence is exothermic. The positive values of ΔS° suggest increased randomness during adsorption and a high affinity of the adsorbent towards the adsorbate.

4.3.5. Fourier Transform Infrared Spectroscopy.

The absorption bands of FTIR spectra listed in Table 4.4reveal the changes in absorption bands of the surface functional groups of PSP, APSP, SAPSP, PAPSP, 9AAC and MPSP after chromium adsorption.

The metal loaded adsorbents showed a shift in the absorption frequencies of OH group indicating the binding of chromium to the –OH groups present in the adsorbents. The intensitiesof the peaks at ~1430, ~1250, ~893 and ~840cm^{-1} decreased whilethose at 1635 and 1556cm^{-1} increased. The peaks at 1430 and1250cm^{-1} were attributed to the C–O–CH_3 (methoxyl) deformationand C–OH (hydroxyl) bending of phenolic structure in lignin and those at 893 and 840 cm^{-1} were assigned to the out-of-plane CH bending vibrations of lignin (Table 4.4) [48-50]. The decreases in the intensities of these peaks indicated the oxidation of lignin in the adsorbents under study upon Cr^{6+} reaction.

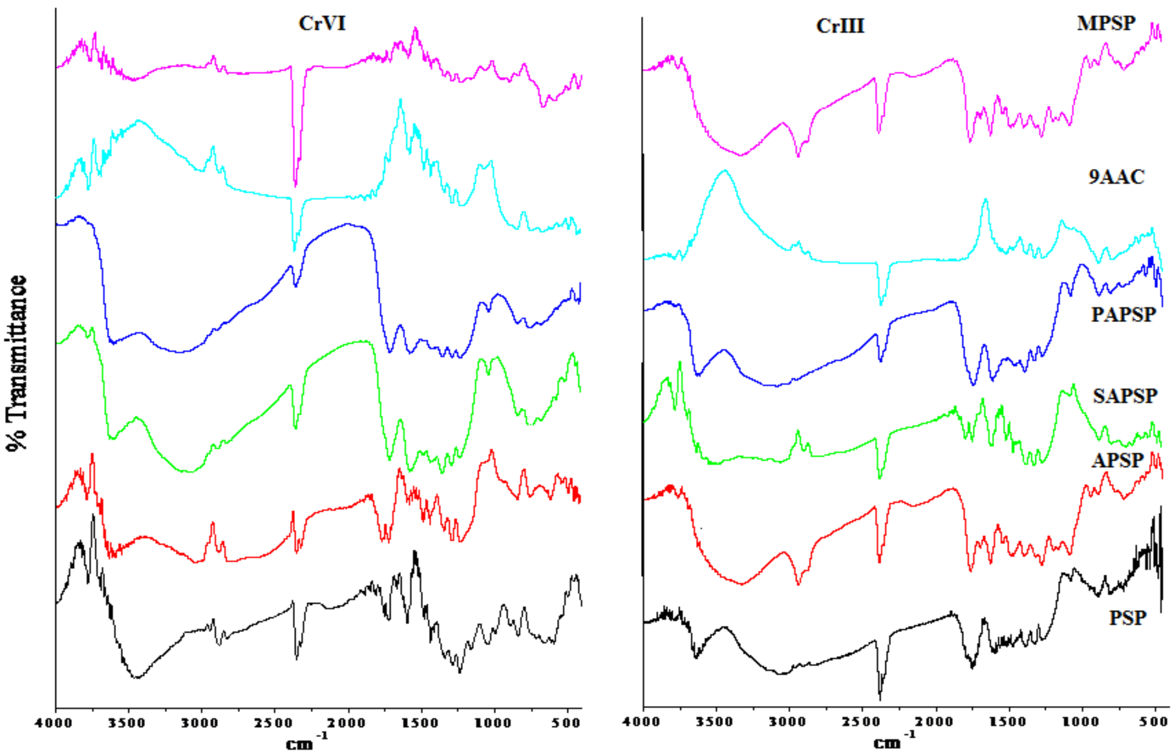

Figure 4.8. FTIR spectra for Cr^{6+} and Cr^{3+} loaded adsorbents

According to Elovitz and Fish[51]the oxidation of phenols leads to the formation of quinones containing carbonyl groups. Further oxidation of quinones may lead to the formation of carboxylate anions [52]. Thus, upon Cr^{6+} reaction, the increasing intensities at 1700 and 1556cm^{-1} were attributed to the formation of carbonyl and carboxyl groups in the adsorbents under study.

Table 4.4. Typical Absorption frequencies and Carbonyl stretching frequencies of Infra red spectra for free and metal loaded adsorbents

PSP-Cr^{3+}/Cr^{6+}	**APSP-Cr^{3+}/Cr^{6+}**	**SAPSP-Cr^{3+}/Cr^{6+}**	**PAPSP-Cr^{3+}/Cr^{6+}**	**9AAC-Cr^{3+}/Cr^{6+}**	**MPSP-Cr^{3+}/Cr^{6+}**	**Assignment**
3642/ 3438	3311/ 3618	3518/ 3615	3627/ 3601	-/-	3344/ 3463	-N-H, -O-H stretching
3016,2891/ 2886,2821	2913,2861/3007,2886	3023,2894/3088,2908	3076,2922/3087,2895	2979,2880/2986,2870	2914,2836/2988,2885	$-CH_3$, $-CH_2$ symmetric stretch
2335/ 2347	2361/ 2347	2357/ 2356	2348/ 2355	2361/ 2356	2355/ 2359	Free CO_2
1722/ 1756, 1717	1719/ 1769, 1717	1776, 1711/ 1727	1707/ 1713	-/-	1752/ 1717	-C=O stretch for acids or aldehyde
1556/ 1589	1573/ 1573	1582/ 1573	1559/ 1571	1512/ 1573	1602/ 1589	-C=O& C=C Aromatic stretch for cellulose/ N-H bending of amide
1437/ 1487, 1435	1445/ 1496, 1435	1432/ 1444	1431/ 1430	1480,1435/ 1496, 1432	1451/ 1434	$-CH_2$- stretch/ -C=C- Aromatic stretching
1346/ 1354	1346/ 1355	1361/ 1367	1354/ 1349	1358/ 1342	1365/ 1345	-C-H stretch/ N-H bending
1291/ 1293, 1229	1242/ 1274, 1213	1260/ 1243	1277/ 1288, 1227	1292/ 1290, 1201	1258/ 1290, 1229	-C-O bending of carboxylic acids/ phenolic O-H stretch/ N-H bending
1224/ 1152	1126/ 1175	-/-	1221	1236	-/-	-O-H stretch (2^0 Alcohol), -C-O-C- stretching
1024/ 1063	1060/ 1046	1041/ 1045	1037/ 1060	1049/ 1060	1042/ 1062	-C-H stretch, -C-O stretch (1^0 Alcohol)
849/ 831	838/ 841	858/ 853	838/ 841	850/ 861	837/ 831	-C-H out of plane bending
785, 507/ 809, 512	798, 508/ 801, 501	718, 525/ 771, 519	786, 516/ 780, 520	793, 518/ 797, 503	801, 507/ 778, 526	Cr-O bending vibrations

The suppression of the peaks located at 1450-1750 cm^{-1} and the decrease of the ratio of the COOH and COO- groups intensities canbe observed. Also there is a shiftin the frequencies of the absorption band of both C=O and C-O in carboxyl group (-COOH) due to metal binding. The C-O band shifts to higher frequencies 1217-1289 cm^{-1}probably due to high electron density induced by the adsorption of chromium on the adjacent carbonyl groups [53, 54]. Thus carboxylic groups are involved in sorption of chromium as seen by comparison of IR spectra of the adsorbents and the chromium loaded-adsorbents. The interaction between chromium and carboxylic group of the adsorbent causes a diminution of the distance between C=O and C-O stretching peaks [55].A decrease in the ratio of the COOH and COO-groups intensities can also be observed. The carboxyl and carbonyl groups may further provide the binding sites for Cr^{3+} resulting from Cr^{6+} reduction. These observations suggest that Cr^{6+} induces an oxidation of lignincomponents which is not observed in Cr^{3+} loaded spectra and that the retention of Cr ions occurs througha complexation reaction involving carboxylate moieties. Similar observations were made by Dupont et al.[56].After Cr^{3+} adsorption intensity of the peak around 1630 cm^{-1} (C=O chelate stretching) increased.

4.3.6. X-Ray Photoelectron Spectroscopy.

Figure 4.9depicts the XPS spectra for the adsorbents under study after chromium adsorption. Table 4.5summarizes the identification of the bands observed in Figure4.9.

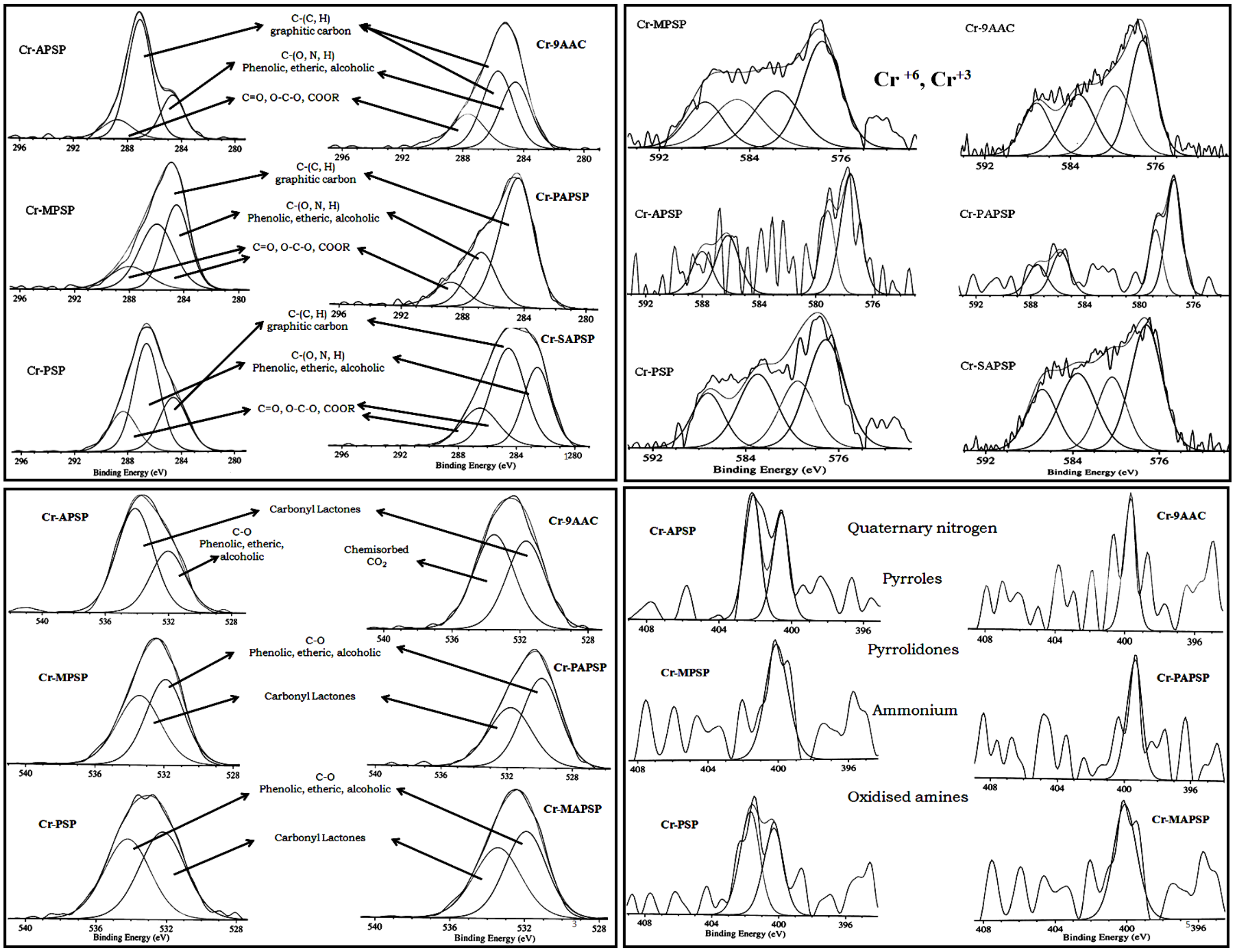

Figure 4.9. XPS spectra

It is also evident from the table that the five modified adsorbents of palm shell powder explored in this study have different amounts of carboxyl groups, differing by a factor up to 10. Furthermore, XPS results (Figure4.9 and Table 4.5) also showed an increase of carboxylate groups after Cr^{6+}adsorption.

Table 4.5. Summary of binding energy and area ratios of pristine and Cr-loaded adsorbents

Sample Surface	Proposed components	Binding Energy eV	FWHM eV	Relative Quantity %
C1s Valence State				
PSP	C-(C, H) graphitic C	284.661	2.310	0.6906
	C-(O, N, H) phenolic, alcoholic, etheric	285.984	1.774	0.1871
	C=O, O-C-O, COOR -carbonyl or quinine	287.200	2.495	0.1223
Cr-PSP	C-(C, H)	284.604	2.470	0.2820
	C-(OH, OR)	286.626	2.224	0.5119
	O=C-O carboxyl or ester	288.356	2.425	0.2061
APSP	C-(C, H)	284.647	2.462	0.6716
	C-(OH, OR)	286.599	2.074	0.2112
	O=C-O	288.577	2.605	0.1172
Cr-APSP	C-(C, H)	284.696	2.027	0.2219
	C-(OH, OR)	287.172	2.087	0.6459
	O=C-O	288.791	2.552	0.1239
SAPSP	C- (C, H)	284.524	2.264	0.5272
	C-(OH, OR)	286.342	1.894	0.2499
	O=C-O	288.073, 289.791	1.973, 2.181	0.1471, 0.0758
Cr-SAPSP	C-(C, H)	282.615	2.189	0.3139
	C-(C, H)	284.600	2.724	0.4839
	C-(OH, OR)	286.573	2.938	0.2019
PAPSP	C-(C, H)	284.590	2.051	0.6297
	C-(OH, OR)	286.071	2.204	0.2552
	C=O, O-C-O, COOR	287.979	1.527	0.0817
	O=C-O	289.308	1.424	0.0334
Cr-PAPSP	C-(C, H)	284.631	2.542	0.6439
	C-(OH, OR)	286.903	2.251	0.2379
	C=O, O-C-O, COOR, O=C-O	288.830	2.510	0.1179
9AAC	C-(C, H)	284.507	2.336	0.5552
	C-(OH, OR)	286.511	2.284	0.2822
	C=O, O-C-O, COOR	288.384	2.572	0.1155
	C=C, occluded CO, π electrons in aromatic ring, CO_2	290.295	3.464	0.0471
Cr-9AAC	C-(C, H)	284.607	2.325	0.3610
	C-(OH, OR)	285.755	2.352	0.1744
	C=O, O-C-O, COOR	287.709	2.360	0.0829
MPSP	C-(C, H, R), C-(C, H)	284.624	2.460	0.5456

	C-(OH, OR)	286.116, 286.346	1.718, 2.120	0.2137, 0.1311
	C=O, O-C-O, COOR O=C-O	288.517	2.491	0.1095
Cr-MPSP	C-(C, H, R), C-(C, H)	284.600	2.265	0.4149
	C-(OH, OR)	286.044	2.970	0.4189
	C=O, O-C-O COOR	287.993	3.355	0.1661
O1s Valence State				
PSP	C=O, C-O (Lactones, phenolic and etheric)	531.400	2.050	0.4424
	Singly bonded oxygen C-O	532.846	2.072	0.5576
Cr-PSP	C=O, C-O (Lactones, phenolic and etheric)	532.261	3.015	0.5219
	Singly bonded oxygen C-O	534.258	3.038	0.4819
APSP	C=O, C-O (Lactones, phenolic and etheric)	531.770	2.606	0.8160
	Singly bonded oxygen C-O	533.570	2.394	0.4796
Cr-APSP	C=O, C-O (Lactones, phenolic and etheric)	532.068	2.568	0.6411
	Singly bonded oxygen C-O	534.179	2.696	0.5067
SAPSP	C=O (Carboxylic acid)	532.209, 534.596	3.492, 3.517	0.8032, 0.1968
Cr-SAPSP	C=O, C-O (Carboxylic acid, etheric, lactonic, anhydrides, pyrones and phenols)	530.624, 532.541	2.964, 3.082	0.6129, 0.3871
PAPSP	C=O, C-O (Carboxylic acid, etheric, lactonic, anhydrides, pyrones and phenols)	531.656 533.388	2.449 3.347	0.4576 0.5424
Cr-PAPSP	C=O, C-O (Carboxylic acid, etheric, lactonic, anhydrides, pyrones and phenols)	529.984 531.841	2.771 3.095	0.5679 0.4320
9AAC	C=O, C-O (Carboxylic acid, etheric, lactonic, anhydrides, pyrones and phenols)	533.080	3.389	0.8437
	Occluded CO, chemisorbed CO_2, O_2 and H_2O	535.638	3.618	0.1563
Cr-9AAC	C=O, C-O (Carboxylic acid, etheric, lactonic, anhydrides, pyrones and phenols)	531.691 533.576	2.643 2.790	0.4701 0.5299
MPSP	C=O, C-O (Carboxylic acid, etheric, lactonic, anhydrides, pyrones and phenols)	531.367 532.931	2.440 2.978	0.3795 0.6205
Cr-MPSP	C=O, C-O (Carboxylic acid, etheric, lactonic, anhydrides, pyrones and phenols)	531.990 533.503	2.576 2.916	0.5219 0.4781
N1S				
PSP	C-N-C (pyrrolic nitrogen, pyridines)	399.839, 398.597,	1.492, 1.512,	0.6129, 0.2141,

		400.846	1.258	0.1729
Cr-PSP	C-N-C (pyrrolic nitrogen, pyridones)	400.382, 401.790	1.366, 1.368	0.4569, 0.5430
APSP	C-N-C (pyrrolic nitrogen, pyridones)	399.98, 400.075	1.228, 1.468	0.3556, 0.2780
	Quartenary nitrogen, protonated pyridinic ammonium ions, nitrogen atoms replacing carbon in graphene	401.278	1.908	0.3664
Cr-APSP	C-N-C (pyrrolic nitrogen, pyridones)	400.622	1.044	0.4709
	Oxidised nitrogen functionalities or NO_2 groups	402.245	1.000	0.5290
SAPSP	C-N-C (pyrrolic nitrogen, pyridones)	399.797	1.366	0.3883
	Quartenary nitrogen, protonated pyridinic ammonium ions, nitrogen atoms replacing carbon in graphene	401.477	1.941	0.6118
Cr-SAPSP	C-N-C (pyrrolic nitrogen, pyridones)	399.279	1.051	1.000
PAPSP	C-N-C (pyrrolic nitrogen, pyridones)	398.584, 399.774	1.097, 1.319	0.2677, 0.4869
	Quartenary nitrogen, protonated pyridinic ammonium ions, nitrogen atoms replacing carbon in graphene	401.074	1.032	0.2454
Cr-PAPSP	C-N-C (pyrrolic nitrogen, pyridones)	399.483	1.047	1.000
9AAC	C-N-C (pyrrolic nitrogen, pyridones)	397.686, 400.803	1.516, 1.596	0.3000, 0.3745
	Oxidised nitrogen functionalities or NO_2 groups	402.300	1.639	0.3255
Cr-9AAC	C-N-C (pyrrolic nitrogen, pyridones)	399.800	0.841	1.000
MPSP	C-N-C (pyrrolic nitrogen, pyridones)	398.703, 400.000	1.889, 1.679	0.2787, 0.5613
	Quartenary nitrogen, protonated pyridinic ammonium ions, nitrogen atoms replacing carbon in graphene	401.606	1.570	0.1599
Cr-MPSP	C-N-C (pyrrolic nitrogen, pyridones)	400.085	1.497	1.000

The presence of adsorbed chromium has been detected on the metal loaded adsorbents, and the Cr2p peaks have been analyzed. It consists of two contributions corresponding to 2p1/2 and 2p3/2 energy levels respectively as shown in table 4.6. The two contributions of Cr2p peaks are at 577.2,577.6,577.3, 577.5, 577.2, 577.8 eVand 587.2, 588.0,586.9,587.5, 587.2, 588.0eV for PSP,APSP,SAPSP, PAPSP, 9AAC and MPSP respectively. These values compare well with the binding energy of Cr^{3+}[56]. The slight difference between the Cr 2p1/2 peaks (586.8-587 eV) Cr2p3/2 peaks (577.2-577.7 eV) is attributed to different chemical environments. The Cr2p peaks which appear at 579.6, 579.2, 580.4,578.9,579.98, 581.7and 583.0, 586.2, 583.6, 585.8, 583.3, 585.2eV indicate the presence of hexavalent chromium and that reduction is not still complete. Similar observations were made by Dupont et al. [56].

Table 4.6. Summary of binding energy, area ratios, spin orbit splitting of Cr-loaded carbons

Sample Surface	Proposed components	Binding Energy eV	FWHM eV	Relative Quantity%	Spin orbit splitting
Cr-PSP	Cr2p 3/2 Cr^{3+}	577.210, 587.292	3.791, 3.193	0.3700, 0.1571	10.08
	Cr2p 1/2 Cr^{3+}	583.048	3.897	0.2579	
	Cr2p3/2 Cr^{6+}	579.596	3.582	0.2149	
Cr-APSP	Cr2p 3/2 Cr^{3+}	577.574, 588.019	1.590, 1.645	0.4059, 0.1480	10.5
	Cr2p 1/2 Cr^{3+}	586.227	1.872	0.2320	
	Cr2p3/2 Cr^{6+}	579.200	1.192	0.2129	
Cr-SAPSP	Cr2p 3/2 Cr^{3+}	577.246, 586.852	3.393, 3.268	0.3659, 0.1711	9.6
	Cr2p 1/2 Cr^{3+}	583.611	4.025	0.2659	
	Cr2p3/2 Cr^{6+}	580.424	3.146	0.1980	
Cr-PAPSP	Cr2p 3/2 Cr^{3+}	577.518, 587.514	1.357, 1.682	0.4469, 0.1461	10.0
	Cr2p 1/2 Cr^{3+}	585.803	1.590	0.1940	
	Cr2p3/2 Cr^{6+}	578.860	1.144	0.2130	
Cr-9AAC	Cr2p 3/2 Cr^{3+}	577.274, 587.224	2.843, 3.070	0.3419, 0.1671	10.0
	Cr2p 1/2 Cr^{3+}	583.290	3.601	0.2279	
	Cr2p3/2 Cr^{6+}	579.856	3.649	0.2630	
Cr-MPSP	Cr2p 3/2 Cr^{3+}	577.796, 588.053	3.931, 3.912	0.3739, 0.1591	10.3
	Cr2p 3/2 Cr^{6+}	581.715	4.875	0.2470	
	Cr2p1/2 Cr^{3+}	585.253	5.142	0.2210	

XPS results also showed the presence of Cr^{3+}(~40-50%) on Cr^{6+}loaded adsorbents. The carboxyl and carbonyl groups may further provide the binding sites for Cr^{3+}resulting from Cr^{6+}reduction. This is also supported by the fact that the adsorption capacity of all the adsorbents under study is greater for Cr^{6+} than Cr^{3+}. This observation is in agreement with the ICP analysis, which showed that almost no Cr^{3+} can be detected in the supernatants of the contacted solutions suggesting that the reduced $Cr^{3+}$is also strongly adsorbed at pH1 leading to maximum adsorption of total Cr at pH 1.Low pH also accelerates the redox reactions in aqueous and solid phases, since the protons participate in these reactions as Eq. (1).

$$HCrO_4^- + 7H^+ + 3e^- \leftrightarrow Cr^{3+} + 4H_2O \quad (1)$$

An increase in the O/C ratio is also observed from the XPS data which can be attributed to the conversion of $C1$ into $C2$ and$C3$ carbon types and generation of oxidized functional groups like alcoholic and carboxylic sites as also evidenced by IR spectral analysis. This interpretation is supported by thestudies of Pizzi[57] and Ostmeyer and Elder [58].

4.3.7. Column studies.

The column breakthrough curves for chromium adsorption by adsorbents under study are shown in Figure 4.10. The effluent concentration is seen to have the typical 'S' shape. A total of ~ 2.3 L of 1000 mg/L metal ion solution was passed through the column containing 5 g of adsorbent under study.Cr^{6+}adsorption in column mode showed adsorption upto155, 388, 375, 356, 164,162 bed volumes for PSP, APSP, SAPSP, PAPSP, 9AAC, MPSP respectively and 144, 347, 325, 335, 312, 131bed volumes for PSP, APSP, SAPSP, PAPSP, 9AAC and MPSP respectively for Cr^{3+}.

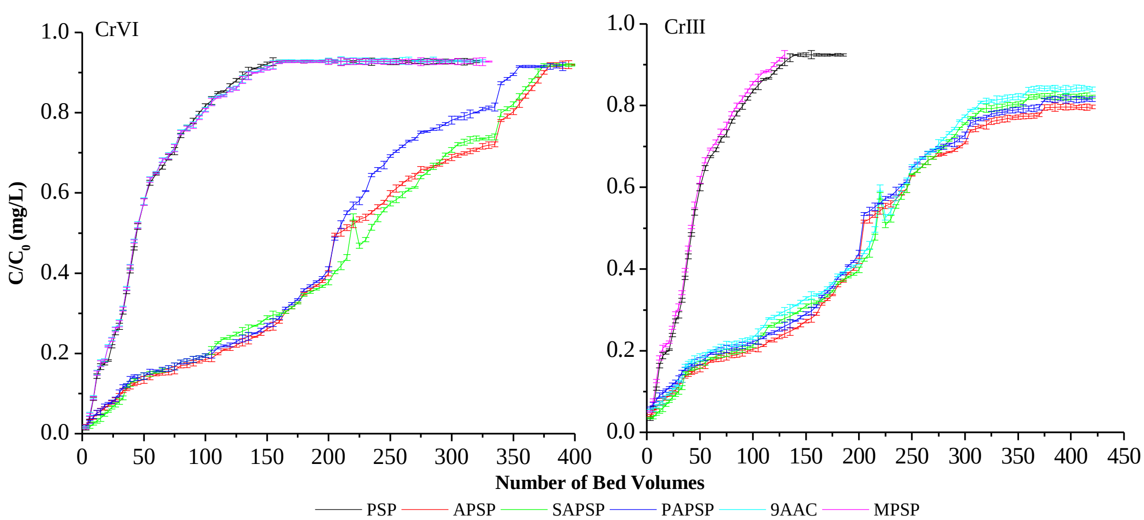

Figure 4.10. Column studies

Thomas and Yoon–Nelson models were also applied to the column adsorption data at a flow rate of 1 mL/min at an initial metal ion concentration of 1 g/L and bed height 5 cm with all the adsorbents under study.Thomas rate constant (k_{Th}) and bed capacity (q_{Th}) were calculated and are presented in Table 4.7.

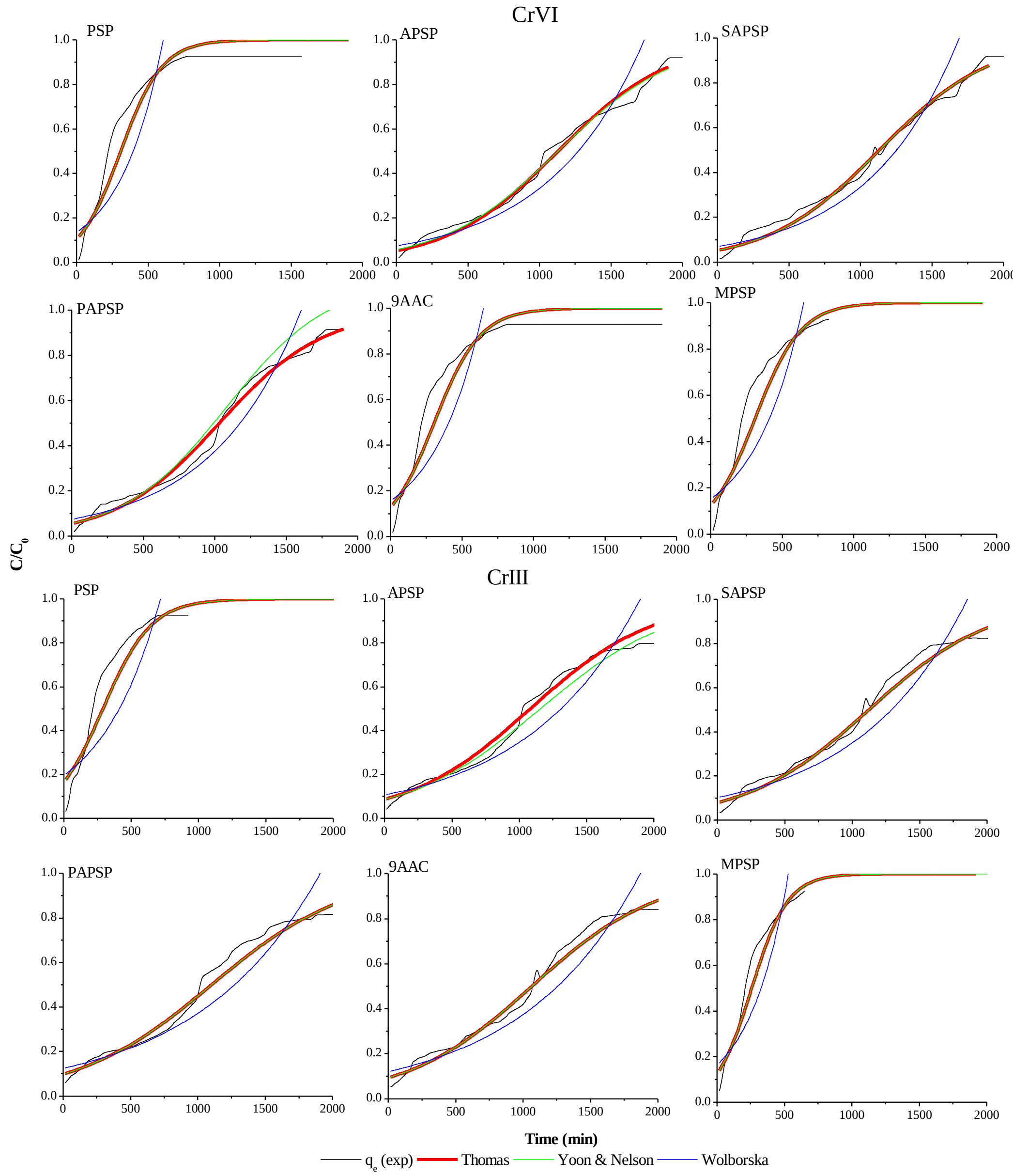

Figure 4.11. Column Modeling studies for Cr^{6+}& Cr^{3+}

The theoretical predictions based on the model parameters are compared in Figure 4.11 with the observed data. Similarly, from the plot of sampling time (t) versus $\ln[C_e/(C_0-C_e)]$, the Yoon and Nelson constant K_{YN} and τ (the time necessary to reach 50% of the retention) were calculated and are shown in Table 4.7. The well fit of the experimental data on to the Thomas and Yoon-Nelson model indicate that external and internal diffusion will not be the limiting step.

Table 4.7. Column Isotherms parameters for different adsorbents

Cr^{6+}/ Cr^{3+}	PSP	APSP	SAPSP	PAPSP	9AAC	MPSP
Thomas Model						
K_{TH}	0.000007/ 0.000006	0.000003/ 0.000002	0.000003/ 0.000002	0.000003/ 0.000002	0.000006/ 0.000002	0.000006/ 0.000008
q_0	61.739/ 58.097	225.910/ 216.514	226.406/ 224.771	206.349/ 220.310	61.312/ 213.084	62.080/ 51.531
r^2	0.937/ 0.938	0.986/ 0.982	0.976/ 0.980	0.984/ 0.985	0.938/ 0.985	0.935/ 0.969
SD	0.086/ 0.090	0.045/ 0.054	0.093/ 0.085	0.066/ 0.025	0.086/ 0.043	0.063/ 0.077
Yoon & Nelson Model						
K_{YN}	0.007/ 0.006	0.002/ 0.002	0.003/ 0.002	0.003/ 0.002	0.006/ 0.002	0.006/ 0.008
$t_{0.5(exp)}$	225/ 300	1050/ 1175	1100/ 1125	1050/ 1100	225/ 1075	225.000/ 250
$t_{0.5(cal)}$	309/ 291	1129/ 1157	1133/ 1124	1033/ 1102	307/ 1065	310/ 257
r^2	0.938/ 0.938	0.986/ 0.982	0.975/ 0.980	0.984/ 0.985	0.938/ 0.985	0.934/ 0.969
SD	0.086/ 0.090	0.091/ 0.054	0.096/ 0.085	0.066/ 0.025	0.086/ 0.043	0.064/ 0.077
Wolborska Model						
β	0.509/ 0.416	0.662/ 0.571	0.680/ 0.581	0.662/ 0.529	0.474/ 0.538	0.479/ 0.461
N_0	154424/ 182606	441653/ 483688	430902/ 472726	408938/ 486223	165709/ 476453	165752/ 134924
r^2	0.789/ 0.796	0.950/ 0.946	0.923/ 0.932	0.949/ 0.954	0.788/ 0.944	0.782/ 0.866
SD	0.062/ 0.096	0.082/ 0.060	0.077/ 0.091	0.089/ 0.023	0.067/ 0.057	0.084/ 0.093

From the equations in Chapter 3 Table3.1 it is evident that the characteristic parameter associated with Thomas and Yoon and Nelson models vary but both the models predict essentially same uptake capacity and C/C_0 values for a particular experimental set of data. Hence same r^2 and SD values were obtained as also suggested by Baral et al. [59].

4.3.8. Desorption.

The XPS results indicate that about 50% of Cr is present as Cr^{3+} and the rest as Cr^{6+}. As mentioned previously, ICP analysis was done to find the total Cr remaining in solution during the course of our adsorption studies. There was negligible difference in total chromium(obtained from ICP) and Cr^{6+}concentration(obtained from diphenylcarbazide method) due to the fact that Cr^{3+} was also retained almost quantitatively at pH1as indicated during pH studies. This led us to believe that complete reduction of $Cr^{6+}$to Cr^{3+} was taking place by the adsorbents under study as observed in many reports available in literature[60].Theanalysis thus not gives us a clue of only partial reduction Cr^{3+}.So no attempt was made to study the desorption of Cr as we felt that chromium present in the adsorbents under study need not be separated since the end product is a Cr^{3+} salt[61].

The partial reduction of $Cr^{6+}$to $Cr^{3+}$by the adsorbents under study was identified only from XPS studies, the results of which were unfortunately obtained only when we had almost come to an end of the compilation of this report. So further studies need to be done regarding desorption of Cr from the adsorbents under study and also to try to achieve complete reduction using a suitable desorbent as achieved by Luis K. [29].

4.4.Mechanism.

The aqueous phase pH governs the speciation of metals and also the dissociation of active functional sites on the sorbent. In this study, the pH values of initial solutions were adjusted to below 4.0 and the acidic chromate ion species ($HCrO_4^-$) was the major form of Cr^{6+} at this pH range [62]. At low pH conditions, there is easier protonation of functional groups such as amino, carboxyl and sulfonate groups of biomaterials making the adsorbent material surfaces more positive [63, 64].Furthermore, the point of zero charge (pH_{ZPC}) of the adsorbents under study was determined to be about in the range 3.5-4.0, suggesting that the adsorbents have a large surface charge density at pH 1, resulting in a strong electrostatic attraction between theadsorbents and the anionic adsorbates.

This results in the removal rate of Cr^{6+}in the aqueous phase being faster, since the binding of anionic Cr^{6+}species with the positively charged groups is enhanced as a result of electrostatic interaction.Thus, Cr^{6+}sorption, similar to other metals, could easily be attributed to ion exchange, surfacecomplexation, and precipitation.The reason being reduction of $Cr^{6+}$to Cr^{3+}could not be evidenced by the presence of Cr^{3+} in solution as observed by other researchers. However, low pH is also known to accelerate the redox reactions in aqueous and solid phases, since the protons participate in these reactions as[65].The chromium reduction can take place through variousreactions, mainly the following;

$$\mathrm{CrO_4^{2-} + 8H^+ + 3e^- \leftrightarrow Cr^{3+} + 4H_2O} \qquad E^0=1.48\ V$$

$$\mathrm{HCrO_4^- + 7H^+ + 3e^- \leftrightarrow Cr^{3+} + 4H_2O} \qquad E^0=1.35\ V$$

$$\mathrm{H_2CrO_4 + 6H^+ + 3e^- \leftrightarrow Cr^{3+} + 4H_2O} \qquad E^0=1.33V$$

The electron donor groups of the biomass reduce $Cr^{6+}$to Cr^{3+}. After that, Cr^{3+}forms complexes with the adsorbent materials under study.Furthermore,XPS analyses suggested the presence of both $Cr^{3+}$and Cr^{6+} species on the adsorbent surfaces. This suggests that Cr^{6+} anions were easily adsorbed on the adsorbents by electrostatic interaction and were reduced to Cr^{3+} ions on the biomass surface.The adsorption of $Cr^{3+}$was also found to be quantitative at low pH probably due to chelation of $Cr^{3+}$with hydroxyl and phenolic groups. After reduction, either $Cr^{3+}$was occluded in the solid phase or slow to diffuse back to aqueous phase that Cr^{3+} was undetectable in the filterate.FT-IR observations also suggest that hexavalent Cr induces an oxidation of lignin components and that the retention of Cr ions occurs through a complexation reaction involving carboxylate moieties.

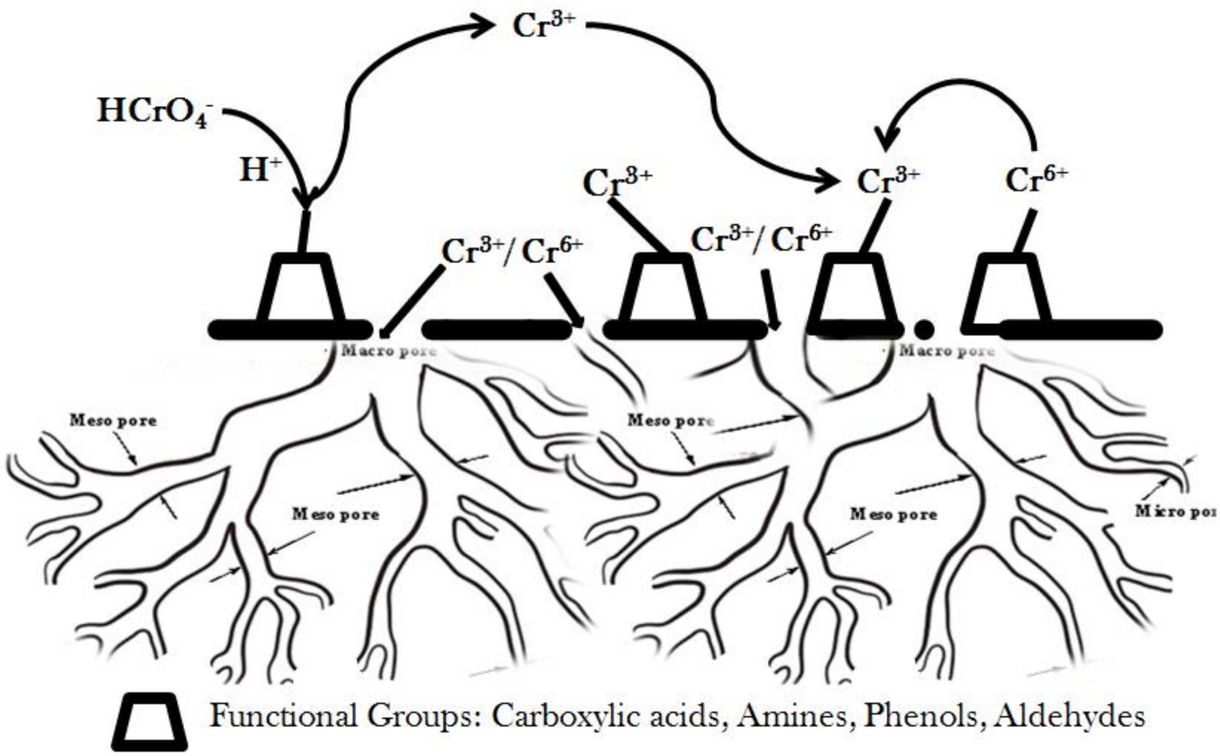

Figure 4.12. Mechanism for Cr^{6+} and Cr^{3+} adsorption and reduction of chromium involved

The adsorption process thus probably involves three steps as depicted in Figure 4.12: (1) the binding of anionic Cr^{6+} ions with the positively charged groups present on the biomass surface; (2) the reductionof Cr^{6+} to Cr^{3+} by adjacent electron-donor groups; (3) the formation of complexes of the Cr^{3+} with adjacent groups capable of Cr-binding. This statement was consistent withthat of Park et al. [66-68].

Literature Cited:

1. V.P. Evangelou, *Environmental Soil and Water Chemistry*: *Principles and Applications*; John Wiley&Sons: NewYork, **1998**; 476.
2. R. Eisler, *Chromium Hazards to Fish*, *Wildlife*, *and Invertebrates*: *A Synoptic Review*; Biological Report 85 1.6; Contaminated Hazard Reviews Report 6; U.S. Department of the Interior, Fish and Wildlife Service: Laurel, MD, **1986**.
3. S.D. Faust, O. M. Aly, *In Adsorption Processes of Water Treatment*; Butterworth Publishers: Stoneham, MA, **1987**.
4. C. Raji, T. S.Anirudhan.*Water Res.* **1998**, *32*, 3772.
5. L.J. Yu, S.S. Shukla, K.L. Dorris, A. Shukla, J.L. Margrave. *J. Hazard. Mater.* **2003**, *100*, 53.
6. F.N. Acar, E. Malkoc.*Bioresource Technol.* **2004**, *94*, 13.
7. H. Ucun, Y.K. Bayhan, Y. Kaya, A. Cakici, O.F. Algur.*Bioresource Technol.* **2002**, *85*, 155.
8. J.S. Melo, S.F. D'Souza.*Bioresource Technol.* **2004**, *92*, 151.
9. R.S. Bai, T.E. Abraham.*J. Sci. Ind. Res.* **1998**, *57*, 821.
10. J.S. Merrin, R. Sheela, N. Saswathi, R.S. Prakasham, S. V.Ramakrishma.*Indian J. Exp. Biol.* **1998**, *36*, 1052.
11. R.S. Prakasham, J.S. Merrie, R. Sheela, N. Saswathi, S.V. Ramakrishna. *Environ. Pollut.***1999**, *104*, 421.
12. Y. Sag, A. Yalcüuk, T. Kutsal.*Hydrometallurgy*.**2001**, *59*, 77.
13. M. Nourbakhsh, Y. Sag, D. Ozer, Z. Aksu, T. Kutsal, A.A. Cuaglar.*Process Biochem.* **1994**, *29*, 1.
14. G. Ozdemir, T. Ozturk, N. Ceyhan, R. Isler, T. Cosar.*Bioresource Technol.* **2003**, *90*, 71.
15. A.I. Zouboulis, M.X. Loukidou, K.A. Matis.*Process Biochem.* **2004**, *39*, 909.
16. Z. Aksu,U. Acüikel, T. Kutal. *J. Chem. Technol. Biotechnol.* **1997**, *70*, 368.
17. G.C. Donmez, Z. Aksu, A. Ozturk, T. Kutsal.*Process Biochem.* **1999**, *34*, 885.
18. Z. Aksu, U. Acüikel.*Biochem. Eng. J.* **2000**, *4*, 229.
19. V.K. Gupta, A.K. Shrivastava, N. Jain.*Water Res.* **2001**, *35*, 4079.
20. D.C. Lee, C.J. Park, J.E. Yang, Y.H. Jeong, H.I. Rhee.*Appl. Microbiol. Biotechnol.* **2000**, *54*, 445.
21. D. Park, Y.S. Yun, J.M. Park.*Environ. Sci. Technol.***2004**, 38, 4860.
22. L. Chun, C. Hongzhang, L. Zuohu.*Process Biochem.* **2004**, *39*, 541.
23. N.R. Bishnoi, M. Bajaj, N. Sharma, A. Gupta.*Bioresource Technol.* **2004**, *91*, 305.
24. K. Selvaraj, S. Manonmani, S. Pattabhi.*Bioresource Technol.* **2003**, *89*, 207.

25. D. Mohan, C. Pittman.*J. Hazard. Mater*. **2006**,*B137*, 762.
26. C. Raji, T.S. Anirudhan.*Indian J. Chem. Technol.* **1997**, *4*, 228.
27. M. Zhao, J.R. Duncan.*Biotechnol. Appl. Biochem.* **1997**, *26*, 179.
28. D. Kratochvil, P. Pimentel, B. Volesky.*Environ. Sci. Technol.* **1998**, *32*, 2693.
29. L.K. Cabatingan, R.C. Agapay, J.L. Rakels, M. Ottens, L.A.M. Van der Wielen.*Ind. Eng. Chem. Res.* **2001**, *40*, 2302.
30. D.C. Sharma, C.F. Forster.*Water Res.* **1993**, *27*, 1201.
31. J.L. Gardea-Torresdey, K.J. Tiemann, V. Armendariz, L. Bess-Oberto, R.R. Chianelli, J. Rios, J.G. Parsons, G. Gamez.*J. Hazard. Mater.* **2000**, *80*, 175.
32. In-situ treatment of soil and groundwater con-taminated with chromium, Technical Resources Guide, United States Environmental Protection Agency, US EPA/625/R-00/005.
33. Dionex, Determination of Cr(VI) in water, wastewater and solid waste extracts,Technical Note 26LPN34398-011M7/96, Dionex Corporation, **1996**.
34. V.M. Nurchi, G. Crisponi, I. Villaescusa. *CoordChem Rev.***2010**, *254*, 2181.
35. R. Ramos, A. Martinez, R. Coronado.*Water Sci. Technol.***1994**, *30*, 19.
36. M. Lopez-Garcia, P. Lodeiro, J.L. Barriada, R. Herrero, M.E. Sastre de Vicente. *Chem. Eng. J.* **2010**, *165*, 517.
37. S.K. Das, A.R. Das, A.K. Guha. *Environ. Sci. Technol*. **2007**, *41*, 8281.
38. B. Xiao, K.M. Thomas. *Langmuir* **2005**, *21*, 3892.
39. J. Febrianto, A.N. Kosasih, J. Sunarso, Y.H. Ju, N. Indraswati, S. Ismadji. *J. Hazard. Mater*. **2009,** 162.
40. R.S. Vieira, M.M. Beppu. *Colloids Surf. A.***2006,** *279*, 196.
41. Y.S. Ho, G. McKay. *Chem. Eng. J*. **1998**, *70*, 115.
42. S. Schiewer, S.B. Patil. *Biores. Technol*. **2008**, *99*, 1896.
43. Z. Reddad, C. Gerente, Y. Andres, P.L. Cloirec. *Environ. Sci. Technol*. **2002,** *36*, 2067.
44. K. Vijayaraghavan, K. Palanivelu, M. Velan. *Biores. Technol*. **2006**, *97*, 1411.
45. J. Sarma, A. Sarma, K.G. Bhattacharyya. *Ind. Engg. Chem. Res.***2008,** *47*, 5433.
46. V.K. Gupta, I. Ali, V.K. Saini, T.V. Gerven, B.V. Bruggen, C. Vandecasteele. *Ind. Eng. Chem. Res*.**2005**, *44*, 3655.
47. G.J.L. Torresdey, K. Dokken, K.J. Tiemann, J.G. Parsons, J. Ramos, N.E. Pingitore, G. Gamez. *Microchem. J.* **2002,** *71*, 157.
48. R.K. Samal, B.B. Panda, S.K. Rout, M. Mohanty.*J. Appl. Polym. Sci.* **1995,** *58*, 745.
49. K.K. Pandey.*J. Appl. Polym. Sci*. **1999**, *71*, 1969.
50. H. Yang, R. Yan, H. Chen, D.H. Lee, C. Zheng.*Fuel.***2007,** *86*, 1781.

51. M.S. Elovitz, W. Fish.*Environ. Sci. Technol*. **1995**, *29*, 1933.
52. A. Santos, P. Yustos, A. Quintanilla, S. Rodriguez, F. Garcia-Ochoa.*Appl. Catal.B.* **2002,** *39*, 97.
53. E. Fourest, B. Volesky. *Environ. Sci. Technol*. **1996**, *30*, 277.
54. N.B. Clothup, L.H. Daly, S.E. Wiberley. *Introduction to Infrared and Raman Spectroscopy, 3rd ed.;* Academic Press: London, **1990**.
55. S. Fonglim, Y. Mingzheng, S. Wenzou, J.P. Chen. *Environ. Sci. Technol*. **2008**, *42*, 2551.
56. L.Dupont, E.Guillon. *Environ. Sci. Technol*. **2003**, *37,* 4235.
57. A. Pizzi, *Holzforschung***1990**, *44*, 419.
58. J. G.Ostmeyer, T. J. Elder, *J. Wood Technol*. **1988**, 8, 413.
59. S.S. Baral, N. Das, T.S. Ramulu, S.K. Sahoo, S.N. Das, G.R. Chaudhury. *J. Hazard. Mater*.**2009,** *161*, 1427.
60. J. Li, Q. Lin, X. Zhang, Y. Yan.*J. Colloid Interface Sci*. **2009**,*333*, 71.
61. R. Aravindhan, B. Madhan, J.R. Rao. *Environ. Sci. Technol.***2004**, *38,* 300.
62. R. Ramos, A. Martinez, R. Coronado, *Water Sci. Technol*. **1994,** *30*, 191.
63. D.C. Sharma, C.F. Forster, *Bioresour. Technol*. **1994**, *47*, 257.
64. G. Cimino, A. Passerini, G. Toscano, *Water Res*. **2000,** *34*, 2955.
65. D. Park, S.R. Lim, Y.S. Yun, J.M. Park, *Bioresour. Technol*. **2008**, *99*, 8810.
66. D. Park, Y.S. Yun, J.M. Park, *Environ. Sci. Technol*. **2004**, *38*, 4860.
67. D. Park, Y.S. Yun, J.M. Park, *Chemosphere.***2005**, *60*, 1356.
68. D. Park, Y.S. Yun, D.S. Lee, S.-R. Lim, J.M. Park, *J. Hazard. Mater*. **2006,** *137*, 1377.

Chapter 5

Mechanistic and Spectroscopic study for adsorption of U^{6+} onto the adsorbents prepared from Palm Shell Powder

Outline:

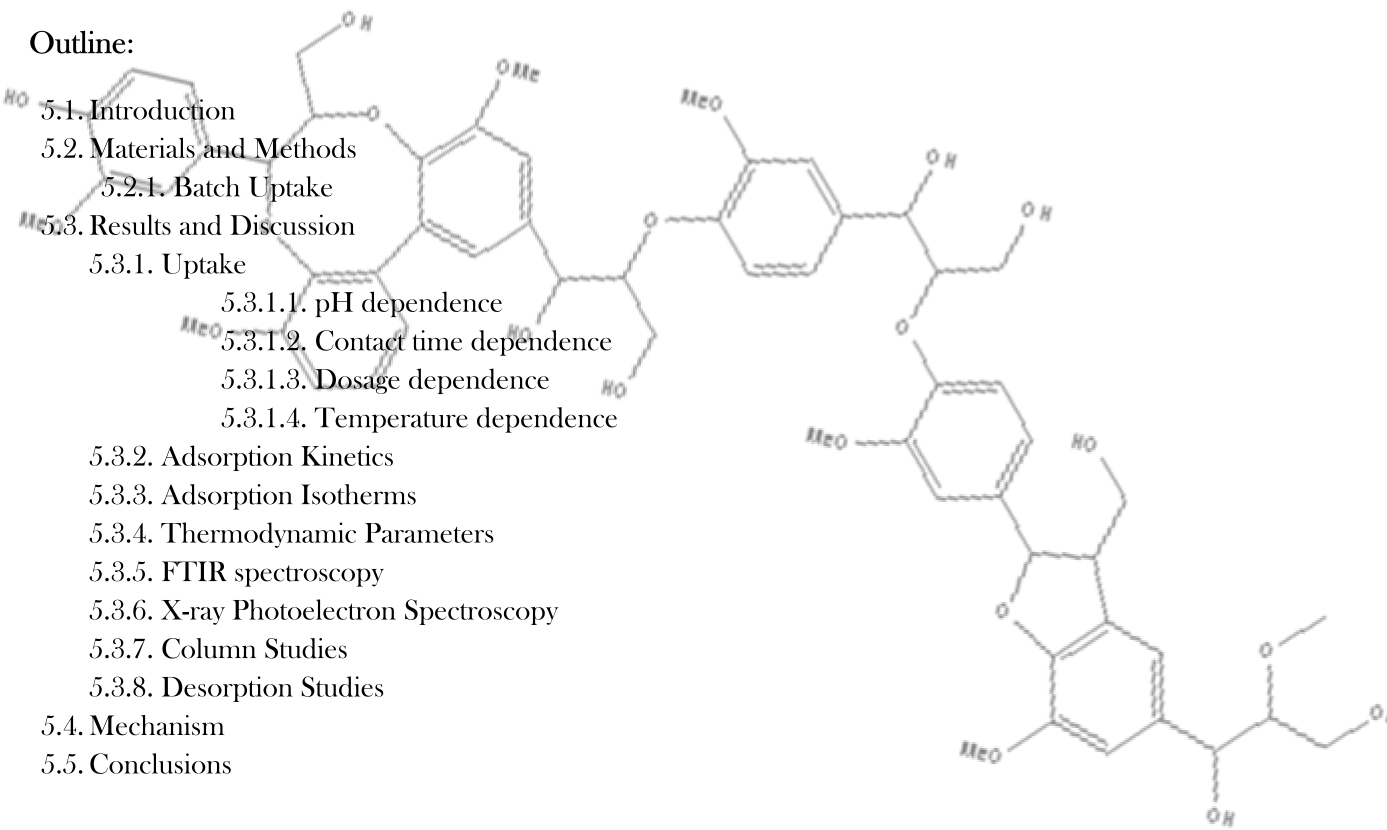

5.1. Introduction

Biomaterials have also been investigated for their potential use in the remediation and/or recovery of uranium from aqueous solutions, high salt concentration solutions, acid mine drainage, and uranium process solutions (Table1.1 of chapter1) [1-8]. For uranium uptake, biosorbents of different origins viz., bacteria, fungi and plant biomass showing efficient metal uptake (>15% loading capacity) across the pH range 4–5.5 are common [9-11]. Yang and Volesky have investigated the interactions of uranyl cations with *Sargassum* seaweed, and they have modeled the interactions of proton exchange with uranyl cations [4]. In addition they have investigated the effect of pH on adsorption, which showed a pH-dependent trend and an increase in binding with an increase in pH. Jansson-Charrier et al. investigated the adsorption of uranium ions onto chitosan and found that it was effective in the treatment of leachates from mines [6]. Psareva et al. have investigated the sorption of uranium onto cork biomass [7]. Whereas, Liu et al. have studied the effects of cations and anions on the biosorption processes for uranium and found little or no effect from various cations and anions [8]. To the best of our knowledge there are no reports in the literature on biomass exhibiting good performance (>15% loading capacity) at low pH(~1). Hence use of these biosorbents for biosorption technology in treating such wastewaters becomes technically non-feasible. Furthermore, although studies on the biosorption of uranium have been performed, the investigation into the mechanism(s) of biosorption has not been studied to any great extent.

Spectroscopic techniques have been a valuable aid in determining functional groups that are responsible for metal binding. Parsons et al have investigated the mechanism of uranium adsorption onto alfalfa biomass and have found that the primary functional group on alfalfa biomass responsible for the binding of uranyl cations from aqueous solution was the carboxyl functionality [12]. Several investigations have shown that U(IV) is formed during the adsorption of U(VI) [13-15]. However no investigation on speciation of uranium on biomass has been reported.

The objectives of the study were:

1) To explore the potential use of palm shell and palm shell based adsorbents for adsorption of uranium.

2) To study the influence of various parameters on adsorption.

3) To understand the adsorption mechanism through XPS and FT-IR spectroscopic techniques.

5.2. Material and Methods.

5.2.1. Batch Uptake.

A stock solution of U^{6+} was prepared by dissolving 2.11 g of uranyl nitrate (Sulab) in slightly acidified double distilled water and making upto 1L to give 1000 mg/L of uranyl solution. Working standards were prepared by diluting different volumes of the stock solution to obtain the desired concentration. Batch adsorption experiments were conducted as discussed in Chapter 3.

At the end of the predetermined time intervals, the suspensions were filtered and the filterate was analysed to find the uptake of uranium by the adsorbents under study. The U^{6+} concentration in the filterate was analysed spectrophotometrically by UV spectrophotometer (Elico SL177) after using Arsenazo as complexing agent [16].

5.3. Results and Discussion.

5.3.1. Uptake studies.

5.3.1.1. ***pH dependence.*** The effect of pH on the removal of uranyl ion (initial concentration 100ppm) was studied in the range 1 to 10.

Figure 5.1 shows that adsorption of uranyl ion was not much dependent on pH. Maximum adsorption occurs at pH 1 for all the adsorbents under study, followed by slight decrease till pH 5 and then remains constant for the remaining range of pH studied. However the percent adsorption varies to a maximum of around 6% in the entire pH range studied.

E. M. Saad et al. reported that the uptake of uranyl (II) ions is low at acidic pH≤5. The protonation of the available active sites (amino acids, hydroxyl and carboxyl groups) in the date pits most likely inhibit their binding towards the uranyl (II) ions as reported earlier by the same group [17-19] for the solid sorbent polyurethane foams thus lowering the UO_2^{2+} ions uptake from the aqueous media [20].

The maximum uranium adsorption at pH 1 suggests that electrostatic forces cannot explain the adsorption mechanism and that covalent bonding contributes significantly to the adsorption. However, the high extent of adsorption that occurs at higher pH values is likely due to a range of adsorption reactions because the aqueous speciation of uranium is so complex in this pH range.

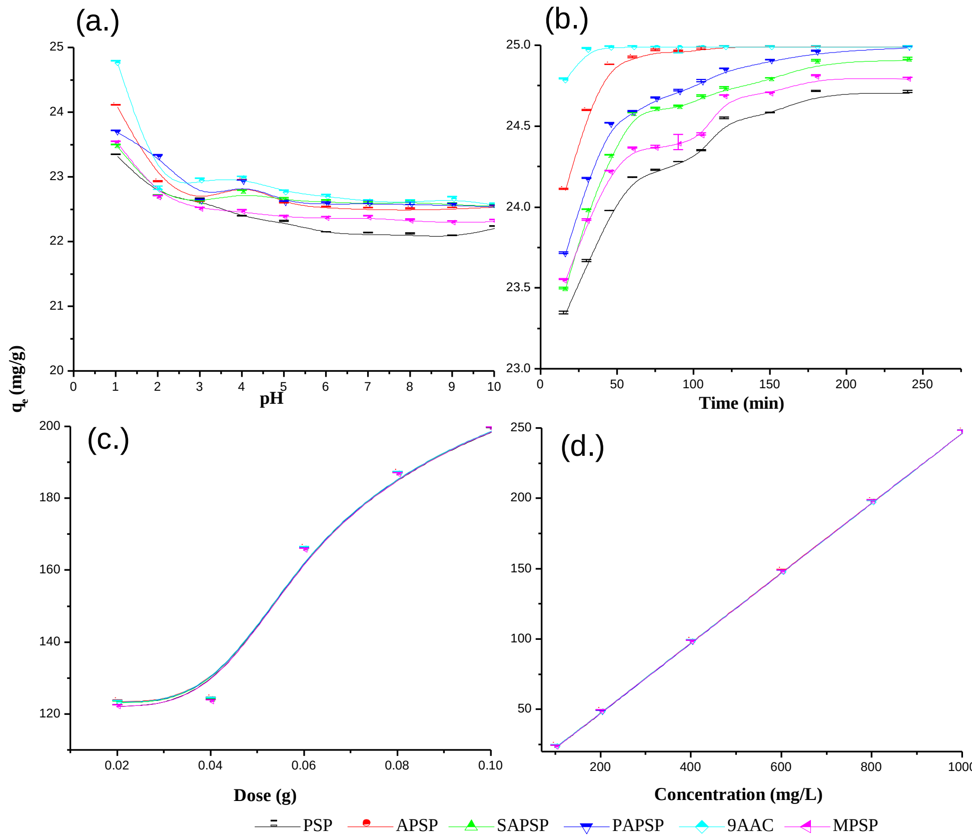

Operating parameters: 30 ^{0}C, 180 rpm, pH 1, 100ppm of U^{6+}, 0.1g adsorbent, time 180 min, temperature 30 ^{0}C; Time variation: 30-180 min, pH variation: pH 1-10, Conc. variation: 100-1000 ppm, Dose variation: 0.02-0.10 g adsorbent

Figure 5.1. Effect of a) pH, b) time, c) dose, d) initial concentration of U^{6+}

The predominate species in acidic solution up to pH =4.8 is UO_2^{2+} [21, 22]. The uranyl ion does not exist in the free state above pH 4, with uranyl hydroxide and uranyl-carbonate complexes dominating above pH 5, suggesting the adsorption of other uranium complexes to a significant extent. The relatively high extent of adsorption under these high pH conditions is likely caused by adsorption of the uranyl aqueous complexes themselves onto the adsorbent surface. The pK_a values of the protonation of the different functional groups in the adsorbents under study may account for the observed trend. The uptake at acidic pH could be attributed to the reducing action of aldehydes.

5.3.1.2. *Contact time dependence.* Contact time variation shows that equilibrium is achieved faster (30 & 80 min) when 9AAC & APSP was used as the adsorbent as compared to other adsorbents under study (PSP, SAPSP, PAPSP and MPSP) where equilibrium was achieved in 180 min (Figure 5.1). The rate of adsorption is very fast initially with about 96% of total uranium being removed within few minutes followed by a decreased rate with the approach of equilibrium. The removal rate is high initially due to the presence of free binding sites which gradually become saturated with time resulting in decreased rate of adsorption as equilibrium approaches. This indicates that the adsorption is mainly through surface binding. Similar observations were made by Das et al [23].

5.3.1.3. *Amount of adsorbent variation*. The effect of dose of adsorbents under study on the removal of uranium is shown in Figure 5.1, which illustrates the adsorption of uranyl ion with change of the adsorbent dose from 200 to 1000 mg. As inferred from Figure 5.1, for a fixed metal initial concentration, increasing the adsorbent dose provided greater surface area and availability of more active sites [24], thus leading to the enhancement of metal ion uptake. Adsorption increased from 98 to >99% with increase in adsorbent dose.

5.3.1.4. *Temperature variation*. Temperature studies showed (Figure 5.2) almost the same trend for all the adsorbents under study. From the figure it can be seen that uptake decreases as temperature increases indicating that the mechanism of adsorption is exothermic in nature for all the adsorbents under study.

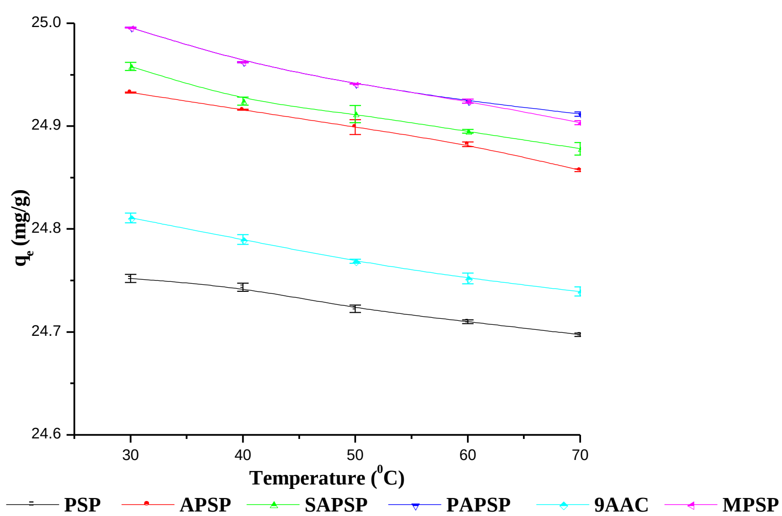

Operating parameters: 180 rpm, 0.1g adsorbent, time 240 min, optimum pH

Figure 5.2. Effect of temperature on uptake of uranyl ions by PSP, MPSP, APSP, SAPSP, PAPSP and 9AAC

5.3.2. Adsorption Kinetics.

Figure 5.3 shows the adsorption kinetics conducted at pH 1 for U^{6+} removal by PSP, APSP, SAPSP, PAPSP, 9AAC and MPSP. Adsorption of U^{6+} ions onto the adsorbents under study was carried out for 240 min. to ensure attainment of equilibrium. The kinetic models of Pseudo First order, Pseudo Second order, Intraparticle diffusion, Bangham, Elovich and Liquid film diffusion models were studied and the kinetic constants for the adsorption of mercury by all the adsorbents under study are presented in Table 5.1.

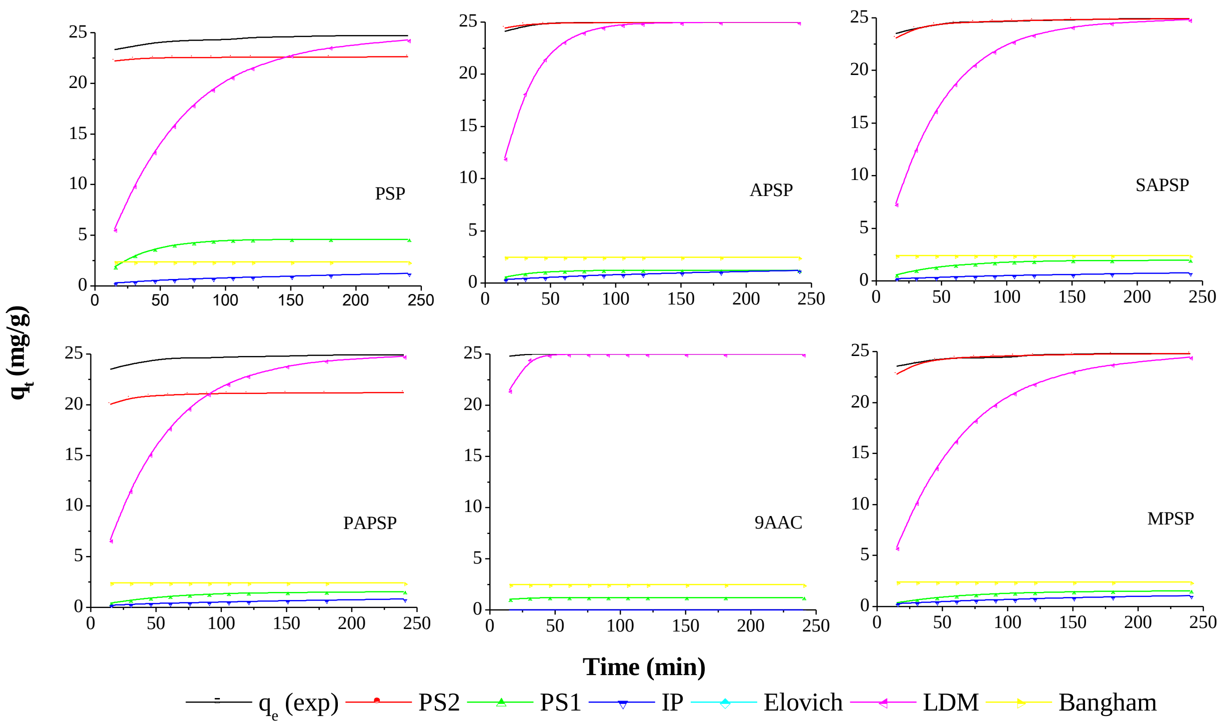

Operating parameters: 15-240 min, pH 1, 100 ppm of U^{6+}, 0.1 g adsorbent, 30 ^{0}C, 180 rpm.

Figure 5.3. Kinetic studies

Table 5.1. Kinetics parameters for uranium adsorption

pH1						
	PSP	**APSP**	**SAPSP**	**PAPSP**	**9AAC**	**MPSP**
q_e (exp)	24.714	25.000	24.920	24.996	25.000	24.802
Pseudo 2nd order						
q_e ($mg.g^{-1}$)	22.629	25.056	25.044	21.286	62.112	24.944
K_2 ($g.mgmin^{-1}$)	0.154	0.104	0.031	0.047	0.094	0.028
r^2	0.999	1.000	1.000	1.000	0.999	0.999
SD	0.017	0.005	0.008	0.007	6.24E-04	0.016
Lagergren						
q_e ($mg.g^{-1}$)	4.604	1.223	1.971	1.546	1.197	1.545
K_1 (min^{-1})	-0.035	-0.043	-0.023	-0.021	-0.129	-0.018
r^2	0.795	0.970	0.942	0.989	0.986	0.954
SD	0.082	0.067	0.101	0.075	0.098	0.111
Intra Particle Diffusion						
K_{ip}(mg/g/min)	0.079	0.008	0.049	0.054	0.000	0.070
r^2	0.951	0.806	0.976	0.967	0.000	0.921
SD	0.072	0.016	0.030	0.039	0.000	0.082
Elovich						
β ($g.mg^{-1}$)	1.907	3.478	1.969	2.204	1.865	2.158
α ($mg.g^{-1}min^{-1}$)	3.788E+41	3.66E+81	4.32E+43	3.83E+49	7.70E+45	8.89E+47
r^2	0.989	0.859	0.964	0.971	0.711	0.981
SD	0.065	0.107	0.119	0.096	0.046	0.079
Liquid film diffusion model						
K_{FD} (min^{-1})	0.017	0.043	0.023	0.021	0.129	0.018
r^2	0.979	0.970	0.942	0.989	0.987	0.954
SD	0.095	0.085	0.097	0.103	0.106	0.163
Bangham						
K_{BM} ($mL.g^{-1.}.L^{-1}$)	-114.160	-113.179	-113.807	-113.635	-112.841	-113.918
α	1.02E-04	4.43E-05	9.15E-05	8.20E-05	7.28E-06	8.88E-05
r^2	0.881	0.616	0.798	0.811	0.455	0.863
SD	0.004	0.004	0.005	0.004	0.001	0.004

The pseudo second order kinetics provided the best fit for the kinetic data at all pH values. The q_e values were very close to the experimental q_e value and correlation coefficient values were 0.99-1 at all the pH values for PSP, APSP, SAPSP, PAPSP, 9AAC and MPSP suggesting rate limiting step in adsorption of uranium could be chemisorption involving valence forces through the exchange of electrons between sorbent and sorbate [25, 26], complexation, coordination and/ or chelation.

In pseudo first order model the $q_{e(exp)}$ values were much higher than q_e fitted values showing large discrepancies demonstrating that the reaction cannot be classified as pseudo first order although this plot has reasonably good correlation coefficient from the fitting process. This underestimate of the amount of binding sites is probably due to the fact that q_e was determined from the y-intercept (0, 1). This has been observed by several other workers [27-30]. This could be due to boundary layer controlling the beginning of the adsorption process [30].

The curves for Liquid Film Diffusion Model (Table 3.1 Chapter 3) did not pass though origin as required by the model for all the adsorbents under study but had very small intercepts (curves not shown) indicating that diffusion of uranium from the liquid phase to the adsorbent surface might be having some role in deciding the rate processes.

The Weber and Morris adsorption kinetic model was plotted using the equation given in Table 3.1 (Chapter 3). The plots obtained for PSP, APSP, SAPSP, PAPSP, 9AAC and MPSP do not pass through origin implying that intraparticle diffusion is not the only operative mechanism. The intraparticle diffusion rate is fastest in PSP and APSP, the order being APSP~PSP>MPSP>PAPSP>SAPSP>9AAC as evident from intraparticle diffusion rate constants. Finally, in order to further confirm the occurrence of intraparticle diffusion, Bangham equation (Table 3.1 of Chapter 3) was applied to the adsorption data. The double logarithmic plots obtained with very less correlation coefficients (>0.455) indicated very less contribution of pore diffusion towards adsorption process. The lowest r^2 value for 9AAC is in agreement with the results of intraparticle diffusion. The not so linear curves indicated the diffusion of adsorbate into pores of the sorbent is not the only rate controlling step.

Adsorption capacity of the adsorbents for uranium was highest at pH 1 hence kinetics was studied at pH1, which is consistent with results of others [31]. Initial rapid uptake implies the binding of adsorbate ions on the surface of adsorbents under study through proton exchange at pH 1. Later on slower adsorption might be due to intraparticle diffusion, and diffusion of uranium from the aqueous phase to the adsorbent due to weak acidic and basic groups such as carboxyl, hydroxyl, amino groups at pH >1.

5.3.3. Adsorption Isotherms.

For modeling of mercury uptake Freundlich, Langmuir, Temkin, Dubinin-Radushkevich (DR), Flory-Huggins, Elovich and Halsey isotherm models were employed. Adsorption isotherms of the type q_e vs C_e were also used to verify the isotherm models. Model fits for all the isotherms along with experimental data for adsorption of U^{6+} on PSP, APSP, SAPSP, PAPSP, 9AAC and MPSP are presented in Figure 5.4. The values of model constants along with their correlation coefficients, r^2 and SD values for all the systems studied are presented in Table 5.2.

Freundlich equation describes adsorption (possibly multilayer in nature) on a highly heterogeneous surface consisting of non identical and energetically non uniform sites. The value of $n \approx 1$ for the Freundlich model indicates favorable adsorption. The Langmuir isotherm model is basically developed for gas-phase adsorption on homogeneous surfaces of glass and metals and predicts a single maximum binding capacity. The parameters K_L (equilibrium sorption constant) and q_{max} were calculated from the intercept and slope of the plot of C_e/q_e versus C_e. Based on the correlation coefficient r^2 and standard deviations for Langmuir it varied from 0.958 to 0.999 with very less SD values. Langmuir monolayer adsorption capacity was found in good agreement with the experimental adsorption capacities.

Table 5.2. Isotherms parameters for different adsorbents

	PSP	**APSP**	**SAPSP**	**PAPSP**	**9AAC**	**MPSP**
$q_{e\ (exp)}$ (mg/g)	248.440	248.280	248.364	248.415	248.427	248.280
Freundlich						
K_F(mg.g^{-1})(dm^3/mg)$^{1/n}$	3.739	4.618	5.989	5.207	4.226	5.474
n	0.714	0.893	1.248	1.008	0.770	1.188
r^2	0.989	0.977	0.991	0.988	0.961	0.998
SD	0.045	0.068	0.042	0.048	0.089	0.020
Langmuir						
K_L (dm^3.mg^{-1})	0.157	0.985	0.269	0.395	0.067	0.216
q_m (mg.g^{-1})	249.376	253.807	252.525	232.558	244.498	235.849
ΔG (kJ.mol^{-1})	-4.810	-0.039	-3.407	-2.416	-7.017	-3.979
r^2	0.986	0.989	0.972	0.999	0.993	0.958
SD	1.90E-05	9.72E-04	0.001	2.48E-04	0.002	9.91E-04
Temkin						
-ΔH (kJ.mol^{-1})	3.614	4.551	6.399	4.774	3.715	5.822
K_T (dm^3.mg^{-1})	0.639	0.867	0.570	0.869	0.748	0.725
r^2	0.995	0.995	0.994	0.989	0.994	0.978
SD	0.078	0.081	0.085	0.053	0.099	0.086
DR						
q_m (mg.g^{-1})	284.292	256.466	214.862	232.758	304.904	207.265
E^0 (KJ)	14.041	17.330	12.883	12.918	1.498	15.377
r^2	0.991	0.985	0.964	0.973	0.998	0.953
SD	0.095	0.023	0.093	0.087	0.044	0.022
Halsey						
K_H (mg.g^{-1})(dm^3/mg)$^{1/n}$	0.114	0.035	0.006	0.022	0.078	0.010
n_H	-0.714	-0.949	-1.248	-1.008	-0.770	-1.176
r^2	0.989	0.977	0.991	0.988	0.961	0.998
SD	0.094	0.056	0.098	0.098	0.094	0.046
Flory-Huggins						
K_{FH} (mg.g^{-1})(dm^3/mg)$^{1/n}$	0.956	0.983	1.025	1.026	1.016	1.038
N_{FH}	-0.994	-0.998	-0.997	-0.997	-0.998	-0.995
r^2	1.000	1.000	1.000	1.000	1.000	1.000
SD	4.97E-04	4.06E-04	3.69E-04	7.78E-04	2.57E-04	6.08E-04
Elovich						
q_m (mg.g^{-1})	237.461	232.758	208.513	217.022	262.434	198.3434
K_E (dm^3.mg^{-1})	0.846	0.092	0.018	0.419	0.080	0.238
r^2	0.986	0.996	0.974	0.978	0.983	0.989
SD	7.39E-04	0.012	0.030	0.079	0.030	0.037

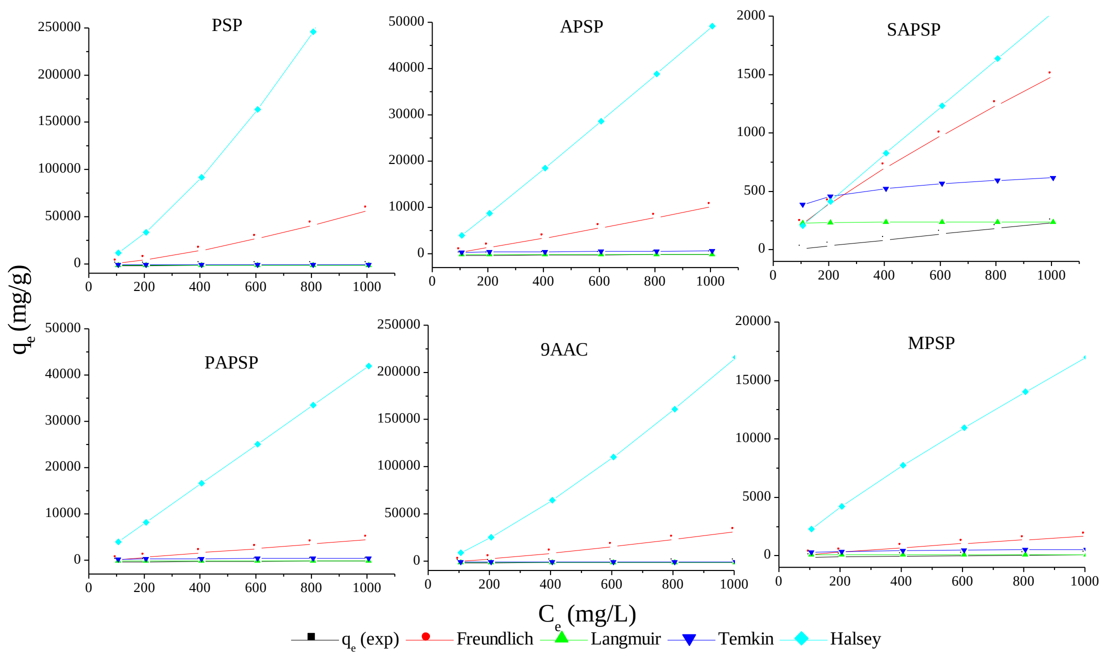

Operating parameters: 100-1000 ppm of U^{6+}, pH 1, 240 min, 0.1 g adsorbent, 30 ^{0}C, 180 rpm.

Figure 5.4. Adsorption Isotherms for U^{6+}

The correlation coefficients of Temkin Model (0.978 to 0.995) indicate a satisfactory fit of the model to the experimental data. The variation of adsorption energy, ΔQ = (3.614, 4.551, 6.399, 4.774, 3.715 and 5.822) is positive for all the sorbents under study, which indicated the adsorption process to be exothermic.

The Dubinin–Radushkevich model is applied in the form of linear equation as given in Table 3.1 (Chapter 3). The adsorption energy values calculated for U^{6+} on PSP (14.041 KJmol^{-1}), APSP (17.330 KJmol^{-1}), SAPSP (12.883 KJmol^{-1}), PAPSP (12.918 KJmol^{-1}), 9AAC (1.498 KJmol^{-1}) and MPSP (15.377 KJmol^{-1}). The magnitude of E is useful for estimating the mechanism of the sorption reaction. In case of E < 8.0 kJ/mol, physical forces may affect the sorption; for E in the range 8–16 kJ/mol, ion exchange is the working mechanism, while for E > 16 kJ/mol sorption may be dominated by particle diffusion [32, 33]. It is thus evident from D-R model that for 9AAC physisorption is the predominant mechanism, while for APSP, SAPSP, PAPSP and MPSP ion-exchange is the predominant mechanism.

Multilayer adsorption is generally discussed by the Halsey equation and is found to fit well with the experimental data having r^2 ($\geq$ 0.971) [25] indicating that the mechanism may be multilayer sorption for adsorbents under study while the low values of K_H suggest that multilayer sorption might be playing only a small role.

The Flory-Huggins model was used to assess the isotherm data. From the linear plots of $\log(\theta/C_0)$ versus $\log(1-\theta)$ (Figure not shown) for uranium adsorption on the adsorbents under study and the correlation coefficient values (r^2 =1.00) , it is apparent that the model shows good fits for the adsorbent under study. However the negative values of n and low values of k_{FH} imply that the model cannot be used to describe the adsorption data.

5.3.4. Thermodynamic Parameters.

The thermodynamic parameters of the sorption process could be determined from the experimental data obtained at various temperatures using the equations:

$$\Delta G^0 = \Delta H^0 - T\Delta S^0$$

The values of ΔH^0 and ΔS^0 can be calculated from the slope and intercept of the plots of ΔG^0 against T (Figure 5.5).

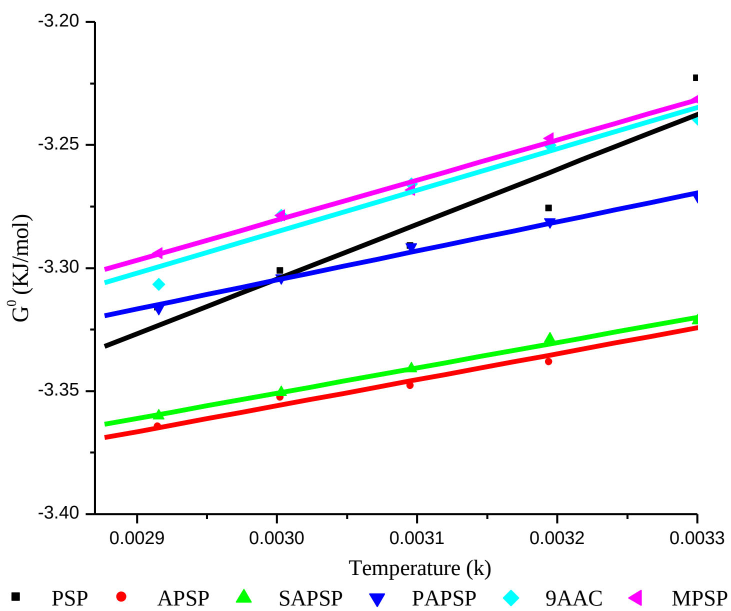

Operating parameters: 30-70 ^{0}C, 180 min, pH 1, 1000 ppm of U^{6+}, 0.1 g adsorbent, 180 rpm.

Figure 5.5. Thermodynamic studies

The negative value of ΔH^0 indicates that the adsorption of U^{6+} on PSP, APSP, SAPSP, PAPSP, 9AAC and MPSP is exothermic. Generally the absolute magnitude of the change in energy for physisorption is between (-20 and 0 KJ/mol); chemisorption has a range of (-400 and -80 KJ/mol). The negative value of ΔG^0 in table 5.3 indicates that sorption of uranyl ion by PSP, APSP, SAPSP, PAPSP, 9AAC and MPSP to be physisorption and is spontaneous and thermodynamically favorable [34].

Table 5.3. Thermodynamic Parameters for uranyl ions by PSP, APSP, SAPSP, PAPSP, 9AAC and MPSP

	ΔG (KJ/mol)	**ΔS (KJ/molK)**	**ΔH (KJ/mol)**	**r^2**	**SD**
PSP	-11.862	0.033	-1.854	0.945	0.001
APSP	-10.134	0.031	-0.881	0.986	0.003
SAPSP	-10.076	0.030	-0.856	0.997	0.002
PAPSP	-10.201	0.030	-0.981	0.996	0.002
9AAC	-10.941	0.032	-1.396	0.977	0.006
MPSP	-10.852	0.031	-1.355	0.997	0.002

Also the ΔG^0 values become less negative with increase in temperature suggesting that adsorption is favored at lower temperatures and hence is exothermic. The positive values of ΔS^0 suggest increased randomness during adsorption and a high affinity of the adsorbent towards the adsorbate.

5.3.5. FT-IR Spectroscopic Analysis.

FTIR spectra of uranium loaded PSP, APSP, SAPSP, PAPSP and MPSP are presented in Figure 5.6. The absorption bands of FTIR spectra listed in Table 5.4 reveal the changes in absorption bands of the surface functional groups of PSP, APSP, SAPSP, PAPSP, 9AAC and MPSP after uranium adsorption.

The band at 1720-1762 cm^{-1} band is associated with C=O stretching mode of carbonyls in carboxylic acids and lactones while 1280-1000 cm^{-1} band is associated with C-O stretching and O-H bending modes of groups such as phenols and carboxylic acids [35]. Also there is a shift in the frequencies of the absorption band of both C=O and C-O in carboxyl group (-COOH) due to metal binding.

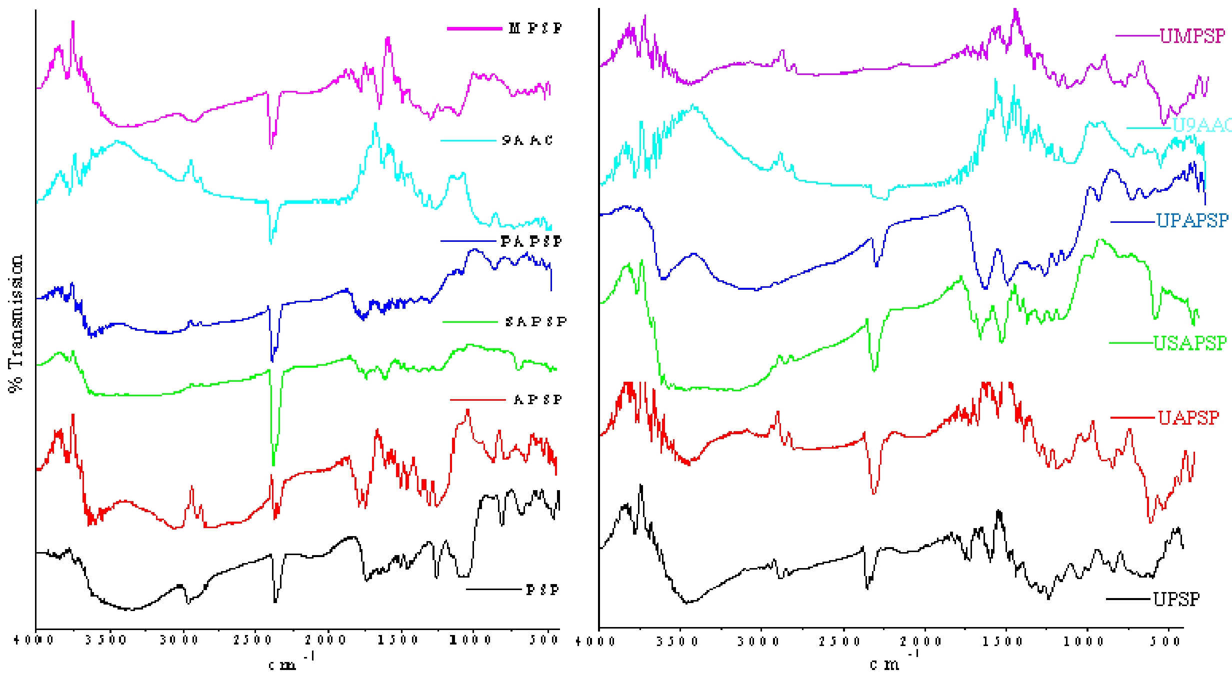

Figure 5.6. FTIR spectra of uranium loaded adsorbents

The C-O band shifts to higher frequencies 1217-1289 cm^{-1} probably due to high electron density induced by the adsorption of U(VI) on the adjacent carbonyl groups [36, 37]. This showed that the carboxyl groups and metal ion were coordinated, which may have been caused by the oxygen atom of carboxyl groups coordinating with the metal ion and leading to the shifting of symmetrical stretching vibration of carboxyl groups (νC=O). Similar observations were also made by Liu and Lin et al. [38, 39].

The band at 1720- 1732 cm^{-1} which is the absorbing band of carboxyl groups almost disappeared after adsorption of uranium. This can be interpreted by the decarboxylation of carboxyl groups and the oxidation of quinone groups [41-42]. Thus carboxylic groups are involved in adsorption of uranium as seen by comparison of IR spectra of the adsorbents and the uranuim loaded-adsorbents.

The interaction between uranium and carboxylic group of the adsorbent causes a diminution of the distance between C=O and C-O stretching peaks [43]. New peaks at wave numbers of 905-916 cm^{-1} were observed in the uranium treated samples, theses peaks can be assigned to the asymmetric stretching vibration of UO_2^{2+} [44, 45]. This peak was stronger in APSP, SAPSP, PSP than in MPSP, PAPSP and 9AAC suggesting higher uranium adsorption.

Table 5.4. Typical Absorption frequencies and Carbonyl stretching frequencies of Infra red spectra for free and metal loaded adsorbents

PSP-U	**MPSP-U**	**APSP-U**	**SAPSP-U**	**PAPSP-U**	**9AAC-U**	**Assignment**
3451	3478	3465	3454	3613	-	-N-H, -O-H stretching
2878, 2819	2979, 2875	2982, 2876	2893	3092, 2929	2990, 2876	-CH_3, -CH_2 symmetric stretch
2361	2345	2312	2335	2346	2335	Free CO_2
1718	1742 U^{4+}	1752	1751	1688	-	-C=O stretch for acids or aldehyde
1600	1586	1588	1589	1557	1591	-C=O stretch cellulose/ C=C Aromatic stretch (skeletal vibration)/ N-H bending of amide
1487	1466	1482	1483	1415	1482	-CH_2- stretch/ -C=C- Aromatic stretching
1420	-	-	-	-	-	U^{5+}
1346	1331	1344	1351	1325	1347	-C-H stretch/ N-H bending
1287	1274	1286	1289	1263	1217	-C-O bending of carboxylic acids/ phenolic O-H stretch/ N-H bending
1163	1149	1168	-	1194	-	-O-H stretch (2^0 Alcohol), -C-O-C-stretching
1061 U^{6+}	1051	1063 U^{6+}	1041	1041	-	-C-H stretch, -C-O stretch (1^0 Alcohol)
888	889	-	-	-	-	Anomeric C-H bending of cellulose
819	837 U^{6+}	840	-	830 U^{6+}	846	-C-H out of plane bending pentavalent uranium asymmetric stretch
995 U^{6+}, 850,571	947 U^{6+}, 852,556	962 U^{6+}, 844,570	948 U^{6+}, 847, 573	950 U^{6+}, 853, 569	950 U^{6+}, 851,572	U-O bending vibrations ν_{as} axial strong band of U=O, Equatorial U-O stretching

Biosorbent	$\upsilon_{C=O}$	υ_{C-O}	$\Delta = \upsilon_{C=O} - \upsilon_{C-O}$	**Biosorbent**	$\upsilon_{C=O}$	υ_{C-O}	$\Delta = \upsilon_{C=O} - \upsilon_{C-O}$
PSP	1732	1250	482	PSP-U	1718	1287	431
APSP	1720	1229	491	APSP-U	1752	1286	468
SAPSP	1723	1229	494	SAPSP-U	1751	1289	462
PAPSP	1723	1256	467	PAPSP-U	1688	1263	425
MPSP	1727	1238	489	MPSP-U	1742	1274	468

This indicates that part of uranium adsorption occurs by chemical adsorption (complexation) of uranyl species without reduction. The axial strong bands pertaining to the νas(U=O) vibrational modes, were found at 995, 947, 962, 948, 950 and 950 cm^{-1}, respectively. The two equatorial U-O stretching bands were at 571, 556, 570, 573, 569 and 572 cm^{-1} respectively [46]. The uranyl asymmetric stretch for pentavalent uranyl complexes is observed in the IR spectrum at ~800 cm^{-1} and is at significantly lower energy than the hexavalent uranium (~900 cm^{-1}) [47].

5.3.6. X-ray Photoelectron Spectroscopic analysis.

To evaluate adsorption mechanism for adsorption of uranium onto PSP, APSP, SAPSP, PAPSP, 9AAC and MPSP was analysed by XPS. The XPS survey spectrum consisted of carbon, oxygen, nitrogen and uranium. Figure 5.7 shows the U 4f spectra of U(VI) adsorbed on PSP, APSP, PAPSP, SAPSP, 9AAC and MPSP at pH 1.0. The chemical shift in the U 4f7/2 peak position is directly related to the oxidation state of uranium. Its binding energy decreases as the oxidation state is decreased from VI to IV. However, uranium V and uranium VI oxidation states exist as UO_2^{+} and UO_2^{2+} ions [48]. As a consequence of this oxygen bonding, the chemical shift between V and VI states are reported to differ only marginally in the BE scale [49]. Furthermore, low intensity excitations result in shake-up satellites for both U 4f7/2 and U 4f5/2 states [49], as a consequence of the change in electrostatic potential during the photoelectron excitation process. The BE of the U 4f satellite peak is much more sensitive to the valence state than the BE of the main U 4f peak, so that they can be used as a probe to identify the oxidation state of uranium [50].

The BE's and the FWHM's of the peaks were obtained by a fit which includes four peaks on a Shirley background. The unusually large FWHM and the asymmetry towards low binding energies of these peaks suggest the presence of at least three different chemical environments inducing a different chemical shift. The results from XPS suggest that adsorption of uranyl ion from an aqueous solution results in a mixture of U(VI), U(V) and U(IV) oxidation states on the surface of all the adsorbents under study. The intense peaks at about 380 and 392eVcorrespond to the spin–orbit (L–S) split U 4f7/2 and U 4f5/2 states, respectively. The 4f peak separation was found to be ~9 to 10 ev for each oxidation state of uranium. However, there also appears satellite peaks at a few eV slightly higher than the normal BE. Since the spin–orbit interaction separates these two levels by 10.85 eV, and hence the satellites of 4f7/2 which generally appear in this energy range are buried in the intense 4f5/2 peak or as a shoulder. These, satellite peaks carry the valence band information and are a good probe to identify chemical state and understand the chemical interaction [50]. This is applicable for both the U4f7/2 and U4f5/2 peaks. Since the spin–orbit interaction separates these two levels by 10.85 eV, and hence the satellites of 4f7/2 which generally appear in this energy range buried in the intense 4f5/2 peak or may appear as shoulder.

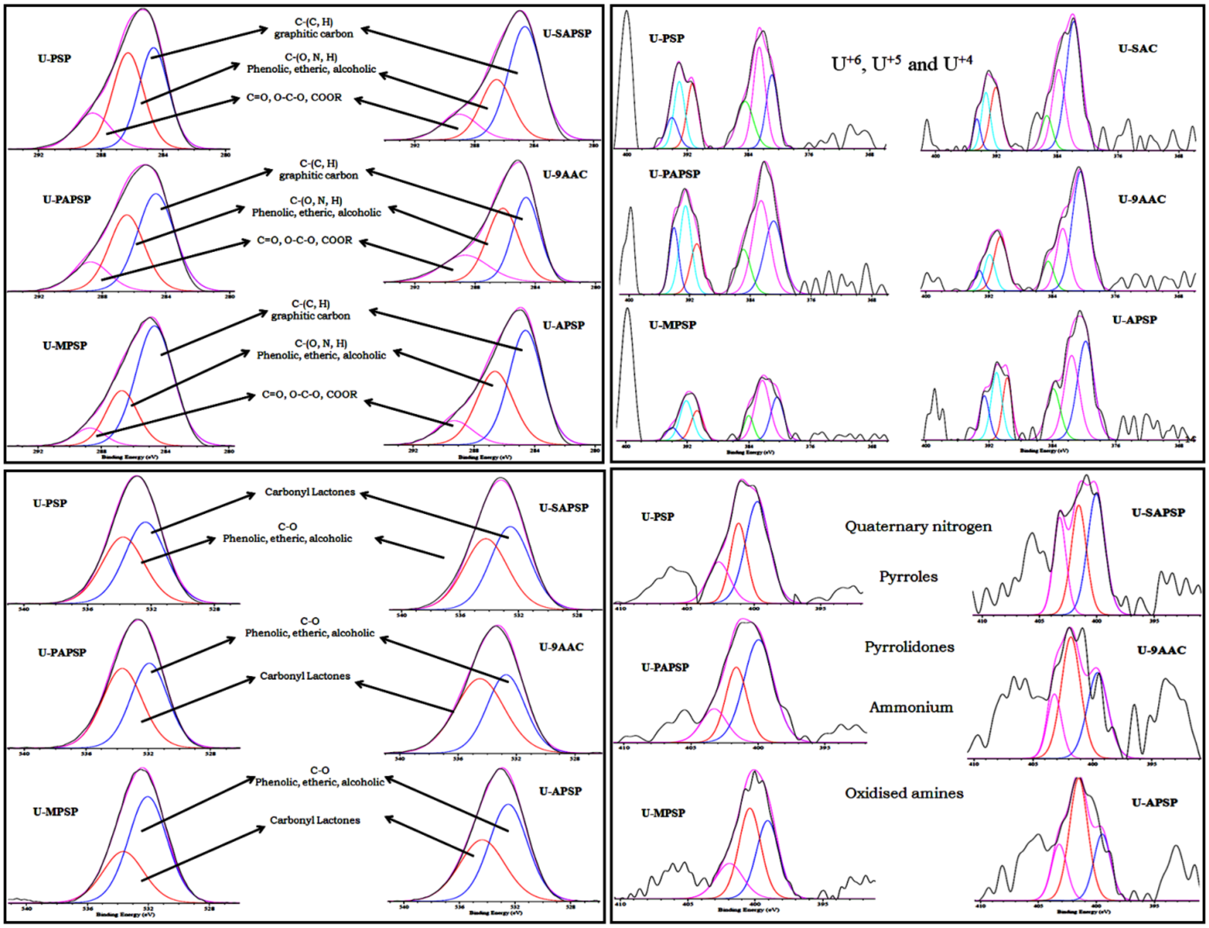

Figure 5.7. Deconvoluted XPS spectra of U

In the case of U (IV), the 5.8 and 16 eV satellites of 4f7/2 are clearly seen. Pireaux et al. [51] have reported satellites for U(IV) at 5.8, 8.2 and 16 eV higher binding energy than 4f photo peak position. The satellite peak observed at 397.0 eV, 397.6 eV which are approximately 7 eV from the U(4f5/2) peak, may be attributed to a shake-up transition from the oxygen-derived 2p band to the U(5f) Fermi level of UO_2 [50, 52]. The spectra contains two O1s peaks positioned at ~532 and ~534 eV, which can be assigned to terminal OH and sorbed H_2O, respectively [53]. The peak position of U(V) was found to be 381.6 eV with FWHM 2.2 eV [49] and the satellite peaks appear at 7.9-8.1 eV from the main U4f7/2 and U4f5/2 peaks [50].

5.3.7. Column.

The column breakthrough curves for uranium adsorption by adsorbents under study are shown in Figure 5.8. The effluent concentration is seen to have the typical 'S' shape. A total of ~ 2.8 L of 1000 mg/L metal ion solution was passed through the column containing 5 g of adsorbent under study. As seen from Figure 5.8 the breakthrough for uranium is seen to take place at 279.3, 147.2, 135.1, 129.1, 179.3 and 239 bed volumes for PSP, APSP, SAPSP, PAPSP, 9AAC and MPSP respectively.

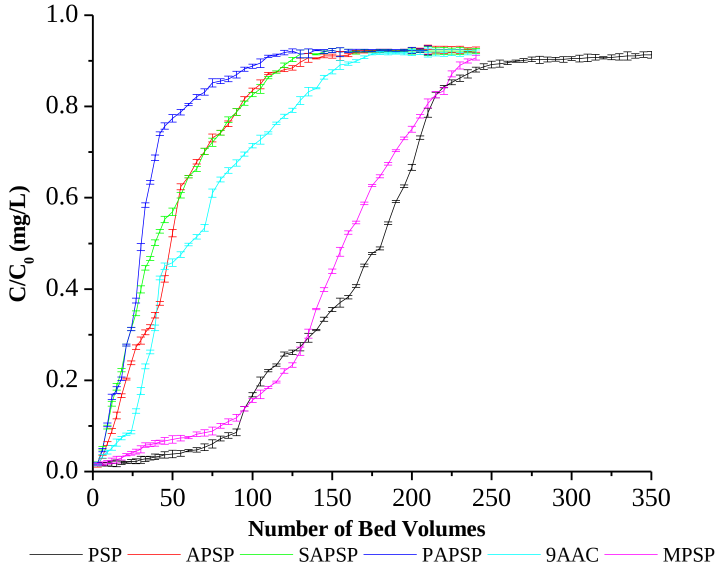

Figure 5.8. Column studies

Table 5.5. Column Isotherms parameters for different adsorbents

	PSP	APSP	SAPSP	PAPSP	9AAC	MPSP
Thomas Model						
K_{TH}(dm^3/(mg min))	0.00000443	0.00000435	0.00000389	0.00000424	0.00000453	0.00000503
q_0 (mg.g^{-1})	184.198	67.310	54.498	37.981	88.609	158.767
r^2	0.980	0.882	0.877	0.818	0.915	0.995
SD	0.074	0.085	0.086	0.093	0.766	0.091
Yoon & Nelson Model						
K_{YN} (min^{-1})	4.43E-03	4.35E-03	0.00389	0.00424	0.00453	0.00503
$t_{0.5}$ (exp) (min)	950	335	292	189	451	789
$t_{0.5}$ (cal) (min)	920.993	336.551	272.494	191.038	443.046	794.035
r^2	0.980	0.882	0.877	0.818	0.915	0.996
SD	0.073	0.088	0.086	0.093	0.076	0.081
Wolborska Model						
β (min^{-1})	0.917	0.423	0.346	0.337	0.509	0.894
N_0(mg.dm^{-3})	348775.700	229873.900	231018.700	199769.200	241528.663	293228.900
r^2	0.936	0.724	0.697	0.646	0.774	0.973
SD	0.063	0.067	0.068	0.073	0.095	0.069

Thomas and Yoon–Nelson models were also applied to the column adsorption data at a flow rate of 1 mL/min at an initial metal ion concentration of 1 g/L and bed height 5 cm with all the adsorbents under study. From the linear plots of $\ln[(C_o/C_t)-1]$ versus V_{eff} (Figure not shown) Thomas rate constant (k_{Th}) and bed capacity (q_{Th}) were calculated and are presented in Table 5.5.

The theoretical predictions based on the model parameters are compared in Figure 5.9 with the observed data. Similarly, from the plot of sampling time (t) versus $\ln[C_e/(C_0 - C_e)]$, the Yoon and Nelson constant K_{YN} and τ (the time necessary to reach 50% of the retention) were calculated and are shown in Table 5.5.

The well fit of the experimental data on to the Thomas and Yoon-Nelson model indicate that external and internal diffusion will not be the limiting step. From the equations in Table 3.1 (Chapter 3) it is evident that the characteristic parameter associated with Thomas and Yoon and Nelson models vary but both the models predict essentially same uptake capacity and C/C_0 values for a particular experimental set of data. Hence same r^2 and SD values were obtained as also suggested by Baral et al. [54].

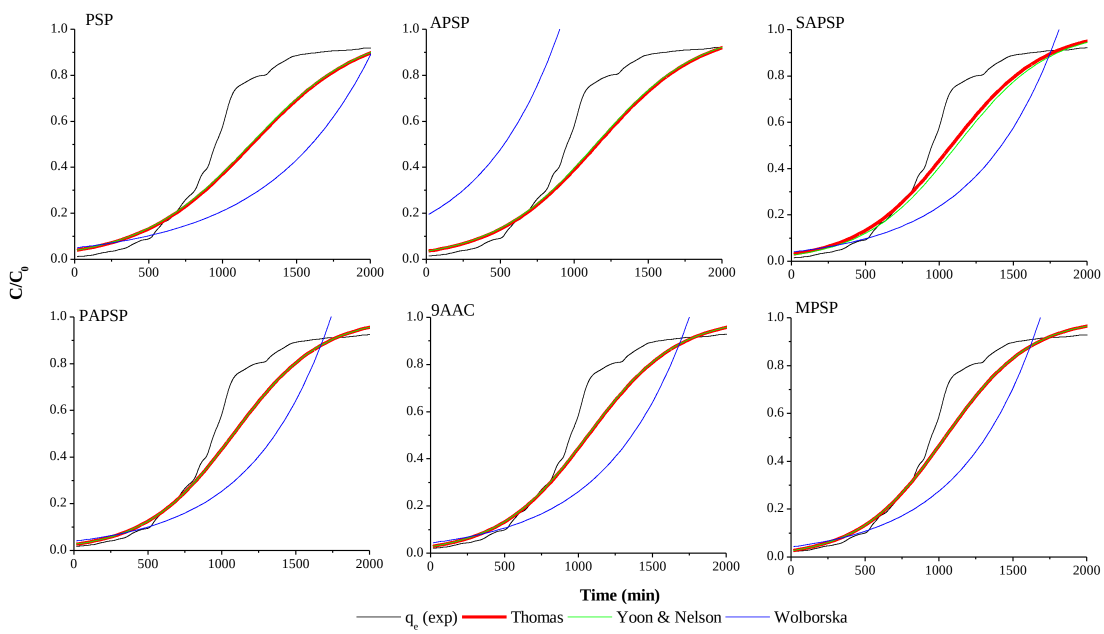

Figure 5.9. Column Modeling studies

5.3.8. Desorption.

Solutions of 0.1 M HCl, 0.1 M EDTA and 0.1 M NH_3 have been studied as eluents for desorption of U^{6+}. From Figure 5.10 it is evident that desorption of U^{6+} from the metal-loaded adsorbents with 0.1M EDTA resulted in >99% recovery.

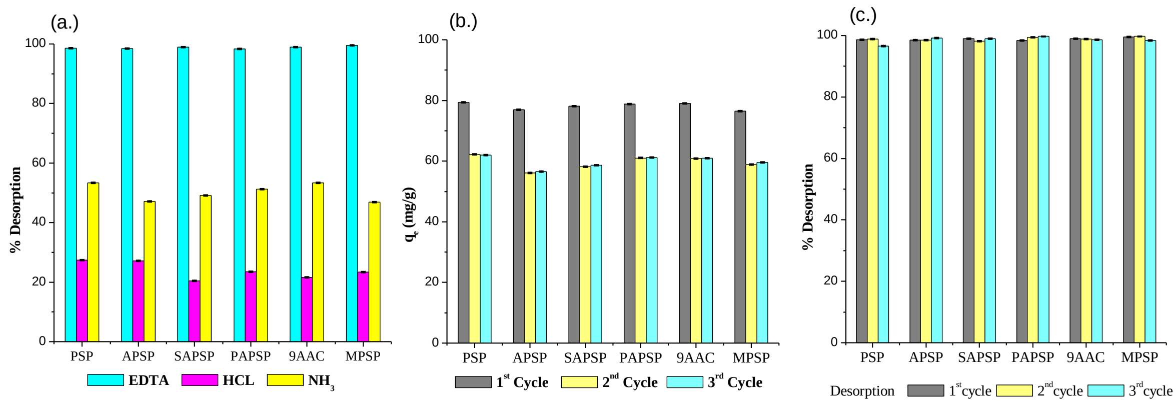

Operating parameters: Adsorption: 30 ^{0}C, 180 min, pH 1, 1000 ppm, 0.1 g adsorbent, 180 rpm. Desorption: 0.1 N desorbent, desorbing time: 30 min, 30 ^{0}C.

Figure 5.10. Desorption and cycles of adsorption (a) Effect of desorbents (b) Cycles of adsorption (c) Cycles of desorption

This indicates that ion exchange is involved in the adsorption process [55]. However, the use of 0.1M NH_3 and 0.1 M HCl resulted in >48 and >20 % recovery of U^{6+} respectively. It was observed that U^{6+} was easily desorbed within 30 min, which would prove highly advantageous for metal recovery. From Figure 5.10 it is evident that the removal capacity of adsorbents shows insignificant changes in the second and third cycle. Thus regeneration and reuse of the adsorbents under study is an economical and efficient method for removal of U^{6+} from water.

5.4. Mechanism.

The possible mechanisms for the removal of uranium include: complexation or chelation of uranyl or reduced uranous species by organic ligands, adsorption by weak van der waals and hydrogen bonding. Although sorption onto the adsorbents under study is likely to be responsible for the initial removal of U from solution, some subsequent surface reduction of U(VI) to U(IV) occurs. The reduction of uranium occurred concurrently with the oxidation of hydroxyl and aldehydic groups. Interestingly, U(V) which is not supposed to be stable is seen to be stabilized by the reducing groups present in the adsorbents under study.Reduction of uranyl species by the reducing groups under right pH conditions to relatively insoluble UO_2 and U(V) and precipitation could be taking place.

The reduction of $[UO_2]^{2+}$ to U(IV) is thought to proceed *via* single electron transfer to pentavalent uranyl, $[UO_2]^+$ and further reduction to $[UO_2]$ as shown in scheme 5.1.

$$[UO_2]^{2+} + e^- \rightarrow [UO_2]^+ + e^- \rightarrow [UO_2]$$

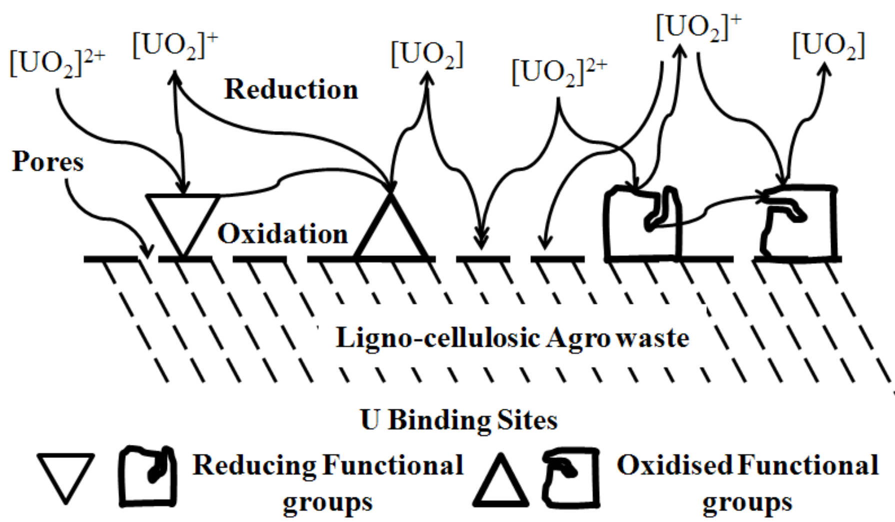

Scheme 5.1. Redox mechanism for uranium adsorbed species

The interaction of uranyl ions with the adsorbents under study can take place as below. Formation of uranyl carbonyl complexes:

$$2RCOOH + UO_2^{2+} \rightarrow RCOO^- - UO_2^{2+} - {}^-OOCR + 2H^+$$

Oxidation of hydroxyl groups in the adsorbents into carbonyl groups:

$$> CH - OH + UO_2^{2+} \rightarrow > C = O + UO_2 + 2H^+$$

Dehydrogenation of aliphatic hydro-carbonaceous moieties are known to be 'catalyzed' by uranium species [56].

$$RH_2 + UO_2^{2+} \rightarrow R + UO_2 + 2H^+$$

5.5. Conclusions

The adsorption potential of PSP, APSP, SAPSP, PASP, 9AAC and MPSP towards adsorption of uranium was evaluated. The parameters influencing the adsorption process like pH, dose of adsorbent and agitation time were optimized. Sorption isotherms of U(VI) on the adsorbents under study were evaluated using Freundlich, Langmuir, Temkin, Dubinin-Radushkevich (DR), Flory-Huggins, Elovich and Halsey isotherms. The values of E_0 derived from DR model suggest ion exchange as the working mechanism for APSP, SAPSP, MPSP and PAPSP, particle diffusion for PSP while for 9AAC the value suggests physisorption. The ΔG^0 values from Langmuir and thermodynamic calculations indicate physisorption as the major mechanism for adsorption of uranium. The adherence to pseudo second order kinetic model and Halsey model indicate multilayer and ion exchange as the mode of adsorption thus justifying our hypothesis that a range of mechanisms are involved in the adsorption process to different extents for the adsorbents under study. We have observed for the first time that the adsorption of uranium takes place by adsorption followed by reduction, the reduced species being both U(IV) and U(V). The sorption process was found to be exothermic, spontaneous and accompanied by decrease in entropy.Furthermore data also suggest that the adsorbents under study prepared from biomass, particularly APSP and PAPSP may be an inexpensive and viable means to remediate UO_2^{2+} from contaminated acidic solutions as till date adsorbents with good adsorption capacity at low pH(~1) are not available in literature.

Literature Cited.

1. A. Nakajima, T. Tsuruta. *J. Nucl. Sci. Technol.* **2002**, 528.
2. K.C. Bhainsa, S.F. D'Souza. *J. Environ. Sci. Health, Pt. A: Toxic/Hazard. Subst. Environ. Eng.* **2001**, *A36*, 1621.
3. M.T. Gonzalez-Munoz, M.L. Merroun, N.B. Omar, J.M. Arias. *Int. Biodeterior. Biodegrad.* **1997**, *40*, 107.
4. J. Yang, B. Volesky. *Environ. Sci. Technol.* **1999**, *33*, 4079.
5. K. Popa, A. Cecal. *Environ. Eng. Manage. J.* **2003**, *2,* 69.
6. M. Jansson-Charrier, E. Guibal, J. Roussy, R. Surjous, P. Le Cloirec. *Water Sci. Technol.* **1996**, *34*, 169.
7. T.S. Psareva, O.I. Zakutevskyy, N.I. Chubar, V.V. Strelko, T.O. Shaposhnikova, J.R. Carvalho, M.J.N. Correia. *Colloids Surf. A* **2005**, *252*, 231.
8. W.J. Liu, W.C. Xu, B.E. Wang. *Youkuangye* **2004**, *23*, 143.
9. T.A. Davies, B. Volesky, A. Mucci. *Water Res.* **2003**, *37*, 4311.
10. M. Kalin, W.N. Wheeler, G. Meinrath. *J. Environ. Radioactiv*. **2005**, *78*, 151.
11. J. Wang, C. Chen. *Biotechnol. Adv.* **2006**, *24*, 427.
12. K.J. Tiemann, G. Gamez, K. Dokken, J.G. Parsons, J.L. Gardea-Torresdey. *Microchem. J.* **2002**, *71*, 287.
13. A.A. Atia, *Hydrometallurgy* **2005**, *80*, 13.
14. E.D. Vecchia, H. Veeramani, E.I. Suvorova, N.S. Wigginton, J.R. Bargar, R.B. Latmani. *Research in Microbiology* **2010**, *161*, 765.
15. L. Alidokht, A.R. Khataee, A. Reyhanitabar, S. Oustan. *Desalination* **2011**, *270*, 105.
16. S.B. Savvin, *Talanta* **1961**, *8*, 673.
17. M.M. Abou-Mesalam, I.M. El-Naggar, M.S. Abdel-Hai, M.S. El-Shahawi, *J. Radioanal. Nucl. Chem.* **2003**, *258*, 619.
18. M.S. El-Shahawi, M.A. Othman, M.A. Abdel-Fadeel, *Anal. Chim. Acta* **2005**, *546*, 221.
19. M.S. El-Shahawi, M.A. Othman, H.M. Nassef, M.A. Abdel-Fadeel, *Anal. Chim. Acta* **2005**, *536*, 227.
20. E.M. Saad, R.A. Mansour, A. El-Asmy, M.S. El-Shahawi. *Talanta* **2008**, *76*, 1041.
21. G. Meinrath. *Journal of Radioanalytical and Nuclear Chemistry* **1998b**, *232*, 179.

22. W. Dong, S.C. Brooks. *Environ. Sci. Technol*. **2006**, *40*, 4689.
23. S.K. Das, A.R. Das, A.K. Guha. *Environ. Sci. Technol.* **2007**, *41*, 8281.
24. K.V. Kumar, K. Porkodi. *J. Hazard. Mater.* **2007**, *146*, 214.
25. J. Febrianto, A.N. Kosasih, J. Sunarso, Y.H. Ju, N. Indraswati, S. Ismadji. *J. Hazard. Mater.* **2009**, *162*, 616.
26. R.S. Vieira, M.M. Beppu. *Colloids Surf. A.* **2006**, *279*, 196.
27. Y.S. Ho, G. McKay. *Chem. Eng. J.* **1998**, *70*, 115.
28. S. Schiewer, S.B. Patil. *Biores. Technol*. **2008**, *99*, 1896.
29. Z. Reddad, C. Gerente, Y. Andres, P.L. Cloirec. *Environ. Sci. Technol*. **2002**, *36*, 2067.
30. K. Vijayaraghavan, K. Palanivelu, M. Velan. *Biores. Technol*. **2006**, *97*, 1411.
31. J. Sarma, A. Sarma, K.G. Bhattacharyya. *Ind. Engg. Chem. Res*. **2008**, *47*, 5433.
32. C. Gerente, V.K.C. Lee, P.L. Cloirec, G. Mckay. *Crit. Rev. Environ. Sci. Technol*. **2007**, *37*, 41.
33. V.K. Gupta, I. Ali, V.K. Saini, T.V. Gerven, B.V. Bruggen, C. Vandecasteele. *Ind. Eng. Chem. Res*. **2005**, *44*, 3655.
34. G.J.L. Torresdey, K. Dokken, K.J. Tiemann, J.G. Parsons, J. Ramos, N.E. Pingitore, G. Gamez,. *Microchem. J.* **2002**, *71*, 157.
35. M.M. Figueira, B. Volesky, H.J. Mathieu. *Environ. Sci. Technol*. **1999**, *33*, 1840.
36. E. Fourest, B. Volesky. *Environ. Sci. Technol*. **1996**, *30*, 277.
37. N.B. Clothup, L.H. Daly, S.E. Wiberley, Introduction to Infrared and Raman Spectroscopy, 3rd ed.; Academic Press: London, **1990**.
38. Z.Y. Lin, J.M. Wu, B.Q. Fu, R. Xue, J.Z. Zhou, Q.X. Zheng, Y.Y. Liu, J.K. Fu. *Acta Chim. Sinica* **2004**, *62*, 1829.
39. W.J. Liu, W.C. Xu, B.E. Wang. *Environ. Prot. Sci*. **2004**, *30*, 39.
40. M.A. Rashid. *Chem. Geol*. **1972**, *9*, 241.
41. P. Ioselis, R. Ikan, M. Frenkel. Thermal degradation of metal complexed humic substances. In: A.G. Douglas and J.R. Maxwell (Eds), Advances in Organic Geochemistry, Pergamon Press, **1979**, 547.
42. Y.K. Kharaka, W.W. Carothers, R.J. Rosenbauer. *Geochim. Cosmochim. Acta* **1983**, *47*, 397.
43. S. Fonglim, Y. Mingzheng, S. Wenzou, J.P. Chen. *Environ. Sci. Technol*. **2008**, *42*, 2551.
44. R.L. Frost. *Spectroc. Acta. A. Mol. Biomol. Spectrosc*. **2006**, *64*, 308.
45. M. Tsezos, B. Volesky. *Biotechnol. Bioeng*. **1982**, *24*, 385.

46. C.A. Tellez Soto, M. Arissawa, J. Gomez Lara, M.A. Mondragon. *Polyhedron* **2000**, *19*, 2353.
47. P.L. Arnold, J.B. Love, D. Patel. *Coordination Chemistry Reviews* **2009**, *253*, 1973.
48. F.A. Cotton, G. Wilkinson, *Advanced Inorg. Chem*. Willey Eastern Pvt, **1969**.
49. S. Bera, S.K. Sali, S. Sampath, S.V. Narasimhan, V. Venugopal. *Journal of Nuclear Materials* **1998**, *255*, 26.
50. J.H. Liu, S. Vanden Berghe, M.J. Konstantinovic. *Journal of Solid State Chemistry* **2009**, *182*, 1105.
51. J.J. Pireaux, J. Riga, E. Thibaut, C. Tenret-Neol, R. Caudano, J.J. Verbist, *Chem. Phys.* **1977**, *22*, 113.
52. G.C. Allen, P.M. Tucker, J.W. Tyler, *J. Phys. Chem*. **1982**, *86*, 224.
53. X. Tan, Q. Fan, X.B. Wang. *Environ. Sci. Technol*. **2009**, *43*, 3115.
54. S.S. Baral, N. Das, T.S. Ramulu, S.K. Sahoo, S.N. Das, G.R. Chaudhury. *J. Hazard. Mater*. **2009**, *161*, 1427.
55. L. Xiaomin, Y. Tang, C. Xiuju, L. Dandan, L. Fang, W. Shao. *Colloids and Surfaces A: Physicochem. Eng. Aspects* **2008**, *317*, 512.
56. S. Choudhary, P. Sar. *Journal of Hazardous Materials* **2011**, *186*, 336.

Chapter 6

Application of the adsorbents to some Real and Synthetic Samples

Outline:

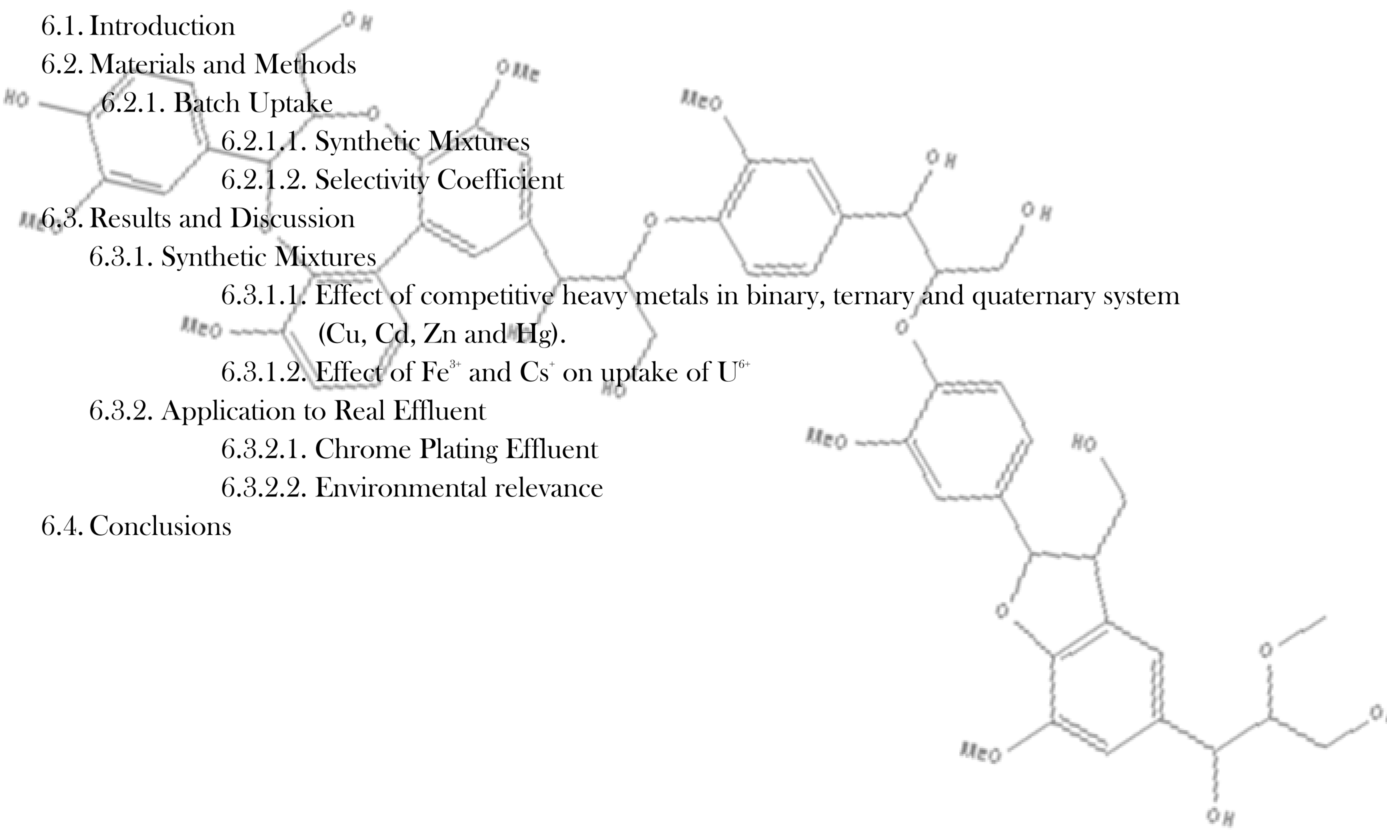

6.1. Introduction.

In the environment, contamination rarely occurs for single metals and is invariably due to complex mixtures. Nonetheless, routine evaluation of adsorbates is made based on single adsorbate components. Competitive adsorption on the adsorbent surface can take place where components with similar properties (i.e., size, polarity, interaction energy) compete for a limited number of adsorption sites.

Nuclear technology has resulted in release of radioactive isotopes of cesium into environment. ^{137}Cs is one of the most abundant radionuclides in the nuclear fission having long radiological half-life (30 years) and can be present along with uranium [1-3]. Its metabolic similarities to potassium favour its uptake and accumulation by plants after radio-contamination of water body and ultimately agricultural field. It enters into many food chain pathways to cause radiation exposure to human being and other ecological biota of the ecosystem [4]. Futhermore Fe^{3+} is known to be present in mining feed solution and also is a major constituent in high and low level nuclear industry effluents [5, 6].

Thus, a better understanding of the multi-component adsorption from aqueous solutions is needed.

The removal of heavy metals from industrial wastewaters is gaining significance in the present context of global ecology. Chromic acid is used in the plating and anodizing operations in the surface finishing industry. Chromate eventually finds its way to a company's waste treatment system through the dumping of the spent plating baths, contaminated rinse waters, and fume scrubber blow down. Both the spent plating bath and contaminated rinse waters are acidic; however, they generally differ in the amount of chromate contained. The former is apparently very concentrated (ranging from 45 to 470 g of Cr^{6+}/L), while the latter can be relatively dilute and can be further classified as high strength, typical strength, or dilute wastewaters with typical Cr^{6+} levels of 500, 100, and 20 ppm, respectively [7].

So our objectives were:

i) To investigate the adsorption ability of the adsorbents under study (PSP, APSP, SAPSP, PAPSP, 9AAC and MPSP) for Cu, Cd, Zn and Hg in binary, ternary and quaternary metal solution mixtures

ii) To study the effect of the presence of Fe^{3+} and Cs^{+} on the adsorption of uranium using the adsorbents under study

iii) To study the application of the adsorbents under study for the removal of chromium from chrome plating effluents

6.2. Materials and Methods.

6.2.1. Batch Uptake.

Adsorption experiments were performed in batch mode for Cu^{2+}, Cd^{2+}, Zn^{2+} and Hg^{2+} (from stock solutions as described in Chapter 3) conducted at 30°C by agitating 0.1 g of adsorbent with respective metal ion solution in 100mL stoppered conical flasks in a thermostated rotary mechanical shaker at 150 rpm for 4 hours.

6.2.1.1. *Synthetic Mixtures.* Binary mixtures contained 25 ppm of each metal ion, ternary mixtures contained 11 ppm of each metal ion and quaternary mixtures contained 6.25 ppm of each metal ion. Batch experiments were performed by taking 20 mL of adsorbate solution containing different mixtures of metal ions under study maintained at pH 4 and 0.1 g of adsorbent in 25 mL stoppered flasks. The contents were shaken by a thermostated water bath shaker with a constant speed of 150 rpm at 30°C and the samples were withdrawn at appropriate time intervals and filtered. The filtrate was analyzed for each of the metals Cu, Cd, Zn and Hg by AAS at their respective wavelengths.

6.2.1.2. *Selectivity Coefficient.* The effectiveness of the removal of each metal ion is reflected in the percentage adsorption and selectivity coefficient as reported in Figures 6.1, 6.2, 6.3 and Table 6.1 respectively. The selectivity coefficient k was calculated using the equation [8, 9]:

$$k = \frac{molar\ fraction\ of\ component\ i\ in\ the\ carbon\ adsorbed\ mixture}{molar\ fraction\ of\ component\ i\ in\ the\ aqueous\ solution\ mixture} = \frac{q_i/(q_i+q_j)}{C_{Li}/\ (CL_i+CL_j)}$$

6.3. Results and Discussion.

6.3.1. Synthetic Mixtures

6.3.1.1. *Effect of competitive heavy metals in binary, ternary and quaternary system (Cu, Cd, Zn and Hg).* In quaternary mixtures PAPSP, APSP, SAPSP, 9AAC and MPSP showed higher selectivity towards zinc while PSP showed greater preference towards mercury followed by zinc. SAPSP and PAPSP showed their next preference to copper followed by mercury while APSP, 9AAC and MPSP showed their next preference to mercury over copper.

In ternary mixtures containing Cu, Cd and Hg where zinc was absent all the adsorbents under study showed higher selectivity towards mercury except for SAPSP which showed preference to copper over mercury as also seen in quaternary mixtures. Even in solutions containing Hg, Zn and Cu PSP, MPSP and APSP showed selectivity towards mercury. However, PAPSP and 9AAC again showed better selectivity towards zinc followed by mercury. SAPSP showed selectivity towards copper followed by mercury and zinc. Between copper and cadmium no specific trend was observed with some adsorbents showing selectivity towards copper (PSP, APSP, MPSP) and some towards cadmium (PAPSP) after Hg and Zn.

In bimetallic mixtures of copper and mercury greater selectivity towards mercury was observed by PSP, PAPSP, 9AAC and MPSP. PAPSP showed five times higher selectivity for mercury over copper. On the other hand APSP and SAPSP showed better selectivity towards copper.

Adsorption studies on binary mixtures containing Cd and Hg revealed that all the adsorbents under study showed higher selectivity towards mercury as compared to Cd. Similar studies on binary mixtures containing Zn and Hg revealed that all the adsorbents were selective towards Zn over mercury. However MPSP had almost equal selectivity coefficient values for Zn and Hg.

In binary mixtures containing Cu and Cd, the selectivity coefficients were higher for Cu than Cd in the case of APSP, SAPSP, PAPSP and 9AAC while PSP and MPSP had greater selectivity coefficient values for Cd. APSP, SAPSP, PAPSP and 9AAC displayed higher selectivity towards copper in binary mixtures containing Cu and Zn while PSP and MPSP showed greater selectivity towards zinc. On the other hand, in binary mixtures containing Cd and Zn, PSP, 9AAC, APSP and MPSP showed higher selectivity coefficient for Cd while SAPSP, PAPSP had higher selectivity coefficient for Zn.

In summary, SAPSP seems to show a clear preference for copper except in quaternary mixtures where Zn has a slightly higher selectivity coefficient, however the difference is very less. PSP on the other hand displayed a greater selectivity towards mercury except for binary mixtures. In binary mixtures probably where individual metal concentrations are higher though the total metal ion concentration continues to be the same PSP showed a different trend by displaying greater selectivity towards Cd in the presence of Cu and Zn, a greater selectivity towards mercury in the presence of Cd and Cu and a greater selectivity towards Zn in Hg-Zn mixtures. PAPSP showed a clear preference to Zn in quaternary and ternary mixtures and in Cd-Zn and Hg-Zn binary mixtures. Surprisingly, PAPSP showed six times higher selectivity coefficient for copper over Zn in their binary mixtures. MPSP seems to show a clear preference towards mercury in binary and ternary mixtures. However in quaternary mixtures it showed preference towards Zn. APSP and 9AAC did not show any specific trend in the present studies with its selectivity coefficients changing in quaternary, ternary and binary mixtures. This variation in specificity could be because the binding strength of a metal ion to a given adsorbent depends on various properties of the adsorbent and the adsorbate namely ionic radius, hydrolysis constant and electro-negativity of the adsorbate as well as the functional groups and porosity of the adsorbent. It also depends on multiple mechanisms involved in adsorption like ion exchange, chemisorptions, physic-sorption, dipole interactions, intra-particle diffusion, pore diffusion etc. However, it is observed that mercury and zinc showed quantitative adsorption (>90%) in binary, ternary and quaternary mixtures with most of the adsorbents under study. Thus further studies using different concentrations and adsorption models are definitely warranted to get a clear picture of the selectivity.

Table 6.1. Selectivity of binary, ternary and quaternary mixtures of Cu, Cd, Zn and Hg

Binary Mixtures

	Cu+Hg		Cd+Hg		Zn+Hg		Cu+Cd		Cu+Zn		Cd+Zn	
	Cu	Hg	Cd	Hg	Zn	Hg	Cu	Cd	Cu	Zn	Cd	Zn
PSP	0.720	1.508	0.748	1.452	1.054	0.948	0.721	1.457	0.993	1.006	1.377	0.755
APSP	1.297	0.808	0.607	2.368	2.816	0.559	1.106	0.910	1.647	0.681	1.118	0.901
SAPSP	1.125	0.898	0.710	1.621	1.672	0.706	1.372	0.774	1.958	0.635	0.777	1.388
PAPSP	0.576	2.978	0.652	2.055	1.019	0.981	1.490	0.734	3.378	0.535	0.669	1.925
9AAC	0.809	1.261	0.731	1.487	1.161	0.866	1.648	0.688	1.567	0.683	1.485	0.714
MPSP	0.878	1.143	0.719	1.540	0.965	1.036	0.743	1.401	0.944	1.060	1.535	0.701

Ternary Mixtures

	Cu+Cd+Zn			Cu+Cd+Hg			Hg+Zn+Cu			Hg+Zn+Cd		
	Cu	Cd	Zn	Cu	Cd	Hg	Hg	Zn	Cu	Hg	Zn	Cd
PSP	1.144	0.563	1.591	0.787	0.662	2.644	2.385	0.755	0.751	15.966	0.957	0.495
APSP	1.107	0.749	1.257	1.069	0.771	1.266	1.299	0.761	1.066	6.724	1.055	0.481
SAPSP	0.923	0.799	1.467	1.118	0.840	1.086	1.029	0.904	1.081	11.567	2.988	0.359
PAPSP	0.450	1.150	3.450	0.666	1.076	1.627	0.938	1.957	0.697	8.531	2.901	0.373
9AAC	0.808	0.842	1.482	0.799	0.725	1.938	0.889	12.807	0.492	1.590	12.857	0.366
MPSP	0.980	0.777	1.338	0.823	0.608	2.714	1.730	0.736	0.903	9.669	1.772	0.353

Quaternary Mixtures

	Cu+Cd+Zn+Hg			
	Cu	Cd	Zn	Hg
PSP	1.38E-02	2.95E-03	0.033	0.960
APSP	0.059	0.065	0.271	0.155
SAPSP	0.188	1.78E-02	0.203	0.133
PAPSP	0.124	0.063	0.227	0.055
9AAC	5.96E-03	1.91E-03	0.172	9.33E-03
MPSP	1.09E-02	2.75E-03	0.041	0.027

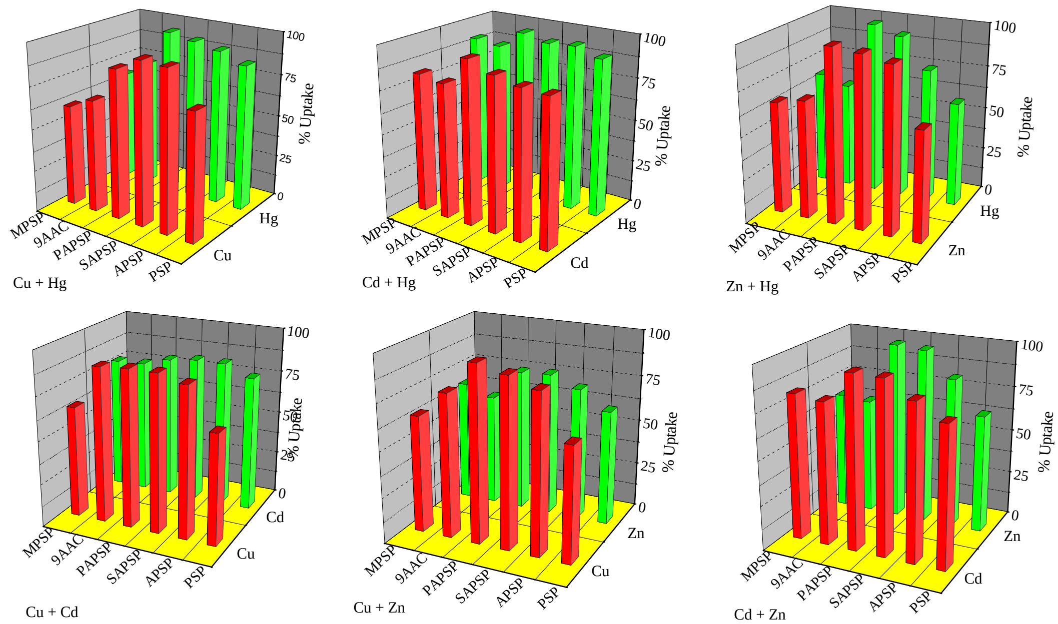

Figure 6.1. % Uptake for Binary Mixtures

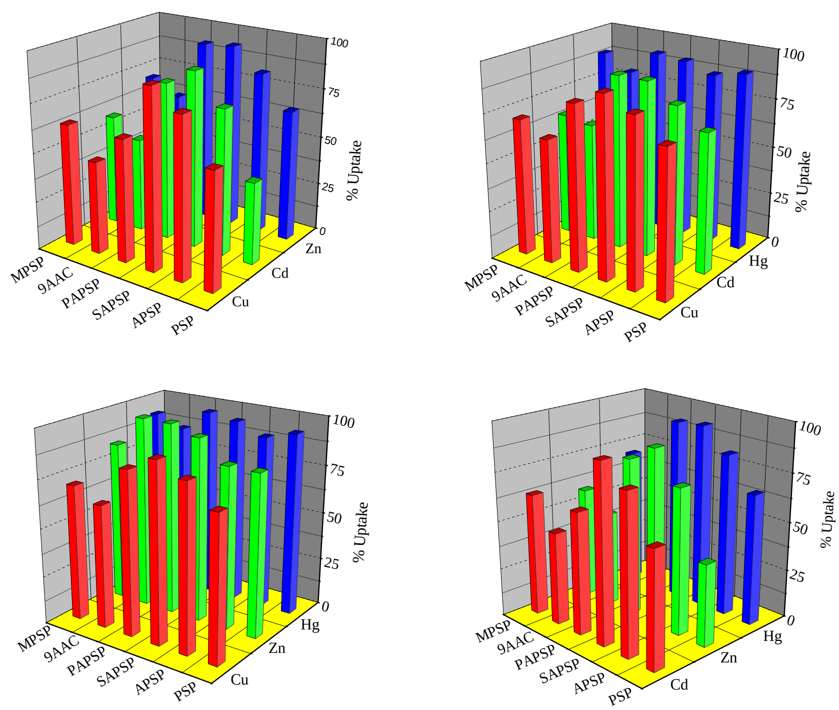

Figure 6.2. % Uptake for Ternary Mixtures

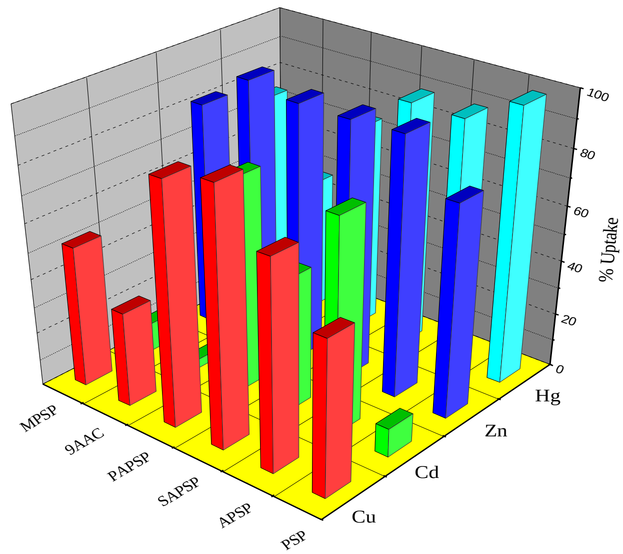

Figure 6.3. % Uptake for Quaternary Mixtures

6.3.1.2. ***Effect of Fe^{3+} and Cs^{+} on uptake of U^{6+}.*** The effect of co-ions like Fe^{3+} and Cs^{+} on the adsorption of U^{6+} by the adsorbents under study was tested in binary and ternary metal systems. About 0.1 g of each adsorbent under study was agitated with 25mL of binary or ternary metal solutions containing equimolar concentrations (1000 mg/L) of UO_2^{2+}, Cs^{+} and Fe^{3+} maintained at pH 1.0, at 30°C. After the established contact time (4 h) was attained, the suspension was filtered, and filterate was analyzed for the metal concentration. The adsorption processes are represented by the distribution coefficient K_d where K denotes the distribution of the ion of interest between the solid phase and the aqueous phase [10].

The obtained results as adsorbed amount of each cation are summarized in Table 6.2. It is evident from the table that the presence of Cs^{+} and Fe^{3+} cations, in binary systems and ternary systems did not cause any interference in the uptake of U^{6+} and the uptake of all the three ions was quantitative at high concentrations of all the three ions when present simultaneously (1000 ppm each). Similar observations were made by Sudhir et al [11].

Table 6.2. Selectivity of Uranium over iron and cesium

% Extraction						
U+Fe						
	PSP	APSP	SAPSP	PAPSP	9AAC	MPSP
Fe	97.02	98.82	98.26	98.96	98.56	96.14
U	97.98	98.8	98.54	99.36	98.62	96.86
U+Cs						
Cs	98.16	99.18	98.74	99.26	98.82	96.48
U	96.86	98.16	98.38	98.54	97.58	97.02
U+Cs+Fe						
Cs	97.56	97.98	97.7	99.02	98.02	96.06
Fe	96.14	97.38	97.14	98.44	97.54	95.18
U	96.38	98.06	97.74	99.06	98.3	95.62
K_d						
U+Fe						
Fe	6.611	16.849	11.394	19.131	13.789	5.081
U	9.801	16.566	13.598	31.150	14.393	6.269
U+Cs						
Cs	10.769	24.290	15.773	26.927	16.849	5.582
U	6.269	10.769	12.245	13.598	8.164	6.611
U+Cs+Fe						
Cs	8.096	9.801	8.595	20.308	10.001	4.976
Fe	5.081	7.533	6.893	12.720	8.030	4.049
U	5.425	10.209	8.749	21.176	11.664	4.466
Selectivity Coefficient						
U+Fe						
Fe	1.482	0.983	1.193	1.628	1.044	1.234
U+Cs						
Cs	0.582	0.443	0.776	0.505	0.485	1.184
U+Cs+Fe						
Cs	0.670	1.042	1.018	1.043	1.166	0.898
Fe	1.067	1.355	1.269	1.665	1.453	1.103

6.3.2. Application to Real Effluent

6.3.2.1. *Chrome Plating Effluent.* The adsorbents under study were tested for their efficacy to remove chromium from chromium plating waste water collected from a chrome plating industry of GIDC, Ankleshwar, India. Exact concentrations of the metals of interest were measured by ICP analysis. The waste water was acidified using 1M HNO_3 to dissolve the precipitates, and pH of the solution found to be pH 1. Solution was analysed using ICP analysis for finding out the presence of metal ions and their concentration. Further the acidified chrome plating effluent was treated with adsorbents under study. A series of flasks containing 25 mL acidified effluent, along with 100mg adsorbents under study were placed for shaking in a thermostated rotary mechanical shaker for 180 mins. The amount of metal remaining in the solution was determined by ICP analysis.

Table 6.3. Composition of the chrome plating effluent sample

Metal ions	Conc. (ppm)	Metal ions	Conc. (ppm)	Metal ions	Conc. (ppm)
Al	13.0	Ni	10.7	Zn	76.0
K	19.9	Cr	51.8	Ca	214
Mg	35.9	Pb	3.35	Na	480
Cu	7.57	Fe	136.0	Cd	0.5
Hg	0.14	V	0.11	As	0.09

A detailed composition of the plating effluent sample collected from chrome plating industry in GIDC, Ankleshwar, India is presented in Table 6.3. The chromium concentration in the effluent is 51.8 ppm. The results of the experiments with the percent extraction, K_d value and selectivity coefficient are shown in table 6.4. It is seen that SAPSP is the most effective adsorbent capable of removing more than 90% of Fe, Ni, Cd and Cr, more than 80% of Zn, V and As, 78% of Hg and 64% of Pb. PSP, APSP and SAPSP were able to remove Cr quantitatively from plating effluent. Selectivity coefficient was found to be highest for Cr over other metals (103 times over Fe, Ni, Pb and Hg) present in the effluent for APSP.

6.3.2.2. *Environmental relevance.* Because chrome-plating rinsewaters are acidic, it is an advantage that the maximum uptake for chromate by biosorbents is obtainable at pH 1. Adjustment of the rinse-water pH will thus only require less volume of mineral acid/base solution. The disadvantage lies in the fact that biosorbent-bound chromate cannot be recovered completely as chromate but also as Cr(III). However, unlike other adsorbents reported in literature wherein the reduced Cr(III) is observed in solution , in the present study the reduced Cr(III) remained adsorbed onto the adsorbents under study. Although only tested in laboratory scale, the removal of chromium from plating waste water using palm shell based adsorbents appears to be a promising approach APSP seems to be the most promising adsorbent because of its high chromium selectivity coefficients with respect to Zn, Pb, Hg, Ni and Fe. Thus there is excellent potential to remove toxic heavy metals from the plating effluent using these adsorbents under study, providing a viable and cost-effective technology for waste water treatment.

Table 6.4. Selectivity of Chromium over other inorganic ions present in chrome plating effluent

% Extraction						
	PSP	APSP	SAPSP	PAPSP	9AAC	MPSP
Zn	17.11	11.84	85.92	22.63	16.45	15.79
Cd	40.00	98.00	98.00	98.00	40.00	50.00
Pb	40.29	37.31	64.18	55.22	49.25	40.29
Hg	78.57	21.43	78.57	85.71	92.86	92.86
V	63.64	90.91	81.82	86.36	90.91	90.91
As	33.33	88.89	88.89	88.89	44.44	66.67
Cu	85.47	99.87	32.63	28.67	2.25	6.21
Ni	91.59	21.49	95.33	45.79	33.64	41.12
Fe	23.38	27.94	93.46	47.79	27.94	31.62
Cr	95.95	99.83	94.98	53.67	44.02	42.08
Distribution ratio K_d						
	PSP	APSP	SAPSP	PAPSP	9AAC	MPSP
Zn	0.052	0.034	1.526	0.073	0.049	0.046
Cd	0.167	12.250	12.250	12.250	0.167	0.250
Pb	0.169	0.149	0.448	0.308	0.243	0.168
Hg	0.917	0.068	0.917	1.500	3.250	3.250
V	0.438	2.500	1.125	1.583	2.500	2.500
As	0.125	2.000	2.000	2.000	0.200	0.500
Cu	1.470	189.000	0.121	0.100	0.006	0.016
Ni	2.722	0.068	5.100	0.211	0.127	0.174
Fe	0.076	0.097	3.570	0.229	0.097	0.115
Cr	5.917	143.639	4.731	0.289	0.197	0.181
Selectivity Coefficient						
	PSP	APSP	SAPSP	PAPSP	9AAC	MPSP
Zn	114.756	4277.280	3.101	3.960	3.994	3.882
Cd	35.520	11.725	0.386	0.023	1.179	0.728
Pb	35.081	965.260	10.562	0.939	0.810	1.078
Hg	6.4581	2106.720	5.161	0.193	0.060	0.056
V	13.531	57.456	4.205	0.182	0.078	0.072
As	47.360	71.820	2.365	0.144	0.983	0.364
Cu	4.025	0.760	39.073	2.882	34.231	10.997
Ni	2.174	2098.393	0.927	1.371	1.550	1.042
Fe	77.592	1481.760	1.325	1.265	2.028	1.574

6.4. Conclusions.

Competetive adsorption in case of binary ternary and quaternary mixtures of Cu, Cd, Zn and Hg was found in agreement with the adsorption of particular metal ions in Chapter 3 but no particular trend is been observed. Further in case of uranium adsorbents showed better affinity towards uranium in presence of its competitive inorganic ions (Fe and Cs). Adsorbents were found to have satisfying selectivity coefficients for chromium over other adsorbates in chrome plating effluent.

Literature Cited.

1. B.W. Mercer, L.L. Ln Ames Jr., L.B. Sand, F.A. Mumplon (Eds.), Zeolite Ion Exchange in Radioactive Municipal Wastewater Treatment in Natural Zeolites, Occurrence, Properties Use, Pergamon Press, Oxford, **1978**, 451.
2. K.C. Song, H.K. Lee, H. Moon, K.J. Lee. *Sep. Purif. Technol.* **1997**, *12*, 215.
3. International Commission of Radiological Protection Individual Monitoring for Internal Exposure of Worker: Replacement of ICRP Publication 54, Pergamon Press, ICRP Publication, **1998**, 78.
4. R.R. Jalali, H. Ghafourian, Y. Asef, S.T. Dalir, M.H. Sahafipour, B.M. Gharanjik. *J. Hazard. Mater.* **2004**, *B116*, 125.
5. C. Kutahyali, M. Eral. *Separation and Purification Technology* **2004**, *40*, 109–114
6. J.W. Patterson, E. Gasca, Y. Wang. *Water Sci. Technol.* **1994**, *29* (9), 275.
7. D. James, G. Venkateswaran, T. Prasada Rao. *Microporous and Mesoporous Materials* **2009**, *119*, 165.
8. F. Stoeckli, M.V. Lopez-Ramon, D. Hugi-Cleary, A. Guillot. *Carbon* **2001**, *39*, 1115.
9. A.R. Khan, I.R. Al-Waheab, A. Al-Haddad. *Environ. Technol.* **1996**, *17*, 13.
10. M. Shamsipur, J. Fasihi, K. Ashtari. *Anal. Chem.* **2007,** *79*, 7116.
11. Sudhir Dahiya, R.M. Tripathi, A.G. Hegde. *Journal of Hazardous Materials* **2008**, *150*, 376.

Chapter 7

Preparation and characterization of specific adsorbents for Mercury

Outline:

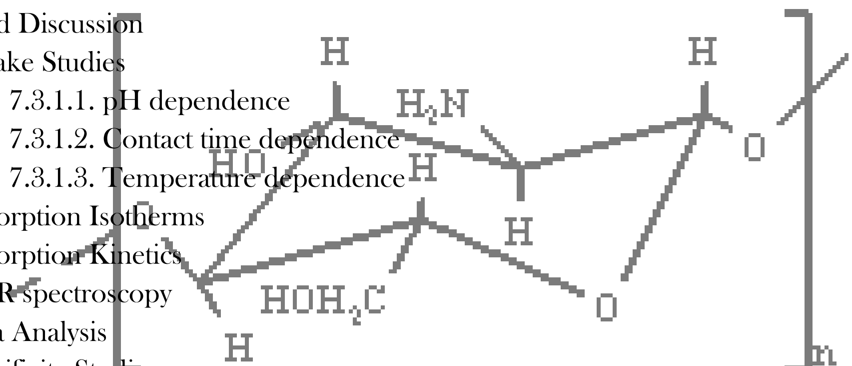

7.1. Introduction

Agricultural waste materials as we have seen in chapter 1 and 2 are usually composed of lignin and cellulose as the main constituents. Other components are hemicellulose, extractives, lipids, proteins, simple sugars, starches, water, hydrocarbons, ash and many more compounds that contain a variety of functional groups present in the binding process. Cellulose is a crystalline homo-polymer of glucose with $\beta 1 \rightarrow 4$ glycosidic linkage and intra-molecular and intermolecular hydrogen bonds [1, 2]. Hemicellulose is a heteropolymer of mainly xylose with $\beta 1 \rightarrow 4,4$ glycosidic linkage with other substances of acetyl feruoyl and glycouronyl groups [3]. Lignin is three dimensional polymer of aromatic compounds covalently linked with xylans in hardwoods and galactoglucomannans in softwoods [4, 5]. The functional groups present in biomass molecules acetamido groups, carbonyl, phenolic, structural polysaccharides, amido, amino, sulphydryl carboxyl groups alcohols and esters [6, 7]. These groups have the affinity for metal complexation. Some biosorbents are non-selective and bind to a wide range of heavy metals with no specific priority, whereas others are specific for certain types of metals depending upon their chemical composition.

Similar observations of non selectivity or selectivity for a group of metals has been made by us with the adsorbents under study namely PSP, APSP, SAPSP, PAPSP, 9AAC and MPSP. Surface modification has become a common technique in providing a material with desirable functional properties one of which is selectivity.

Chitosan is a linear polysaccharide composed of β (1→4) linked 2-amino-2-deoxy-D-glucose and 2-acetamido-2-deoxy-D-glucose units. Chitosan is soluble in all organic and mineral acids and has reduced diffusivity of sorbate due to its low porosity and high crystallinity. It is biodegradable and has gelling ability. Chitosan, has widely been studied as an adsorbent with good metal-chelating properties for the removal of various heavy metal ions from water or wastewater [7, 11-15]. It is generally known that the amine groups in chitosan are the main binding sites for the heavy metal ions, but the amine groups do not show specific selectivity toward individual heavy metal species [16]. In recent years, surface modification has become a popular method for providing a material with desirable properties for practical applications, and many methods of surface modification have been developed [17,18]. Thanks to its amino groups, chitosan is reactive towards many chemicals: this results in a number of chitosan derivatives having a wide range of uses, and in particular as transition metal chelates [10-17].

Chitosan and its derivatives have been used for removal of metal ions from waste water [34-44]. The suitability of chitosan and cross-linked chitosan have been studied for adsorption of mercury [37, 38]. Elemental mercury removal on chitosan, iodine (bromide) or sulfuric acid modified chitosan has been studied [36]. Limited reports have been found in the literature on removal of methyl mercury and phenyl mercury using chitosan as an adsorbent. Methyl mercury adsorption has been studied using chitosan as an adsorbent in a column [34]. Several investigations were done to modify chitosan to facilitate mass transfer and to expose the binding sites to enhance the adsorption capacity [45]. Chitosan and chitosan grafted polyacrylamide beads, thiol modified chitosan have been reported for the adsorption of inorganic mercury [35, 46].

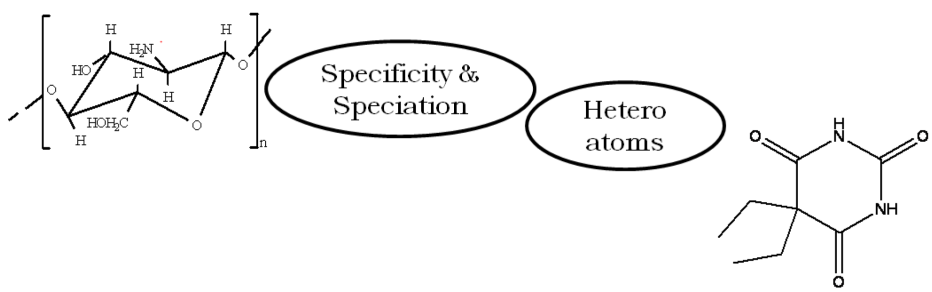

Many reviews are available in literature regarding adsorption of mercury onto chitosan [18-20], Table 7.1 also describes the reports available in literature for adsorption of mercury by different chitosan derivatives along with their maximum adsorption capacities.

Table 7.1. Chitosan based adsorbents with their adsorption capacity and adsorption parameters

Adsorbent	Metal	Operating Conditions		Max. Ads. Cap. (mg/g)	References
		Temp.	pH		
Natural chitosan	Hg(II)	313K	5.0	16.1	[21]
	Hg(II)	313K	6.0	25.3	
	Hg(II)	313K	7.0	24.7	
Glutraladehyde cross linked chitosan	Hg(II)	313K	5	22.3	
	Hg(II)	313K	6	75.5	
	Hg(II)	313K	7	37.5	
Epichlorohydrin cross linked chitosan	Hg(II)	313K	5	16.3	
	Hg(II)	313K	6	30.3	
	Hg(II)	313K	7	22.9	
Ethylenediamine modified chitosan magnetic microspheres	Hg(II)	298K	5	2.69	[22]
	Hg(II)	308K	5	2.45	
	Hg(II)	318K	5	2.19	
	Hg(II)	328K	5	1.96	
Thiourea-modified magnetic chitosan microspheres	Hg(II)	-	-	625.2	[23]
	Cu(II)	-	-	66.7	
	Ni(II)	-	-	15.3	
	Hg(II)	-	-	-	
	Cu(II)	-	-	-	
	Ni(II)	-	-	-	
	Hg(II)	-	-	-	
	Cu(II)	-	-	-	
	Ni(II)	-	-	-	
Chitosan	Cu(II)	333K	2.5	135	[24]
	Hg(II)	-		357	
	Cu(II)	333K	4.5	238	
	Hg(II)	-		454	
Chitosan coated cotton fibres SCCH	Hg(II)	278K	-	0.32	[25]
		278K	-	-	
	Hg(II)	288K	-	0.16	
		288K	-	-	
	Hg(II)	298K	-	0.42	
		298K	-	-	
	Hg(II)	308K	-	0.52	
		308K	-	-	
Chitosan coated cotton fibres RCCH	Hg(II)	278K	-	0.28	
		278K	-		
	Hg(II)	288K	-	0.20	
		288K	-	-	
	Hg(II)	298K	-	0.48	
		298K	-		
	Hg(II)	308K	-	0.38	
		308K	-	-	
Chitosan	Hg(II)	<383K	2	647.4	[26]

Thiocarbomoyl derivative of chitosan S2	Hg(II)	<383K	2	459.5	
	Hg(II)	<383K	5	617.9	
	Hg(II)	<383K	7	1445.0	
	Hg(II)	<383K	7	365.3	
Thiocarbomoyl derivative of chitosan SC2	Hg(II)	<383K	2	459.9	
	Hg(II)	<383K	5	606.9	
	Hg(II)	<383K	7	1271.2	
	Hg(II)	<383K	7	330.7	
Magnetic chitosan resin chemically modified by a Schiff's base cross-linker.	Hg(II)	303K	<7.5	3.060	[27]
	Hg(II)	313K	<7.5	2.688	
	Hg(II)	323K	<7.5	2.520	
	Hg(II)	333K	<7.5	2.214	
Thiol-grafted chitosan beads	Hg(II)	-	2	-	[28]
	Hg(II)	-	4	-	
	Hg(II)	-	4	-	
	Hg(II)	-	5	-	
	Hg(II)	-	7	-	
Aminated chitosan bead prepared through chemical reaction with EDA	Hg(II)	-	4	89	[29]
	Hg(II)	-	5.5	191	
	Hg(II)	-	7	496	
Chemically modified chitosan	Pb(II)	298K	7	-	[30]
	Cu(II)	298K	7	-	
	Cd(II)	298K	7	-	
HDI-crosslinkeddeacetylated Chitin	Cu(II)	323K	7	-	[31]
	Cu(II)	323K	7	-	
TMA-crosslinkeddeacetylated Chitin	Cu(II)	323K	7	-	
	Cu(II)	323K	7	-	
Coarse chitin	-	343K	7	70 ± 8	[32]
	-	343K	7	-	
Fine chitin	-	343K	7	66 ± 8	
	-	343K	7	-	
thiourea-modified chitosan derivative (TMCD)	Hg(II)	299K	-	6.690	[33]
	Hg(II)	309K	-	5.734	
	Hg(II)	319K	-	5.277	
	Hg(II)	329K	-	5.107	

Most of the studies have been done to optimize sorption performances, especially sorption isotherms with some suggesting uptake mechanisms, but little has been done on the identification of the sorption sites and interpretation of the molecular interactions between sorbent and solute by FTIR and mechanistic modeling using potentiometric titrations. The ability of mercury(II) to form a complex with barbital (5,5-diethyl barbituric acid) has been used as the basis for the separation and determination of barbiturates where barbital was treated with excess mercury(II) to form a chloroform extractable complex [47]. Advantage was taken of the ability of mercury to form a mercury barbital complex for the determination of mercury [48]. This suggested that more detailed study could be done to find the suitability of grafting barbital onto chitosan (BC), cross-linked chitosan using glutaraldehyde (G-Chitosan) and Barbital Glutaraldehyde cross-linked Chitosan (BG-Chitosan) and their use as adsorbents for the removal of inorganic, methyl and phenyl mercury.

Our objectives were

i) Evaluation of C, BC, CL and BCL for the removal of inorganic mercury (Hg^{2+}), methyl (CH_3Hg^{2+}) and phenyl mercury ($PhHg^{2+}$) and optimization of parameters for their maximum removal.
ii) Detailed studies using spectroscopic, potentiometric techniques as well as kinetic and isotherm models to understand the mechanism during the adsorption of different forms of mercury onto C, BC, G-Chitosan and BG-Chitosan.

7.2. Material and method

7.2.1. Sorbent Preparation.

Chitosan flakes (87.6 % deacetylated and molecular weight 5.5 x 10^5 g/mol) from Sigma Aldrich were used to prepare chitosan beads. 1 % (w/w) chitosan solution was prepared by dissolving chitosan flakes in 1 % (w/w) acetic acid solution at room temperature for homogenizing the mixture for 48 hrs. The homogeneous chitosan solution was injected dropwise into 0.41 N NaOH solution for the formation of beads. After the formation of beads it was left overnight in a freezer for hardening (Scheme 7.1). The beads were extensively washed with distilled water until neutral and then used for the preparation of barbital immobilized chitosan and for further experimental studies as adsorbent (C).

For the preparation of barbital immobilized chitosan [BC] (Scheme 7.1), a solution of neutralized beads of chitosan with 1 % sodium barbiturate (dissolved in double distilled water) in the ratio of 1:1 was stirred for 24 h at 50 ^{0}C, filtered, washed with double distilled water until neutral and then left for air drying.

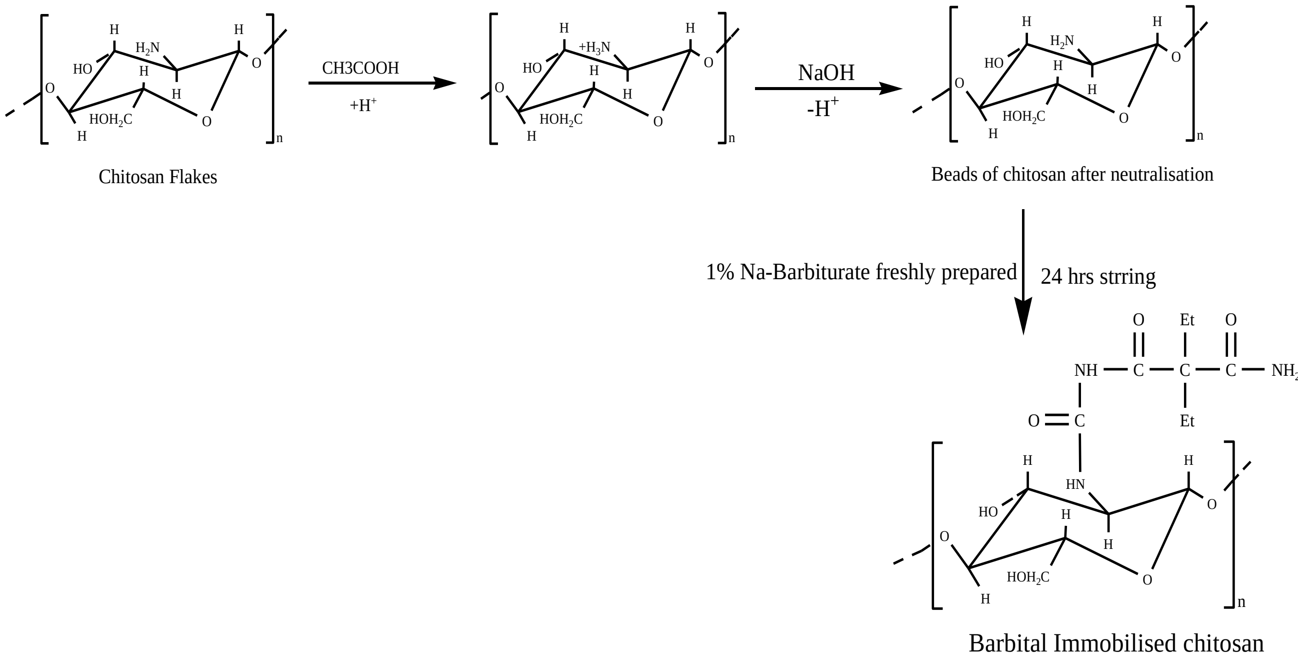

Scheme 7.1. Scheme for preparation of chitosan beads and Barbital Immobilized chitosan

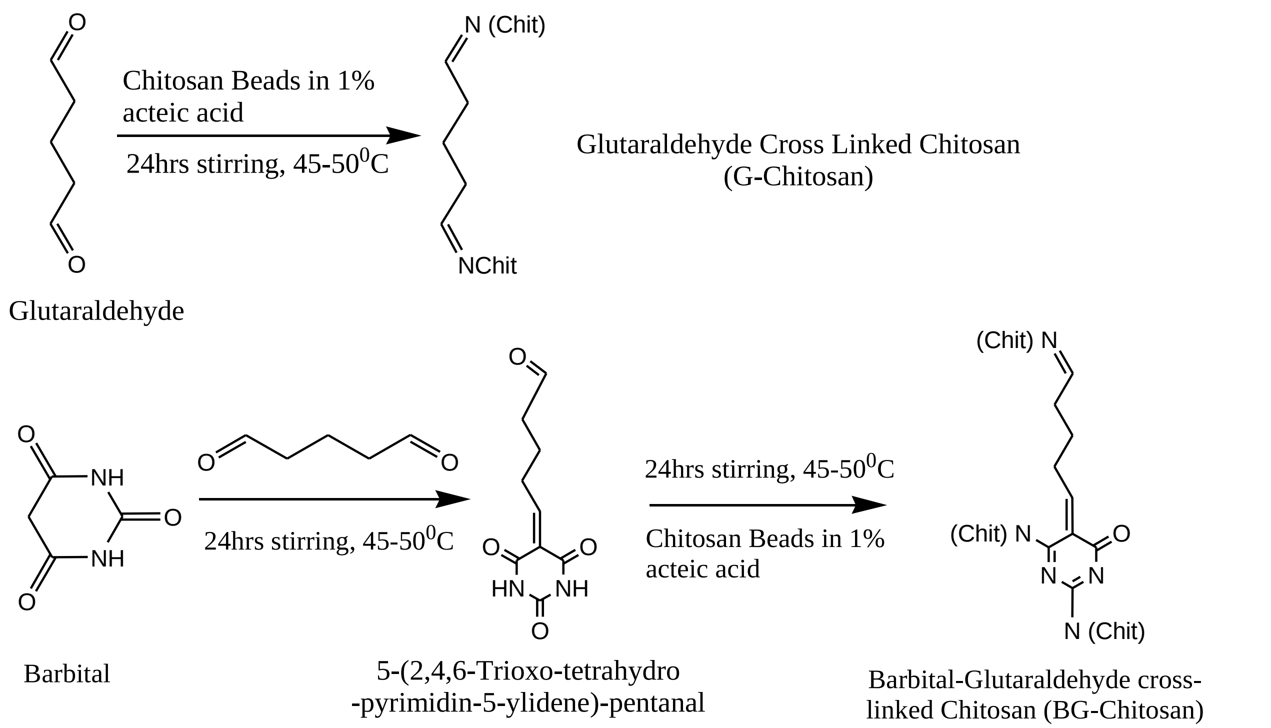

Scheme 7.2. Cross-linking with Glutaraldehyde and Barbital with glutaraldehyde

A 100mL of 0.1% solution of gultaradehyde was added to 100mL of 1% homogenized solution of chitosan in 1% acetic acid and allowed to react for 24hrs at 45-50^{0}C to form an imine [G-

Chitosan] through a Schiff's base reaction between aldehyde ends of glutaraldehyde and amine moieties of Chitosan. Glutaraldehyde cross-linked chitosan (G-Chitosan) was then filtered, washed with double distilled water until neutral and then left for air drying(Scheme 7.2).

Barbital Glutaraldehyde cross-linked Chitosan (BG-Chitosan) was formed by initial condensation of glutaraldehyde and barbiturate moiety followed by cross-linking with chitosan(Scheme 7.2).. A 100mL of 0.1% solution of glutaraldehyde was mixed with 100mL of 0.1% solution of freshly prepared sodium barbiturate and were allowed to react at 45-50^{0}C for 24hrs. This solution was added to 100mL of 1% solution of chitosan in acetic acid and stirred for 24 hrs at 50^{0}C, filtered, washed with double distilled water until neutral and then left for air drying. The barbital glutaraldehyde condensation product (5-(2,4,6-Trioxo-tetrahydro-pyrimidin-5-ylidene)-pentanal) undergoes cross-linking with chitosan resulting in the formation of BG-Chitosan. BG-Chitosan was found to be less soluble, hard and had greater swelling capacity compared to G-Chitosan.

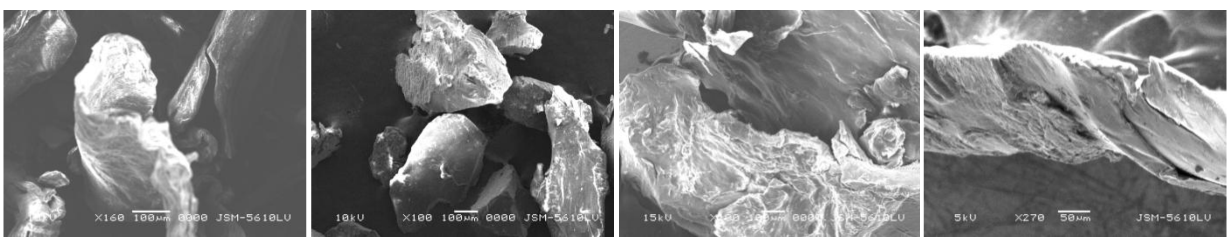

Figure 7.1. Scanning Electron Micrograph of C, BC, G-Chitosan and BG-Chitosan

Scanning Electron Micrograph of G-Chitosan displays an open porous and heterogeneous structure (Figure 7.1). Crosslinking with BG-Chitosan is seen to bring about conspicuous textural and morphological changes with BG-Chitosan forming a more compact and rigid structure. The pores are in the range 100 µm in G-Chitosan which reduce in BG-Chitosan to 50 µm.

7.2.2. Batch Adsorption Experiments.

A series of metal sorption experiments were conducted to study the effect of various parameters i.e. pH, dose and temperature for the removal of inorganic, methyl and phenyl mercury on C, BC, G-chitosan and BG-chitosan. For each experiment 25mL of Hg^{+2}, CH_3Hg^{+2} and $C_6H_5Hg^{+2}$ solution of known initial concentration and pH were taken in a 100mL stoppered conical flask. A suitable adsorbent dose was added to the solution and the mixture was shaken at a constant speed. The supernatant was separated from the adsorbent by filtration and analyzed for the presence of unadsorbed Hg^{2+} by CVAAS (MA-5840 analyzer ECIL). All the experiments were conducted in triplicate and the average results are reported. The mercury uptake by chitosan was calculated as follows:

$q_e = (C_i - C_e)/m;$ (1)

where, C_i-initial concentration of metal ion mg/L; C_e – Equilibrium concn. of metal ion (mg/L); m – Mass of adsorbent (g/L); q_e – Amount of metal ion adsorbed per gram of adsorbent.

The experiments done without adsorbent were treated as blanks and they showed no precipitation of metal ions occurred under the conditions selected.

7.2.3. Selectivity Studies.

Selectivity coefficient of inorganic mercury over other inorganic cations like copper, cadmium and zinc were studied by batch procedure for C, BC, CL and BCL. The concentration of the metals was determined by ICP-AES (Thermo Jarrel Ash, Model TraceScan) at wavelengths of 409.014 nm. The selectivity of the mercury ions versus another cation was determined by shaking 100 mg of adsorbent with an aliquot of 10 mL each of 100 ppm of each individual inorganic ions (Cu^{2+}, Cd^{2+}, Zn^{2+} and Hg^{2+}) were taken at pH 4 to give a total volume of 40 mL. The selectivity coefficient ($S\ Hg^{2+}/M^{n+}$) is defined as

$$S_{\mathrm{Hg^{2+}/M^{n+}}} = \frac{D_{\mathrm{Hg^{2+}}}}{D_{\mathrm{M^{n+}}}}$$

where $D\mathrm{Hg}^{2+}$ and $D\mathrm{M}^{n+}$ are the distribution ratios of the mercury ion and other inorganic species, respectively. Distribution ratios were calculated using the formula

$$D_{\mathrm{M^{n+}}} = \frac{C^{\mathrm{i}}_{\mathrm{M^{n+}}} - C^{\mathrm{f}}_{\mathrm{M^{n+}}}}{C^{\mathrm{f}}_{\mathrm{M^{n+}}}} \times \frac{v}{m}$$

where $C_{\mathrm{i}}\ \mathrm{M}^{n+}$ and $C_{\mathrm{f}}\ \mathrm{M}^{n+}$ are the concentrations of inorganic ions in aqueous phase before and after extraction, v is the volume of the solution, and m is the mass of the adsorbent. The percent extraction (%E) of inorganic ion is defined as

$$\%E = \frac{C^{\mathrm{i}}_{\mathrm{M^{n+}}} - C^{\mathrm{f}}_{\mathrm{M^{n+}}}}{C^{\mathrm{i}}_{\mathrm{M^{n+}}}} \times 100$$

7.3. Results and discussion

7.3.1. Uptake Studies.

7.3.1.1. ***pH dependence.*** Effect of pH was studied as a function of % uptake of the adsorbate under study (Hg^{+2}, CH_3Hg^{+2}, $C_6H_5Hg^{+2}$) in the range of pH 1-10, using metal ion concentration of 0.8mg/L with an adsorbent dose of 4g/L for C, BC, G-Chitosan and BG-Chitosan. There exists a large number of binding sites on C, BC, G-Chitosan and BG-Chitosan like amine, amide and hydroxyl groups. The nitrogen atom of the amino group and oxygen atoms of the hydroxyl groups can bind to a proton or a metal ion by electron pair sharing. The electronegativity of oxygen being more than that of nitrogen, the donation of lone pair of electrons from the nitrogen atom will be more facile than the oxygen atom for bond formation with mercury. In the case of chitosan under highly acidic condition (pH 1-2) there was no sorption of mercury because the binding sites are protonated which causes repulsion of the approaching mercury cation. As pH increases (3-7) the sorption of mercury increases because electron rich binding sites are exposed which allow the metal ions to get bound to the biosorbent [49].

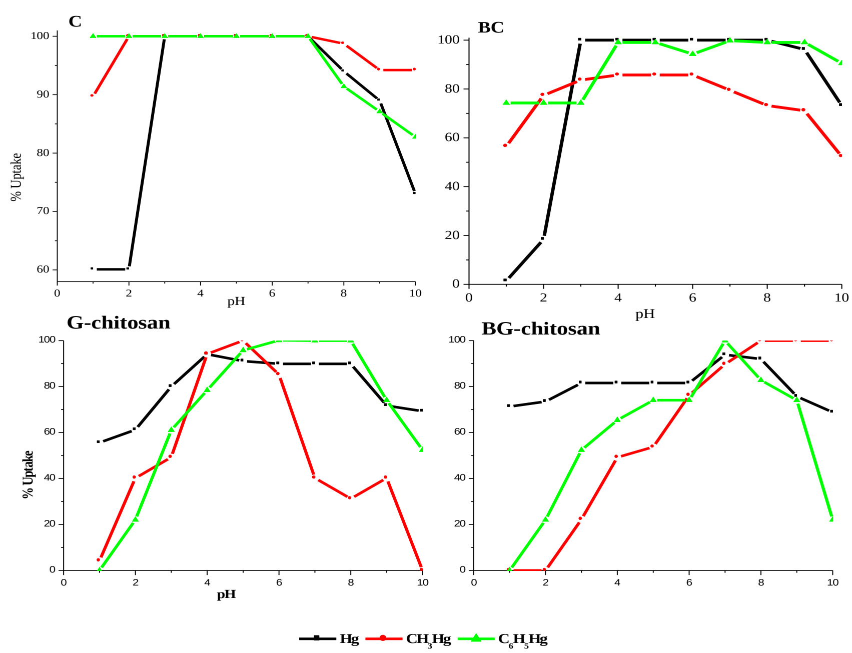

Initial metal conc. 0.1mg/L, amount of sorbent 4.0g/L, temperature 30^{0}C

Figure 7.2. Effect of pH on uptake of Hg^{2+}, CH_3Hg^{2+}, $C_6H_5Hg^{2+}$ using C, BC, G-Chitosan and BG-Chitosan

Inorganic Hg uptake was found to increase with increase in pH and reach equilibrium at pH 4 and 7 in case of G-Chitosan, BG-Chitosan respectively. Organic Hg uptake also was found to increase with increase in pH. Methyl mercury was found to reach equilibrium at pH 5, >8 in case of G-Chitosan, BG-Chitosan respectively while phenyl mercury was found to reach equilibrium at pH 6-8, 7 in case of G-Chitosan, BG-Chitosan respectively. This is in contrast to what is observed in general that adsorption of mercury decreases from pH 6 onwards due to precipitation [50]. This could be due to the fact that all the mercury species which are likely to exist in the investigated pH range (0.5–8), might remain in soluble form due to the low concentrations of mercury studied [51]. Furthermore, considerable uptake of Hg^{+2} is observed even under acidic pH conditions.

Beyond pH 7 sorption decreases due to precipitation as shown in Figure 7.2. At low and high pH, hydrogen bonding can also result between metal/mercuric hydroxide to hydroxyl groups of C, BC, G-chitosan and BG-chitosan. So the total uptake of mercury could be by electrostatic attraction, hydrogen bonding and weak van der Waals forces.

$$\mathrm{R-NH_2 + H^+ \leftrightarrow R- NH_3^+}$$

$$\mathrm{R-NH_2 + Hg^{2+} \rightarrow R- NH_2Hg^{2+}}$$

$$\mathrm{R-NH_3^+ + Hg^{2+} \rightarrow R- NH_2Hg^{2+} + H^+}$$

In BC which has an amide group both C-N and C-O bonds possess comparable amounts of single and double bond character resulting in considerable delocalization of negative charge on the amide carbonyl oxygen atom causing predominant proton metal ion interactions. As the pH increases the hydroxyl groups become deprotonated resulting in negative charge

$$\mathrm{R-OH + OH^- \leftrightarrow R- O^- + H_2O}$$

$$\mathrm{R' - O^- + Hg^{2+} \leftrightarrow R' - O - Hg^+}$$

Thus due to stronger electrostatic attraction between the lone pairs of the nitrogen atom and Hg^{2+} and also the electrostatic attraction between the negatively charged hydroxyl group and positive or neutral mercury species, adsorption occurs in the pH range 3-7. The adsorption of Hg^{2+} at low pH values for C was found to be comparatively higher than BC, G-chitosan and BG-chitosan due to strong electrostatic attraction between the lone pair of nitrogen and Hg^{2+} species than the competing protons. The adsorption is higher in the case of BC with a concomitant increase in pH values due to deprotonation of amide groups and formation of covalent bonds between O, N and Hg.

7.3.1.2. ***Contact time dependence.*** The effect of agitation time on the uptake of Hg^{+2}, CH_3Hg^{+2}, and $PhHg^{+2}$ on G-Chitosan and BG-Chitosan is shown in Figure 7.3. Uptake study with respect to time showed >99% uptake after 3 h for C, whereas BC shows full uptake after 2 h, but the time needed to attain equilibrium is longer when using G-Chitosan than BG-Chitosan.

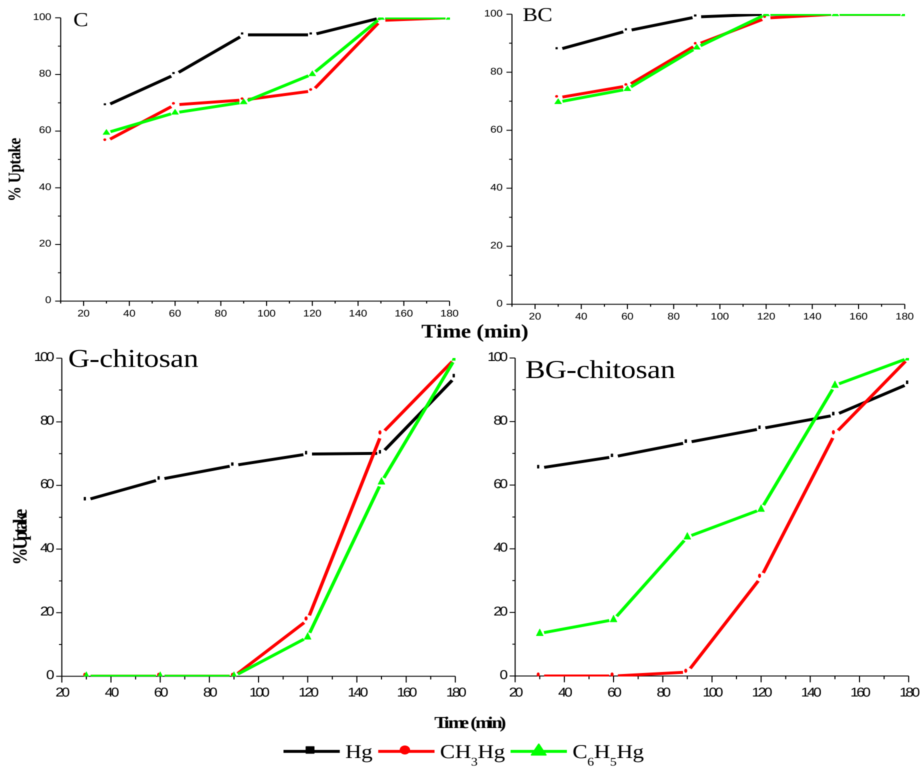

Initial metal conc. 0.1mg/L, amount of adsorbent 4.0 g/L, temperature 30^0C, optimum pH

Figure 7.3. Effect of Time on uptake of Hg^{+2}, CH_3Hg^{+2}, $C_6H_5Hg^{+2}$ using C, BC, G-Chitosan and BG-Chitosan

Hg^{2+} was found to adsorb at a faster rate with higher percentage removal than organic mercury ions. Since the mercury(II) ion has a smaller ionic radius, it is possible that mercury(II) ions diffuse faster through the adsorbent pores than the bulkier organic mercury. Also Hg^{+2} was found to adsorb at a faster rate followed by $C_6H_5Hg^{+2}$ and CH_3Hg^{+2}. More than 99% of total mercury was removed within a period of 120 min using BC, 160 min using C and 180 min using G-chitosan and BG-chitosan. This rapid initial binding rate suggests an instantaneous binding of mercury on surface binding sites followed by slower and non specific binding to other components.

7.3.1.3. ***Temperature dependence.*** The effect of temperature on the sorption of Hg^{+2}, CH_3Hg^{+2}, $C_6H_5Hg^{+2}$ was studied by carrying out a series of experiments at 30-70^{0}C at equilibrium times of the respective sorbates. Figure 7.4 shows that effect of temperature on adsorption is different for both the adsorbates. Temperature studies (Figure 7.4) showed adsorption of inorganic mercury is endothermic in all the cases whereas adsorption of both the forms of organic mercury showed exothermic nature with all the adsorbents except C (endothermic).

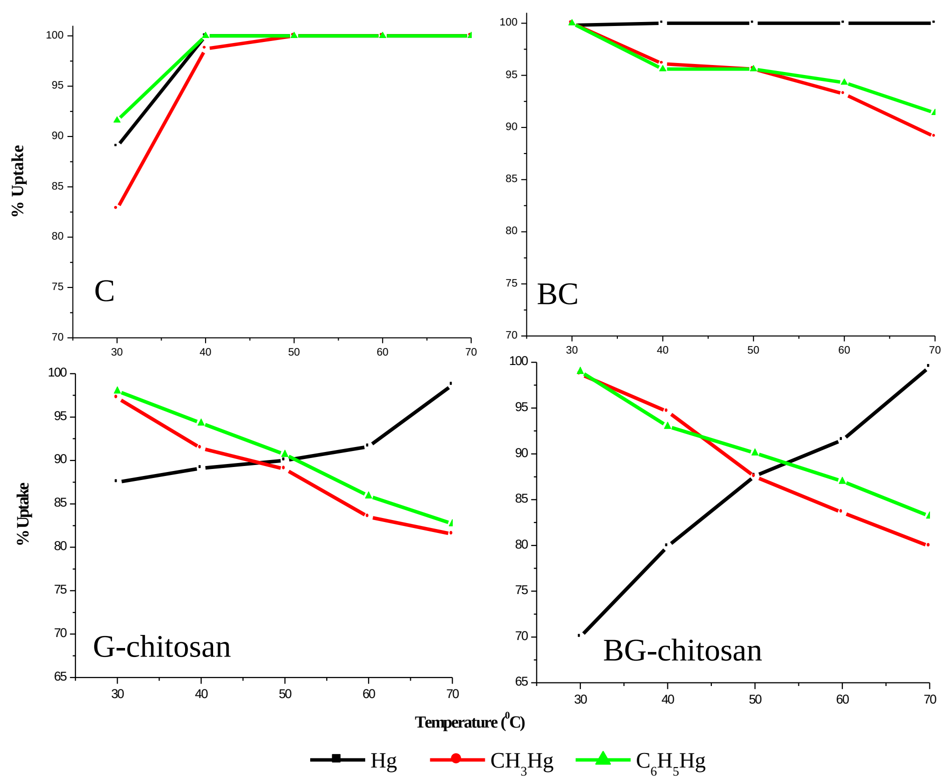

Initial metal conc. 0.1mg/L, amount of adsorbent 4.0 g/L, optimum pH, 180 min

Figure 7.4. Effect of Temperature on uptake of Hg^{+2}, CH_3Hg^{+2}, $C_6H_5Hg^{+2}$ using C, BC, G-Chitosan and BG-Chitosan

Uptake of inorganic mercury was found to increase with increase in temperature in the case of all the sorbents under study C, BC, G-Chitosan and BG-Chitosan but sorption of organic mercury decreased with increase in temperature for BC, G-Chitosan and BG-Chitosan suggesting chemisorption mechanism in the latter case [52]. Whereas increase in inorganic mercury adsorption with increasing temperature might be due to an enhanced rate of intraparticle diffusion of the adsorbate, as diffusion is an endothermic process. Chemisorption in case of organomercury can be explained due to the greater softness of organomercury compounds.

7.3.2. Adsorption Isotherms.

The adsorptive capacity of chitosan derivatives used for mercury removal was determined through adsorption isotherm studies. The Langmuir and Freundlich models were used to determine the adsorption capacity of mercury on chitosan derivatives and model parameters are presented (Table 7.2 and Figure 7.5).

From the correlation coefficient values (r^2) obtained for the two models, it can be seen that the Langmuir and Freundlich models cannot be applied to these data. Both Langmuir and Freundlich models could not be applied to the data obtained for mercury using chitosan based adsorbents. This could be due to mercury ions penetrating the adsorbent, adsorbing onto amine/ amide sites and forming metal clusters which might block the pores. This might render the active sites lying in the interior inaccessible for adsorption.A similar behavior was observed by Gregory et al. during the study of Cd^{2+} ions on porous magnetic chitosan beads [53]. The negative values obtained for Gibbs free energy, enthalpy and entropy suggest that the adsorption process is feasible and spontaneous in the case of G-Chitosan and BG-Chitosan.

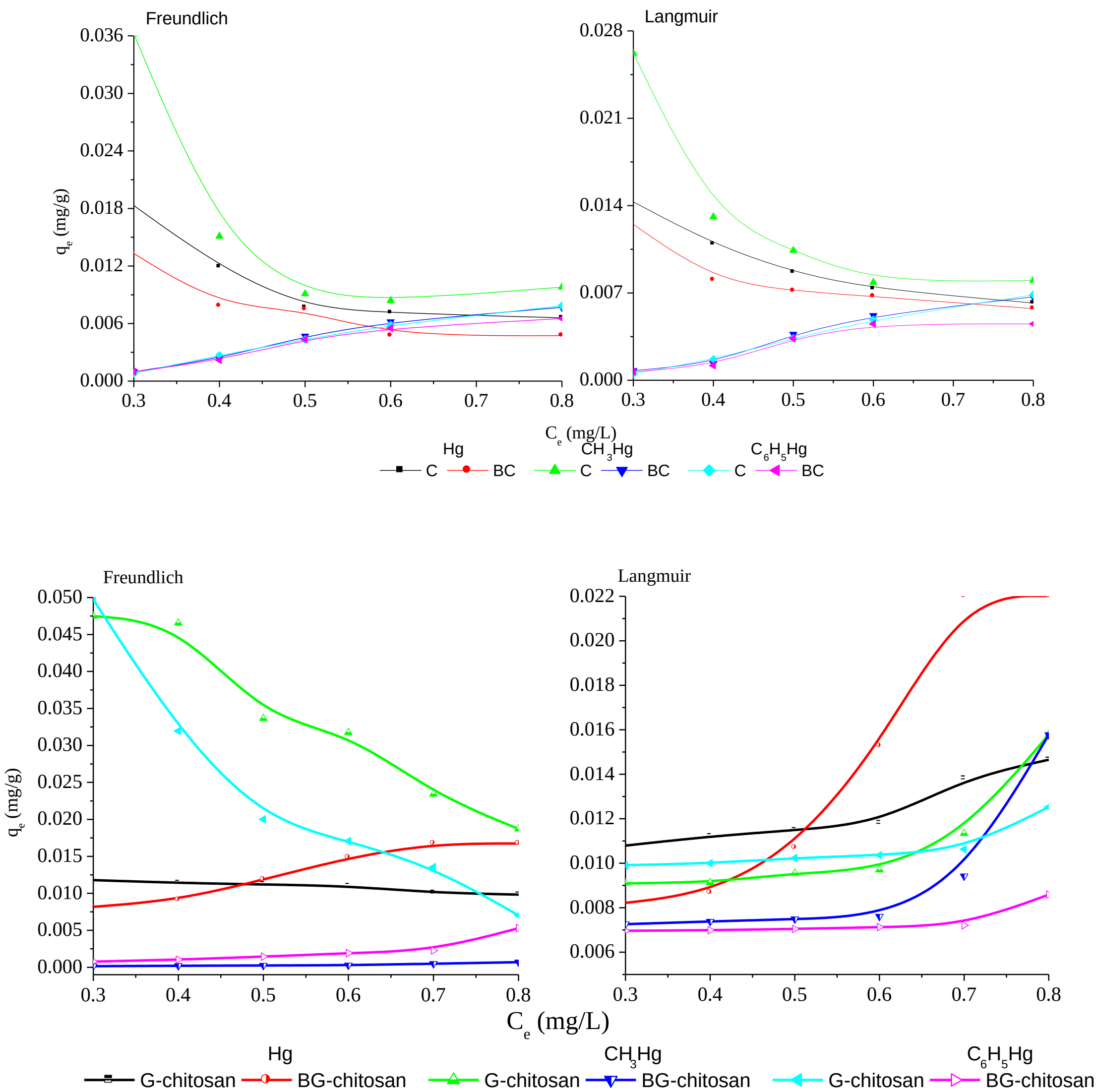

Figure 7.5. Freundlich and Langmuir Isotherm plots for C and BC

7.3.3. Adsorption Kinetics.

In order to investigate the possible mechanism of sorption process three kinetic models were used including Pseudo first order model, Pseudo second order model and Intra-particle diffusion model. Kinetics was examined for the sorption of Hg^{2+}, CH_3Hg^{2+}, and $PhHg^{2+}$ on chitosan derivatives under study using a series of measurements extending from 30 min to 240 min at 25 ^{0}C (Table 7.2 and Figure 7.6).

Table 7.2. Isothermal and kinetic parameters for adsorption of inorganic and organic mercury

Kinetics and Isotherms		C			BC		
		Hg^{2+}	CH_3Hg^{2+}	$C_6H_5Hg^{2+}$	Hg^{2+}	CH_3Hg^{2+}	$C_6H_5Hg^{2+}$
Pseudo 1st order	q_e (mg/g)	0.0410	0.0330	0.0650	1.1980	0.0100	1.0140
	K (min^{-1})	0.2000	0.1000	0.2300	0.1500	0.0790	0.0010
	r^2	0.9590	0.9700	0.9520	0.9850	0.8170	0.9190
Pseudo 2nd order	q_e (mg/g)	0.0500	0.0620	0.0540	0.0294	0.0023	0.00129
	K (g/mgmin)	0.2480	0.0670	0.2810	0.5090	107.70	4.1500
	r^2	0.9680	0.8960	0.9900	0.9950	0.6040	0.7130
Intra-particle	K_i(mg/gmin$^{0.5}$)	0.0030	0.0030	0.0440	0.0020	0.0008	0.0011
	r^2	0.9810	0.9790	0.9080	0.9860	0.9800	0.9990
Langmuir	q_m (mg/g)	0.0130	0.0100	0.0250	0.0040	0.0060	0.0200
	K_a (L/mg)	-184.0	-156.0	-927.0	-887.3	-73.5	-179.3
	r^2	0.9300	0.9450	0.9850	0.9940	0.9440	0.9560
Freundlich	K_f (mg/g)(dm^3/mg)$^{1/n}$	0.455	0.0002	0.004	0.003	$4.4x10^{-5}$	$5.4x10^{-5}$
	N	-1.790	-0.9360	-8.880	-3.3400	-0.1790	-0.9860
	r^2	0.8700	0.8670	0.9960	0.8010	0.7050	0.9130
Kinetics and Isotherms		G-Chitosan			BG-Chitosan		
		Hg^{+2}	CH_3Hg^{+2}	$C_6H_5Hg^{+2}$	Hg^{+2}	CH_3Hg^{+2}	$C_6H_5Hg^{+2}$
Pseudo 1st order	q_e (mg/g)	0.0170	0.0151	0.0190	0.0355	0.0295	0.0478
	K (min^{-1})	0.0090	0.0081	0.0102	0.0195	0.0018	0.0213
	r^2	0.9170	0.9560	0.9290	0.9490	0.9590	0.9880
Pseudo 2nd order	q_e (mg/g)	0.0210	0.2310	0.2030	0.0625	0.0591	0.0716
	K (g/mgmin)	0.5600	0.6730	0.4950	0.0001	0.0003	0.0002
	r^2	0.9170	0.9210	0.9330	0.9100	0.9230	0.9190

Intra-particle	K_i(mg/gmin$^{0.5}$)	0.001	0.0008	0.0021	0.0018	0.0076	0.0082
	r^2	0.9780	0.9890	0.9880	0.9920	0.9230	0.8190
Langmuir	q_m (mg/g)	0.0080	0.0089	0.0098	0.0065	0.0072	0.0069
	K_a (L/mg)	228.10	234.50	257.80	240.50	189.57	314.00
	r^2	0.9940	0.9800	0.9960	0.9680	0.6670	0.8190
	ΔG (KJ/mol)	-13.70	-13.75	-13.99	-13.81	-13.21	-14.48
Freundlich	K_f (mg/g)(dm^3/mg)$^{1/n}$	0.0530	0.0817	0.0919	0.0008	0.0001	0.0006
	N	2.7800	3.1400	1.5670	1.815	2.321	1.513
	r^2	0.4760	0.5140	0.6780	0.9490	0.9590	0.8990

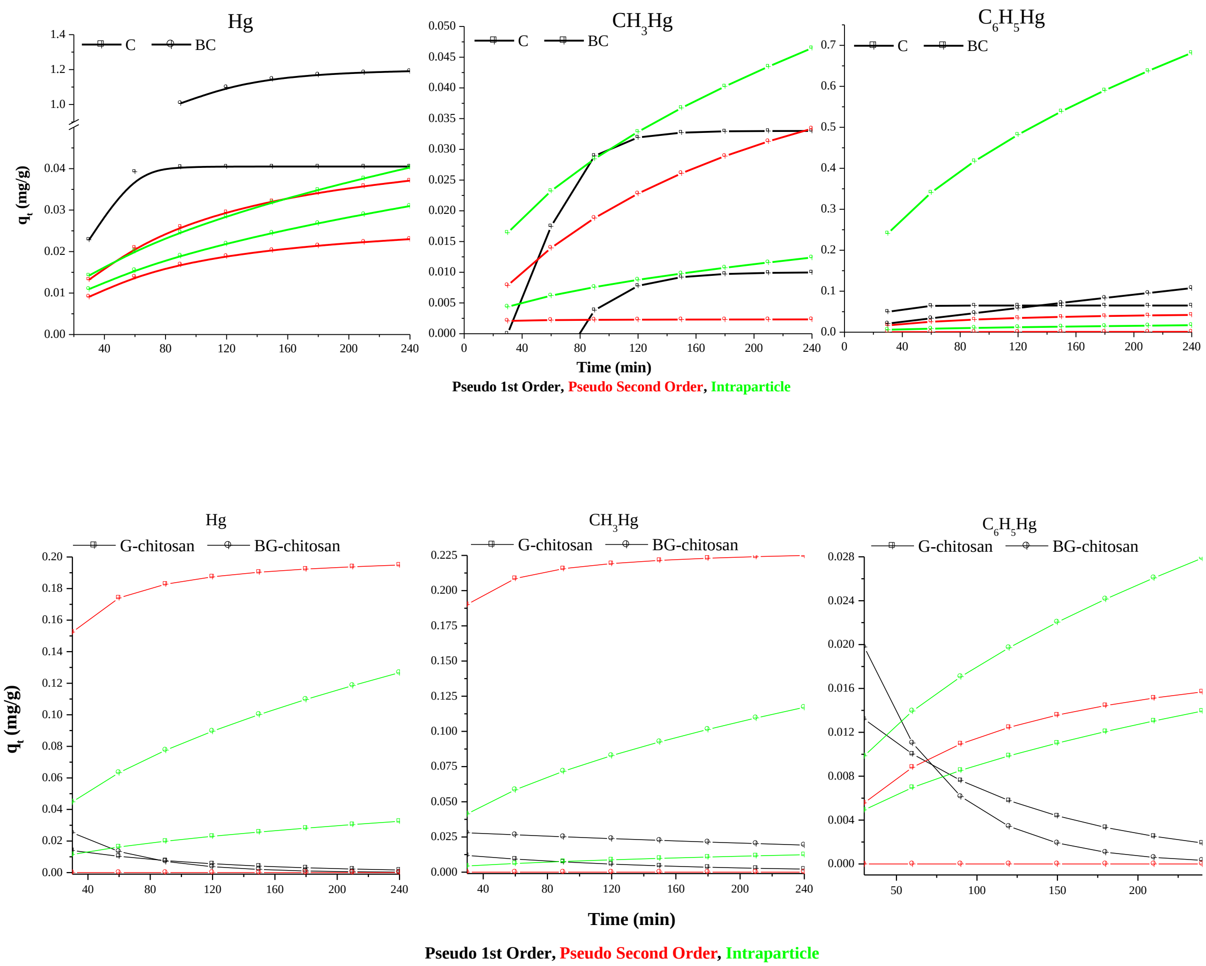

Figure 7.6. Different Kinetic plots for C, BC, G-chitosan and BG-chitosan

Pseudo first order model was fitted with a correlation coefficient of >0.917 for all the three forms of mercury. Values of regression coefficients are shown in Table 7.2. It is seen that the rate of adsorption is fast for the adsorbents under study in the case of Hg^{2+}, CH_3Hg^{2+}, and $C_6H_5Hg^{2+}$ adsorption. However the time needed to attain equilibrium is longer when using C, G-chitosan and BG-chitosan than BC (120 min using BC, 160 min using C and 180 min using G-chitosan and BG-chitosan). This could be explained by the presence of a larger number of functional groups for bonding in the case of BC (potentiometric titrations and FTIR). However Hg^{2+} was found to adsorb at a faster rate followed by CH_3Hg^{2+} and $C_6H_5Hg^{2+}$. This could be due to the smaller ionic radius of Hg^{2+} which enables it to diffuse faster than the bulkier $C_6H_5Hg^{2+}$ and CH_3Hg^{2+}. More than 99 % of total mercury was removed within the period of 180 min. This rapid initial binding rate suggests an instantaneous binding of mercury on surface sites followed by slower and non specific binding to other components.

But in the case of Pseudo 2^{nd} order rate equation the correlation coefficients were found to be >0.90. Intraparticle diffusion mechanism was found to be followed by G-Chitosan for all the three species of mercury but in BG-Chitosan phenyl mercury did not follow intraparticle diffusion whereas others did with a correlation coefficient >0.92. This suggests that multiple mechanisms like fast ion exchange, inter and intra-molecular binding and diffusion are operating in the sorption of mercury on C, BC, G-Chitosan and BG-Chitosan.

7.3.4. FTIR Spectroscopy.

Typical absorption frequencies of FTIR for C, BC, G-Chitosan, BG-Chitosan and mercury loaded species with their corresponding assignments are summarized in Table 7.3.

The strong broad band in region of 3300 to 3500 cm^{-1} is characteristic of the N-H stretching vibration in C, BC, G-Chitosan and BG-Chitosan although there is the possibility of overlapping between the N-H and the O-H stretching vibrations corresponding to pyranose structure. For BC the FTIR spectra shows a peak at 1654 cm^{-1} specifically for the amide groups indicating the grafting of barbital on chitosan. The band corresponding to free amino groups is observed at 1632, 1629.95 and 1599.31cm^{-1} for C, G-Chitosan and BG-Chitosan respectively.

Table 7.3. Typical absorption frequencies of infrared spectra of the C and BC

Sample	C/ BC	C/BC-Hg	C/BC-CH_3Hg	C/BC-PhHg	Assignment
Wave numbers (cm^{-1})	3447/ 3425	3432/ 3449	3445/ 3432	3441/ 3435	N-H & OH Stretching
	2929/ 2924	2920/ 2924	2921/ 2924	2921/ 2923	C-H stretching
	1632/1654	1599/ 1636	1597/ 1636	1597/ 1637	N-H bending
	-/ 1560	-/ 1512	-/ 1511	-/ 1509	N-H bending
	1383/ 1380	1384/ 1384	1383/ 1384	1383/ 1382	C-H bending
	1074/ 1073	1086/ 1077	1089/ 1024	1090/ 1080	C-N, C-O stretch
Samples	G-chitosan	G-chitosan-Hg	G-chitosan-CH_3Hg	G-chitosan-PhHg	Assignment
Wave numbers (cm-1)	3434/ 3431	3431/ 3431	3431/ 3427	3431/ 3433	N-H Stretching
	2925/ 2924	2933/ 2933	2924/ 2926	2926/ 2926	C-H stretching
	1725/ -	1685/ -	1651/ -	1757/ -	C=Ostretching(Aldehyde)
	1629/ 1599	1635/ 1635	1599/ 1618	1637/ 1637	N-H bending
	1379/ 1380	1384/ 1384	1384/ 1383	1383/ 1383	C-H bending
	-/ 1153	-/ 1155	-/ 1159	-/ 1155	C-N, C-O Stretching
	1074/ 1084	1066/ 1070	1068/ 1029	1062/ 1063	C-N, C-O Stretching

But the frequency is shifted to a lower wave number in case of BG-Chitosan due to consumption of these groups during cross linking of chitosan with 5-(2,4,6-Trioxo-tetrahydro-pyrimidin-5-ylidene)-pentanal, the condensation product of glutaraldehyde and barbital. A band at 1725cm^{-1} in G-Chitosan can be attributed to carbonyl groups of unreacted aldehyde functional groups of glutaraldehyde which are found to be absent in BG-Chitosan suggesting the condensation of these aldehydic groups of gltaraldehyde with barbiturate. A new band in BG-Chitosan at 1153cm^{-1} appeared due to the formation of new C-N bonds after complexation of glutaraldehyde with barbital and cross-linking with chitosan. This 1153cm^{-1} peak can be attributed to asymmetric stretching of C-O-C and C-N stretch.

The amide stretching frequency shifts from 1654 cm^{-1} to a lower frequency of 1636 cm^{-1} after mercury adsorption showing the possible interaction of metal linkage with O and N of the amide group [54]. The FTIR spectra after sorption of mercury on G-Chitosan shows a shift in 1725cm^{-1} band to 1655 and 1700cm^{-1} after mercury binding in case of Hg^{+2} and $CH3Hg^{+2}$ respectively suggesting the involvement of carbonyl arising from unbound sites of glutaraldehyde in binding of mercury. This behavior is consistent with previous reported results on uranium removal by chitosan and molybdate removal by cross-linked chitosan beads [55]. A decrease in transmittance in the wave number region of 3434 to 3431cm^{-1} after mercury sorption indicates that N-H vibration was affected due to sorption of mercury. In the case of BG-Chitosan the FTIR data showed that C-N stretching frequency at wave number of 1084cm^{-1} shifted to 1070, 1028, 1062cm^{-1} after mercury sorption suggesting the attachment of mercury to N and O bond of amide moiety A shift in the band at 1153cm^{-1} to higher wavenumbers was also observed in BG-Chitosan suggesting that N and O of amide involved in the sorption process. After mercury sorption there is a large shift in N-H bending absorption frequency from 1599cm^{-1} to 1635cm^{-1}, 1618cm^{-1} and 1637cm^{-1} for Hg^{+2}, CH_3Hg^{+2} and $PhHg^{+2}$ respectively in BG-Chitosan. A shift in 1074cm^{-1} band to 1066cm^{-1}, 1068cm^{-1} and 1062cm^{-1} related to C-N stretching indicates that nitrogen atoms are main sorption sites in both. Thus all the bands are suggestive of involvement of bonds with N atoms and C=O of unreacted aldehyde in the case of G-Chitosan and C-N and C-O of amide in BG-Chitosan for sorption mercury.

Thus we can conclude that for G-Chitosan sorption sites may be free aldehyde group of glutaraldehyde which has not been used in cross linking of chitosan and amino groups in chitosan. In the case of BG-Chitosan the sorption sites could be amide groups of barbital where mercury can coordinate bidentately to both amide nitrogen and oxygen atoms [56].

Frequencies for N-H stretching and bending were found to decrease after mercury adsorption in the case of C and BC showing the bonding of Hg^{2+} with the N of amine where the lone pair of electrons of the nitrogen atom was donated to the shared bond between the N and Hg^{2+} and as a consequence, the electron cloud density of the nitrogen atom was reduced, causing the shift. Mercury adsorption is found to affect the frequencies of all the bonds with N atoms of amine and amide, indicating that nitrogen atoms (amine group) are the main adsorption sites for mercury adsorption on C while in the case of BC it is N and O (amide and amine group).

7.3.5. Data analysis.

Results of potentiometric titration curves are used to generate a simplified mathematical model using Matlab [57-59].

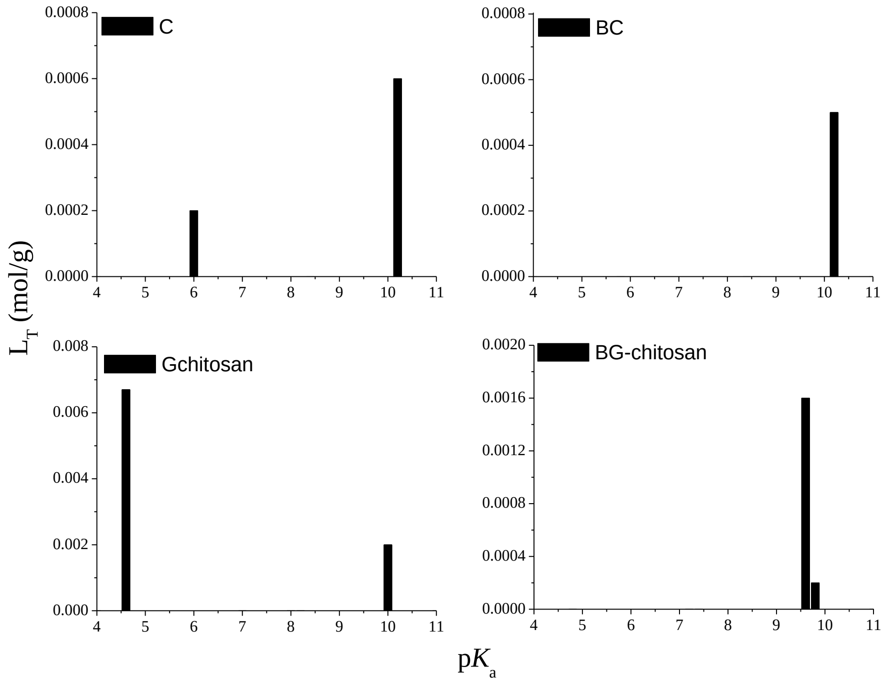

Figure 7.7. pK_a spectra determined by linear programming analysis

The pK_a spectra resulting from fitting the data using weighted mean value calculations are shown in Figure 7.7 and Table 7.4.

Table 7.4. Three-Site model from pK_a Analysis of C & BC Titration Data by Linear Programming

Ligand Class		1	2
Range of pK_a		4.0– 7.0	9.7 – 11.0
Functional Group		Self assembled amine/ protonated amine	Hydroxyl/ Amine
Chitosan	pK_a	10.2	-
	L_T	0.0006 mol/g	-
BC	pK_a	-	10.2
	L_T	-	0.0005 mol/g
G-chitosan	pK_a	4.6	10.0
	L_T	0.0067	0.0020 mol/g
BG-chitosan	pK_a	-	9.7
	L_T	-	0.0009 mol/g

Surface pK_a values for Site 1 falls in the range of 4-7 pK_a which have been reported for amino groups in self-assembled monolayers or protonated amines. Usually high pK_a sites (~10) are attributed to phenolic hydroxyl sites. Since both C and BC do not have phenolic protons, it is likely that high pK_a sites are for CH_2OH groups, or for 1^0 or 2^0 amines which have pK_a values in the range 9-11. In summary the pK_a sites that are observed here are likely to correspond to site 1 amino groups in self assembled monolayers or protonated amines, for site 2 it corresponds to hydroxyl or amines.

7.3.6. Specificity studies.

The % extraction, distribution ratio and selectivity coefficients of mercury ion with respect to metal ions like Cu^{2+}, Cd^{2+} and Zn^{2+} using C, BC, CL and BCL are studied.

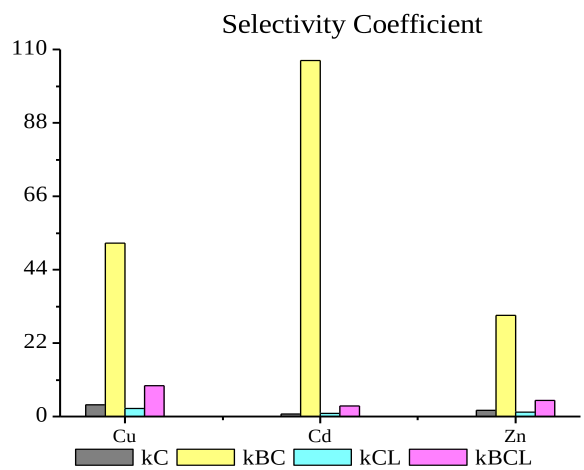

Figure 7.8. % Extraction, Distribution Coefficient and Selectivity coefficient

The obtained results are depicted in Figure 7.8. It is clear from the results that BC shows good selectivity for mercury (102) as compared to C, CL and BCL in the concentration range studied. A significant difference between the binding of mercury ion and other competitor metal ions on the adsorbents under study can be explained on the basis of Pearson's classification [60] according to which mercury is the softest of the metals which have been studied and can attach to soft bases (functional groups) present in the materials under study.

7.4. Conclusions

New adsorbents C, BC, G-chitosan and BG-Chitosan were prepared. BG-Chitosan was found more rigid and had more swelling capacity compared to other sorbents under study. Grafting barbital on C improves the equilibrium time for uptake of phenyl, methyl and inorganic Hg^{2+} when compared. Mercury adsorption to C, BC, G-chitosan and BG-Chitosan are strongly pH-dependent. There must be more than one mechanism responsible for mercury removal. Sorption of all the three forms of mercury showed similar behavior except for the fact that the process is endothermic for Hg^{+2} and exothermic for CH_3Hg^{+2}, $C_6H_5Hg^{+2}$. C showed higher adsorption capacity as compared to other sorbents under study. Amine, amide, amine and aldehyde, amide groups are involved in binding through complexation, weak van der Waals forces and electrostatic interactions in C, BC, G-Chitosan and BG-Chitosan respectively. More than 99 % of total mercury was removed within 160 min suggesting instantaneous binding of mercury on surface sites followed by slower and non specific binding to other components. Due to the different nature of the adsorbate-adsorbent system and the low initial metal ion concentration used comparison with other adsorbents is not possible. Appreciable selectivity was obtained for mercury with BC as adsorbent.

Literature Cited.

1. A. Demirbas. *Energy Edu. Sci. Technol.* **2000**, *5*, 21.
2. A. Demirbas. *Energy Edu. Sci. Technol*. **2000**, *6*, 19.
3. U.K. Garg, M.P. Kaur, V.K. Garg, D. Sud. *Biores. Technol.* ***in press.***
4. U.K. Garg, M.P. Kaur, V.K. Garg, D. Sud. *J. Hazard. Mater.* **2007**, *140*, 60.
5. E. Sjotrom. Wood Chemistry Fundamentals and Applications. *Academic Press Inc., New York* **1981.**
6. T.J. Beveridge, R.G.E. Murray. *J. Biotechnol.* **1980**, *141*, 876.
7. V.K. Gupta, I. Ali. *J. Colloid Interface Sci.* **2004**, *271*, 321.
8. Y. A. Koyama, C. P. Taniguchi, B. D. W. Haung. *Journal of Applied Polymer Science*, **1986**, *31*, 1951.
9. K. Kurita, T. Sannan, Y. J. Iwakura. *Applied Polymer Science* **1979**, *23*, 511.
10. J. D. Merrifield, W. G. Davids, J. D. MacRae, A. Amirbahman. *Water Research* **2004**, *38*, 3132.
11. A. Zhang, J. Xiang, L. Sun, S. Hu, P. Li, J. Shi. *Industrial Engineering & Chemistry Research* **2009**, *48*, 4980.
12. R. S. Vieira, M. M. Beppu. *Adsorption*. **2005**, *11*, 731.
13. K. Oshita, M. Oshima, Y. H. Gao, K. H. Lee, S. Motomizu. *Analytical Sciences* **2002**, *18*, 1121.
14. J. Choong. *Journal of Microbiology and Biotechnology* **2005**, *15*, 497.
15. J. Choong, W.H. Holl. *Water Research*, **2003**, *37*, 4770.
16. E. Guibal. *Industrial Engineering & Chemistry Research*, **1998**, *37*, 1454.
17. R. A. A. Muzzarelli, O. Tubertini. *Talanta* **1969**, *16*, 1571.
18. P. Miretzky, A. Fernandez Cirelli. *Journal of Hazardous Materials* **2009**, *167*, 10.
19. A.J. Varmaa, S.V. Deshpandea, J.F. Kennedy. *Carbohydrate Polymers* **2004**, *55*, 77.
20. A. Bhatnagar, M. Sillanpaa. *Advances in Colloid and Interface Science* **2009**, *152*, 26.
21. R.S. Vieira, M.M. Beppu. *Colloids and Surfaces A: Physicochem. Eng. Aspects* **2006**, *279*, 196.
22. L.M. Zhou, Y.P. Wang, Q.W. Huang. *J. Nucl. Radiochem*. **2007**, *29*, 184.
23. L. Zhou, Y. Wang, Z. Liu, Q. Huang. *J. Hazard. Mater*. **2009**, *161*, 995.

24. G. Cardenas, P. Orlando, T. Edelio. *International Journal of Biological Macromolecules* **2001**, *28(2)*, 167.
25. R. Qu, C. Sun, F. Ma, Y. Zhang, C. Ji, Q. Xu, C. Wang, H. Chen. J. Hazard. Mater. 167 (2009) 717–727.
26. K. Campos Gavilan, A.V. Pestov, H. Maldonado Garcia, Y. Yatluk, Jean Roussya, E. Guibal. *Journal of Hazardous Materials* **2009**, *165*, 415.
27. A.M. Donia, A.A. Atia, K.Z. Elwakeel. *J. Hazard. Mater.* **2008**, *151*, 372.
28. J.D. Merrifield, W.G. Davids, J.D. MacRae, A. Amirbahman, *Water Res.* **2004**, *38*, 3132.
29. C. Jeon, W.H. Holl, *Water Res.* **2003**, *37*, 4770.
30. A. Khan, S. Badshah, C. Airoldi. *Colloids and Surfaces B: Biointerfaces* **2011**, *87*, 88.
31. K.D. Trimukhe, A.J. Varma. *Carbohydr. Polym*. **2008**, *71*, 66.
32. J.L. Barriada, R. Herrero, D.P. Rodriguez, M.E. Sastre de Vicente. *Reactive & Functional Polymers* **2008**, *68*, 1609.
33. L. Wang, R. Xing, S. Liu, S. Cai, H. Yu, J. Feng, R. Li, P. Li. *International Journal of Biological Macromolecules* **2010**, *46*, 524.
34. R.A.A. Muzzarelli, R. Rocchetti. *J. Chromatogr. A* **1974**, *96*, 115.
35. J.D. Merrifield, W.G. Davids, J.D. MacRae, A. Amirbahman. *Water Res.* **2004**, *38*, 3132.
36. A. Zhang, J. Xiang, L. Sun, S. Hu, P. Li, J. Shi, P. Fu, S. Su. *Ind. Eng. Chem. Res.* **2009**, *48*, 4980.
37. R.S. Vieira, M.M. Beppu. *Adsorption* **2005**, *11*, 731.
38. K. Oshita, M. Oshima, Y.H. Gao, K.H. Lee, S. Motomizu. *Anal. Sci.* **2002**, *18*, 1121.
39. J. Choong. *J. Microbiol. Biotechnol.* **2005**, *15*, 497.
40. J. Choong, W. H. Holl. *Water Res.* **2003**, *37*, 4770.
41. W. M. Arguelles, C. C. Peniche. *Appl. Macromol. Chem. Phys./Angew. Makromol. Chem.* **1993**, *207*, 1.
42. C. C. Peniche, L. W. Alvarez, W. M. Arguelles. *J. Appl. Polym. Sci.* **2003**, *46*, 1147.
43. R. A. A. Muzzarelli, I. Antonio. *Water, Air Soil Pollut.* **1971**, *1*, 65.
44. C. Karol, E. Guibal, P. Francisco, M. Ly, M. Holger. *Adv. Mater. Res.* **2007**, *20-21*, 635.
45. G. M. Gadd. Biosorption. *Chem. Ind.* **1990**, *13*, 421.
46. L. Nan, B. Renbi, L. Changkun. *Langmuir* **2005**, *21*, 11780.

47. P. Padmaja. Concentration, separation and determination of trace amounts of Hg. Ph.D. Thesis, IIT Madras, 1994.
48. P. Ahuja, R. Gupta, B. K. Saxena. Zn^{+2} biosorption by Oscillatoria anguistissima. *Process Biochem.* **1999**, *34*, 77.
49. M. D. Ahmed, A. A. Asem, M. Heniesh. *Separation and Purification Technology* **2008**, *60*, 46.
50. C. F. Baes Jr., & R. E. Mesmer. The hydrolysis of cations. New York*: Wiley* **1976**, 301.
51. F. Jonathan, N. K. Aline, S. Jaka, J. Yi-Hsu, I. Nani, I. Suryadi. *Journal of Hazardous Materials* **2009**, *162*, 616.
52. L. R. Gregory, H. Tzu-Yang. *Ind. Eng. Chem. Res.* **1993**, *32*, 2170.
53. S. Hasan, A. Krishnaiah, T. K. Ghosh, D. S. Viswanath. *Ind. Eng. Chem. Res.* **2006**, *45*, 5066.
54. R. A. A. Muzzarelli. *Carbohydrate Polymers* **2011**, *84*, 54.
55. T. Hui-Chung, L. Carmay. *Journal of Physical Chemistry A* **2006**, *110*, 452.
56. P. Brassard, J. R. Kramer, P. V. Collins. *Environ. Sci. Technol.* **1990**, *24*, 195.
57. J. S. Cox, D. S. Smith, L. A. Warren, F. G. Ferris. *Environ. Sci. Technol.* **1999**, *33*, 4514.
58. M. Dittrich, S. Sibler. *Langmuir* **2006**, *22*, 5435.
59. I. Sokolov, D. S. Smith, G. S. Henderson, Y. A. Gorby, F. G. Ferris. *Environ. Sci. Technol.* **2001**, *35*, 341.
60. R.G. Pearson. *J. Am. Chem. Soc.* **1963**, *85*, *3533*.

Chapter 8

Preparation and characterization of Specific Adsorbent for Uranium

Outline:

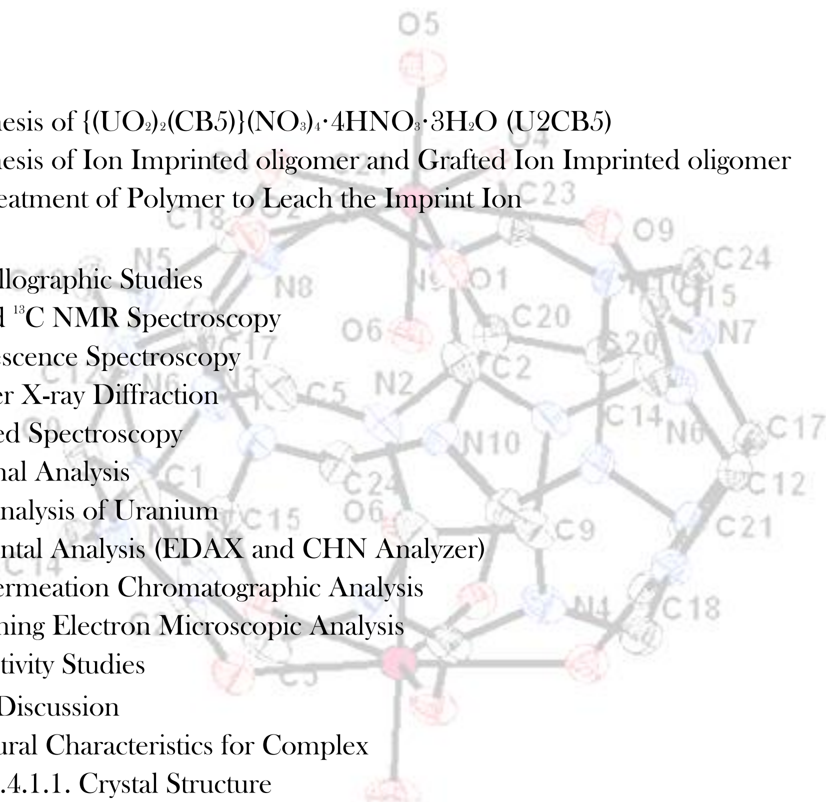

8.1. Introduction
8.2. Materials
    8.2.1. Synthesis of $\{(UO_2)_2(CB5)\}(NO_3)_4 \cdot 4HNO_3 \cdot 3H_2O$ (U2CB5)
    8.2.2. Synthesis of Ion Imprinted oligomer and Grafted Ion Imprinted oligomer
    8.2.3. Pretreatment of Polymer to Leach the Imprint Ion
8.3. Methods
    8.3.1. Crystallographic Studies
    8.3.2. ^{1}H and ^{13}C NMR Spectroscopy
    8.3.3. Fluorescence Spectroscopy
    8.3.4. Powder X-ray Diffraction
    8.3.5. Infrared Spectroscopy
    8.3.6. Thermal Analysis
    8.3.7. ICP Analysis of Uranium
    8.3.8. Elemental Analysis (EDAX and CHN Analyzer)
    8.3.9. Gel Permeation Chromatographic Analysis
    8.3.10. Scanning Electron Microscopic Analysis
    8.3.11. Selectivity Studies
8.4. Results and Discussion
    8.4.1. Structural Characteristics for Complex
        8.4.1.1. Crystal Structure
        8.4.1.2. Powder- X-Ray Diffraction
        8.4.1.3. ^{1}H and ^{13}C Nuclear Magnetic Resonance
        8.4.1.4. Thermal Analysis
        8.4.1.5. Fourier Transform Infra Red Spectroscopic Analysis
        8.4.1.6. Fluorescence Spectroscopy
    8.4.2. Structural Characteristics for Oligomer
        8.4.2.1. Gel Permeation Chromatographic Analysis
        8.4.2.2. Thermal Analysis
        8.4.2.3. Scanning Electron Microscopic Analysis
        8.4.2.4. Fourier Transform Infra Red Spectroscopic Analysis
    8.4.3. Uranium Selectivity Studies
8.5. Conclusions

8.1. Introduction

Molecular imprinting polymers (MIP) which have the ability for high selective adsorption of target chemical species from various media are presently of great interest [1, 2]. In recent years, some imprinting polymers have been prepared and used for selective removal, pre-concentration and extraction of metal ions [3-20] which are termed as ion imprinting polymers (IIP).

The high selectivity of these imprinted polymers arises from the memory effect of the polymer to the imprinted ions, including the specificity of interaction of ligand with the metal ions, the coordination geometry and coordination number of metal ions, the charge of the metal ions, and the size of the metal ions [21].

Important steps for synthesis of imprinted polymer include selection of a functional monomer that can form a complex with template, polymerization of the monomer containing imprint ion and leaching of the imprint ion to obtain an imprint which can recognize the template from a mixture of chemical species (Scheme 8.1). The bonding between the template and the functional monomer can be either covalent or non-covalent.

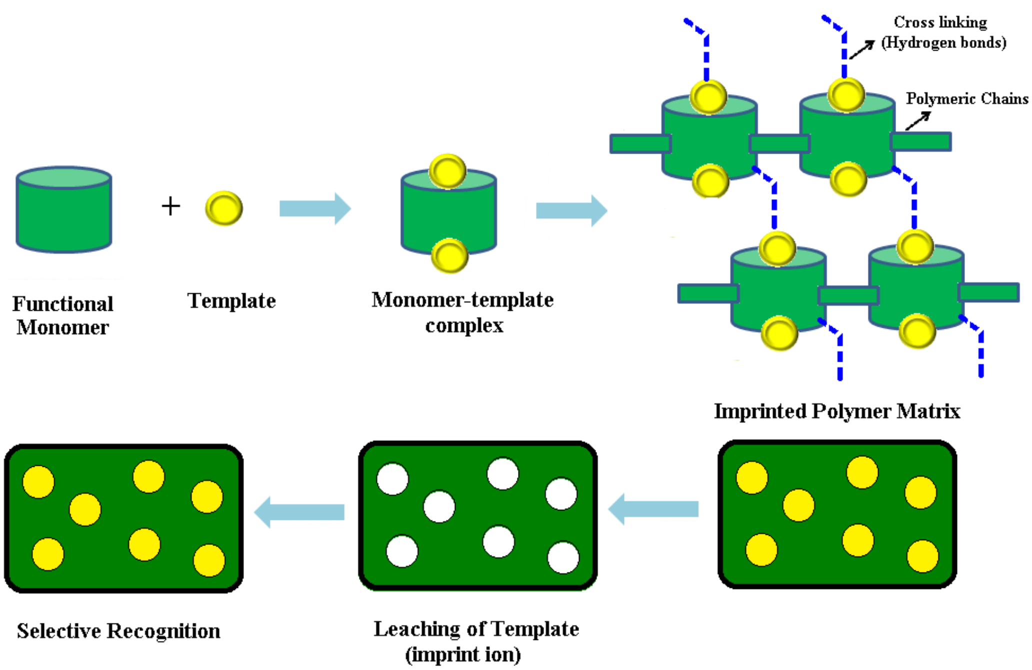

Scheme 8.1. Scheme for complexation involving template, imprinting by formation of matrix, leaching of template and selective recognition

Hydrogen bonding is the most common interaction during non-covalent molecular imprinting. Previous studies have shown that an imprinted polymer prepared based on hydrogen bonding interactions lost its molecular recognition ability in aqueous media or organic solvents with high polarity [21, 22]. The covalent bonding system employs a template-monomer complex which is formed by a reversible covalent bonding.

Traditionally, MIPs, prepared by bulk polymerization, exhibit highly selective recognition but with poor site accessibility to the target molecules, as the template molecules and functional groups are totally embedded inside the polymer network and the binding kinetics is low [23]. They also have other limitations such as non-uniform distribution of particle size [24, 25-27], high consumption of template and material [25, 27, 28] thermal instability, and swelling and shrinkage effects [26]. Therefore, much attention has been paid to novel surface imprinting techniques which offer fast mass transfer kinetics [29-36]. Recently, the problems associated with bulk polymerization have also been overcome by grafting techniques wherein the MIPs layers are coated onto substrates with known surface morphologies [27, 28, 38-41]. We were interested in the development and evaluation of the grafting of ion imprinting oligomers onto agrowaste materials.

Industrial activities and mining operations have exposed man to the toxic effects of uranium. Uranium is an emerging pollutant and can cause irreversible renal injury and may lead even to death. Due to the biological, environmental and industrial impacts of uranyl ion, development of imprinting polymers for selective separation of uranyl ion is of continuing interest [3-20].

In the race of nuclear empowerment, every country is consuming more and more of nuclear fuel leads to increased incidents of seepage and residual fuel and distribution of radioactivity to the our surroundings. Recently number of reports has focused on uranium poisoning. Times Of India (TOI) reported in March 2009 high levels of uranium while analyzing the hair and urine samples of ~150 children in Punjab. Children were reported to be affected from birth with physical deformities, neurological and mental disorders. Further, TOI of June 2010 reported that studies carried out amongst mentally retarded children of Punjab, revealed uranium levels high enough to cause diseases. The recent Fukushima Nuclear accident in March 2011, resulted in a hovering radioactive cloud and seepage of fuel to the sea water. Hence selective extraction and recovery of uranium from these discharges is essentially required in view of its extreme toxicity and environmental aggressiveness.

The combination of cross-linking with macromolecular functional monomers for production of selective imprinted polymers for uranium ion which does not exhibit directional bonding, prepared by bulk polymerization, ATRP, Free radical copolymerization, cross linked matrix, thermal polymerization and sol-gel surface imprinting etc. are summarized in Table 8.1.

Table 8.1. Summary of Retention capacity/ Distribution Coefficient for uranium

Sr. No.	Functional monomer/ Polymer	Technique	Cross Linker	pH	Eluent	Retention capacity/ Distribution Coefficient		References
						Imprinted sorbent	Control Sorbent	
1.	MAA	Free Radical	EGDMA	3.0	1M HCl	4950.0	35.5	[3]
	HEMA/ VP/ Amidoxime	Free Radical	EGDMA	8.0	1N HCl	26 μmol/g	-	
2.	Chitosan	-	Glutraldehyde/ glyoxal	4.0	1:1 HCl	-	-	[42]
3.	2-chloroacrylic acid	Free Radical	EGDMA	<3.0	Conc. HNO_3	-	-	[5]
4.	TMOS	Sol-Gel (Surface imprinting)	-	~5.0	HNO_3	-	-	[6]
5.	DCQ/ Styrene	Thermal	DVB	6.0	1:1HCl	99.0	3.16	[8]
6.	Quinoline-8-ol/ DCQ/ DBQ/ DIQ/ VP/ Styrene	Free Radical	DVB	6.0	1:1HCl	30 mg/g	-	[9]
7.	DCQ/ VP/ Styrene	Free Radical	DVB	6.0	1MHCl	34 mg/g	25 mg/g	[10]
8.	VP/ Styrene	Free Radical	DVB	6.0	1MHCl	886.3	-	[12]
9.	SALO/ Catechol/ succinic acid/ DCQ/ VP/ HEMA	Free Radical	EGDMA	>5.0	5MHCl	99x5x10E +4	-	[13]
10.	SALO/ VP/	Free	DVB	~3.	1MHCl	99x5x10E	0.15x5x10E	[14]

	Styrene	Radical		5		+3	+3	
11.	Chitosan/ PVA	Cross Linking	EG diglycidyl ether	5.0	0.1MHNO3	495.0	86.0	[15]
12.	SALO/ VP/ DCQ	Thermal	DVB	7.0	5.0MHCl	-	-	[16]
13.	PPMP/ MAA	Thermal	EGDMA	3.0	5MHCl	37.58 mg/g	25.44 mg/g	[43]
14.	VBA/ Styrene	Free Radical	DVB	3.0	1MHNO_3	-	-	[44]
15.	Piroxicam/ VP/ Styrene	Free Radical	DVB/ EGDMA	6.0	6MHCl:MeOH (1:1)	38.58 mg/g, 14.0	-	[17]
16.	SALO/ VP/ 2-methoxy ethanol/ Methacrylic acid	Thermal	EGDMA	5.0	2MHCl	-	-	[18]
17.	3-(Triethoxysilyl) propylacrylamide/ acrylamide (Aam)/ (TEA)/ 3-(triethoxysilyl)propyl acrylate/ PVC	Sol-Gel	TEOS	-	12%HNO_3 in ultra-sonicator	-	-	[45]
18.	VP/ HEMA	Thermal/ Surface imprinting	EGDMA	5.0 - 7.0	1MHCl	97.1 µmol/g	-	[19]
19.	1-hydroxy-2-(prop-20-enyl)-9,10-anthraquinone	Free Radical	EGDMA	1.0 - 3.0	2MHCl	52.1 µmol/g	-	[20]

However, most of these IIPs are not suitable for removal of uranium from nuclear power reactor effluents as they are reported to contain free acidity and not much research has been attempted to selectively remove uranium from a number of coexisting inorganic ions present in weakly acidic to acidic solutions using IIP's [14]. Say et al. [46] selectively removed uranium using glutamic acid ion imprinted polymeric beads from weakly acidic solutions (pH 3.5) containing Fe(III), Th(IV) and Mn(II) but had a number of drawbacks like requirement of 75 min adsorption time, crucial dependence on the pH of equilibration which made the process tedious and time consuming. Recently, Prasada Rao et al. prepared IIP based on ternary mixed ligand (UO_2^{2+}-SALO-VP) prepolymer complexes for the selective removal of uranium from dilute aqueous solutions [13].

Interest in the family of cucurbit[n]urils (CB[n], n=5–10), comprising n glycoluril units joined by pairs of methylene bridges, having a hydrophobic cavity accessible through two carbonyl-fringed portals as hosts has been increasing [47]. Cucurbiturils were developed after cyclodextrins, crown ethers and calixarenes [48-50]. The metal complexing properties of cucurbiturils have been widely investigated [51-53], particularly in the case of alkali, alkaline-earth [54-60], lanthanide cations [61] and d-block metal ions [62-66]. In the case of actinides, the crystal structures of only two compounds have been reported by Fedin et al., one having Th(IV) cation bound to three adjacent carbonyl groups complexed at each portal of CB6, and the other $[(UO_2)_4(\mu 3\text{-}O)_2(\mu 2\text{-}Cl)_4(H_2O)_6]$ [67]. CB6, having no uranium−carbonyl bond, the tetranuclear uranyl complex being only hydrogen bonded to the macrocycle [68]. These molecules exhibit wide range of applications including molecular catalysis, molecular recognition, ion channel, and supramolecular assemblies [69-71].

Recent synthesis of cucurbituril homologues (CB[*n*], *n* = 5, 7 and 8) has broadened the scope of the cucurbituril chemistry [72]. Thuery was the first to report complexes between uranyl ions and CB5, the heterometallic uranyl lanthanide complexes having direct uranyl-carbonyl bonds and hydrogen bonded channels [73-75]. Polynuclear complexes were also reported by him where uranyl ions were bound to two carbonyl groups from two different molecules [91-93]. CB5 is known to form capsules when capped by alkali metal or lanthanide ions, and Zn, K with different cations at its two portals [65, 73, 76-80]. In the absence of other reactants (alkali metal/lanthanide ions, Zn and K) the problem of formation of insoluble powders and/or small quantity of crystals was reported by Thuery under hydrothermal conditions [73-75].

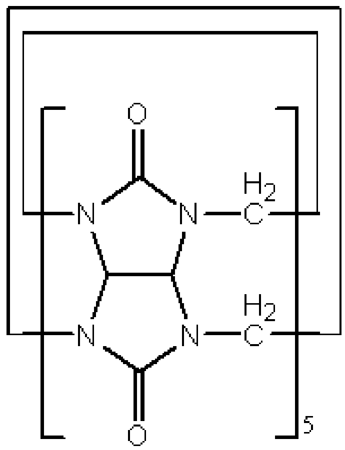

Scheme 8.2. Cucrbit[5]uril

The environment and the size of the two carbonyl fringed portals [2.4 Ǻ] led us to believe that CB5 (Scheme 8.2) would be a perfect molecule for the complexation of uranyl ions [0.81Ǻ] at each of its portals. Literature search prominently showed that very few of the studies have reported selective extraction and recovery of uranium using ion imprinted polymers in the acidic pH range. Our objectives were:

i) To prepare U2CB5 complex and characterize the complex by XRD, NMR, UV, IR and fluorescence studies.

ii) To explore the possibility of U2CB5 complex being a suitable monomer for the preparation of ion imprinted oligomer.

iii) Due to their structural morphology and low cost explore the possibility of the use of agro-waste palm shell powder as potential support material for the grafting of imprinted oligomer.

However, during the course of our attempt to prepare a complex of uranyl nitrate with CB5 under ambient conditions we were pleasantly surprised to get yellow crystals of U2CB5 at ambient temperature conditions, in which both the portals are closed by uranyl ions. We thus report herein the synthesis, characterization and single crystal X-ray structure analysis of (U2CB5). This monomer containing uranyl ion as the template would be further polymerised for the preparation of ion imprinted oligomer. The imprinted polymer would then be non-covalently grafted onto palm shell powder as described in scheme 8.3.

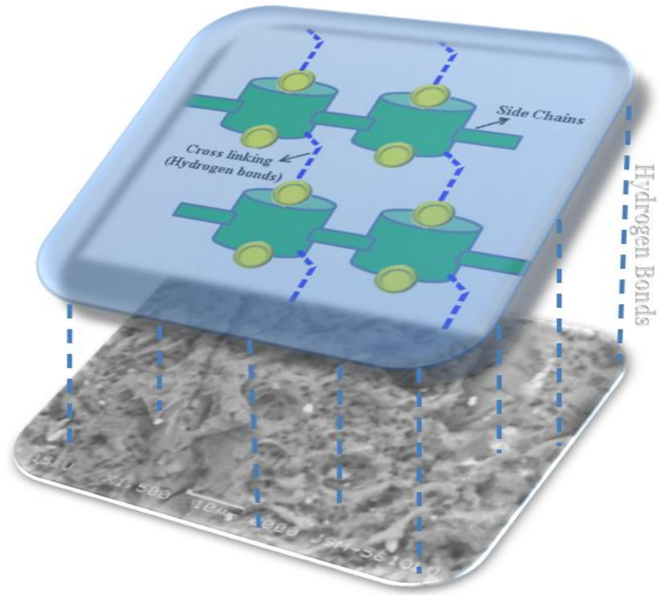

Scheme 8.3. Ion imprinted oligomer grafted on PSP

8.2. Materials.

8.2.1. Synthesis of $\{(UO_2)_2(CB5)\}(NO_3)_4 \cdot 4HNO_3 \cdot 3H_2O$ (U2CB5).

$UO_2(NO_3)_2.6H_2O$ was purchased from Sulab chemicals, HNO_3 was purchased from E-Merck and cucurbit[5]uril from Aldrich. Cucurbit[5]uril (20 mg, 0.020 mmol) was dissolved in 4.6 mL of demineralized water and 0.4 mL of HNO_3 (69% w/v) was added to it. A 10-fold excess of $UO_2(NO_3)_2 \cdot 6H_2O$ (116 mg, 0.232 mmol) was dissolved in 4.9 mL of demineralized water and 0.1 mL of HNO_3 (69% w/v) was added to it. The uranyl nitrate solution was added dropwise to cucurbituril solution with continuous stirring and was left for 24 h at 40°C under stirring conditions and the complex is readily synthesized. Light yellow color crystals of the complex U2CB5 were deposited in solution. Good quality single crystals of light yellow color could be separated within 24 h, which if left further for another 24 h resulted in crystalline material. Anal. Calcd. for $C_{30}H_{40}N_{28}O_{41}U_2$: C, 18.75; H, 2.08; N, 20.42. Found C, 18.82; H, 1.97; N, 20.54%. The observed percentage of U was found to be 12.41% (Anal. Calcd. 12.39%). 1H NMR (D_2O/HCl 300K): δ (ppm) 6.873, 8.190 (d, $-CH_2-$) and 8.073 (s, $-CH-$) for U2CB5. 13C NMR (D_2O/HCl 300K): δ (ppm) 51.13, 71.78, and 172.88 for U2CB5. Amount of water or dilution and pH of the reaction is an important part playing role for synthesizing U2CB5 as it serves as mineralizing agent as well as counter cation.

8.2.2. Synthesis of Ion Imprinted oligomer and Grafted Ion Imprinted oligomer.

U2CB5 (107 mg) was allowed to react with $K_2S_2O_8$ (418 mg)[1:15 mole ratio] in water at 85 °C for 6 h in presence of nitrogen atmosphere. After cooling to room temperature acetone vapor diffusion into the solution gave light yellow precipitates were filtered washed with acetone and dried in vacuum oven (50°C) to give hydroxylated U2CB5. Allylation was done by adding hydroxylated U2CB5 (48.2 mg) to a solution containing NaH (27.13) (60% dispersion in mineral oil in 10 mL anhydrous DMSO) in 1:20 mole ratio at 0 °C and stirred at RT for 1 h, followed by addition of alkyl bromide (0.42 mL) to this reaction mixture at 0 °C and stirred at RT for 12 h. The reaction mixture was poured into ice-water (300 mL) resulting in a light yellow solid which was washed thoroughly with water and ether, and finally dried in vacuum to obtain allyl derivative of hydroxylated U2CB5. The product was purified number of times by washing with ether or hexane to remove the unreacted alkyl bromide. Allyl derivative of hydroxylated U2CB5 is the template complexed monomer which was polymerized using free radical solution polymerization to obtain uranyl ion imprinted polymer.

About 25 mg of allyl derivative of hydroxylated U2CB5 (Monomer) in 10 mL solution of methanol along with 10 mg recrystalised AIBN (Initiator) was taken in a three neck flask at 55 °C under nitrogen atmosphere in thermostatically controlled oil bath with constant stirring for 10 h. After completion of reaction, excess methanol was distilled off under reduced pressure and traces of solvent were removed by drying under reduced pressure in vaccum oven for 12 hours. The resulting polymer was then dried to obtain ion imprinted polymer [IU2CB5]. Imprinted polymer IU2CB5 was then grafted to a lignocellulosic agrowaste, *palm shell powder (PSP)* by dry impregnation method or forced impregnation for 12h. A grafted ion imprinted polymer [PGIU2CB5] was thus obtained.

Control polymer was similarly prepared by omitting the imprint ion $(UO_2)^{2+}$ (Controlled polymer [CU2CB5] and Controlled polymer grafted to *PSP* [CPGIU2CB5]).

8.2.3. Pretreatment of Polymer to Leach the Imprint Ion.

The imprint ion $(UO_2)^{2+}$ was leached from the imprinted polymer [LIU2CB5] and grafted imprinted polymer [LPGIU2CB5] by sonication with 10 ml of 1N $HClO_4$ for 6 h. The resultant polymer material was dried in a vacuum oven at 60^0C to obtain imprinted polymer [IU2CB5] and grafted imprinted polymer [PGIU2CB5] for possible selective extraction of $(UO_2)^{2+}$ over other metal ions.

8.3. Methods.

8.3.1. Crystallographic Studies.

A yellow single crystal of suitable size and uniform shape was selected and mounted on a glass fiber with epoxy and aligned on a Bruker SMART APEX CCD X-ray diffractometer. Intensity measurements were performed using graphite monochromated Mo Kα radiation [λ = 0.71073 Å]. Each set had a different Φ angle for the crystal, and each exposure covered a range of 0.3° in ω. A total of 2400 frames were collected with an exposure time per frame of 40 s. ω scan width of 0.3°, each for 8 s, crystal-detector distance 60 mm, collimator 0.5 mm. The data were reduced by using SAINTPLUS and a multiscan absorption correction was done using SADABS [76-78]. Structure solution and refinement were performed using SHELX-97 [79]. All non hydrogen atoms were refined anisotropically. The final cell parameters were determined using a least-squares fit to 4713 reflections. During the crystallography 25040 reflections were collected, among which 4713 unique ones were used to solve the structure with R(int) = 0.0343.

8.3.2. ^{1}H and ^{13}C NMR Spectroscopy.

High-resolution ^{1}H and ^{13}C NMR spectra were recorded using a Varian-500 spectrometer operating at 500 MHz in D_2O/HCl. The chemical shifts δ, expressed in parts per million [ppm], were referenced relative to the signal of tetramethylsilane ($Si(CH_3)_4$) at δ = 0 ppm.

8.3.3. Fluorescence Spectroscopy.

Fluorescence and absorption data were acquired for the solutions of ligand and the compound using a Jasco spectrofluorimeter quartz cell and Lamda-35 Perkin-Elmer UV−visible spectrophotometer. Excitation was achieved using 365 nm light from a Xenon lamp for the fluorescence spectroscopy. The absorption spectra are provided in the Supporting Information. Absolute emission quantum yields were determined by comparison of the integrated emission intensity with that of quinine sulfate under identical conditions such as exciting wavelength, optical density, and apparatus parameters.

8.3.4. Powder X-ray Diffraction.

Powder X-ray diffraction pattern of the samples were collected on a PHILIPS PW-1830. XRPD pattern of the ingredients was taken by holding in place on quartz plate for exposure to CuKα radiation of wavelength 1.5406 Å. The sample was analyzed at room temperature over a range of 10−70° 2θ with sampling intervals of 0.02° 2θ and scanning rate of 2°/min.

8.3.5. Infrared Spectroscopy.

Infrared spectra were obtained from single crystals of U2CB5 and oligomers using a Perkin-Elmer RX1 model FTIR spectrometer. FT-IR spectra for the crystal was obtained by first mixing with KBr and then ground in a mortar at an appropriate ratio of 1/100 for the preparation of the pellets. The resulting mixture was pressed at 10 tons for 5 min and sixteen scans with 8 cm^{-1} resolution were applied in recording spectra. The background obtained from the scan of pure KBr was automatically subtracted from the sample spectra.

8.3.6. Thermal Analysis.

The thermal behavior of the crystal as well as oligomers was evaluated by using thermo-gravimetric analyzer (TG/DTA 6300 (INCARP EXSTAR 6000), under air at a heating rate of 10 °C min^{-1} up to 450 °C. Differential Scanning Calorimetry for oligomers was obtained by using Seiko SSC 5200H Differential Scanning Calorimeter at a uniform heating rate of 10°C/min over a temperature range of 30-550°C in nitrogen atmosphere.

8.3.7. ICP Analysis of Uranium.

For the ICP analysis, the U2CB5 complex (5 mg) was dissolved in 10 mL of water. After complete dissolution, the solution was transferred to a 25 mL volumetric flask and diluted to final volume with deionized water. Five standard solutions of uranium were used to obtain calibration curves with concentrations of 1−10 mg L^{-1} prepared from a 1000 mg L^{-1} stock solution. The standards and sample were analyzed by an inductively coupled plasma atomic emission spectrophotometer (ICP-AES, Thermo Jarrel Ash, Model Trace Scan) at wavelengths of 409.014 nm.

8.3.8. Elemental Analysis (EDAX and CHN Analyzer).

Elemental analysis was carried out using a JSM5610LV instrument combined with INCA-EDX-SEM analyzer and confirmed by Perkin-Elmer 2400 CHN analyzer for the quantitative identification.

8.3.9. Gel Permeation Chromatographic Analysis.

The weight-average molecular weight (M_w), number-average molecular weight (M_n) and polydispersity index (M_w/M_n) were obtained on a Waters 150C GPC using RI detector (1000-Å HT column).

8.3.10. Scanning Electron Microscopic Analysis.

The surface morphology and topographic analysis of the adsorbent samples was examined by Scanning Electron Microscope (JEOL, Model JSM-5610LV).

8.3.11. Selectivity Studies.

The selectivity of IU2CB5, PGIU2CB5, CU2CB5, CPGIU2CB5 for uranium over other inorganic ions was determined by shaking 20 mg of polymer particles with 25 ppm of Cu^{2+}, Cd^{2+}, Zn^{2+}, Cr^{6+}, Fe^{3+}, Cs^{+} and U^{6+} present in 10 mL of deionized water at pH1 adjusted using HNO_3. The selectivity coefficient (S UO_2^{2+}/M^{n+}) is defined as

$$S_{\mathrm{UO_2^{2+}/M^{n+}}} = \frac{D_{\mathrm{UO_2^{2+}}}}{D_{\mathrm{M^{n+}}}}$$

where DUO_2^{2+} and DM^{n+} are the distribution ratios of the uranyl ion and other inorganic species, respectively, with polymer particles (CU2CB5 or IU2CB5). These distribution ratios were calculated using the formula

$$D_{\mathrm{M^{n+}}} = \frac{C^{\mathrm{i}}_{\mathrm{M^{n+}}} - C^{\mathrm{f}}_{\mathrm{M^{n+}}}}{C^{\mathrm{f}}_{\mathrm{M^{n+}}}} \times \frac{v}{m}$$

where C_i M^{n+} and C_f M^{n+} are the concentrations of inorganic ions in aqueous phase before and after extraction, v is the volume of the solution, and m is the mass of the polymer. The percent extraction (%E) of inorganic ion is defined as

$$\%E = \frac{C^{\mathrm{i}}_{\mathrm{M^{n+}}} - C^{\mathrm{f}}_{\mathrm{M^{n+}}}}{C^{\mathrm{i}}_{\mathrm{M^{n+}}}} \times 100$$

8.4. Result and discussion

8.4.1. Structural Characteristics for Complex.

8.4.1.1. ***Crystal Structure*****.** The title compound $\{(UO_2)_2(CB5)\}(NO_3)_4{\cdot}4HNO_3{\cdot}3H_2O$ (U2CB5) crystallizes in monoclinic system with space group of *C*2/*c*. The asymmetric unit in the crystal structure of U2CB5 is composed of half of the moiety with four units of nitrate anion (two for charge compensation and other two for lattice HNO_3 molecules) and three lattice water molecules. Coordination complexes having two uranyl ions in the same molecular unit to form the internal complex are extremely rare and exhibit interesting properties. But here, in contrast to the reported results we are presenting the first internal complex of uranyl nitrate and cucurbit[5]uril under normal bench conditions.

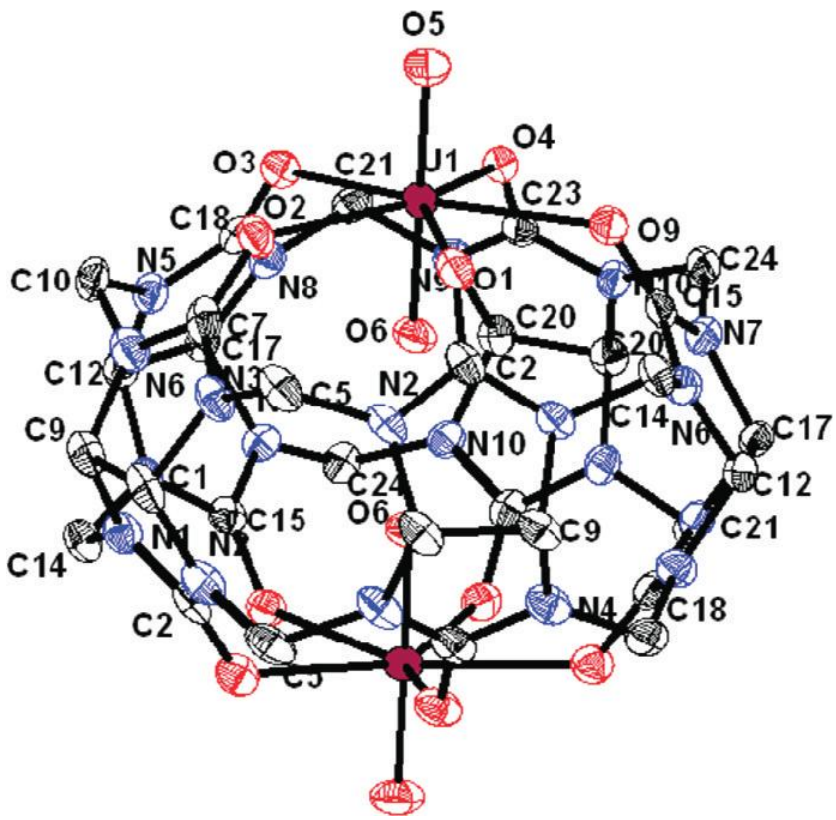

Figure 8.1. Oak Ridge thermal ellipsiodal diagram of the U2CB5 with 40% probability (Hydrogens, counteranion and solvent water molecules are omitted for clarity): Color code: C, gray; O, red: N, blue;.

The full molecule of the U2CB5 as shown in Figure 8.1 is a biuranyl complex with cucurbit[5]uril (CB5) and crystallographic data with structural refinement parameters are provided in Table 8.2.

Table 8.2. Crystallographic Data and Structural Refinement

Entry	U2CB5
Formula	$C_{30}H_{30}N_{28}O_{41}U_2$
Volume	1914.88
Crystal system	Monoclinic
Space group	C2/c
a/Å	15.0886 (15)
b/Å	14.5869 (14)
c/Å	24.889 (2)
β /deg	93.6340(10)
U/Å^3	5340.6 (9)
Z	4
F(000)	3672
ρ_{cal}/ Mg m^{-3}	2.382
Crystal size(mm^3)	0.36 x 0.22 x 0.14
Completeness to θ =25.0	100 %
Theta range for data collection(deg)	1.68 to 25.0
Reflections collected/ unique	25040/ 4713 [R(int) = 0.0343]
$R_1(F^2_0)$ [$I > 2\ \sigma(I)$]	0.0349
wR_2 (F^2_0) [$I > 2\ \sigma(I)$]	0.0957
$R_1(F^2_0)$ (all data)	0.0395
wR_2 (F^2_0) (all data)	0.0992
Largest diff. peak and hole(Å^{-3})	1.323 and -1.427

Here, uranyl cations fit into both open portals of CB5 molecule. The U−O bond lengths with the five carbonyls of CB5 is in the range of 2.413(4)-2.454(4) Å while in the case of pendant uranyl oxygens it is 1.748(5)−1.759(5) Å. The hydrogen bonding environment around $\{(UO_2)_2(CB5)\}^{4-}$ is quiet interesting, which is shown in the Figure 8.2 where the length of C−H···O is 2.40 to 2.80 Å. The hydrogen bonding distances and angles are represented in Table 8.3.

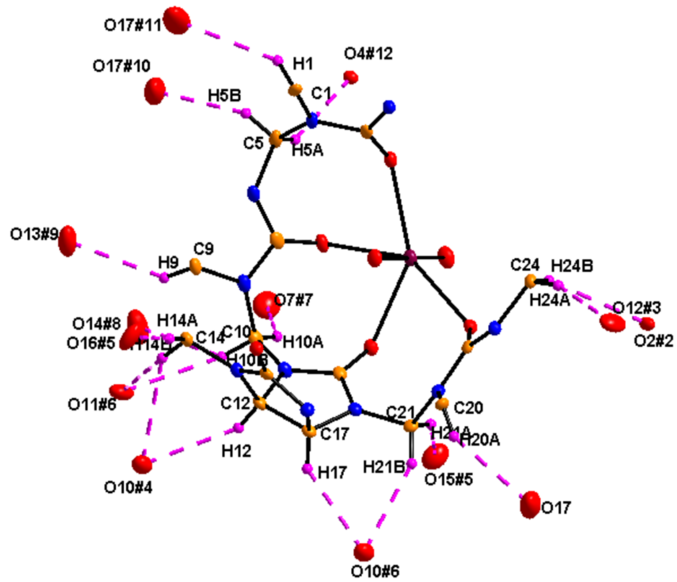

Figure 8.2. Hydrogen bonding situation around the asymmetric unit of the U2CB5: Color code: C, grey; O, red: N, blue; H, purple.

Table 8.3. Hydrogen bonds for U2CB5 [Å and deg.]

D-H...A	d(D-H)	d(H...A)	d(D...A)	<(DHA)
C(24)-H(24A)...O(2)#2	0.97	2.74	3.460(7)	131.3
C(24)-H(24B)...O(12)#3	0.97	2.39	3.324(8)	162.4
C(20)-H(20A)...O(17)	0.85(6)	2.51(6)	3.275(12)	150(5)
C(21)-H(21B)...O(10)#4	0.97	2.48	3.353(8)	149.4
C(21)-H(21A)...O(15)#5	0.97	2.45	3.297(9)	146
C(17)-H(17)...O(10)#4	0.92(5)	2.47(5)	3.248(9)	142(4)
C(12)-H(12)...O(10)#6	0.87(7)	2.54(7)	3.313(8)	148(5)
C(14)-H(14B)...O(10)#6	0.97	2.81	3.591(9)	138.5
C(14)-H(14A)...O(16)#5	0.97	2.49	3.460(9)	176.6
C(10)-H(10A)...O(7)#7	0.97	2.63	3.429(11)	139.6
C(10)-H(10B)...O(14)#8	0.97	2.89	3.586(10)	129.4
C(10)-H(10B)...O(11)#6	0.97	2.67	3.565(9)	153.2
C(14)-H(14B)...O(11)#6	0.97	2.39	3.331(9)	162.4
C(9)-H(9)...O(13)#9	0.94(7)	2.53(6)	3.226(9)	131(5)
C(5)-H(5B)...O(17)#10	0.97	2.4	3.285(12)	150.7
C(1)-H(1)...O(17)#11	0.89(6)	2.68(6)	3.416(13)	141(5)
C(5)-H(5A)...O(4)#12	0.97	2.47	3.257(7)	138.6

Symmetry transformations used to generate equivalent atoms: #1 -x,y,-z+1/2 #2 -x+1/2,y+1/2,-z+1/2 #3 x-1,y,z #4 -x+1,y,-z+1/2 #5 x-1/2,y-1/2,z #6 x-1,-y+1,z+1/2 #7 -x+1/2,-y+1/2,-z+1 #8 -x+1,-y+1,-z+1 #9 x-1,y-1,z #10 x,y-1,z #11 -x,y-1,-z+1/2 #12 -x+1/2,y-1/2,-z+1/2

The environment of nitrate anion around $\{(UO_2)_2(CB5)\}^{4-}$ looking like a wheel is shown in Figure 8.3, C−H···O interaction being responsible for the whole architecture.

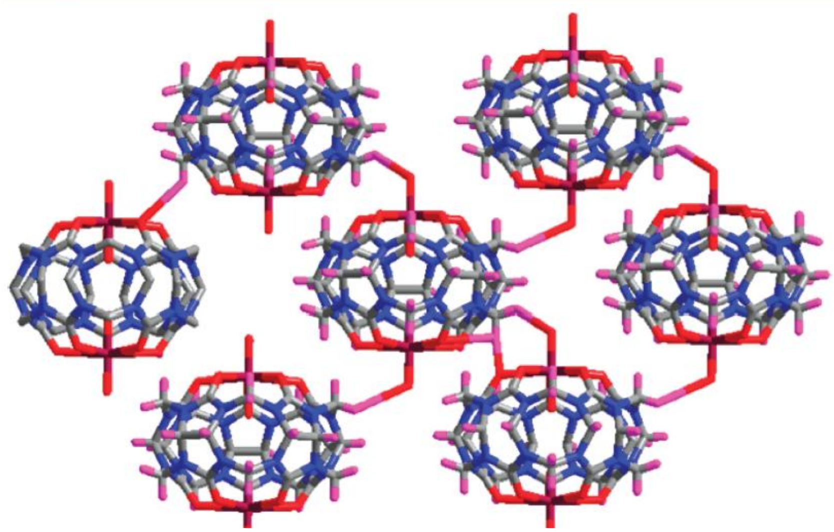

Figure 8.3. C−H···O interaction

Extensive O−H···O interaction has been found in the crystal structure of U2CB5, which leads to a 2-dimensional network as represented in Figure 8.4.

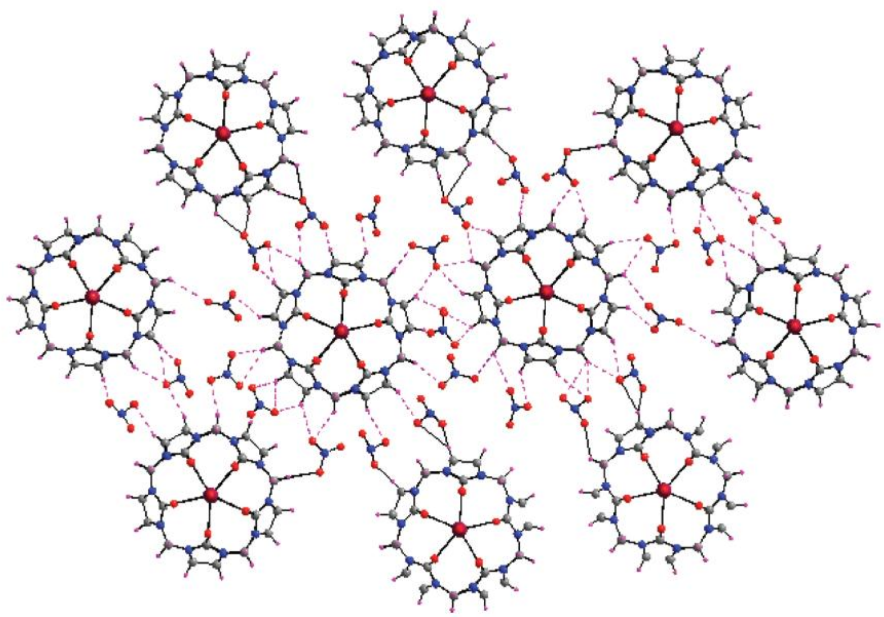

Figure 8.4. Environment of nitrate ions

The water molecules are involved in both intra- and intermolecular hydrogen bonding. The distance between the uranium atoms is 6.079 Å, and the separation between the inner oxo groups is 2.562 Å. The water molecules are located in the intermolecular spaces. The uranyl ion is perpendicular to the O plane, with an angle of ~94° with the normal to the plane and the uranium environment is thus a regular pentagonal bipyramid.

8.4.1.2. *Powder- X-Ray Diffraction*. The phase purity of U2CB5 was confirmed by XRPD patterns (Figure 8.5 a–c). Peak positions of the experimental and simulated spectra are in good agreement with each other indicating overall homogeneity of the samples and showing that single crystal and bulk properties remains the same.

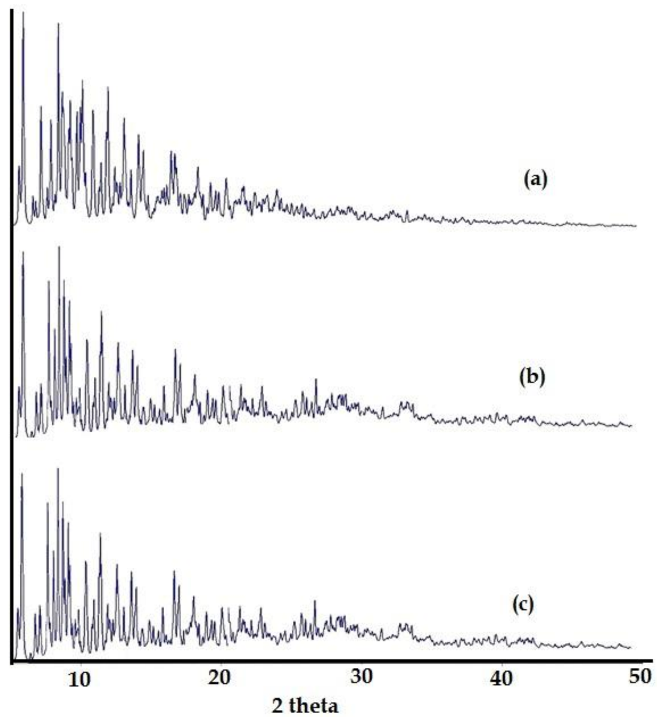

Figure 8.5. (a) Simulated pattern of U2CB5 (b) Powder diffraction pattern of U2CB5 Single crystal (c.) Powder diffraction pattern of U2CB5 crystalline material

The unit cell parameters from the powder data were found to be in good agreement with that of single crystal. X-ray powder diffraction patterns showed numerous reflections in the low to high angle regions, indicative of crystalline phases. The high intensity Bragg reflections (7.2, 8.7, 12.6, 15.4, 16.9, 18.0, 18.6, 19.9, 20.9, 21.7 Å) are likely due to the strongly scattering uranyl cations [12, 80].

8.4.1.3. ***^{1}H and ^{13}C Nuclear Magnetic Resonance*.** The ^{1}H decoupled NMR spectrum showed upfield shifting of the signals due to deshielding of protons after complexation. Two doublets (−CH_2−) and a singlet (−CH−) along with a very broad signal (D_2O) appeared at ~4.2 and 5.6 (d), ~5.4 (s) and ~4.7 ppm for CB5 which shifted upfield to ~6.9 and 8.2 (d), 8.1 (s), and 7.3 ppm, respectively, after complexation with uranium (Figure 8.6). The ^{13}C NMR spectrum (Figure 8.6) showed chemical shifts at 49.91, 68.95, and 156.23 ppm, which can be attributed to N−CH_2-N, N−CH−N, and –C=O groups, respectively, in CB5. While there were small changes in chemical shifts attributed to N−CH_2−N and N−CH−N in U2CB5, the chemical shift of –C=O at 156.23 ppm shifted downfield to 172.88 ppm. This probably indicates the formation of covalent bond between highly electronegative uranyl ion to the carbonyl moiety of CB5.

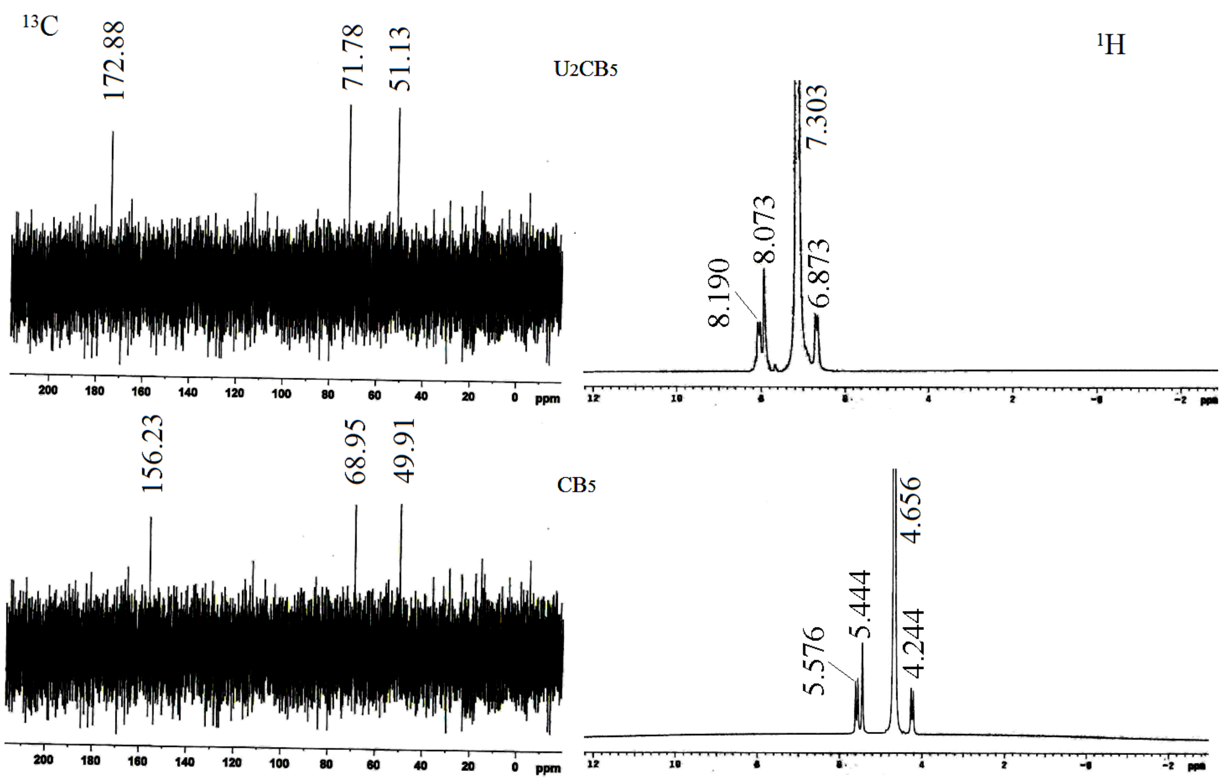

Figure 8.6. ^{1}H and ^{13}C spectra for CB5 and U2CB5

8.4.1.4. ***Thermal Analysis*.** The DTA curve of CB5 (Table 8.4 and Figure 8.7) shows an endothermic transition in the temperature interval 67.704−151.24 °C, which corresponds to a mass loss of 9.13% in the TG curve. This weight loss corresponds to the loss of 4.6 lattice water molecules. CB5 loses most of its weight (52%) around 400 °C.

Table 8.4. Thermal analysis for CB5 and U2CB5

	CB5		U2CB5	
	Temperature	% weight loss	Temperature	% weight loss
TGA Analysis	21.618 - 67.704	8.699	38.761 – 85.051	3.331
	67.704 - 151.24	9.13	85.051 - 137.09	2.703
			137.09 - 172.243	2.391
	151.24 - 332.932	1.763	172.243 - 270.619	7.015
			270.619 - 355.758	16.183
	332.932 - 547.72	52.391	355.758 - 549.087	8.776
Total % Weight loss	71.983		40.399	

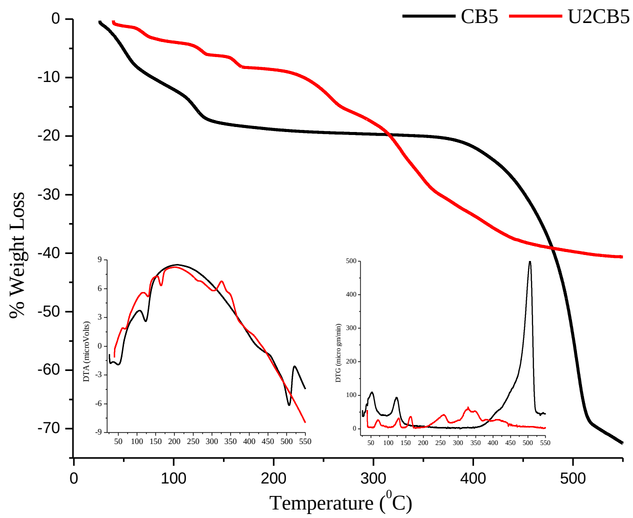

Figure 8.7. Thermal analysis of CB5 and U2CB5

After complexing, DTA curve of U2CB5 showed an endothermic transition in the temperature interval 85.051−172.243 °C. This corresponds to a mass loss of 5.094% in the TG curve equivalent to 5.6 lattice water molecules. An exothermic transition in the temperature interval 270.619−355.758 °C, corresponding to a mass loss of 16.183% in the TG curve occurs due to decomposition of ligand and formation of UO_3 [81]. Thus the weight loss is less in U2CB5 around 400 °C in contrast to CB5, but it overlaps with the ligand decomposition and gives a continuous weight loss until the final product UO_3 is formed at about 450 °C.

8.4.1.5. *Fourier Transform Infra Red Spectroscopic Analysis*. The selected vibrations from FT-IR spectra of CB5 and U2CB5 with the suggested assignments, are listed in Table 8.5. The very strong and broad bands found at ~3439 and 3423 cm^{-1} and sharp bands at 1636 cm^{-1} in the spectra are consistent with the presence of water molecules in the ligand and complex, also supported by the single crystal XRD.

Table 8.5. FTIR frequencies for ligand and complexes

	CB5	U2CB5
-C=O Stretching	1738	1695
-CH Stretching & bending	3002 2941 1485 1382	3020 2924 2830 1381
-NO_3 stretching	-	1766
Stretching & bending of H_2O	3439 1636	3423 1653
U-O Bending	-	579, 480 , 445, 948, 859

Frequencies of the stretching and bending vibrations of the C−C, C−N, and C−H groups of cucurbituril were also observed. The IR spectra of the complex show strong and weak absorption bands between 950 and 850 cm^{-1}, and weak bands in the region 580−450 cm^{-1} (Figure 8.8).

The bands at about 948, 579, and ∼480 cm^{-1} are assigned to the asymmetric U−O stretching modes and those at about 859 and 445 cm^{-1} to the symmetric U−O stretching modes of the uranyl moiety [82]. The strong absorption band observed at 1766 cm^{-1} may be assigned to the nitrate. Infrared spectral studies as well as X-ray structural determinations have established that in the complex, nitrate groups are acting as counterions. Stretching frequencies in the complex is significantly shifted toward lower wave-numbers Table 8.5 as a result of oxygen−uranium coordination. The formation of a U−O bond, leads to a decrease in the π character of the C=O bond.

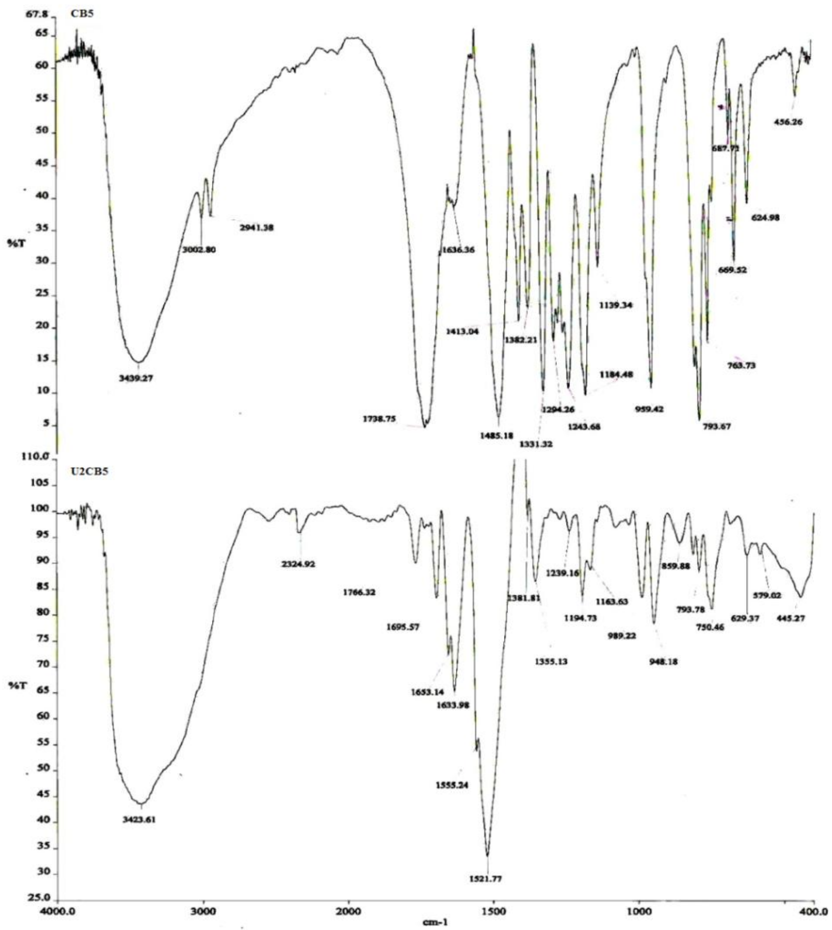

Figure 8.8. FTIR spectra for the CB5 and U2CB5

8.4.1.6. ***Fluorescence Spectroscopy*****.** Uranyl nitrate was found to exhibit the typical greenish-yellow fluorescence with vibronic transitions [107-109] of uranyl ion when excited at 266 nm Figure 8.9.

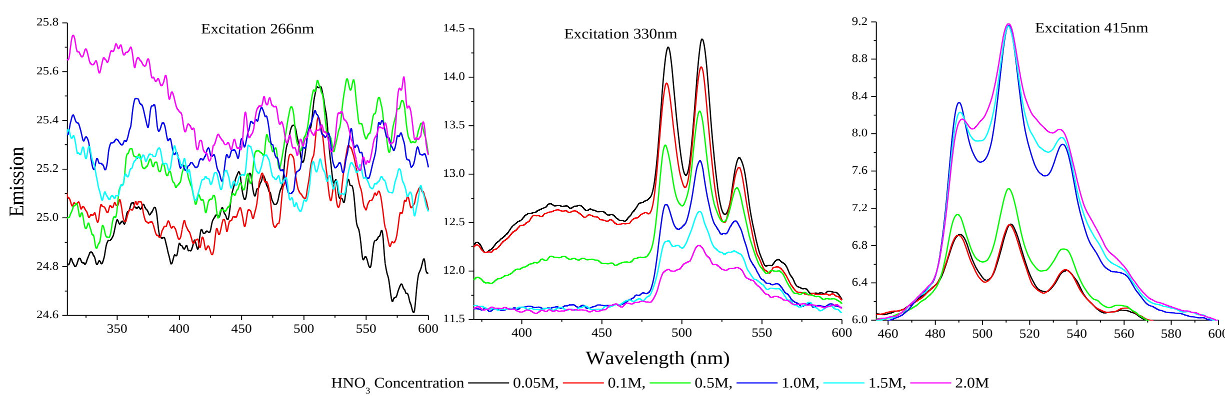

Figure 8.9. Emission spectra of uranyl nitrate with variation in excitation wavelength and HNO_3 concentration

The acidity of the medium seemed to play a vital role in the characterisitics of the emission spectra of uranyl nitrate (Figure 8.10) [83]. Change in excitation wavelength from 266 to 330 nm to 415 nm led to an increase in resolution of the individual vibronic transitions with decrease in the intensity of emission (Figure 8.10 (inset)).

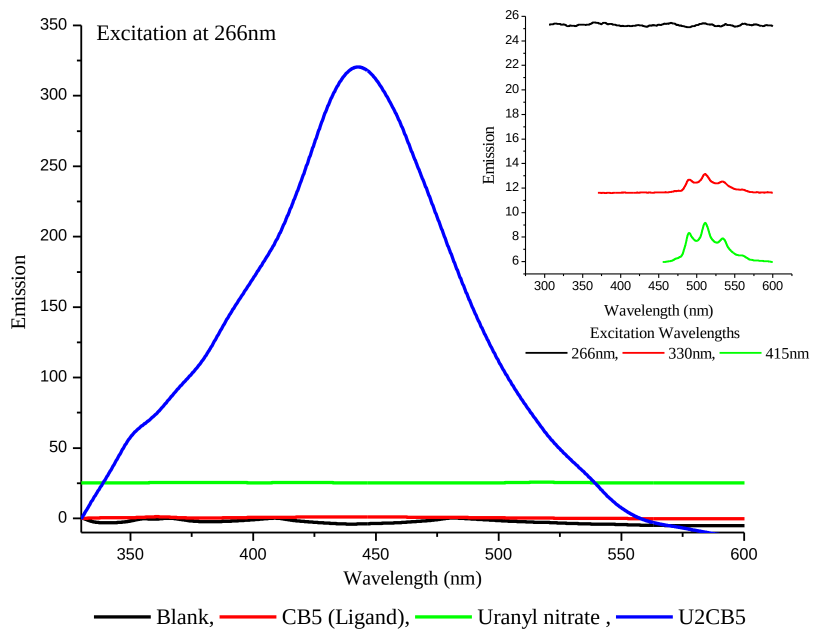

Figure 8.10. Emission spectra of CB5, Uranyl nitrate and U2CB5 excited at 266nm and emission intensity measured at 432nm, inset emission intensities of uranyl nitrate excited at 266nm, 330nm and 415nm

Hence, emission for U2CB5 was measured in ~1.0 M HNO_3 by excitation at 266 nm at room temperature where maximum emission intensity and a well resolved spectrum was observed for uranyl nitrate at 516 nm. The fluorescence intensity of uranyl ion increased remarkably (25.53−319), and the emission peak gradually shifted from 516 to 432 nm upon complexation with CB5 (Figure 8.10). The bonding of uranium to carbonyl groups and hence formation of complex with a macrocycle like CB5 suppresses the various vibrational modes present in uranyl ion [84]. Furthermore the presence of two uranyl ions bound to CB5 could also be responsible for enhanced fluorescence. Thus the formation of inclusion complex of uranyl ion with CB5, led to a hypsochromic shift with fluorescence enhancement. Increase in excitation wavelength from 266 to 330 to 415 nm led to an increase in resolution of the individual vibronic transitions while at the same time decrease in the intensity of emission was observed. The effect of acidity of the medium was also investigated by performing the experiments in 0.05, 0.10, 0.50, 1.00, 1.50, 2.0 M nitric acid. The spectra obtained by excitation at 330 nm were found to be of high emission intensities and well resolved in <1 M nitric acid, while they were broad, unresolved and of lesser intensity in media containing higher concentration of nitric acid. On the other hand, the spectra obtained by excitation at 415 nm in <1 M nitric acid are found to be well resolved with maxima at 516 nm. When the concentration is increased above 1 M the peak at 518 nm is prominent with increased intensity while the other peaks appear only as shoulders. The extinction coefficient, however was much higher and the spectra were better structured for the 330 nm excitation wavelength in comparison with the 415 nm excitation wavelength. Thus the formation of inclusion complex of uranyl ion with CB5, led to a hypsochromic/blue shift with a fluorescence enhancement.

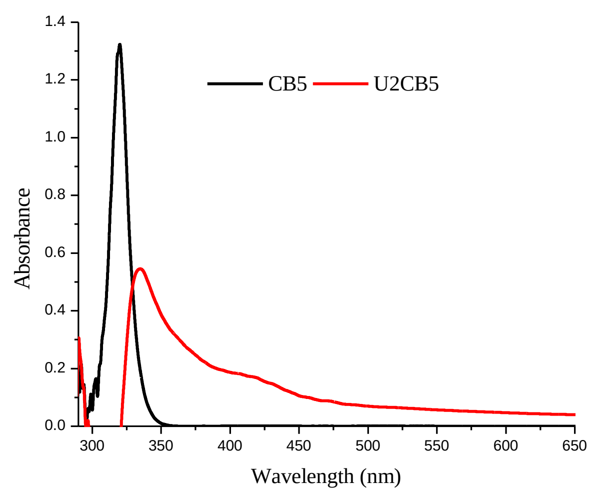

Figure 8.11. UV-Visible absorption spectra of CB5 and U2CB5

Absorption spectral characteristics of U2CB5 showed a bathochromic shift of the charge transfer band (uranium to oxygen) from 319 to 334 nm and a less intense broad shoulder in the visible region at 420 nm (Figure 8.11). The broad character of the U2CB5 could be due to electron transfer involving π- bond contribution (d $\rightarrow$ f transition).

The luminescence spectrum of a solution of uranyl nitrate (0.15 M, pH 1.3) is shown in Figure 8.11. The quantum yield of uranyl nitrate has been previously determined using fluorescein as reference, since its emission spectrum closely overlaps with that of the uranyl ion. However, fluorescein is reported to have some drawbacks as fluorescent standard because of its instability in solution and the dependence of its emission spectrum on pH [85]. We have, thus, determined the luminescence quantum yield for uranyl nitrate solution using, quinine sulfate in 1 M sulfuric acid (quantum yield = 0.546) [86] at excitation wavelength 282 nm. Luminescence quantum yields of 2.7×10^{-3} and 0.75 were obtained for uranyl nitrate and U2CB5 respectively using quinine sulfate as standard. A quantum yield of 0.75 was also reported for the complex $[UO_2(bipyO_2)H_2O](ClO_4)_2$ by Hnatejko et al. [87].

8.4.2. Structural Characteristics for Oligomer.

8.4.2.1. *Gel Permeation Chromatographic Analysis*. The molecular weight of the prepared oligomer was determined using size exclusion chromatography (Figure 8.12) and it is clearly seen that the oligomer was of low degree of polymerization with a molecular weight of 11968 dalton and poly-dispersity index of 1.783.

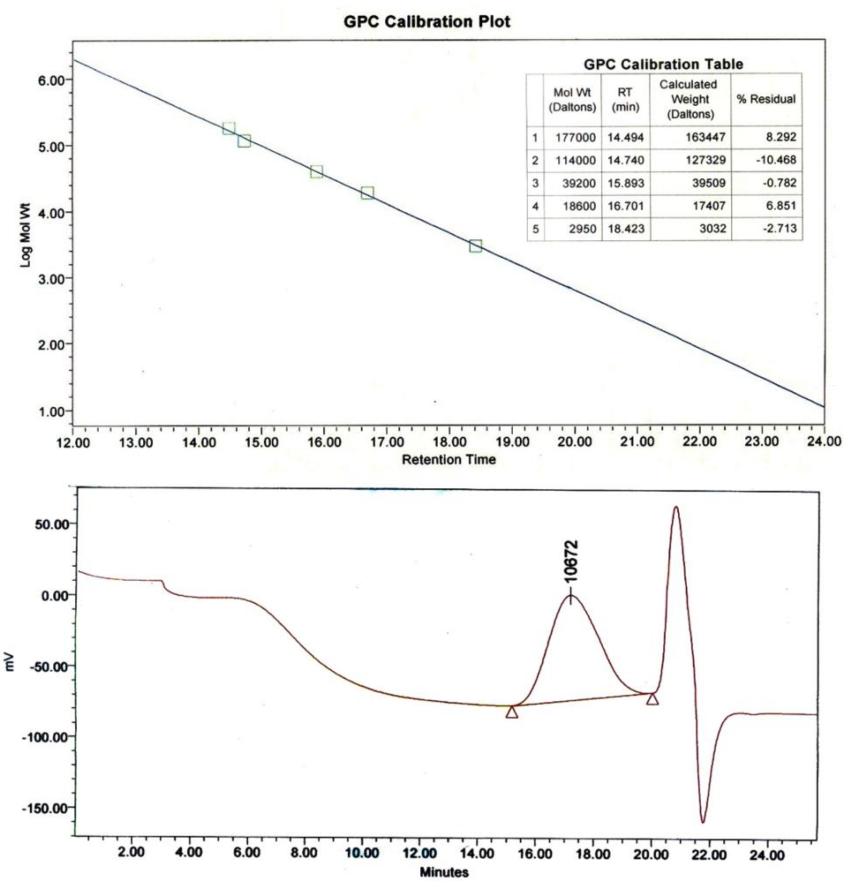

GPC Calibration Table

	Mol Wt (Daltons)	RT (min)	Calculated Weight (Daltons)	% Residual
1	177000	14.494	163447	8.292
2	114000	14.740	127329	-10.468
3	39200	15.893	39509	-0.782
4	18600	16.701	17407	6.851
5	2950	18.423	3032	-2.713

GPC Results

	Dist Name	Mn	Mw	MP	Mz	Mz+1	Mv	Polydispersity	MW Marker 1	MW Marker 2
1		6712	11968	10672	18765	25910		1.783096		

Figure 8.12. GPC calibration and experimental results for IU2CB5

8.4.2.2. *Thermal Analysis*. The TGA curves of IU2CB[5], PGIU2CB[5], LIU2CB[5] and LPGIU2CB[5] (Table 8.6 and Figure 8.13) show gradual loss of mass in the temperature range 28-165^{0}C which corresponds to a loss of adsorbed water molecules.

Table 8.6. Thermal analysis of IU2CB[5], PGIU2CB[5], LIU2CB[5] and LPGIU2CB[5]

<table>
<tr><th colspan="2">IU2CB[5]</th><th colspan="2">LIU2CB[5]</th><th colspan="2">PGIU2CB[5]</th><th colspan="2">LPGIU2CB[5]</th></tr>
<tr><td>Temperature (^{0}C)</td><td>% weight loss</td><td>Temperature (^{0}C)</td><td>% weight loss</td><td>Temperature (^{0}C)</td><td>% weight loss</td><td>Temperature (^{0}C)</td><td>% weight loss</td></tr>
<tr><td>34.64-90.97</td><td>1.93</td><td>28.07–72.71</td><td>9.21</td><td>34.76-107.60</td><td>2.21</td><td>33.81-144.5</td><td>3.11</td></tr>
<tr><td>90.97-162.31</td><td>3.93</td><td>72.71-142.43</td><td>8.44</td><td rowspan="2">107.60-328.18</td><td rowspan="2">14.03</td><td rowspan="2">144.5-265.09</td><td rowspan="2">4.51</td></tr>
<tr><td>162.31-329.95</td><td>35.24</td><td>142.43–354.26</td><td>2.82</td></tr>
<tr><td rowspan="2">329.95-559.58</td><td rowspan="2">10.99</td><td>354.26-516.57</td><td>48.84</td><td>328.18-519.88</td><td>14.30</td><td>265.09-486.85</td><td>14.10</td></tr>
<tr><td>516.57-557.96</td><td>4.49</td><td>519.88-559.58</td><td>1.96</td><td>486.85-560.12</td><td>2.61</td></tr>
<tr><td colspan="8">Total % Weight loss</td></tr>
<tr><td colspan="2">52.44</td><td colspan="2">73.21</td><td colspan="2">32.519</td><td colspan="2">24.33</td></tr>
</table>

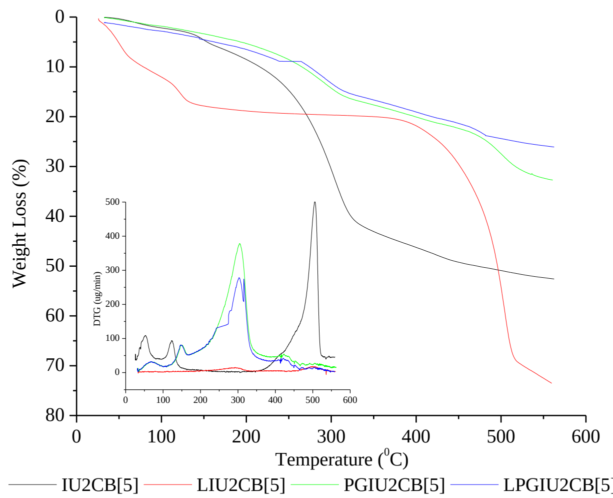

Figure 8.13. Thermal analysis TGA and DTG of IU2CB[5], PGIU2CB[5], LIU2CB[5] and LPGIU2CB[5]

IU2CB[5] and PGIU2CB[5] showed a continuous weight loss upto 450^0C in the TGA curve due to decomposition of oligomer [88]. After formation of stable UO_3 there is not much change in weight of the oligomer whereas leached oligomer showed a sharp decrease in weight loss till 550^0C. It can be interpreted that PGIU2CB[5] (32.52 % mass loss) is more stable than IU2CB[5] (52.44 % mass loss) while LIU2CB[5] (73.21 % mass loss) was found to be least stable. DSC analysis presented the glass transition temperatures for IU2CB[5], PGIU2CB[5], LIU2CB[5] and LPGIU2CB[5] at 105.41, 98.77, 102.18 and 88.2 ^{0}C showing the polymeric nature (Figure 8.14). The lower T_g of PGIU2CB[5] suggests the absence of chemical interactions between the oligomer and PSP.

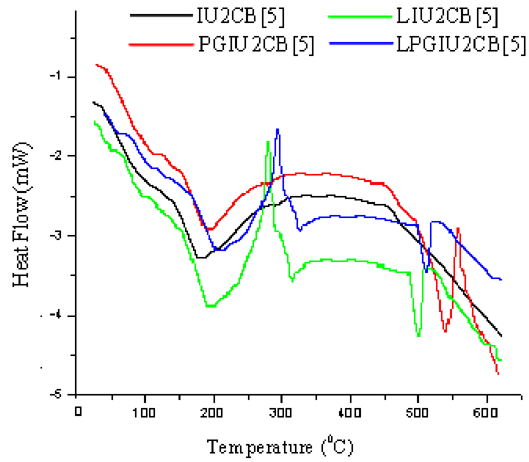

Figure 8.14. DSC analysis of IU2CB[5], PGIU2CB[5], LIU2CB[5] and LPGIU2CB[5]

8.4.2.3. ***Scanning Electron Microscopic Analysis*****.** The scanning electron micrographs are shown in Figure 8.15. The micrograph for IU2CB[5] showed the presence of some non-charged species and an agglomerate of amorphous particles could be seen anchored on the surface of PSP in PGIU2CB[5]. The oligomers were monolithic in nature. After leaching LIU2CB[5] showed very bright images which could probably be due to less electron density and amorphous nature of the oligomer in the absence of uranium. The presence of holes strongly indicated that a template imprint was formed.

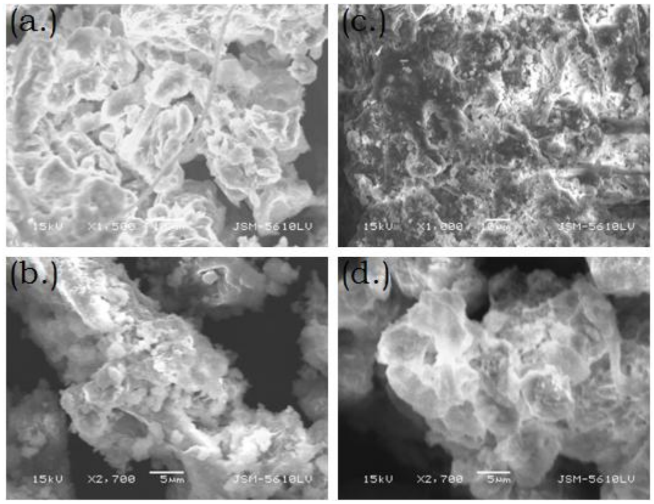

Figure 8.15. Scanning Electron Micrographs (a.)IU2CB[5] (b.)PGIU2CB[5] (c.)LIU2CB[5] and (d.) LPGIU2CB[5]

8.4.2.4. ***Fourier Transform Infra Red Spectroscopic Analysis*****.** The selected infrared bands of IU2CB[5], PGIU2CB[5], LIU2CB[5] and LPGIU2CB[5] with the suggested assignments (frequency in cm^{-1}), are listed in Table 8.7.

Table 8.7. FTIR spectral assignments (frequency in cm^{-1})

Functional groups	CB5/ U2CB[5]	CU2CB[5]/ IU2CB[5]	LIU2CB [5]/ LPGIU2CB[5]	PSP	CPGU2CB[5]/ PGIU2CB[5]
-C=O Stretch	1738/ 1766	1745/ 1759	1750/ 1732	1732	1742/ 1764
-CH Stretch & bend	3002, 2941, 1485, 1382/ 3020, 2924, 2830, 1381	2989, 2915, 2827, 1380/ 2930, 2915, 2827, 1380	2994, 2932, 2825, 1390/ 2959, 2895, 1454, 1373	2959, 2895 1454, 1430 1373	2991, 2940, 2833, 1390/ 2991, 2928, 2832, 1385
Stretch & bend of H_2O	3439, 1636/ 3445, 1695, 1653	3429, 1680/ 3396, 1692	3401, 1642, 1670/ 3391, 1648	1648	3402, 1640, 1670/ 3402, 1639, 1669
-OH stretch & bend (1^0 alcohol)	-/ -	-/ -	-/ 3391	3361	-/ 3402
-C-O- bend	-/ -	1044/ 1256, 1044	1235, 1052/ 1254, 1059	1250, 1049	1051/ 1215, 1057
$CH=CH_2$ bend	-/ -	-/ -	-/ -	-	-/ -
-C-H bend	959, 793, 630/ 964, 788, 624	-/ -	964, 788, 624/ -	893, 809	-/ 962, 878, ~710
U-O Stretch	-/ 579, 480, 445, 948, 859	-/ 580, 481, 448, 951, 864	-/ -	-	-/ 583, 483, 450, 952, 859

The very strong and broad band found at ca. ~3440cm^{-1} and sharp bands at ~1636, ~1695 cm^{-1} in the spectra are consistent with the presence of water molecules in all the samples. All the reported frequencies of the stretching and bending vibrations of cucurbituril were also observed confirming that there is no adverse affect on cucurbituril after complexation and during polymerisation and grafting. Furthermore, the bands at about ~948, ~579 and ~480 cm^{-1} assigned to the asymmetric U-O stretching modes and at about 859.88 and 445.27 cm^{-1} to the symmetric U–O stretching modes of the uranyl moiety [81] were present in all the intermediates as well as imprinted and grafted oligomer but were found to be absent in leached and control oligomer. The IR spectra of IU2CB[5], LIU2CB[5] and PGIU2CB[5], LPGIU2CB[5] respectively were similar, indicating that the leaching process was not affecting the oligomer network and also that cucurbituril remains intact even after leaching. Leaching, left cavities with a predefined cucurbituril array that is able to selectively recognize and rebind the uranyl ion.

8.4.3. Uranium Selectivity Studies.

The distribution ratio, selectivity coefficients and imprinting coefficient of uranyl ion with respect to metal ions like Cu^{2+}, Cd^{2+}, Zn^{2+}, Fe^{3+}, Cs^{+} and Cr^{6+} using CU2CB[5], CPGU2CB[5], IU2CB[5] and PGU2CB[5] are shown in Table 8.8, Table 8.9 and comparison with reported literature is provided in 8.10.

Table 8.8. Imprinting Coefficient

k'	CU2CB[5]	IU2CB[5]	CPGU2CB[5]	PGIU2CB[5]
	1st adsorption		2nd Adsorption	
Cu	4729.005	1652.276	11321.300	2712.278
Cd	8347.820	2344.075	7518.860	2426.503
Zn	4612.201	1295.023	4380.860	1326.225
Cr	3029.618	667.289	3109.912	860.125
Fe	987.349	754.706	967.029	824.912
Cs	555.048	181.451	484.932	207.130

Table 8.9. Distribution ratio and selectivity coefficient

Distribution ratio K_d/ Selectivity Coefficient k								
	CU2CB[5]	IU2CB[5]	CPGU2CB[5]	PGIU2CB[5]	CU2CB[5]	IU2CB[5]	CPGU2CB[5]	PGIU2CB[5]
1st adsorption					2nd Adsorption			
Cu	0.181/ 0.554	0.008/ 2619	0.164/ 2.142	0.007/ 3539	0.171/ 0.593	0.003/ 6710	0.156/ 2.079	0.004/ 5640
Cd	0.431/ 0.232	0.011/ 1934	0.412/ 0.851	0.012/ 1994	0.408/ 0.248	0.010/ 1865	0.379/ 0.855	0.011/ 2074
Zn	0.328/ 0.305	0.015/ 1406	0.205/ 1.714	0.011/ 2219	0.305/ 0.332	0.013/ 1453	0.192/ 1.691	0.010/ 2242
Cr	0.263/ 0.380	0.018/ 1152	0.145/ 2.417	0.015/ 1612	0.251/ 0.403	0.015/ 1254	0.149/ 2.168	0.012/ 1865
Fe	0.379/ 0.263	0.081/ 260	0.460/ 0.763	0.042/ 576	0.318/ 0.319	0.061/ 309	0.395/ 0.820	0.033/ 676
Cs	0.239/ 0.417	0.091/ 232	0.167/ 2.107	0.063/ 383	0.206/ 0.492	0.079/ 238	0.139/ 2.332	0.047/ 483
U	0.099/ -	21.124/ -	0.351/ -	24/ -	0.101/ -	18/ -	0.324/ -	22/ -

The selectivity coefficients (K) of uranyl ion over Cu^{2+}, Cr^{6+}, Zn^{2+}, Cd^{2+} ranged from >103 to $3.82x10^2$ over Fe^{3+} and Cs^{+}. The selectivity coefficients for CPGU2CB[5] were greater by 2 to 8 fold as compared to CU2CB[5]. The selectivity coefficient of PGIU2CB[5] increased $7.7x\ 10^2$ fold to $1.6x10^3$ fold over CPGU2CB[5] owing to the size and shape specific cavities created in PGIU2CB[5] unlike CPGU2CB[5]. Similarly the selectivity coefficient of IU2CB[5] was $5.5x10^2$ to $4.7\ x10^3$ times higher over CU2CB[5]. This observation is attributed to imprinting effect. Interestingly the selectivity coefficient increased during second cycle of adsorption by 1.2 to 1.5 times in presence of Fe^{3+}, Cs^{+}, Cu^{2+} and Cd^{2+} for PGIU2CB[5] which could be probably due to improved memory effect. This improvement was not observed in case of IU2CB[5] in presence of other metal ions except copper while in CU2CB[5] it was not observed in presence of all the metal ions under study. Based on the results shown in Table 8.10, it is clear that U(VI) can be removed selectively from several inorganic species present in dilute aqueous solutions and it is evident that the prepared imprinted oligomer's efficiency is comparable to those reported in literature. Furthermore the material also shows selectivity towards uranium over iron which is a major constituent in front end nuclear industry effluents.

Table 8.10. Comparison with IIP's reported in literature

Ion	Wt. of IIP (mg)	Concentration	K	(k')	Reference
Salo & Vinyl Pyrindine					
Cu^{2+}	100	100 μg/L	1650	157	[18]
Zn^{2+}			825	412	
Fe^{2+}			582	529	
CrO_4^{2-}			9900	309	
Styrene & DVB					
Cu^{2+}	100	0.5 mg/L	277	-	[12]
Zn^{2+}			219	-	
Piroxicam					
Cu^{2+}	100	15 μg/L	104	-	[17]
Zn^{2+}			96	-	
Fe^{3+}			43	-	
Cu^{2+}	100	20 mg/L	130	2.7	[13]
Zn^{2+}			630	1.7	
Fe^{3+}			25	4.9	
Cu^{2+}	100	20 mg/L	1500	6.8	[13]
Zn^{2+}			9500	20.2	
Fe^{3+}			200	1.6	
Cu^{2+}	20	25 mg/L	3539	1652	This work
Zn^{2+}			2219	1295	
Fe^{2+}			576	754	
CrO_4^{2-}			1613	667	

8.5. Conclusions.

Uranyl complex reported herein is the first molecular capsule ever reported with CB5 where both the portals are closed by uranyl ions bound to five oxygen donors obtained in a single step under ambient conditions. Another novelty is the fluorescence study of U2CB5 molecular capsule under ambient conditions which may provide new avenues for research in actinide sensing and molecular recognition. A uranyl complexed cucurbituril oligomer grafted noncovalently led to a rigid, cost-effective ion imprinting oligomer selective for uranium in acidic conditions. Neither this approach nor any other method for synthesis of ion imprinting oligomers based on cucurbiturils has been reported. The prepared imprinted oligomer using cucurbituril, with high imprinting coefficients especially over iron and retention capacity offer possible application towards removal of uranium from front end nuclear effluents.

Literature Cited.

1. G. Wulff. *Angew. Chem., Int. Ed. Engl.* **1995**, *34*, 1812.
2. N. Masquee, R. M. Marcee, F. Borrull, *Trends Anal. Chem.* **2001**, *20*, 477.
3. M . Shamsipur, J. Fasihi, K.Ashtari, *Anal. Chem.* **2007**, *79*, 7116.
4. X. Zhang, C. Ding, H. Liu, L. Liu, C. Zhao, *Toxicology* **2011**, *286*, 75.
5. G. D. Saunders, S. P. Foxon, P. H. Walton, M. J. Joyce, S. N. Port, *Chem. Commun.* **2000**, 273.
6. S. Dai, Y. S. Shin, C. E. Barnes, L. M. Toth, *Chem. Mater*. **1997**, *9*, 2521.
7. M. Kruppa, B. Konig, *Chem. Rev.* **2006**, *106*, 3520.
8. J. M. Gladis, T. P. Rao, *Microchim. Acta* **2004**, *146*, 251.
9. J. M. Gladis, T. P. Rao, *Anal. Lett.* **2003**, *36*, 2107.
10. P. Metilda, J. M. Gladis, T. P. Rao, *Anal. Chim. Acta* **2004**, *512*, 63.
11. C. F. Poole, *Trends Anal. Chem.* **2003**, *22*, 362.
12. S. J. Ahmadi, O. N. Kalkhoran, S. S. Arani, *J. Hazard. Mater.* **2010**, *175*, 193.
13. P. Metilda, J. M. Gladis, G. Venkateswaran, T. P. Rao, *Anal. Chim. Acta* **2007**, *587*, 263.
14. C. R. Preetha, J. M. Gladis, T. P. Rao, *Environ. Sci. Technol.* **2006**, *40*, 3070.
15. Y. Liu, X. Cao, R. Hua, Y. Wang, Y. Liu, C. Pang, Y. Wang, *Hydrometallurgy* **2010**, *104*, 150.
16. P. Metilda, K. Prasad, R. Kala, J. M. Gladis, T. P. Rao, G. R. K. Naidu, *Anal. Chim. Acta* **2007**, *582*, 147.
17. S. Sadeghi, A. A. Mofrad, *React. Funct. Polym.* **2007**, *67*, 966.
18. D. K. Singh, S. Mishra, *Anal. Chim. Acta* **2009**, *644*, 42.
19. T. E. Milja, K. P. Prathish, T. P. Rao, *J. Hazard. Mat.* **2011**, *188*, 384.
20. J. Fasihi, S. A. Alahyari,; M. Shamsipur, H. Sharghi, A. Charkhi, *React. Funct. Polym.* **2011**, *71*, 803.
21. M. Karabo1rk, A. Ersoiz, A. Denizli, R. Say, *Ind. Eng. Chem. Res.* **2008**, *47*, 2258.
22. C. Yu, K.Mosbach, *J. Chromatogr. A* **2000**, *888*, 63.
23. Q. Li, H. J. Su, T. W. Tan, *Biochem. Eng. J.* **2008**, *38*, 212.
24. C. Alexander, H. S. Andersson, L. I. Andersson, R. J. Ansell, N. Krisch, I. A. Nicholls, J. O'Mahony, Whitcombe, M.J. *J. Mol. Recognit.* **2006**, *19*, 106.

25. O. Bruggemann, K. Haupt, L. Ye, E. Yilmaz, K. Mosbach, *J. Chromatogr. A* **2000**, *889*, 15.
26. B. B. Prasad, S. Banerjee, *React. Funct. Polym.* **2003**, *55*, 159.
27. C. Sulitzky, B. Ruckert, A. J. Hall, F. Lanza, K. Unger, B. Sellergren, *Macromolecules* **2002**, *35*, 79.
28. J. Ou, X. Li, S. Feng, J. Dong, X. Dong, L. Kong, M. Ye, H. Zou, *Anal.Chem.* **2007**, *79*, 639.
29. J. Pan, X. Zou, X. Wang, W. Guan, Y. Yan, J. Han, *Chem. Eng. J.* **2010**, *162*, 910.
30. K. Tsukagoshi, K. Y. Yu, M. Maeda, M. Takagi, *Bull. Chem. Soc. Jpn.* **1993**, *66*, 114.
31. Y. M. Ren, M. L. Zhang, D. Zhao, *Desalination* **2008**, *228*, 135.
32. G. H. Wu, Z. Q. Wang, J. Wang, C. Y. He, *Anal. Chim. Acta* **2007**, *582*, 304.
33. X. J. Chang, N. Jiang, H. Zheng, Q. He, Z. Hu, Y. H. Zhai, Y. M. Cui, *Talanta* **2007**, *71*, 38.
34. E. Birlik, A. Ersoz, E. Ac ıkkalp, A. Denizli, R. Say, *J. Hazard. Mater.* **2007**, *140*, 110.
35. N. Candan, N. Tuzmen, M. Andac, C. A. Andac, R. Say, A. Denizli, *Mater. Sci. Eng. C* **2009**, *29*, 144.
36. Y. H. Zhai, Y. W. Liu, X. J.Chang, X. F. Ruan, J. L. Liu, *React. Funct. Polym.* **2008**, *68*, 284.
37. B. Sellergren, C. Sulitzky, B. Ruckert, U.S. Patent 6, **2004**, *488 B1*, 759.
38. F. G. Tamayo, M. M. Titirici, A. M. Esteban, B. Sellergren, *Anal. Chim. Acta* **2005**, *542*, 38.
39. M. Quaglia, E. D. Lorenzi, C. Sulitzky, G. Massoloni, B. Sellergren, *Analyst* **2001**, *126*, 1495.
40. M. Quaglia, E. D. Lorenzi, C. Sulitzky, G. Caccialanza, B. Sellergren, *Electrophoresis* **2003**, *24*, 952.
41. L. Schweitz. *Anal. Chem.* **2002**, *74*, 1192.
42. D. James, G. Venkateswaran, T. P. Rao, *Microporous and Mesoporous Materials* **2009**, *119*, 165.
43. V. Pakade, E. Cukrowska, J. Darkwa, N. Torto, L. Chimuka, Simple and Efficient Ion Imprinted Polymers for Recovery of Uranyl Ion and Chromium (VI) from Environmental Samples, *ANALYTICAL TOOLS AND TECHNIQUES* ,15th ICHMET, 227.
44. S.Y. Bae, G.L. Southard, G.M. Murray, *Analytica Chimica Acta,* **1999,** *397*, 173.
45. F. Caprasse, D. Leroy, L. Martinot, S. Lambert, J. P. Pirard, J. Guillaume, C. Jeromeand R. Jeromed, *J. Mater. Chem.* **2002**, *12*, 137.
46. R. Say, A. Ersoz, A. Denizli, Sep. Sci. Technol. 38 (2003) 3431–3441.

47. W.L. Mock, In Comprehensive Supramolecular Chemistry; Vogtle, Ed.; Pergamon: Oxford, **1996**, *2*, 477.
48. J.W. Lee, S. Samal, N. Selvapalam, H. J. Kim, K. Kim, *Acc. Chem. Res.* **2003**, *36*, 621.
49. J. Lagona, P. Mukhopadhyay, S. Chakrabarti, L. Isaacs, *Angew. Chem. Int. Ed.* **2005**, *44*, 4844.
50. S.D. Choudhury, J. Mohanty, H. Pal, A. C. Bhasikuttan, *J. Am. Chem. Soc.* **2010**, *132*, 1395.
51. K. Kim, *Chem. Soc. Rev.* **2002**, *31*, 96.
52. O. A. Gerasko, D. G. Samsonenko, V. P. Fedin, *Russ. Chem. Rev.* **2002**, *71*, 741.
53. J. X. Lin, J. Lu, H. X. Yang, R. Cao, *Crys. Grow. Des.* **2010**, *10*, 1966.
54. W. A. Freeman, *Acta Crystallogr. Sect. B* **1984**, *40*, 382.
55. H. J. Buschmann, E. Cleve, E. Schollmeyer, *Inorg. Chim. Acta* **1992**, *193*, 93.
56. Y. M. Jeon, J. Kim, D. Whang, K. Kim, *J. Am. Chem. Soc.* **1996**, *118*, 9790.
57. D. Whang, J. Heo, J. H. Park, K. Kim, *Angew. Chem. Int. Ed.* **1998**, *37*, 78.
58. J. Heo, S. Y. Kim, D. Whang, K. Kim, *Angew. Chem. Int. Ed.* **1999**, *38*, 641.
59. J. Heo, J. Kim, D. Whang, K. Kim, *Inorg. Chim. Acta* **2000**, *297*, 307.
60. F. Zhang, T. Yajima, Y. Z. Li, G. Z. Xu, H. L. Chen, Q. T. Liu, O. Yamauchi, *Angew. Chem. Int. Ed.* **2005**, *44*, 3402.
61. J. X. Liu, L. S. Long, R. B. Huang, L. S. Zheng, *Cryst. Growth Des.* **2006**, *6*, 2611.
62. D. G. Samsonenko, J. Lipkowski, O. A. Gerasko, A. V. Virovets, M. N. Sokolov, V. P. Fedin, J. G. Platas, R. Hernandez-Molina, A. Mederos, *Eur. J. Inorg. Chem.* **2002**, *9*, 2380.
63. D. G. Samsonenko, O. A. Gerasko, J. Lipkowski, A. V. Virovets, V. P. Fedin, *Russ. Chem. Bull.* **2002**, *51*, 1915.
64. D. G. Samsonenko, M. N. Sokolov, O. A. Gerasko, A. V. Virovets, J. Lipkowski, D. Fenske, V. P. Fedin, *Russ. Chem. Bull.* **2003**, *52*, 2132.
65. J. X. Liu, L. S. Long, R. B. Huang, L. S. Zheng, *Inorg. Chem.* **2007**, *46*, 10168.
66. O. A. Gerasko, E. A. Mainicheva, M. I. Naumova, O. P. Yurjeva, A. Alberola, C. Vicent, R. Llusar, V. P. Fedin, *Eur. J. Inorg. Chem.* **2008**, *3*, 416.
67. O. A. Gerasko, M. N. Sokolov, V. P. Fedin, *Pure Appl. Chem.* **2004**, *76*, 1633.
68. O. A. Gerasko, D. G. Samsonenko, A. A. Sharonova, A. V. Virovets, J. Lipkowski, V. P. Fedin, *Russ. Chem. Bull.* **2002**, *51*, 346.
69. S. C. Cui, T. Tachikawa, M. Fujitsuka, T. Majima, *J. Phys. Chem. C* **2011**, *115*, 1824.

70. K. Kim, N. Selvapalam, Y. H. Ko, K. M. Park, D. Kim, Kim, *J. Chem. Soc. Rev.* **2007**, *36*, 267.
71. C. A. Burnett, D. Witt, J. C. Fettinger, L. Isaacs, *J. Org. Chem.* **2003**, *68*, 6184.
72. J. Kim, I.-S. Jung, S.-Y. Kim, E. Lee, J. -K. Kang, S. Sakamoto, K. Yamaguchi, K. Kim, *J. Am. Chem. Soc.* **2000**, *122*, 540.
73. P. Thuery, *Cryst. Growth Des.* **2009**, *9*, 1208.
74. P. Thuery, *Cryst. Growth Des.* **2008**, *8*, 4132.
75. J. C. Berthet, M. Nierlich, M. Ephritikhine, *Angew. Chem. Int. Ed.* **2003**, *42*, 1952.
76. *SAINT: Software for the CCD Detector System*; Bruker Analytical X-ray Systems, Inc.: Madison, WI, **1998**.
77. Bruker SADABS, SMART, SAINTPLUS and SHELXTL, Bruker AXS Inc., Madison, WI, USA, **2003**.
78. G.M. Sheldrick, *SHELXS-97*, *Program for Structure Solution of crystal structure;* University of Gottingen: Germany, **1997**.
79. G.M. Sheldrick, *SHELXL-97, Program for Crystal Structure Analysis;* University of Gottingen: Germany, **1997**.
80. T. Cardinaels, J. Ramaekers, D. Guillon, B. Donnio, K. Binnemans, *J. Am. Chem. Soc.* **2005**, *127*, 17602.
81. Y. Zhang, F. R. Livens, D. Collison, M. Helliwell, F. Heatley, A. K. Powell, S. Wocadlo, Eccles, H. *Polyhedron* **2002**, *21*, 69.
82. Z. Hnatejko, S. Lis, Z. Stryła, Starynowicz, P. *Polyhedron* **2010**, *29*, 2081.
83. Y. Katsumura, H. Abe, T. Yotsuyanagi, K. Ishigure, *J. Photochem. Photobiol., A* **1989**, *50*, 183.
84. E. Rabinowitch, R. L. Belford, *Spectroscopy and Photochemistry of Uranyl Compounds, Pergamon* **1964**, 264.
85. S. J. Formosinho, M. G. Miguel, H. D. Burrows, *J. Chem. Soc., Faraday Trans.* **1984**, *80*, 1717.
86. S. J. Formosinho, H. D. Burrows, M. G. Miguel, M. Emilia, D. G. Azenha, I. M. Saraiva, A. Catarina, D. N. Ribeiro, I. V. Khudyakov, R. G. Gasanov, M. Bolte, M. Sarakha, *Photochem. Photobiol. Sci.* **2003**, *2*, 569.
87. Z. Hnatejko, S. Lis, P. Starynowicz, Z. Stryła, *Polyhedron* **2011**, *30*, 880.

88. S.Y. Jon, N. Selvapalam, D. H. Oh, J. K. Kang, S. Y. Kim, Y. J. Jeon, J. W. Lee, K. Kim, *J. Am. Chem. Soc.* **2003**, *125*, 10186.

Chapter 9

Conclusions

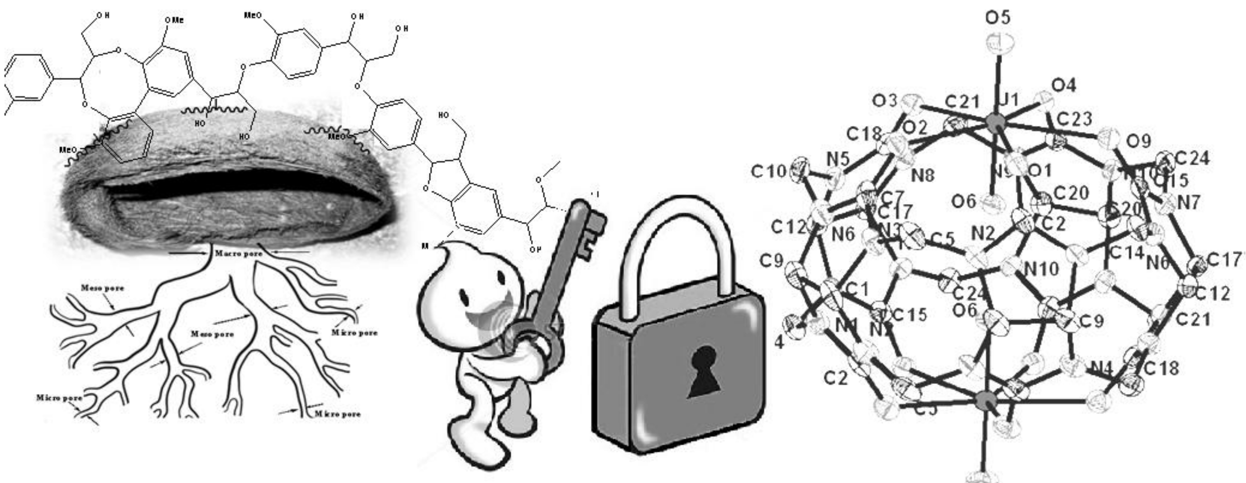

Palm shell powder (PSP) was modified by either charring with sulfuric acid (APSP) or modifying it with formaldehyde (MPSP). A series of adsorbents were prepared from APSP by steam (SAPSP) and persulfate (PAPSP) treatment at 140˚C or thermal activation at 900˚C (9AAC). The materials showed some interesting properties.

- APSP, SAPSP and PAPSP were found to have iodine values of 342.5, 199.8 and 299.7 mg/g respectively and significant pore size in spite of their small BET surface areas suggesting high adsorption capacity.
- FTIR, XPS and ^{13}C NMR spectral data indicate that carboxyl, ether, alcoholic, hydroxyl and amino functional groups may be available for metal binding in PSP, MPSP, APSP, PAPSP and SAPSP.
- The presence of aldehydic groups along with etheric linkages of ligno-cellulosic moiety in higher numbers in PSP and MPSP is also indicated.
- Furthermore the number of oxygen containing functional groups were also found to increase with acid treatment and oxidation, the order being SAPSP>PAPSP>APSP> MPSP>PSP>9AAC.

This led us to evaluate their efficacy towards the removal of several toxic and heavy metal ions like copper, cadmium, zinc, mercury, chromium and uranium.

- The adsorption capacity increased in the order Cr>Cd>U>Zn>Hg>Cu for PSP; Cr>U>Zn>Cd>Cu>Hg for APSP; Cd>Cr>U>Zn>Cu>Hg for SAPSP; Cd> Cr>Zn>U>Cu>Hg for PAPSP; Cd>Cr>U>Zn>Cu>Hg for 9AAC and Cr>Zn>U>Cd>Hg>Cu for MPSP. The low adsorption capacity of mercury could be due to the soft nature of mercury and the hard nature of the dominant carboxyl groups available for binding.
- Column studies have been performed and the breakthrough capacities obtained. However, studies have not been done for optimisation of various parameters like flow rate, bed height had not been done as well as the effect of concentration of the adsorbates has not been studied. These studies would provide useful information for designing pilot- and full scale columns for water and wastewater treatment facilities.

- The materials were found to have adsorption capacity either comparable to or better than those reported in literature.

It is observed that the adsorbents were effective towards adsorption of the metal ions under study in a wide pH range (the amount remaining in solution would be below prescribed limits) in contrast to most of the adsorbents reported in literature due to the presence of functional groups with different pK_a values. Furthermore Cr^{3+}, Cr^{6+} were found to adsorb quantitatively at acidic pH which would be advantageous in the treatment of effluents containing these metal ions which are usually acidic. This is in contrast to the reports in literature where the adsorption of Cr^{3+} was found to be drastically low in acidic pH and even reduced Cr^{6+} was reported to come back into solution. Uranyl ions could be removed effectively in both acidic and alkaline conditions which would be of great advantage as uranium is present in both acidic and alkaline effluents of the nuclear industry.

XPS analysis of metal loaded adsorbents provided interesting results .Mercury loaded PSP showed the presence of elemental mercury which increased the adsorption capacity of mercury in PSP. Chromium (VI) was found to get reduced to Cr(III) on the adsorbents under study while U(VI) was getting reduced to U(V) and U(IV).

- The advantage of the reduction processes being, more number of carboxyl groups are generated leading to greater adsorption capacity as observed for uranium and chromium as well as mercury in the case of PSP.
- Cr (VI) was found to get partly reduced to Cr(III). Studies need to be done to check whether complete reduction would be possible with further change in conditions. The chromium (III) containing adsorbents could then be used as reductant for the preparation of basic chromium sulfate (tanning agent). Another alternative would be to identify conditions where chromium could remain on the adsorbate as Cr(VI) which would be useful in chromate recovery processes in electroplating industries. The stability of the sorbent against oxidation by chromate, the elution efficiency of bound chromate, and the regenerability of chromate-loaded sorbent would be equally relevant considerations.
- The reduction of U(VI) to U(V) and U(IV) by the adsorbents under study is unique and highly advantageous in the remediation of uranium (VI) containing waste waters.

Multiple mechanisms seem to be involved in the adsorption process by the adsorbents under study. The main mechanisms being hydrogen-bonding, physisorption, chemisorption, ion exchange and precipitation. Furthermore in the case of chromium(VI) and uranium(VI) adsorption followed by reduction seems to be a predominant mechanism. However, further studies are needed to find whether reduction is the rate controlling step.

Multicomponent studies have been done by the use of synthetic binary, ternary and quarternary mixtures containing the metal ions under study. The results were encouraging. However, the real samples would not only contain a number of metals but also natural organic matter and other organic pollutants. The effect of these pollutants on the adsorption of metal ions has to be studied.

The study indicates that though palm shell based adsorbents are quite effective in the removal of metal ions, selectivity could not be achieved either during adsorption or during desorption process. The adsorbents can definitely serve as a potential alternative for water treatment though further studies are needed as discussed above. However they cannot be applied for specific recovery of a particular metal. But they can be applied for recovery of metals from specific effluents. Though the ability of the adsorbents for the removal of uranium in the presence of iron and cesium has been demonstrated, further work needs to be done in the presence of other constituents which are usually present in nuclear plant effluents before coming to any conclusion regarding the efficacy of the adsorbents in this direction. The results obtained in this study definitely show that palm shell has some unique constituents which results in its reduction of mercury and uranium which is in contrast to the results reported by other plant based materials. Studies related to analysis of palm shell constituents (sugar palm) in detail are not available in literature. Studies in this direction would be interesting and useful.

Chitosan barbital based adsorbents were prepared and were evaluated for their adsorption potential towards inorganic mercury, methyl mercury and phenyl mercury. Speciation was achieved by sequentially eluting inorganic, methyl and phenyl Hg^{2+} using 0.1N $HClO_4$, 0.015N NaCl and 0.05 N EDTA respectively using barbital grafted chitosan. BCL showed better selectivity for mercury in synthetic mixtures containing copper, cadmium and zinc as compared to C, BC and CL in the concentration range studied.

A novel fluorescent complex {(UO2)2(CB5)}(NO3)8·3H2O (U2CB5) was obtained from cucurbit[5]uril and uranyl nitrate under ambient temperature conditions. The crystal structure revealed that two uranyl ions are coordinated to the two open portals of CB5 giving a closed molecular capsule, which further connected through CB5 molecules to give two-dimensional frameworks.The UCB5 complex was oligomerised and a non-covalent method was used to graft uranyl complexed cucurbituril oligomer onto PSP which led to a rigid, cost-effective ion imprinting oligomer selective for uranium. However, it would be interesting to study the fluorescent properties of the uranyl containing polymer. It could definitely be showing some interesting properties as compared to the U2CB5 complex and could show potential as a sensor. The U2CB5 complex could also be tested for its potential as a catalyst, for instance decomposition of hydrogen peroxide.

PAPERS

PUBLISHED

1. S. Kushwaha, P.P. Sudhakar. Noncovalent Surface Grafting of Uranium complexed Cucurbit[5]uril Oligomer onto Palm Shell Powder: A Novel Approach for selective Uranyl ion Extraction. **Analyst** 2012, 137, 3242-3245.
2. S. Kushwaha, B. Sreedhar and P. Padmaja. A Spectroscopic Study for Understanding the Speciation of Cr on palm shell based adsorbents and their application for the remediation of chrome plating effluents. **Bioresource Technology** 2012, 116, 15-23.
3. S. Kushwaha, B. Sreedhar and P. Padmaja. Adsorption of Hg^{2+} onto *Borassus Flabellifer*: A Redox Mechanism. **Chemical Engineering Journal** 2012, 193-194, 328-338.
4. S. Kushwaha, S.A. Rao, P.P. Sudhakar. A Fluorescent uranyl ion lidded Cucurbit[5]uril capsule. **Inorganic Chemistry** 2012, 51 (1), 267-273.
5. S. Kushwaha, G. Sreelatha and P. Padmaja. Physical and Chemical modified forms of *Palm Shell*: Preparation, Characterization and Preliminary Assessment as Adsorbents. **Journal of Porous Materials**, 2012, 1-16.
6. S. Kushwaha, H. Soni, V. Ageetha and P. Padmaja. An Insight into the Production, Characterisation and Mechanism of Low Cost Adsorbents for removal of Organics from Aqeous Solution. **Critical Reviews in**

Environmental Science & Technology. DOI: 10.1080/10643389.2011.604263.

7. Shilpi Kushwaha, Padmaja P. Sudhakar. Adsorption of mercury(II), methyl mercury(II) and phenyl mercury(II) on chitosan cross-linked with a barbital derivative. **Carbohydrate Polymers**, 86(2), 2011, 1055-1062.
8. S. Kushwaha, B. Sreedhar and P. Padmaja. Sorption of Phenyl Mercury, Methyl Mercury and Inorganic Mercury onto Chitosan and Barbital Immobilized Chitosan: Spectroscopic, Potentiometric, Kinetic, Equilibrium and Selective Desorption Studies. **J. Chem. Engg. Data** 2010, 55 (11), 4691–4698.
9. S. Kushwaha, S. Sodaye and P. Padmaja. Adsorption of Hg(II) from aqueous solution onto *Borassus Flabeliffer*: equilibrium and kinetic studies. **Desalination and Water Treatment**, 2009, 12, 100-107.
10. S. Kushwaha, S. Sodaye and P. Padmaja. Equilibrium, Kinetics and Thermodynamic Studies for Adsorption of Hg (II) on Palm Shell Powder. **Proceedings of World Academy of Science, Engineering and Technology**, 2008, Vol.33, 617-623.

ORAL PRESENTATIONS

1. Proceedings of Sixth All Gujarat Research Scholars Meet, January 2010, Department of Chemistry, The Maharaja Sayajirao University of Baroda.

2. Proceedings of World Academy of Science, Engineering and Technology Volume 33, September-2008, held at Heidelberg, Germany, Issn 2070-3740.

POSTER PRESENTATIONS

1. Proceedings of International Conference on Supramolecules and Nanomaterials-Research and Applications, ICSNA, February-2012 held in Ahmedabad, organized by Gujarat University and GUJCOST.
2. Proceedings of 12^{th} International Symposium on Inorganic Ring Systems, IRIS-12, August-2009 held in Goa, organized by IIT Bombay.
3. Proceedings of International Symposium on Material Chemistry-08, December-2008 held at BARC, Trombay, Mumbai.
4. Proceedings of SESTEC. March-2008 held at Delhi University, Delhi.
5. Proceedings of International Conference on Advanced Materials-February-2008, held at Mahatma Gandhi School of sciences, Kottayam.
6. Proceedings of Modern Trends in Inorganic Chemistry, December 2007, held at IIT Chennai.

WORKSHOPS AND CONFERENCES ATTENDED

1. Workshop on Advances in Materials, January 2010, held at Department of Material Science, S. P. University, Vallabh Vidyanagar.

2. Workshop on Radiochemistry, January 2010, held at Department of Chemistry, The Maharaja Sayajirao University of Baroda.
3. National Symposium on Emerging Horizons in Catalysis (CATSYMP-2009), September 2009, held at Department of Chemistry, The Maharaja Sayajirao University of Baroda.
4. Seminar on Advances in Chemistry, December 2008, held at Welcome Hotel Vadodara.
5. One day Seminar on X-ray Diffraction Technique, ISAS-Baroda Chapter, February 2008, held at Department of Chemistry, The Maharaja Sayajirao University of Baroda.
6. Workshop on Surfactants: Theory and Practice, October 2007, held at Department of Chemistry, The Maharaja Sayajirao University of Baroda.